MYOCARDIAL REMODELING: MECHANISMS AND TRANSLATIONAL IMPLICATIONS

EDITED BY: Oksana Kunduzova, Helene Tronchere, Antonio Lax and Jérôme Roncalli
PUBLISHED IN: Frontiers in Pharmacology

frontiers Research Topics

ISSN 1664-8714
ISBN 978-2-88976-389-4
DOI 10.3389/978-2-88976-389-4

About Frontiers

Frontiers is more than just an open-access publisher of scholarly articles: it is a pioneering approach to the world of academia, radically improving the way scholarly research is managed. The grand vision of Frontiers is a world where all people have an equal opportunity to seek, share and generate knowledge. Frontiers provides immediate and permanent online open access to all its publications, but this alone is not enough to realize our grand goals.

Frontiers Journal Series

The Frontiers Journal Series is a multi-tier and interdisciplinary set of open-access, online journals, promising a paradigm shift from the current review, selection and dissemination processes in academic publishing. All Frontiers journals are driven by researchers for researchers; therefore, they constitute a service to the scholarly community. At the same time, the Frontiers Journal Series operates on a revolutionary invention, the tiered publishing system, initially addressing specific communities of scholars, and gradually climbing up to broader public understanding, thus serving the interests of the lay society, too.

Dedication to Quality

Each Frontiers article is a landmark of the highest quality, thanks to genuinely collaborative interactions between authors and review editors, who include some of the world's best academicians. Research must be certified by peers before entering a stream of knowledge that may eventually reach the public - and shape society; therefore, Frontiers only applies the most rigorous and unbiased reviews.
Frontiers revolutionizes research publishing by freely delivering the most outstanding research, evaluated with no bias from both the academic and social point of view. By applying the most advanced information technologies, Frontiers is catapulting scholarly publishing into a new generation.

What are Frontiers Research Topics?

Frontiers Research Topics are very popular trademarks of the Frontiers Journals Series: they are collections of at least ten articles, all centered on a particular subject. With their unique mix of varied contributions from Original Research to Review Articles, Frontiers Research Topics unify the most influential researchers, the latest key findings and historical advances in a hot research area! Find out more on how to host your own Frontiers Research Topic or contribute to one as an author by contacting the Frontiers Editorial Office: frontiersin.org/about/contact

MYOCARDIAL REMODELING: MECHANISMS AND TRANSLATIONAL IMPLICATIONS

Topic Editors:
Oksana Kunduzova, Institut National de la Santé et de la Recherche Médicale (INSERM), France
Helene Tronchere, Institut National de la Santé et de la Recherche Médicale (INSERM), France
Antonio Lax, University of Murcia, Spain
Jérôme Roncalli, Centre Hospitalier Universitaire de Toulouse, France

Citation: Kunduzova, O., Tronchere, H., Lax, A., Roncalli, J., eds. (2022). Myocardial Remodeling: Mechanisms and Translational Implications. Lausanne: Frontiers Media SA. doi: 10.3389/978-2-88976-389-4

Table of Contents

frontiers | Frontiers in Pharmacology

EDITORIAL
published: 26 May 2022
doi: 10.3389/fphar.2022.930387

Editorial: Myocardial Remodeling: Mechanisms and Translational Implications

Jerome Roncalli[1,2]*, *Hélène Tronchère*[2], *Antonio Lax*[3] and *Oxana Kunduzova*[2]

[1]Department of Cardiology, Institute CARDIOMET, University Hospital of Toulouse, Toulouse, France, [2]INSERM I2MC - UMR1297, Toulouse, France, [3]ICTC Research Group/Heart Failure Health Science Campus, University of Murcia, Murcia, Spain

Keywords: renin-angiotensin-aldosterone system, myocardial remodeling, hypertrophy, inflammation, fibrosis

Editorial on the Research Topic

Myocardial Remodeling: Mechanisms and Translational Implications

Left ventricular remodeling is an adaptive process modifying the ventricular size, shape, structure and mass of the myocardium. The ensuing cardiomyocytes loss, thereby activate intracellular signaling pathways, inflammatory reaction, and stimulate the renin-angiotensin-aldosterone (RAAS) and sympathetic nervous systems (Pfeffer et al., 1990; Rouleau et al., 1993). All of these result in myocardial fibrosis formation and ventricular cavity dilation (Liu et al., 2012; Van Berlo et al., 2013; Xie et al., 2013). Left ventricular remodeling remains the major determinant of cardiac function and survival after recovery from acute myocardial infarction (AMI) (White et al., 1987). Different available and promising therapeutic approaches are available to treat and attenuate the adverse effects of cardiac remodeling process by targeting the underlying pathophysiological mechanisms. Mainly, the RAAS regulates post-AMI cardiac remodeling process (Belge et al., 2014). As a consequence, blocking RAAS acts in a manner to stop left ventricular remodeling, reduce mortality and improve short- and long-term survival (Pfeffer et al., 1990). The goal of this Research Topic was to understand how aberrant cardiac remodeling contributes to the development and progression of heart failure (HF) and how to exploit this knowledge for therapeutic benefits to improve cardiac function and to prevent HF progression. In this Research Topic we have eight original research articles and one review article summarizing the recent advances in myocardial remodeling.

In their study, Zhang et al. intend to investigate the role and mechanisms of Sestrin2 (Sesn2), a stress-induced protein, in cardiac hypertrophy with the use of Sesn2 transgenic and AMPKα2 knockout mice by establishing a pressure overload-induced cardiac hypertrophy model via aortic banding surgery. Regarding cardiac hypertrophy in women, Wang et al. investigated the effects of G protein–coupled estrogen receptor 30 (GPR30), a membrane receptor of estrogen that displays protective roles in diverse cardiovascular diseases and investigated the effects of GPR30, activation on transverse aortic constriction (TAC)-induced cardiac hypertrophy of aged female mice. The novel finding of this study was that GPR30 activation could reduce TAC-induced cardiac fibrosis through downregulation of the MMP-9 level, which may provide the potential therapeutic targets for the treatment of pathological cardiac hypertrophy in postmenopausal women.

Mitochondrial dysfunction also plays an important role in the pathology of cardiac hypertrophy. Findings by Chen et al. suggested that quercetin, a natural flavonol agent, protected mitochondrial function by modulating SIRT3/PARP-1 pathway, contributing to the inhibition of cardiac hypertrophy in spontaneously hypertensive rats (SHRs) and H9c2 cells.

OPEN ACCESS

Edited and reviewed by:
Francesco Rossi,
University of Campania Luigi Vanvitelli, Italy

***Correspondence:**
Jerome Roncalli
roncalli.j@chu-toulouse.fr

Specialty section:
This article was submitted to Cardiovascular and Smooth Muscle Pharmacology, a section of the journal Frontiers in Pharmacology

Received: *27 April 2022*
Accepted: *09 May 2022*
Published: *26 May 2022*

Citation:
Roncalli J, Tronchère H, Lax A and Kunduzova O (2022) Editorial: Myocardial Remodeling: Mechanisms and Translational Implications. Front. Pharmacol. 13:930387. doi: 10.3389/fphar.2022.930387

Then, atrial fibrillation (AF) which is the most common sustained cardiac arrhythmia in clinical setting, is associated with metabolic disorder, especially defective fatty acids oxidation (FAO). Thus, promoting FAO could prevent AF occurrence. Zhang et al. demonstrated that FAO promotion via L-carnitine attenuated obesity-mediated AF and structural remodeling by activating AMP-activated protein kinase (AMPK) signaling and alleviating atrial lipotoxicity. RAAS inhibitors can also inhibited the occurrence and development of AF induced by atrial fibrosis and realized significant benefits for the long-term survival of AF patients (Han et al., 2013; Turin et al., 2018). However, these conventional drugs cannot completely cure atrial fibrosis (McDonagh et al., 2021). Therefore, Hu et al. investigated the mechanisms and interventions of atrial fibrosis to reduce the atrial structural remodeling and electrical remodeling caused by atrial fibrosis in order to reduce the occurrence and development of AF. Jarkovská et al. show that effective suppression of electrical proarrhythmic remodeling and mortality but not hypertrophy indicates that the beneficial therapeutic effects of ACE inhibitor trandolapril in volume overload heart failure might be dissociated from pure antihypertrophic effects.

Moreover, mineralocorticoid receptor antagonists (MRA) have been described to reduce reactive fibrosis and improve cardiac function. However, Demkes et al. failed to demonstrate that combined treatment with GLP-1R agonist exenatide and MRA potassium canrenoate could minimize cardiac injury and limit progression to chronic HF in a pig model of ischemic/reperfusion.

Recently, LCZ696 (valsartan/sacubitril), the first of the new ARNI (angiotensin receptor-neprilysin inhibitor) drug class, has been recently approved for the treatment of chronic HF patients with reduced ejection fraction (HFrEF) after the PARADIGM-HF trial (McMurray et al., 2014; Campbell, 2017). The addition of the neprilysin component in LCZ696 augments plasma levels of natriuretic peptides (Voors et al., 2013) that counteract the RAAS and promote vasodilation, natriuresis, and inhibit fibrosis and hypertrophy. Despite recent formal recognition of ARNI by guideline authorities, there is a striking paucity of mechanistic data on the effect of ARNI on cardiac remodeling (McDonagh et al., 2021). In this Research Topic, Liu et al., investigated the mechanisms underlying the cardioprotective action of ARNI in the context of fibrosis and remodeling after AMI that are mostly unknown. They found that the improvement of cardiac function in the ARNI group was more significant than a single RAAS blocker. Then, they investigated the mechanisms involved in the role of the Wnt/β-catenin axis in the prevention of myocardial fibrosis and improvement of myocardial remodeling in the context of ARNI treatment (Palevski et al., 2017; Fu et al., 2019). Nevertheless, in the PARADISE-MI trial LCZ696 was not associated with a significant lower incidence of death from cardiovascular causes or incident HF compared to ramipril alone after an AMI (Pfeffer et al., 2021). At this stage, it is difficult to conclude, but the interesting findings shown by Liu et al., help to learn how ARNI acts and we will probably learn more from ongoing studies in this area.

Overall, the traditional guideline directed therapies target the RAAS and the sympathetic nervous system, but recently, cyclic guanosine 3′,5′-monophosphate (cGMP) and its downstream protein kinase G (PKG) signaling has attracted attention as a novel therapeutic target (Tsai and Kass, 2009). cGMP is a second messenger regulated through natriuretic peptide and nitric oxide pathways. In their review, Numata and Takimoto highlighted preclinical evidence of the benefits of cGMP/PKG augmentation in HF models.

In conclusion, this Research Topic provides an overview of the novel mechanisms and translational implications involved in myocardial remodeling leading to HF. This field of research is evolving rapidly, and it ultimately holds promise for more reliable and sensitive development of novel treatments.

AUTHOR CONTRIBUTIONS

All authors listed have made a substantial, direct, and intellectual contribution to the work and approved it for publication.

REFERENCES

Belge, C., Hammond, J., Dubois-Deruy, E., Manoury, B., Hamelet, J., Beauloye, C., et al. (2014). Enhanced Expression of β3-adrenoceptors in Cardiac Myocytes Attenuates Neurohormone-Induced Hypertrophic Remodeling through Nitric Oxide Synthase. *Circulation.* 129 (4), 451–462. doi:10.1161/CIRCULATIONAHA.113.004940

Campbell, D. J. (2017). Long-term Neprilysin Inhibition - Implications for ARNIs. *Nat. Rev. Cardiol.* 14 (3), 171–186. doi:10.1038/nrcardio.2016.200

Fu, W. B., Wang, W. E., and Zeng, C. Y. (2019). Wnt Signaling Pathways in Myocardial Infarction and the Therapeutic Effects of Wnt Pathway Inhibitors. *Acta Pharmacol. Sin.* 40 (1), 9–12. doi:10.1038/s41401-018-0060-4

Han, M., Zhang, Y., Sun, S., Wang, Z., Wang, J., Xie, X., et al. (2013). Renin-angiotensin System Inhibitors Prevent the Recurrence of Atrial Fibrillation: a Meta-Analysis of Randomized Controlled Trials. *J. Cardiovasc. Pharmacol.* 62 (4), 405–415. doi:10.1097/FJC.0b013e3182a094a1

Liu, Q., Chen, Y., Auger-Messier, M., and Molkentin, J. D. (2012). Interaction between NFκB and NFAT Coordinates Cardiac Hypertrophy and Pathological Remodeling. *Circ. Res.* 110 (8), 1077–1086. doi:10.1161/CIRCRESAHA.111.260729

McDonagh, T. A., Metra, M., Adamo, M., Gardner, R. S., Baumbach, A., Böhm, M., et al. (2021). 2021 ESC Guidelines for the Diagnosis and Treatment of Acute and Chronic Heart Failure. *Eur. Heart J.* 42 (36), 3599–3726. doi:10.1093/eurheartj/ehab368

McMurray, J. J., Packer, M., Desai, A. S., Gong, J., Lefkowitz, M. P., Rizkala, A. R., et al. (2014). Angiotensin-Neprilysin Inhibition versus Enalapril in Heart Failure. *N. Engl. J. Med.* 371 (11), 993–1004. doi:10.1056/nejmoa1409077

Pfeffer, M. A., Braunwald, E., Moyé, L. A., Basta, L., Brown, E. J., Jr, Cuddy, T. E., et al. (1990). Effect of Captopril on Mortality and Morbidity in Patients with Left Ventricular Dysfunction after Myocardial Infarction. Results of the Survival and Ventricular Enlargement Trial. The SAVE Investigators. *N. Engl. J. Med.* 327 (10), 669–677. doi:10.1056/NEJM199209033271001

Pfeffer, M. A., and Braunwald, E. (1990). Ventricular Remodeling after Myocardial Infarction. Experimental Observations and Clinical Implications. *Circulation.* 81 (4), 1161–1172. doi:10.1161/01.cir.81.4.1161

Pfeffer, M. A., Claggett, B., Lewis, E. F., Granger, C. B., Køber, L., Maggioni, A. P., et al. (2021). Angiotensin Receptor-Neprilysin Inhibition in Acute Myocardial Infarction. *N. Engl. J. Med.* 385 (20), 1845–1855. doi:10.1056/NEJMoa2104508

Rouleau, J. L., De Champlain, J., Klein, M., Bichet, D., Moyé, L., Packer, M., et al. (1993). Activation of Neurohumoral Systems in Postinfarction Left Ventricular

Dysfunction. *J. Am. Coll. Cardiol.* 22 (2), 390–398. doi:10.1016/0735-1097(93)90042-y

Tsai, E. J., and Kass, D. A. (2009). Cyclic GMP Signaling in Cardiovascular Pathophysiology and Therapeutics. *Pharmacol. Ther.* 122 (3), 216–238. doi:10.1016/j.pharmthera.2009.02.009

Turin, A., Bax, J. J., Doukas, D., Joyce, C., Lopez, J. J., Mathew, V., et al. (2018). Interactions Among Vitamin D, Atrial Fibrillation, and the Renin-Angiotensin-Aldosterone System. *Am. J. Cardiol.* 122 (5), 780–784. doi:10.1016/j.amjcard.2018.05.013

Van Berlo, J. H., Maillet, M., and Molkentin, J. D. (2013). Signaling Effectors Underlying Pathologic Growth and Remodeling of the Heart. *J. Clin. Invest.* 123 (1), 37–45. doi:10.1172/JCI62839

Voors, A. A., Dorhout, B., and van der Meer, P. (2013). The Potential Role of Valsartan + AHU377 (LCZ696) in the Treatment of Heart Failure. *Expert Opin. Investig. Drugs.* 22 (8), 1041–1047. doi:10.1517/13543784.2013.797963

White, H. D., Norris, R. M., Brown, M. A., Brandt, P. W., Whitlock, R. M., and Wild, C. J. (1987). Left Ventricular End-Systolic Volume as the Major Determinant of Survival after Recovery from Myocardial Infarction. *Circulation.* 76 (1), 44–51. doi:10.1161/01.cir.76.1.44

Xie, M., Burchfield, J. S., and Hill, J. A. (2013). Pathological Ventricular Remodeling: Therapies: Part 2 of 2. *Circulation.* 128 (9), 1021–1030. doi:10.1161/CIRCULATIONAHA.113.001879

Conflict of Interest: The authors declare that the research was conducted in the absence of any commercial or financial relationships that could be construed as a potential conflict of interest.

Publisher's Note: All claims expressed in this article are solely those of the authors and do not necessarily represent those of their affiliated organizations, or those of the publisher, the editors and the reviewers. Any product that may be evaluated in this article, or claim that may be made by its manufacturer, is not guaranteed or endorsed by the publisher.

frontiers in Pharmacology

ORIGINAL RESEARCH
published: 26 July 2021
doi: 10.3389/fphar.2021.702326

Neutral Effects of Combined Treatment With GLP-1R Agonist Exenatide and MR Antagonist Potassium Canrenoate on Cardiac Function in Porcine and Murine Chronic Heart Failure Models

*Evelyne J. Demkes[1,2], Steven Wenker[3], Max J. M. Silvis[3], Martijn M. J. van Nieuwburg[1], M. Joyce Visser[1], Marlijn S. Jansen[1], Maike A. D. Brans[1], Evelyn Velema[1], Joost P. G. Sluijter[1,2], Imo E. Hoefer[4], Dominique P. V. de Kleijn[5], Leo Timmers[6] and Saskia C. A. de Jager[1]**

[1]Department of Cardiology, Laboratory of Experimental Cardiology, University Medical Center Utrecht, Utrecht, Netherlands, [2]UMC Utrecht Regenerative Medicine Center, Circulatory Health Laboratory, University Utrecht, University Medical Center Utrecht, Utrecht, Netherlands, [3]Department of Cardiology, University Medical Center Utrecht, Utrecht, Netherlands, [4]Central Diagnostic Laboratory, University Medical Center Utrecht, Utrecht, Netherlands, [5]Department of Vascular Surgery, University Medical Centre Utrecht, Utrecht, Netherlands, [6]Department of Cardiology, St. Antonius Hospital, Utrecht, Netherlands

OPEN ACCESS

Edited by:
Jérôme Roncalli,
Centre Hospitalier Universitaire de Toulouse, France

Reviewed by:
Marie-Ange Renault,
Institut National de la Santé et de la Recherche Médicale (INSERM), France
Kentaro Jujo,
Tokyo Women's Medical University, Japan
Rami Al Batran,
Université de Montréal, Canada

***Correspondence:**
Saskia C. A. de Jager
S.C.A.deJager@umcutrecht.nl

Specialty section:
This article was submitted to Cardiovascular and Smooth Muscle Pharmacology, a section of the journal Frontiers in Pharmacology

Received: 29 April 2021
Accepted: 12 July 2021
Published: 26 July 2021

Citation:
Demkes EJ, Wenker S, Silvis MJ M, van Nieuwburg MMJ, Visser MJ, Jansen MS, Brans MAD, Velema E, Sluijter JPG, Hoefer IE, de Kleijn DPV, Timmers L and de Jager SCA (2021) Neutral Effects of Combined Treatment With GLP-1R Agonist Exenatide and MR Antagonist Potassium Canrenoate on Cardiac Function in Porcine and Murine Chronic Heart Failure Models. Front. Pharmacol. 12:702326. doi: 10.3389/fphar.2021.702326

Background: Ischemia-reperfusion and cardiac remodeling is associated with cardiomyocyte death, excessive fibrosis formation, and functional decline, eventually resulting in heart failure (HF). Glucagon-like peptide (GLP)-1 agonists are reported to reduce apoptosis and myocardial infarct size after ischemia-reperfusion. Moreover, mineralocorticoid receptor antagonists (MRAs) have been described to reduce reactive fibrosis and improve cardiac function. Here, we investigated whether combined treatment with GLP-1R agonist exenatide and MRA potassium canrenoate could minimize cardiac injury and limit HF progression in animal models of chronic HF.

Methods and Results: Forty female Topigs Norsvin pigs were subjected to 150 min balloon occlusion of the left anterior descending artery (LAD). Prior to reperfusion, pigs were randomly assigned to placebo or combination therapy (either low dose or high dose). Treatment was applied for two consecutive days or for 8 weeks with a continued high dose *via* a tunneled intravenous catheter. Using 2,3,5-Triphenyltetrazolium chloride (TTC) staining we observed that combination therapy did not affect the scar size after 8 weeks. In line, left ventricular volume and function assessed by three-dimensional (3D) echocardiography (baseline, 7 days and 8 weeks), and cardiac magnetic resonance imaging (CMR, 8 weeks) did not differ between experimental groups. In addition, 36 C57Bl/6JRj mice underwent permanent LAD-occlusion and were treated with either placebo or combination therapy prior to reperfusion, for two consecutive days *via* intravenous injection, followed by continued treatment *via* placement of osmotic mini-pumps for 28 days. Global cardiac function, assessed by 3D echocardiography performed at baseline, 7, 14, and 28 days, did not differ between treatment groups. Also, no

differences were observed in cardiac hypertrophy, assessed by heart weight/bodyweight and heart weight/tibia length ratio.

Conclusion: In the current study, combined treatment with GLP-1R agonist exenatide and MR antagonist potassium canrenoate did not show beneficial effects on cardiac remodeling nor resulted in functional improvement in a small and large animal chronic HF model.

Keywords: chronic heart failure, glucagon-like peptide-1 agonist, mineralocorticoid receptor antagonist, porcine, mouse, myocardial infarction, cardiac function

INTRODUCTION

Chronic heart failure (HF) incidence, most commonly originating from myocardial infarction (MI) is steadily increasing worldwide and remains a major cause of death (Schmidt et al., 2012). Oxygen and nutrient deprivation during MI induces apoptosis of cardiomyocytes. Reperfusion of the occluded coronary artery is essential to limit myocardial damage but is also responsible for ischemia-reperfusion (IR) injury (Yellon and Hausenloy, 2007). As a consequence, a progressive remodeling response is initiated, consisting of reactive fibrosis formation, hypertrophy, and contractile dysfunction, which eventually leads to chronic HF (Bhatt et al., 2017). To prevent progression towards chronic HF, development of novel therapeutics that prevent progressive remodeling is of major importance.

Exenatide is a human glucagonlike peptide-1 receptor (GLP-1R) agonist. GLP-1R agonists are known for the treatment of type 2 diabetes, but have also been shown to be cardio-protective in preclinical and clinical studies by reducing myocardial infarct size and improving ventricular function after ischemia (Noyan-Ashraf et al., 2009; Lonborg et al., 2012; Read et al., 2012). Moreover, in a large animal model of myocardial IR injury, Exenatide specifically reduced myocardial apoptosis, resulting in a smaller infarct size and improved cardiac function (Timmers et al., 2009). Mineralocorticoid receptor (MR) signaling has a critical role in the fibrotic response observed in adverse cardiac remodeling (Brilla and Weber, 1992) treatment with MR antagonists (MRAs) resulted in a significant decrease in interstitial fibrosis and improved left ventricular function in rodents after permanent MI (Wang et al., 2004). In addition, MRAs have proven beneficial effects on mortality and morbidity in patients with established HF (Pitt et al., 1999; Pitt et al., 2003; Zannad et al., 2011), suggesting MR signaling is involved in HF progression.

Combining promising therapies that target the underlying process of IR injury and cardiac remodeling could further minimize cardiac injury and limit progression to HF. Therefore, we aimed to evaluate the effect of combined therapy of GLP-1R agonist exenatide and MRA potassium canrenoate on cardiac function in the development of chronic HF. To establish this, we use a clinically relevant large animal model of severe IR injury and a mice model of permanent myocardial infarction.

METHODS

Animals

All animal experiments were approved by the local animal welfare committee of the University Medical Center Utrecht and were conducted in accordance with the "Guide for the Care and Use of Laboratory Animals." A total of 40 female Dalland Landrace pigs (69.2 ± 4.2 kg) (Topigs Norsvin, Van Beek SPF varkensfokkerij B.V., Lelystad, Netherlands) were used in this study. All animals were conventionally housed in stables with concrete floor and straw bedding with a light/dark cycle of 12 h and were fed a standard diet with water ad libitum. Rubber bite sticks were provided as environmental enrichment. Sample size calculation was based on end-diastolic volume (EDV) measured with cardiac magnetic resonance imaging (CRM) as the primary endpoint. Based on historical data, we expected a 25% improvement on EDV (165 ml with a sigma of 25 ml). This, together with a power of 90%, alpha of 0.05, and an expected post-operative mortality of 25%, resulted in a group size of 10 animals per group. In addition, a total of 36 male C57Bl/6JRj mice were used. All mice were conventionally housed in type III cages with filter top, Aspen Woodchip bedding, and a plastic shelter with light/dark cycles of 12 h and food and water ad libitum. Tissues were provided as environmental enrichment. Sample size calculation was based on end-systolic volume (ESV) as the primary endpoint. With a power of 90%, alpha of 0.05, estimated effect size of 40 μL difference in volume, standard deviation of 29 μL (based on historical data), and estimated post-operative mortality of 25% this resulted in a group size of 18 animals per group.

Porcine Efficacy Study

Premedication, Anesthesia, and Analgesia

Pigs were pre-treated orally with amiodarone for 10 days (1200 mg loading dose, 800 mg/day maintenance), clopidogrel (75 mg/day) and acetylsalicylic acid (320 mg loading dose 7 days before the experiment, 80 mg/day maintenance). One day before surgery, animals received a buprenorphine patch (5 μg/h). On the day of surgery, anesthesia and analgesia was induced by intramuscular injection of ketamine (15 mg/kg), midazolam (0.75 mg/kg) and atropine (0.015 mg/kg) followed by intravenous (*i.v.*) administration of thiopental (4 mg/kg). Animals were intubated and mechanically ventilated with a 1: 2 oxygen-air ratio. Continuous sedation was achieved with *i.v.*

pancuronium (0.1 mg/kg/h), midazolam (0.4 mg/kg/h) and sufentanil (2.5 μg/kg/h).

Surgical Procedure and Intravenous Line Installation

Pigs were subjected to closed-chest LAD coronary artery balloon occlusion for 150 min. After arterial and venous access was obtained, a catheter (8FR JL4 guiding) was placed in the left coronary tree and a coronary angiogram was acquired. Afterward, the LAD diameter was measured and an adequately sized balloon was placed immediately after the first diagonal branch of the LAD. Balloon inflation and LAD occlusion was verified with a coronary angiogram, at the start, after 60 and 120 min occlusion time, and right before deflation of the balloon. After deflation of the balloon LAD passage was verified with a coronary angiogram. During the occlusion procedure, animals were defibrillated in case of ventricular fibrillation (VF) while receiving 150 mg amiodarone bolus *i.v.*, with a maximum of three boluses.

All animals received an *i.v.*-line from the jugular vein canalled to the back. The iv-line was flushed daily with 0.9% NaCl-solution followed by heparin-solution (0.1% heparin in 0.9% NaCl-solution) and a mesh bandage around the thorax to prevent the *i.v.*-line from being damaged. The tunneled catheter was closed for three out of four groups after 7 days and the external part was removed.

Treatment

Twenty min before reperfusion, pigs were randomly assigned to one of four treatment groups (**Supplementary Table 1**). Pigs received either placebo (2 ml saline) or exenatide/potassium canrenoate treatment (low dose, 0.05 μg/kg exenatide and 1 mg/kg of potassium canrenoate; high dose, 0.15 μg/kg exenatide and 1 mg/kg of potassium canrenoate; continuous high dose: 0.15 μg/kg exenatide and 1 mg/kg of potassium canrenoate) as two separate administrations *via* the ear-vein catheter. *I.v.* treatment continued 2 times daily for two consecutive days and one group continued 2 times daily treatment for entire follow-up period (continuous high dose).

Note: Animals treated with the continuous high dose were initially treated with subcutaneous (s.c.) injections (0.05 μg/kg exenatide and 2 mg/kg potassium canrenoate). However, twice daily injections caused significant distress to the animals. Therefore, after the third animal in this group, we decided to leave the tunneled catheter in place to proceed with intravenous administrations for the entire study duration. In these animals, none of the parameters studied differ from the other animals in the group.

Echocardiography

Before induction of ischemia, and 1 and 8 weeks after reperfusion, all pigs underwent transthoracic and 3D transesophageal echocardiography (3D-TEE) as previously described (Ellenbroek et al., 2016). In short, 3D-TEE images were made using a X7-2T transducer on an iE33 ultrasound device (Philips, Eindhoven, Netherlands). The pig was placed in the right lateral position and the echo probe was inserted for 50–60 cm in the esophagus. After selecting the 3D full volume option, mechanical ventilation was switched of temporarily to obtain good images. Images were analyzed with QLab 10.7 software (Philips, Eindhoven, Netherlands).

Cardiac Magnetic Resonance Imaging

Eight weeks after MI, porcine animals underwent cardiac magnetic resonance imaging (CRM) using a 1,5 T magnet device (Achieva, Philips Medical Systems, Netherlands) under general anesthesia, as described above. Animals were placed in a supine position and imaging was performed using a respiratory corrected, cardiac gated steady-state free precession (SSFP) cine sequence. CMR images were analyzed using Medvisio Segment (Medvisio, Lund, Sweden). Cardiac volumes and myocardial mass were determined by summation of ROIs of short axis slices covering the entire left ventricle multiplied by the slice thickness.

Infarct/Scar Size Determination

Ventricular fibrillation was induced by placing a 9V battery on the heart and pigs were sacrificed by exsanguination under anesthesia. The heart was excised and cut in 5 short-axis slices from apex to base. To discriminate between infarct tissue and viable tissue, slices were incubated in 1% pre-warmed 2,3,5-Triphenyltetrazolium chloride (TTC) (Sigma-Aldrich Chemicals, Zwijndrecht, Netherlands) in 0.9% NaCl at 37° for 15 min. Each slice was photographed at the apical and basal side in presence of a ruler and analyzed with ImageJ software (NIH, Bethesda, MD, United States).

Circulating Markers and Histological Analysis

Plasma samples were obtained at different time points after reperfusion by whole-blood centrifugation at 1850 *g* and immediately stored at −80°C. Troponin I levels were measured from samples 24 h after reperfusion using a clinical chemistry analyzer (AU5811, Beckman Coulter). For histological analysis, infarcted myocardial tissue was processed, paraffin-imbedded and cut into 5 μm sections after conserved in 4% paraformaldehyde for at least 7 days. Collagen was visualized using a Masson's Trichrome staining and analysis of interstitial fibrosis in the border zone region was performed semi-quantitative (scored 1–5; 1 = no interstitial fibrosis, 5 = excessive interstitial fibrosis) by two researchers blinded for group assessment.

Mouse Efficacy Study

Anesthesia, Analgesia, and Surgical Procedure

Anesthesia was induced by intraperitoneal injection of medetomidine hydrochloride (1.0 g/kg body weight), midazolam (10.0 mg/kg), and fentanyl (0.1 mg/kg). Mice were intubated and connected to a respirator with a 1:1 oxygen-air ratio. During surgery, a core body temperature of 37°C was maintained by continuous rectal temperature monitoring and an automatic heating blanket. After a left lateral thoracotomy with an incision of the pericardium, the left coronary artery was ligated permanently with an 8–0 Ethilon suture (Ethicon). Ischemia was confirmed by bleaching of the myocardium and tachycardia, and surgical wounds were closed. Atipamezole hydrochloride (3.3 mg/kg), flumazenil (0.5 mg/kg) and

buprenorphine (0.15 mg/kg) was used as an antagonist, and injected s.c. The evening of the day of operation and 12 h thereafter, s.c. injection of buprenorphine (0.15 mg/kg) was administered as analgesia.

Treatment

Prior to permanent ligation, mice were randomly assigned to receive either placebo (100 µL saline) or continued exenatide/potassium canrenoate treatment *i.v.* (continuous high dose, 0.15 µg/kg exenatide and 1 mg/kg of potassium canrenoate). *I.v.* treatment was continued 2 times daily for two consecutive days. On day 3, animals were anesthetized by isoflurane and small incisions were made in the skin. Osmotic mini-pumps containing either saline or exenatide and potassium canrenoate were implanted on the flank of the animal, providing active release of the compounds until termination. In order to prevent mixing of the therapeutics, two mini-pumps were randomly implanted on either side of the animal.

Echocardiography

At baseline, 7, 14, and 28 days after permanent ligation, all mice underwent echocardiography to assess cardiac geometry and function. Anesthesia was induced by inhalation of 2.0% isoflurane in a mixture of oxygen/air (1:1). Heart rate, respiration, and rectal temperature were constantly monitored and body temperature was kept between 36.0 and 38.0°C using heat lamps. Respiration gating, a 3D motor, and trigger points were used to obtain 300 transversal images of the heart during the expiratory phase, either at end-systole or end-diastole for complete 3D reconstruction of the heart. Image acquisition and analyses were performed using the Vevo 2,100 System and Software (Fujifilm VisualSonics Inc., Toronto, Canada).

Histological Analysis

Paraffin embedded hearts were cut in 3 µm thick sections. Before staining, the sections are deparaffinized [2 × 10 min in Ultraclear (1,466, Sakura), 2 × 5 min in 100% EtOH, (4099.9005 Klinipath), 2 × 5 min in 96% EtOH (Klinipath), 2 × 5 min in 70% EtOH (Klinipath), 5 min in Demi H_2O]. Collagen was visualized using a Masson's Trichrome staining and analysis of interstitial fibrosis in the border zone region was performed semi-quantitative (scored 1–5; 1 = no interstitial fibrosis, 5 = excessive interstitial fibrosis) by two researchers blinded for group assessment.

Statistics

All analyses were performed in a blinded, randomized fashion. Data are presented as mean ± SD. A one-way ANOVA was used to test any differences between the four porcine treatment groups. For the mice data, a mixed-models was used for repeated measurements [EDV, ESV, ejection fraction (EF)], with a random intercept for each mouse and as fixed factors group and time point. To determine whether the time course of the parameters was different for the groups, the interaction group*time point of measurement was also taken into the model. Heart weight/tibia length was analyzed with a student's t-test. Statistical analyses were performed using SPSS and GraphPad Prism 8.3. A $p \leq 0.05$ was considered statistically significant.

RESULTS

Survival of Porcine Animals After Ischemia-Reperfusion Injury and Treatment With Exenatide/Potassium Canrenoate Combination Therapy

An overview of the study can be found in **Figure 1A**. A total of 40 porcine animals (69.2 ± 4.2 kg) were subjected to IR for 150 min. Nearly all animals developed ventricular arrhythmia during the occlusion period. Three animals died due to refractory VF not amenable by defibrillation before group assignment and another three animals during the follow-up period (two animals died on day IR + 1, one died on day IR + 3), presumably due to late VF (**Figure 1B**). This resulted in a total of 34 pigs completing the study and allowed a comparison of eight pigs in the placebo group, eight pigs in the low dose (0.05 µg/kg exenatide and 1 mg/kg of potassium canrenoate) group, 10 pigs in the high dose (0.15 µg/kg exenatide and 1 mg/kg of potassium canrenoate) group and eight pigs in the continuous high dose (0.15 µg/kg exenatide and 1 mg/kg of potassium canrenoate) group (**Supplementary Table 1**). Heart rate and mean arterial pressure was similar during the first hours after IR and compound administration (**Supplementary Table 2**).

Exenatide/Potassium Canrenoate Combination Therapy Does not Influence Cardiac Function and Infarct Size in a Severe Porcine IR-Model

To validate the cardio-protective effect of exenatide/potassium canrenoate combination therapy on myocardial injury and dysfunction following severe IR, left ventricular performance was assessed by 3D-TEE and CMR. Baseline cardiac function (EDV, ESV, and EF) determined by echocardiography was similar in all groups (**Figure 1C** + **Supplementary Figure 1**). After 1 week, ESV significantly increased and EF significantly decreased in all four groups ($p < 0.05$, **Figure 1C**), indicative of successful infarct induction. Both at 1 and 8 weeks post-MI, no significant differences were observed between the four groups in end-diastolic and end-systolic volume nor in EF (**Figure 1C** + **Supplementary Figure 1**). Assessment of cardiac volumes and function measured with CMR after 8 weeks also showed no significant differences (**Figure 1D**). In summary, measurements of myocardial volumes and function were similar in all three treatment groups compared to the controls.

Scar Size and Interstitial Cardiac Fibrosis is not Affected by Exenatide/Potassium Canrenoate Combination Therapy

Solo treatment of exenatide has shown to reduce infarct size in a previous porcine MI study performed by our group (Timmers

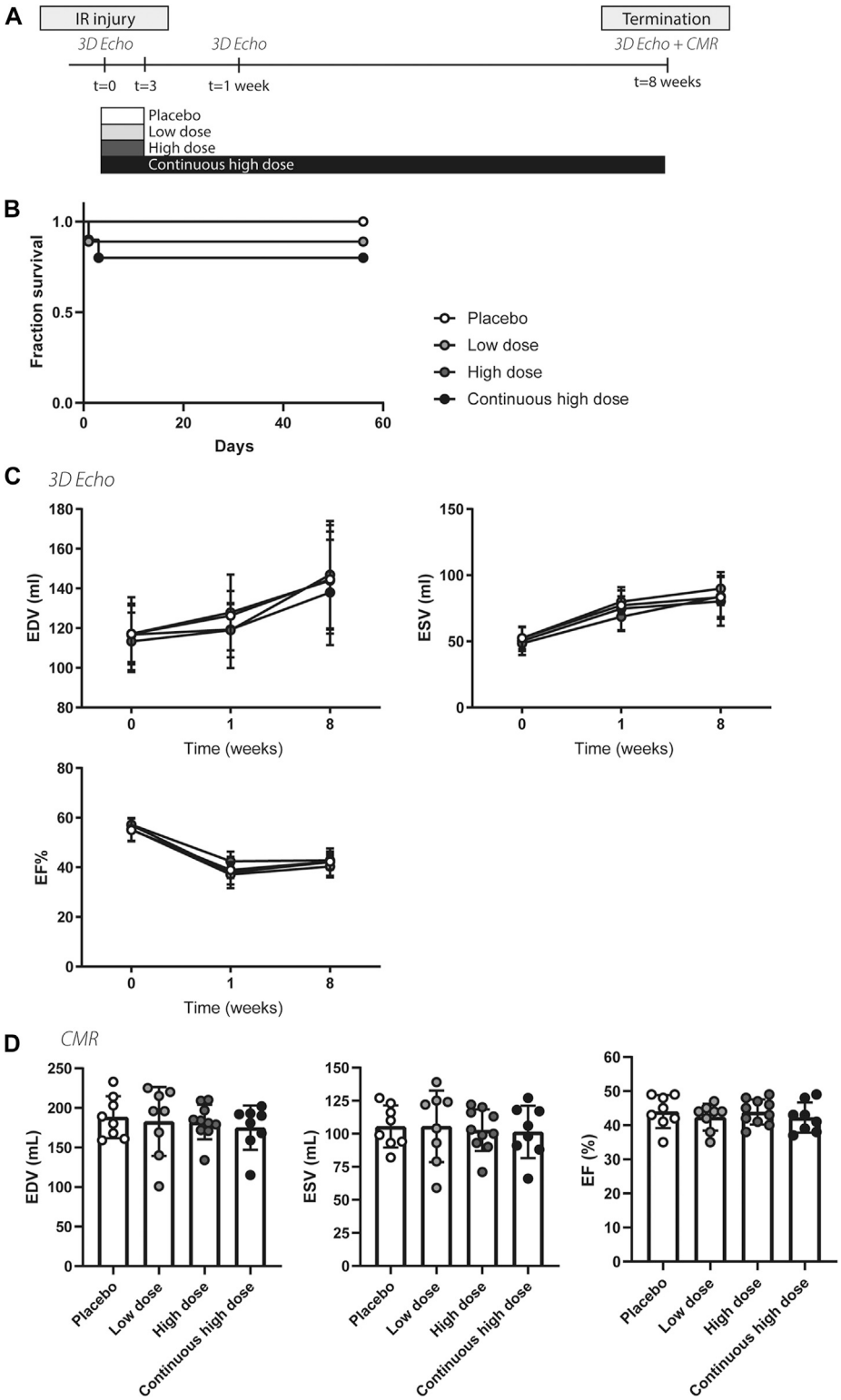

FIGURE 1 | Study design, survival, and global cardiac function of porcine animals after severe ischemia-reperfusion injury. **(A)** Overview of the porcine study. **(B)** Fraction of survival of the different treatment groups, placebo, low dose, high dose, continuous high dose over the entire follow-up. IR, ischemia-reperfusion. **(C)** Similar end-systolic volume (ESV), end-diastolic volume (EDV), and ejection fraction (EF%) at baseline, 1 and 8 weeks post-IR measured by 3D echocardiography between different experimental groups. **(D)** ESV, EDV, and EF% at 8 weeks post-IR measured by cardiac magnetic resonance imaging did not differ between groups.

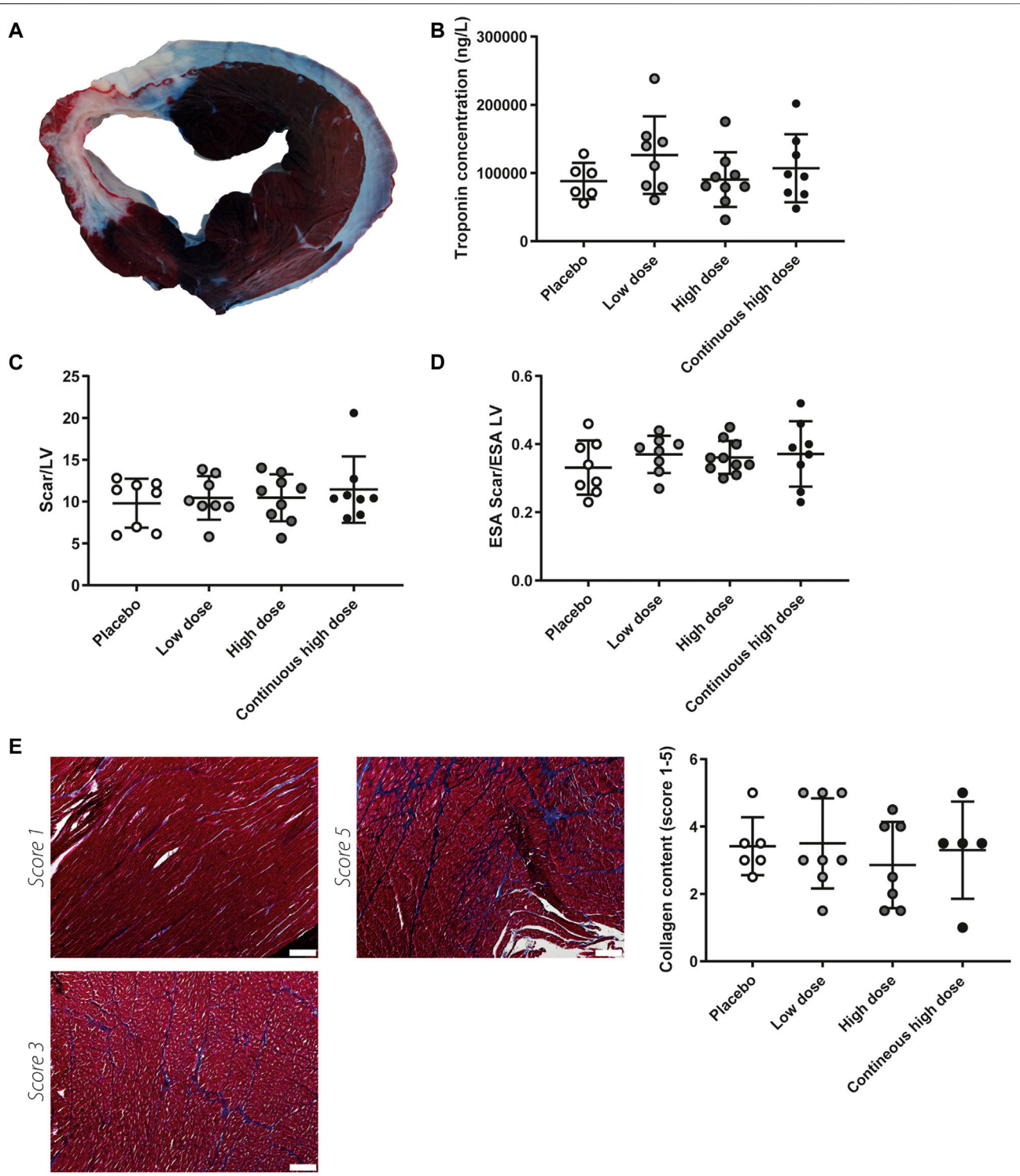

FIGURE 2 | Myocardial damage and after severe ischemia-reperfusion injury. **(A)** Representative picture of myocardial slice; the dark area represents the remote area, white area represents infarcted myocardium. **(B)** Circulating levels of cardiac troponin 24 h after severe ischemia-reperfusion injury. No significant differences were observed between the different experimental groups. **(C)** Infarcted areas did not differ between treatment groups when expressed relative to measurements left ventricle (LV) at 8 weeks follow-up. **(D)** Infarct area as a fraction of LV endocardial surface area (ESA) was not different between treatment groups at 8 weeks follow-up. **(E)** Representative pictures of collagen content score 1, score 3, and score 5 after staining with Masson's Trichrome, quantification showed no differences in interstitial fibrosis in the border zone region. Scale bar = 200 μm.

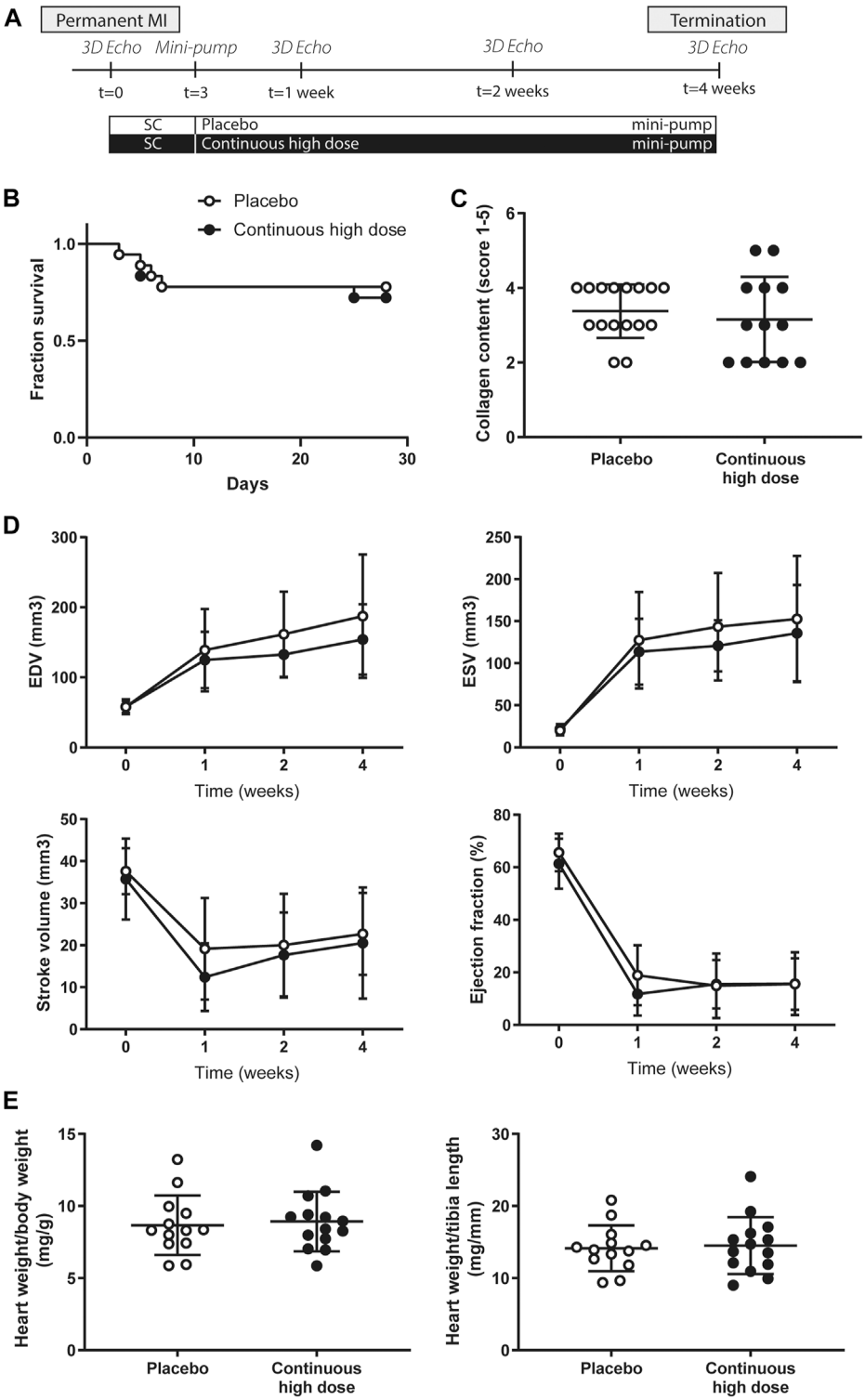

FIGURE 3 | Study design, survival, global cardiac function and cardiac hypertrophy assessment in mice after permanent myocardial infarction. **(A)** Overview of the mice study. **(B)** Fraction of survival of placebo and continuous high dose treated animals over the entire follow-up. MI, myocardial infarction. **(C)** Quantification of collagen content score (1: no collagen—5: extensive collagen) showed no differences in interstitial fibrosis between placebo and continuous high dose treated animals. **(D)** End-systolic volume (ESV), end-diastolic volume (EDV), stroke volume (SV), and ejection fraction (EF) measured by 3D echocardiography at baseline, 7, 14, and 28 days after permanent ligation. No significant differences were observed between the different experimental groups. **(E)** Heart weight/body weight ratio (mg/g) and heart weight/tibia length (mg/mm) between groups were similar 28 days after permanent ligation.

et al., 2009). As a direct reflection of cardiac damage, systemic troponin I levels were measured 24 h after IR. Analysis revealed troponin I levels did not differ between groups, suggesting infarct size is not affected by the combination therapy (**Figure 2B**). Accordingly, infarcted area/LV ratios, assessed by TTC staining, were not significantly different between the groups at 8 weeks follow-up (**Figures 2A,C**). Scar size was also analyzed as a fraction of the endocardial surface area (ESA) of the LV. Yet, scar size as a percentage of ESA was not significantly different among treatment groups (**Figure 2D**). As atrophy of the infarcted area, and hypertrophy of the remote endocardium may have influenced infarct size determination by TTC staining we additionally performed trichrome staining to visualize scar tissue. Histological analysis for interstitial fibrosis also showed no differences between groups (**Figure 2E**).

Survival of Mice After Permanent Coronary Artery Ligation and Treatment With Exenatide/Potassium Canrenoate Combination Therapy

To fully exclude potential effects of the compounds on IR injury and enabling to solely focus on adverse remodeling we tested the effects of continuous administration of exenatide and potassium canrenoate on myocardial function and cardiac remodeling in a severe mouse model of MI with permanent ligation. An overview of the mice study can be found in **Figure 3A**. A total of 36 animals were subjected to permanent LAD ligation. Within 28 days after permanent ligation, nine animals died in total, of which 2 as a direct consequence of the surgery (2 days post-surgery). Other animals died during follow-up (tree animals on day 5, one animal on day 6, two animals on day 7 and one animal on day 25 post ligation) (**Figure 3B**), but without differences between the groups. This resulted in a total of 27 mice completing the study and allowed a comparison of 13 mice in the placebo group and 14 mice in the continuous high dose (0.15 μg/kg exenatide and 1 mg/kg of potassium canrenoate) group (**Supplementary Table 3**).

Neither Cardiac Function nor Cardiac Hypertrophy is Influenced by Exenatide/Potassium Canrenoate Combination Therapy in Mice After Permanent Coronary Artery Ligation

At baseline, 7, 14, and 28 days post-MI, cardiac function was assessed by use of high-frequency 3D ultrasound. Baseline cardiac function (EDV, ESV, SV, and EF) was similar in all groups (**Figure 3D**). As a consequence of the permanent ligation, EDV and ESV increased significantly over time in both groups (**Figure 3D**, $p < 0.05$), while no significant differences were observed between the groups (**Figure 3D** + **Supplementary Figure 2**). Correspondingly, stroke volume and ejection fraction showed a significant decrease over time in both groups after induction of the myocardial infarction (**Figure 3D**, $p < 0.05$), but was not different between placebo and treated animals (**Figure 3D**, **Supplementary Figure 2**). At the end of the follow-up period, heart weight to body weight ratio and heart weight to tibia length (**Figure 3E**) was comparable in both groups indicating no differences in cardiac hypertrophy between the groups. Histological analysis for interstitial fibrosis also showed no differences between groups (**Figure 3B**).

DISCUSSION

In the current study, we hypothesized that combined treatment with GLP-1R agonist exenatide and MR antagonist potassium canrenoate could minimize cardiac injury and limit progression to chronic HF. By using different treatment arms in the pig model we could discriminate between the effect of the combination therapy administered in the early phase after severe IR and long-term administration on adverse cardiac remodeling. Treatment in the acute phase with two different doses of combination therapy did not show effects on cardiac function, scar size or interstitial fibrosis 8 weeks post severe IR injury. The same holds for chronic treatment with high-dose combination therapy. In addition, long-term administration with high dose combination therapy in a mouse model of permanent MI did not show any beneficial effects as well.

Post-MI-cardiac remodeling comprises pathophysiological interactions between cellular and extracellular components resulting in biochemical and metabolic changes, including formation of reactive oxygen species, inflammation, and abrupt changes in pH− and Ca2+ levels, contributing to apoptosis of cardiomyocytes and excessive fibrosis formation (Yellon and Hausenloy, 2007; Nielsen et al., 2019). Separate use of both compounds in different scenarios has shown to have beneficial effects targeting these changes. In an earlier study, we showed increased activity of antioxidant enzymes, reduced nuclear oxidative stress and fewer apoptotic cells in exenatide-treated porcine animals 3 days after IR injury (Timmers et al., 2009) and similar results were found with exenatide pre-treatment for 2 weeks prior to IR in a rat study (Chang et al., 2013). In addition, it was shown that exenatide pre-treatment improved morphological and mechanical changes of mitochondria in response to IR injury in a rat model (Lee et al., 2017). In all studies, these findings were accompanied with reduced infarct size and improved cardiac function compared to control-treated animals. MRAs have shown to reduce collagen accumulation and fibrosis in animal models with permanent MI (Wang et al., 2004; Takeda et al., 2007). In patients, potassium canrenoate treatment also significantly reduced post-infarction collagen synthesis measured by serum N-terminal propeptide of type III procollagen (PIIINP) levels which was accompanied by smaller ventricular volumes (Modena et al., 2001).

Although other combinations of compounds were used, combined treatment of exenatide and with dapagliflozin, a sodium-glucose co-transporter-2 (SGLT2) inhibitor, showed to improve markers associated with liver steatosis and fibrosis in type 2 diabetes patients compared to either exenatide or dapagliflozin administration alone (Gastaldelli et al., 2020). In addition, in rats with post-MI heart failure, a combination of canrenone, the active metabolite of potassium canrenoate and

ramipril, angiotensin-converting enzyme (ACE) inhibitor, attenuated LV dilation and interstitial remodeling and improved cardiac function compared solo-treatment (Cittadini et al., 2003). Building on these results, exenatide, and potassium canrenoate combination therapy could have a synergistic effect on limiting IR injury and cardiac remodeling and thus progression to HF.

One may argue that administered concentrations in this study were not sufficient to realize any beneficial effects. However, the chosen dosing concentrations in this study were comparable with concentrations found in the literature. Apart from the initial administration prior to IR, pigs received the same dose of exenatide compared to a porcine study previously performed by our group (Timmers et al., 2009). During initial dosing, only IV administration was performed as in our study both exenatide and potassium canrenoate was given prior to IR. Potassium canrenoate dose was slightly higher compared to dosages used in clinical studies (Li et al., 2013) but matched the concentration that worked best in reducing infarct size and lowering circulating troponin levels in an acute study performed in mice and rabbits (Schmidt et al., 2010). Differences in pharmacokinetics between species due to differences in volume distribution, clearance, and absorption could be of influence (Frey et al., 1988). Whether this is the case for these compounds is not clear. Higher concentrations of potassium canrenoate (bolus of 200 mg in animals of ~30 kg) were used in a pig model investigating the effect of potassium canrenoate during increased intraabdominal pressure (Gudmundsson et al., 2004). However, here only acute changes in renal hemodynamics and urinary output were investigated and no long-term assessment was carried out. To not risk overdosing or adverse effects in our studies, lower dosing was implemented. In addition, with the current study design, we cannot exclude that drug interaction of exenatide with potassium canrenoate resulted in a neutral result. To the best of our knowledge, no reports on adverse interactions between these drugs have been published, and given the completely different molecular pathways they target, we argue it is unlikely that interaction of the drugs could have contributed to the neutral results.

Apart from dose, the chosen models could play a role in the absence of effect. The rationale of this study was to assess the effects of combined exenatide and potassium canrenoate therapy on adverse cardiac remodeling solely and without affecting infarct size. Therefore, pigs were exposed to prolonged ischemia times and the mice were subjected to permanent ligation. By comparing 60, 75 and 90 min occlusion in the closed chest LAD ligation model in pigs it was recently shown that increasing occlusion times lead to significantly larger infarct sizes, with almost complete transmural infarcts upon 90 min occlusion time (Silvis et al., 2021) In the current study, we used a porcine model of severe IR injury with 150 min occlusion time and a mice model of permanent myocardial infarction. Consequential to the prolonged ischemia time the damage is presumably in an irreversible state, thereby limiting the therapeutic benefit on salvaging myocardial ischemia-reperfusion-related injury. Accordingly, the findings of these studies do not preclude the effects of the combination therapy on myocardial reperfusion injury in pigs with a shorter occlusion times. Although there were difficulties to translate these favorable outcomes to clinical beneficial effects (Roos et al., 2016), we indeed found exenatide can inhibit reperfusion injury in the earlier study performed with exenatide mono-treatment (Timmers et al., 2009). This may suggest exenatide primarily inhibits reperfusion driven injury which is in our severe models very limited or not even present at all. Further direct comparison between these studies is complicated due to methodological differences, including different location of coronary artery occlusion (LCx vs LAD), difference in ischemia time (75 vs. 150 min), time of follow-up (3 days vs. 8 weeks), and different methods to determine cardiac function (echo vs. CMR).

Although our mouse model with permanent ligation resulted in an extreme loss of function (mean EF of 16% at termination), a less but still severe decrease in cardiac function was observed in our porcine model of severe IR injury with 150 min occlusion time (mean EF of 41% at termination). Whether the combination therapy has an effect on pigs with even more severe heart failure (EF < 35%) remains unclear and is difficult to investigate due to low survival rates when occluding the LAD more proximal.

Cardiac remodeling is quickly initiated in response to ischemia. While this remodeling process is focused on wound healing and proper scar formation in the first few days, post-MI progressive collagen deposition in the non-infarcted area is initiated after a few days thereby contributing to late adverse cardiac remodeling and HF progression (Nielsen et al., 2019). Many of the beneficial effects of GLP-1R agonist and MRAs in preclinical models are shown in the acute setting (i.e. short follow-up time) (Timmers et al., 2009; Schmidt et al., 2010; Chang et al., 2013; Roos et al., 2016). In clinical data, treatment with canrenoate did not show any significant differences at entry and at 10 days in echocardiographic parameters such as EDV, ESV, and EF, while at 90 days, and 180 days after treatment it did (Di Pasquale et al., 2005). The same was observed in another patient study with potassium canrenoate (Modena et al., 2001). Here, also collagen synthesis marker PIIINP illustrated a more profound decrease over time (3, 6, 12 months). Evidently, beneficial functional effects can be observed when targeting late cardiac remodeling. Therefore, it may be possible that the timing of our study (8 weeks follow-up) was just outside the optimal therapeutic window: too late to benefit acute-, and too early to benefit long-term effects.

In the current study, combined treatment with GLP-1R agonist exenatide and MR antagonist potassium canrenoate did not show functional benefits on cardiac remodeling and did not result in functional improvement in small and large chronic HF models. Yet, the role of either compound in IR injury and HF progression remains appealing and more studies are necessary to provide complete disclosure concerning their role in this process.

DATA AVAILABILITY STATEMENT

The raw data supporting the conclusion of this article will be made available by the authors, without undue reservation.

ETHICS STATEMENT

The animal study was reviewed and approved by the Central Committee Animal Experimentation (Centrale Commissie Dierproeven), the Hague, Netherlands.

AUTHOR CONTRIBUTIONS

Conception and design of the experiments: IH, LT, DK, SJ. Performing experiments and data analysis: ED, SW, MS, MN, JV, MJ, EV, MB. Writing of the original version of this paper: ED, MS, SJ. Preparation of the figures: ED, MS. Writing, review, and editing of this paper: ED, MS, IH, LT, JS, DK, SJ. All of the authors read and approved the final version of this paper.

FUNDING

This work was financially supported by the Genesis Pharma, Athens, Greece.

ACKNOWLEDGMENTS

The authors gratefully acknowledge Petra van der Kraak and Marian Wesseling from University Medical Center Utrecht, Netherlands for their help regarding histology.

SUPPLEMENTARY MATERIAL

The Supplementary Material for this article can be found online at: https://www.frontiersin.org/articles/10.3389/fphar.2021.702326/full#supplementary-material

REFERENCES

Bhatt, A. S., Ambrosy, A. P., and Velazquez, E. J. (2017). Adverse Remodeling and Reverse Remodeling after Myocardial Infarction. *Curr. Cardiol. Rep.* 19 (8), 71. doi:10.1007/s11886-017-0876-4

Brilla, C. G., and Weber, K. T. (1992). Mineralocorticoid Excess, Dietary Sodium, and Myocardial Fibrosis. *J. Lab. Clin. Med.* 120 (6), 893–901.

Chang, G., Zhang, D., Yu, H., Zhang, P., Wang, Y., Zheng, A., et al. (2013). Cardioprotective Effects of Exenatide against Oxidative Stress-Induced Injury. *Int. J. Mol. Med.* 32 (5), 1011–1020. doi:10.3892/ijmm.2013.1475

Cittadini, A., Monti, M. G., Isgaard, J., Casaburi, C., Stromer, H., Di Gianni, A., et al. (2003). Aldosterone Receptor Blockade Improves Left Ventricular Remodeling and Increases Ventricular Fibrillation Threshold in Experimental Heart Failure. *Cardiovasc. Res.* 58 (3), 555–564. doi:10.1016/s0008-6363(03)00251-7

Di Pasquale, P., Cannizzaro, S., Scalzo, S., Parrinello, G., Fasullo, S., Giambanco, F., et al. (2005). Effects of Canrenoate Plus Angiotensin-Converting Enzyme Inhibitors versus Angiotensin-Converting Enzyme Inhibitors Alone on Systolic and Diastolic Function in Patients with Acute Anterior Myocardial Infarction. *Am. Heart J.* 150 (5), e1–919. doi:10.1016/j.ahj.2005.03.032

Ellenbroek, G. H. J. M., van Hout, G. P. J., Timmers, L., Doevendans, P. A., Pasterkamp, G., and Hoefer, I. E. (2016). Primary Outcome Assessment in a Pig Model of Acute Myocardial Infarction. *J. Vis. Exp.* 116, 54021. doi:10.3791/54021

Frey, B. M., Sieber, M., Mettler, D., Gänger, H., and Frey, F. J. (1988). Marked Interspecies Differences between Humans and Pigs in Cyclosporine and Prednisolone Disposition. *Drug Metab. Dispos* 16 (2), 285–289.

Gastaldelli, A., Repetto, E., Guja, C., Hardy, E., Han, J., Jabbour, S. A., et al. (2020). Exenatide and Dapagliflozin Combination Improves Markers of Liver Steatosis and Fibrosis in Patients with Type 2 Diabetes. *Diabetes Obes. Metab.* 22 (3), 393–403. doi:10.1111/dom.13907

Gudmundsson, F. F., Viste, A., Myking, O. L., Grong, K., and Svanes, K. (2004). Effects of the Aldosterone Receptor Antagonist Potassium Canrenoate on Renal Blood Flow and Urinary Output during Prolonged Increased Intraabdominal Pressure (IAP) in Pigs. *Surg. Endosc.* 18 (10), 1528–1534. doi:10.1007/s00464-003-9295-2

Lee, K. H., Ha, S. J., Woo, J.-S., Lee, G.-J., Lee, S.-R., Kim, J. W., et al. (2017). Exenatide Prevents Morphological and Structural Changes of Mitochondria Following Ischaemia-Reperfusion Injury. *Heart Lung Circ.* 26 (5), 519–523. doi:10.1016/j.hlc.2016.08.007

Li, X., Qi, Y., Li, Y., Zhang, S., Guo, S., Chu, S., et al. (2013). Impact of Mineralocorticoid Receptor Antagonists on Changes in Cardiac Structure and Function of Left Ventricular Dysfunction. *Circ. Heart Fail.* 6 (2), 156–165. doi:10.1161/CIRCHEARTFAILURE.112.000074

Lønborg, J., Vejlstrup, N., Kelbæk, H., Bøtker, H. E., Kim, W. Y., Mathiasen, A. B., et al. (2012). Exenatide Reduces Reperfusion Injury in Patients with ST-Segment Elevation Myocardial Infarction. *Eur. Heart J.* 33 (12), 1491–1499. doi:10.1093/eurheartj/ehr309

Modena, M. G., Aveta, P., Menozzi, A., and Rossi, R. (2001). Aldosterone Inhibition Limits Collagen Synthesis and Progressive Left Ventricular Enlargement after Anterior Myocardial Infarction. *Am. Heart J.* 141 (1), 41–46. doi:10.1067/mhj.2001.111258

Nielsen, S. H., Mouton, A. J., DeLeon-Pennell, K. Y., Genovese, F., Karsdal, M., and Lindsey, M. L. (2019). Understanding Cardiac Extracellular Matrix Remodeling to Develop Biomarkers of Myocardial Infarction Outcomes. *Matrix Biol.* 75-76, 43–57. doi:10.1016/j.matbio.2017.12.001

Noyan-Ashraf, M. H., Momen, M. A., Ban, K., Sadi, A.-M., Zhou, Y.-Q., Riazi, A. M., et al. (2009). GLP-1R Agonist Liraglutide Activates Cytoprotective Pathways and Improves Outcomes after Experimental Myocardial Infarction in Mice. *Diabetes* 58 (4), 975–983. doi:10.2337/db08-1193

Pitt, B., Remme, W., Zannad, F., Neaton, J., Martinez, F., Roniker, B., et al. (2003). Eplerenone, a Selective Aldosterone Blocker, in Patients with Left Ventricular Dysfunction after Myocardial Infarction. *N. Engl. J. Med.* 348 (14), 1309–1321. doi:10.1056/NEJMoa030207

Pitt, B., Zannad, F., Remme, W. J., Cody, R., Castaigne, A., Perez, A., et al. (1999). The Effect of Spironolactone on Morbidity and Mortality in Patients with Severe Heart Failure. *N. Engl. J. Med.* 341 (10), 709–717. doi:10.1056/NEJM199909023411001

Read, P. A., Khan, F. Z., and Dutka, D. P. (2012). Cardioprotection against Ischaemia Induced by Dobutamine Stress Using Glucagon-like Peptide-1 in Patients with Coronary Artery Disease. *Heart* 98 (5), 408–413. doi:10.1136/hrt.2010.219345

Roos, S. T., Timmers, L., Biesbroek, P. S., Nijveldt, R., Kamp, O., van Rossum, A. C., et al. (2016). No Benefit of Additional Treatment with Exenatide in Patients with an Acute Myocardial Infarction. *Int. J. Cardiol.* 220, 809–814. doi:10.1016/j.ijcard.2016.06.283

Schmidt, K., Tissier, R., Ghaleb, B., Drogies, T., Felix, S. B., and Krieg, T. (2010). Cardioprotective Effects of Mineralocorticoid Receptor Antagonists at Reperfusion. *Eur. Heart J.* 31 (13), 1655–1662. doi:10.1093/eurheartj/ehp555

Schmidt, M., Jacobsen, J. B., Lash, T. L., Botker, H. E., and Sorensen, H. T. (2012). 25 Year Trends in First Time Hospitalisation for Acute Myocardial Infarction, Subsequent Short and Long Term Mortality, and the Prognostic Impact of Sex and Comorbidity: a Danish Nationwide Cohort Study. *BMJ* 344, e356. doi:10.1136/bmj.e356

Silvis, M. J. M., van Hout, G. P. J., Fiolet, A. T. L., Dekker, M., Bosch, L., van Nieuwburg, M. M. J., et al. (2021). Experimental Parameters and Infarct Size in Closed Chest Pig LAD Ischemia Reperfusion Models; Lessons Learned. *BMC Cardiovasc. Disord.* 21 (1), 171. doi:10.1186/s12872-021-01995-7

Takeda, M., Tatsumi, T., Matsunaga, S., Hayashi, H., Kimata, M., Honsho, S., et al. (2007). Spironolactone Modulates Expressions of Cardiac Mineralocorticoid Receptor and 11.BETA.-Hydroxysteroid Dehydrogenase 2 and Prevents Ventricular Remodeling in Post-Infarct Rat Hearts. *Hypertens. Res.* 30 (5), 427–437. doi:10.1291/hypres.30.427

Timmers, L., Henriques, J. P. S., de Kleijn, D. P. V., Devries, J. H., Kemperman, H., Steendijk, P., et al. (2009). Exenatide Reduces Infarct Size and Improves Cardiac

Function in a Porcine Model of Ischemia and Reperfusion Injury. *J. Am. Coll. Cardiol.* 53 (6), 501–510. doi:10.1016/j.jacc.2008.10.033

Wang, D., Liu, Y.-H., Yang, X.-P., Rhaleb, N.-E., Xu, J., Peterson, E., et al. (2004). Role of a Selective Aldosterone Blocker in Mice with Chronic Heart Failure. *J. Card. Fail.* 10 (1), 67–73. doi:10.1016/s1071-9164(03)00578-5

Yellon, D. M., and Hausenloy, D. J. (2007). Myocardial Reperfusion Injury. *N. Engl. J. Med.* 357 (11), 1121–1135. doi:10.1056/NEJMra071667

Zannad, F., McMurray, J. J. V., Krum, H., van Veldhuisen, D. J., Swedberg, K., Shi, H., et al. (2011). Eplerenone in Patients with Systolic Heart Failure and Mild Symptoms. *N. Engl. J. Med.* 364 (1), 11–21. doi:10.1056/NEJMoa1009492

Conflict of Interest: The authors declare that the research was conducted in the absence of any commercial or financial relationships that could be construed as a potential conflict of interest.

Publisher's Note: All claims expressed in this article are solely those of the authors and do not necessarily represent those of their affiliated organizations, or those of the publisher, the editors and the reviewers. Any product that may be evaluated in this article, or claim that may be made by its manufacturer, is not guaranteed or endorsed by the publisher.

frontiers in Pharmacology

ORIGINAL RESEARCH
published: 02 September 2021
doi: 10.3389/fphar.2021.724147

Lcz696 Alleviates Myocardial Fibrosis After Myocardial Infarction Through the sFRP-1/Wnt/β-Catenin Signaling Pathway

Jing Liu[1,2], *Xuehui Zheng*[1], *Chen Zhang*[1], *Chunmei Zhang*[1] *and Peili Bu*[1]*

[1]The Key Laboratory of Cardiovascular Remodeling and Function Research, Chinese Ministry of Education, Chinese National Health Commission and Chinese Academy of Medical Sciences, The State and Shandong Province Joint Key Laboratory of Translational Cardiovascular Medicine, Department of Cardiology, Qilu Hospital, Cheeloo College of Medicine, Shandong University, Jinan, China, [2]Department of Cardiology, Heze Municipal Hospital, Heze, China

Background: Lcz696 (ARNI, angiotensin receptor–neprilysin inhibitor; sacubitril/valsartan) shows an inhibitory effect on fibrosis after myocardial infarction (MI). However, the underlying signaling mechanisms are poorly understood. The Wnt/β-catenin signaling pathway is activated after MI and participates in the process of myocardial fibrosis. Here, we aimed to assess the efficacy of ARNI for alleviating myocardial fibrosis after MI and hypothesized that ARNI alleviates myocardial fibrosis by inhibiting the Wnt/β-catenin signaling pathway and overexpressing sFRP-1, an inhibitor of the Wnt/β-catenin signaling pathway.

Methods: Mice randomized at 1 week post-MI were administered lcz696 (60 mg/kg, n = 21), valsartan (30 mg/kg, n = 19), or corn oil (n = 13) orally for 4 weeks, while the sham-operated group received vehicle (corn oil, n = 19). Cardiac function and extent of myocardial fibrosis were measured. Western blotting and quantitative real-time polymerase chain reaction were used to detect the expression of Wnt/β-catenin pathway-related proteins. Furthermore, primary myocardial fibroblasts were stimulated with angiotensin II (Ang II) and cultured with lcz696 and the sFRP-1 inhibitor way316606 to detect the expression of Wnt/β-catenin pathway proteins.

Results: Both lcz696 and valsartan alleviated myocardial fibrosis and improved cardiac function, but lcz696 had superior efficiency compared to valsartan. Furthermore, β-catenin expression was inhibited and sFRP-1 was overexpressed after drug treatment, which could be significantly improved by lcz696 in mice. In addition, lcz696 inhibited β-catenin expression in AngII-stimulated myocardial fibroblasts, and β-catenin expression increased after the inhibition of sFRP-1.

OPEN ACCESS

Edited by:
Jérôme Roncalli,
Centre Hospitalier Universitaire de Toulouse, France

Reviewed by:
Zhuoming Li,
Sun Yat-sen University, China
Firdos Ahmad,
University of Sharjah, United Arab Emirates

***Correspondence:**
Peili Bu
bupeili@outlook.com

Specialty section:
This article was submitted to Cardiovascular and Smooth Muscle Pharmacology, a section of the journal Frontiers in Pharmacology

Received: *12 June 2021*
Accepted: *20 August 2021*
Published: *02 September 2021*

Citation:
Liu J, Zheng X, Zhang C, Zhang C and Bu P (2021) Lcz696 Alleviates Myocardial Fibrosis After Myocardial Infarction Through the sFRP-1/Wnt/β-Catenin Signaling Pathway. Front. Pharmacol. 12:724147. doi: 10.3389/fphar.2021.724147

Abbreviations: A, late peak; AngII, angiotensin II; ARNI, the angiotensin receptor-neprilysin inhibitor sacubitril/valsartan; CFS, cardiac fibroblasts; DBP, diastolic blood pressure; E, early peak; ELISA, enzyme-linked immunosorbent assay; FS, fractional shortening; H&E, hematoxylin and eosin; HR, heart rate; LCA, left coronary artery; LVEF, left ventricular ejection fraction, LVEDd, left ventricular end-diastolic dimension; LV mass, left ventricular mass; MI, myocardial infarction; SBP, systolic blood pressure; sFRP-1, secreted frizzled-related protein 1;

Conclusion: ARNI alleviated cardiac fibrosis and cardiac remodeling by inhibiting the Wnt/β-catenin signaling pathway. In addition, ARNI can lead to overexpression of sFRP-1, which is an inhibitor of the Wnt/β-catenin signaling pathway. These results indicate a new therapeutic target of ARNI to improve myocardial fibrosis and prevent myocardial remodeling.

Keywords: myocardial infarction, myocardial fibrosis, LCZ696, Wnt/β-catenin signaling, SFRP-1

INTRODUCTION

Heart failure following acute myocardial infarction (MI) remains a major public health concern worldwide, exerting a substantial economic burden (Mozaffarian et al., 2016). Cardiac remodeling is viewed as a key determinant of the clinical outcomes in heart diseases. Cardiac fibrosis, which is typically seen in the failing heart, is a major aspect of the remodeling process. Myocardial fibrosis is an important pathophysiological process observed after MI (Zile et al., 2019). Cardiac fibrosis arises from a pathological attempt to repair tissue damage during maladaptive remodeling. The proliferation of interstitial fibroblasts and increased deposition of extracellular matrix components result in myocardial stiffness and diastolic dysfunction, which ultimately leads to heart failure. Treatment options to block or reverse fibrosis are scarce (Burke et al., 2019). Lcz696 (valsartan/sacubitril), the first of the new ARNI (dual-acting angiotensin-receptor–neprilysin inhibitor) drug class, contains equimolar amounts of valsartan which is an angiotensin-receptor blocker, and sacubitril, which is a prodrug for the neprilysin inhibitor, and ARNI has been extensively reported to approve for the treatment of heart failure patients with reduced ejection fraction [(Campbell, 2017). (Voors et al., 2013)]. ARNI, apart from blocking angiotensin II (AngII)-signaling, also augments natriuretic peptides by inhibiting their breakdown by neprilysin (von Lueder, 2015), an endopeptidase that degrades various vasoactive peptides, including ANP (atrial natriuretic peptide) and BNP (brain natriuretic peptide) (Burke et al., 2019). Natriuretic peptides, activated in cardiac dysfunction and HF, counteract the RAAS and promote vasodilation, natriuresis, and inhibit fibrosis and hypertrophy. The addition of the neprilysin component in lcz696 augments plasma levels of natriuretic peptides (Voors et al., 2013). In fact, the PARADIGM-HF trial compared enalapril and sacubitril/valsartan (ARNI) therapies and showed that the latter can significantly reduce cardiovascular death and hospitalization in patients with systolic heart failure (McMurray et al., 2014a). ARNI reportedly can improve cardiac function and remodeling; however, the mechanisms underlying the cardioprotective action of ARNI in the context of fibrosis and remodeling after MI are mostly unknown. Despite recent formal recognition of ARNI by guideline authorities, there is a striking paucity of mechanistic data on the effect of ARNI compared to those on stand-alone RAAS blockade on cardiac remodeling (Ponikowski et al., 2016).

Regarding the underlying molecular mechanisms, ample studies have recently shown an emerging role of the Wnt/β-catenin signaling pathway in the process of cardiac remodeling; inhibition of this pathway has been shown to be cardioprotective, to avert cardiac inflammation and fibrosis, to reduce infarct size and scaring, and to stimulate functional recovery of the heart (Eid et al., 2020).

Wnt signaling pathways are considered essential in heart development and are found to be active in the post-MI heart (Voors et al., 2013; McMurray et al., 2014a). Wnt/β-catenin signaling in the adult heart is quiescent under normal conditions; however, it is reactivated after MI, playing a dominant role in the regulation of cardiac fibrosis [(Palevski et al., 2017). (Fu et al., 2019)]. The expression of several Wnt pathway proteins, such as β-catenin and Dvl-1, is increased in the damaged tissues after experimental MI induction (Barandon et al., 2003a; Chen et al., 2004; Barandon et al., 2005; Kobayashi et al., 2009). In addition, Wnt/β-catenin signaling has been shown to promote cardiac fibrosis by inducing the transition of endothelial and epicardial cells into a mesenchymal state, differentiation of fibroblasts into myofibroblasts, and production of collagen (Mizutani et al., 2016). Importantly, several studies have shown that the inhibition of Wnt/β-catenin signaling after MI is beneficial, as it improves infarct healing and prevents heart failure. This suggests that blocking the Wnt/β-catenin signaling pathway could be a potential novel therapeutic approach to prevent adverse cardiac remodeling after MI.

The secreted frizzled-related protein 1 (sFRP-1), an antagonist of the Wnt/β-catenin pathway (Tao et al., 2015), has been shown to significantly inhibit the proliferation of cardiac fibroblasts, synthesis of collagen, and differentiation of myofibroblasts, and to consequently effectively alleviate the progression of pathological cardiac fibrosis (Sklepkiewicz et al., 2015). Importantly, Barandon et al. demonstrated the upregulation of sFRP-1 in the heart after MI (Ge et al., 2019).

Mechanistically, the beneficial impact of ARNI may partially stem from the inhibition of Wnt/β-catenin signaling. Based on previous studies, we hypothesized that lcz696 could be implicated in post-MI myocardial fibrosis by regulating the Wnt/β-catenin signaling pathway. However, the correlation between ARNI and sFRP-1 has not been studied thus far. Therefore, herein, we evaluated the effects and mechanisms of ARNI in the context of MI, both *in vitro* and *in vivo*. Particularly, we comprehensively investigated the relationship among ARNI, the Wnt//β-catenin pathway, and sFRP-1.

MATERIALS AND METHODS

Animal Protocols

All mouse studies were approved by the Animal Ethics Committee of Shandong University; the care and use of

animals followed the guidelines on animal ethics. Eight-week-old C57BL/6J male mice were purchased from SBF Biotechnology Co. Ltd. (Beijing, China). The mice were housed at a constant temperature (24°C) and provided a normal diet with free access to water. C57BL/6J male mice underwent either a permanent coronary artery ligation to induce MI or sham surgery. Briefly, the left coronary artery (LCA) was positioned using a 6–0 silk suture, stitched, and ligated approximately 3 mm from its starting point (Gao et al., 2010). When the front wall of the left ventricle (LV) turned pale, ligation was considered successful. The sham group received the same surgical procedure but without blocking the LCA. One week following LCA ligation, mice were assessed by echocardiography for study inclusion. Mice were randomly assigned into one of four following groups: sham-operated group (Sham, n = 20; 19 alive), MI group (MI, n = 20; 13 alive), VAL group (VAL; n = 40; 21 alive), and ARNI group (ARNI; n = 40; 19 alive). After a week of adaptive feeding, surviving mice were administered VAL or ARNI via gavage. Some studies have proposed excessive toxic side effects of ARNI. Therefore, we referred to the experimental study of Suematsu et al. and adopted the administration of ARNI (60 mg/kg) or VAL (30 mg/kg) dissolved in corn oil or only corn oil every day in the morning (8–9 AM) for 4 weeks. Moreover, the dose of lcz696 (60 mg/kg/day) was selected based on a previous report (Xia et al., 2017). Of note, there was no difference in feeding conditions among all mice.

Cardiac Function Measurement

Mice were anesthetized via inhalation of isoflurane gas; induction was performed at 2.5% in a chamber, and maintenance was carried out at 1.5% isoflurane via a nose adaptor. The cardiac function was then evaluated using the Vevo770 imaging system (Visual Sonic, Toronto, Canada). The left ventricular ejection fraction (LVEF), fractional shortening (FS), early (E) peak, late (A) peak, left ventricular end-diastolic dimension (LVEDd), and left ventricular mass (LV mass) were measured. The ratios of early-to-late mitral flow velocity (E/A) and diastolic velocity ratio (E'/A') were also calculated. Additionally, the internal diameter of the LV and the thickness of the septum and posterior wall at end-systole and end-diastole were measured from the long-axis view at the level of chordae tendineae. LVEF and FS were then calculated according to these parameters. Echocardiographic imaging and measurements were performed in a blinded manner. All measurements were averaged based on three consecutive cardiac cycles.

Serum NT-proBNP and Blood Pressure Measurements

The serum levels of NT-proBNP were measured using a commercial enzyme-linked immunosorbent assay (ELISA)—Mouse NT-proBNP ELISA Kit (MyBioSource, CA, United States), according to the manufacturer's instructions. Briefly, this assay employs a quantitative sandwich enzyme technique. A microplate is pre-coated with an antibody specific for NT-proBNP; the analyte is captured, and then sandwiched with a biotin-conjugated antibody. Thereafter, avidin-conjugated horseradish peroxidase is added, followed by a specific substrate. Finally, color development is stopped, and the intensity of the color is measured. In our assay system, the intensity of the developed color was positively correlated with the concentration of mouse NT-proBNP in the sample, and the absorbance (OD value) was measured with using an absorbance microplate reader (SpectraMax plus 384, American Molecular Devices Scientific Company) at 450 nm wave length.

The systolic and diastolic blood pressure of awake mice was measured using the tail-sleeve method before and after surgery and before death. The heart rate (HR), systolic blood pressure (SBP), and diastolic blood pressure (DBP) were measured using a noninvasive tail-cuff system (Softron BP-98A, Softron, Tokyo, Japan).

TTC Staining

Animals were humanely euthanized, and their hearts were quickly removed, rinsed with normal saline, and dried. Heart tissues were frozen in a −20°C refrigerator for 30 min until they hardened. Then, from the apex of the heart to the bottom, 1–2 mm thick sections were obtained, along the direction of the atrioventricular groove. A total of five slices were cut. The slices were quickly placed into a TTC phosphoric acid buffer solution (Solarbio, Beijing, China) at 37°C, and were subsequently bathed in water for 15 min. The infarcted area after staining appeared white, while the normal areas appeared red.

Histology and Immunohistochemistry

Mice were anesthetized and euthanized, and their hearts were dissected; the dissected tissues were immediately fixed with 4% formalin. Tissues were then embedded within paraffin and sectioned (5 μm) for histology staining including hematoxylin and eosin (H&E) and immunohistochemistry. Of note, the cardiac tissues were removed from 3 to 4 mm below the ligation site to ensure that the pathological sections of cardiac tissues were at the same level. For the detection of interstitial collagen deposition, heart sections were stained with PicroSirius Red and Masson's trichrome according to the manufacturer's instructions. PicroSirius Red staining images were captured at 10× on a BX51 epifluorescence microscope (Olympus, Shinjuku, Japan) using circularly polarized light to generate a birefringent (red/thick and green/thin) signal from collagen fibers. To evaluate fibrosis, the areas of interest (epicardial, perivascular, and interstitial) were defined using ImageJ. The fraction of the fibrosis area was quantified using ImageProPlus6.0 (Media Cybernetics, Sarasota, FL, United States).

For immunohistochemistry, the slides were incubated overnight at 4°C with specific primary antibodies against SFRP-1 (1:800, Abcam, Cambridge, United Kingdom), β-catenin (1:50, Cell Signaling Technology, Leiden, Germany), GSK-3β (1:50, Santa Cruz Biotechnology, TX, United States), collagen I (1:200, Abcam), and collagen III (1:500, Abcam). The next day, the samples were incubated with secondary antibodies and diaminobenzidine staining (ZSGB-Bio, Beijing, China) was performed following the manufacturer's protocols. Data were analyzed using ImageProPlus6.0 (Media Cybernetics, Sarasota, FL, United States).

TUNEL Assay

Apoptotic cells in myocardium were detected using a *in situ* cell death detection kit (Roche, 12156792910) following the manufacturer's instructions. Heart sections were deparaffinized, hydrated, kept in permeabilization solution (0.1% Triton X-100) for 5 min, and incubated in TUNEL reaction mixture for 60 min at 37°C; the sections were then sealed in Prolong Gold Anti-Fade Reagent with 4-6-diamidino-2-phenylindole (DAPI, Invitrogen). Images were acquired via a fluorescence microscopy (Nikon) and quantified using ImageProPlus6.0 software (Media Cybernetics, Sarasota, FL, United States).

Immunofluorescence

Heart sections were incubated with specific primary antibodies against α-SMA (Abcam, Cambridge, MA, United States) at the appropriate concentrations at 4°C overnight. The next day, horseradish peroxidase-conjugated secondary antibodies were added for 1 h at 37°C. Nuclei were visualized using DAPI staining. Fluorescent images were acquired via a fluorescence microscopy (Nikon) and quantified using Image Pro Plus 6.0 software (Media Cybernetics, Sarasota, FL, United States).

Cellular Cardiac Fibrosis *in vitro* Model

Primary myocardial fibroblasts were obtained from 2–3-day-old mice via enzyme digestion and differential plating (Burke et al., 2019). Briefly, ventricles were isolated and transferred into a solution containing 0.8 mg/ml collagenase type II (Solarbio) and finely minced. Tissues were then agitated in 4–6 ml of collagenase solution in four cycles of 60 min each, and cells were collected at each step by centrifugation. Cells were then strained through 70-μm filters and plated onto 6-well plate for 2 h. Non-adherent cells were then removed, and the adherent cells were considered fibroblasts. The culture medium was then replaced, and the cells were maintained in DMEM (Solarbio) containing 10% FBS and penicillin/streptomycin (Invitrogen, Carlsbad, CA, United States) in a 5% CO_2 humidified incubator at 37°C for 36 h. Before lcz696 or VAL stimulation, the cells were starved in serum-reducing medium (2% FBS) for 12 h. Subsequently, we added different lcz696 (ARNI, HY-18204A; MCE) in varied concentrations (1, 10, and 30 μmol/L) (Ge et al., 2019) and incubated the cells for 1 h; Val (HY-18204; MCE) (30 μmol/L) was used as the positive control. After repeated experiments, the optimal concentration of lcz696 (30 μmol/L) was finally determined. Additionally, to investigate the potential role of sFRP-1, we incubated cells overnight with the sFRP-1 inhibitor way316606 (2 μmol/L; MCE, HY-10858). The stimulation of collagen synthesis with Angiotensin II (*AngII, Sigma*) 100 nmol/L requires 48 h (von Lueder, 2015). Therefore, cells were treated as mentioned above, and only then received AngII, followed by 2 days of incubation. Experiments were repeated at least three times.

Quantitative Real-Time Polymerase Chain Reaction (qRT-PCR) Assay

Total RNA was extracted from the mouse hearts using the TRIzol reagent (Ambion) following the manufacturer's protocol, and the conversion of mRNA into cDNA was performed using the Primescript™ RT reagent kit with gDNA Eraser (RR047A, Takara, Tokyo, Japan). qRT-PCR was performed using SYBR Premix Ex TaqII (RR420A; Takara) in the iQ5 Multicolor Real-Time PCR Detection System (Bio-Rad, Hercules, CA, United States) using gene specific primers (**Table 1**). Relative mRNA expression was quantitated by $2^{-\Delta\Delta Ct}$ comparative quantification method (Liu et al., 2019). All experiments were repeated at least three times.

Western Blot Analysis

Total protein from mouse myocardium tissues and primary cardiac fibroblasts was extracted using a protein extraction kit and protein concentration was measured using BCA Protein Assay kit (Beyotime, China) according to the manufacturer's protocol. The proteins were separated by 10% gradient SDS-polyacrylamide gel electrophoresis (SDS-PAGE) and transferred to a polyvinylidene difluoride (PVDF) membrane using the wet transfer method. The membranes were blocked with 5% defatted milk for 1 h at room temperature and then incubated overnight at 4°C with specific primary antibodies against sFRP-1 (1: 230,Abcam, ab4193), β-catenin (1:1,000, Cell Signaling Technology, D10A8), active β-catenin (1:1,000, EMD Millipore, 05–665), GSK-3β (1:1,000, Santa Cruz Biotechnology, 0011-A),p-GSK-3β (1:1,000, Cell Signaling Technology, 5558T), α-tubulin (1:10,000,Abcam, ab7291), collagen III (1:5,000,Abcam,ab7778) and α-SMA (1:10,000, Cell Signaling Technology, 19245s). All primary antibodies are diluted in proportion with antibody diluent (Boster). The membranes were washed and incubated with the anti-mouse/rabbit secondary antibodies labeled with horseradish peroxidase (1:5,000; ZSGB-Bio, Beijing, China) for 1 h at room temperature. The blots were subsequently detected using a chemiluminescence kit (Millipore, Billerica, MA, United States) as per the manufacturer's instructions. All experiments were repeated at least three times.

Statistical Analysis

All data are expressed as mean ± SEM derived from at least three independent experiments. Statistical analysis was performed using GraphPad Prism 8 (GraphPad, San Diego, CA, United States). The Shapiro-Wilk test was applied for normality assumption. Thereafter, normally distributed data were analyzed using the unpaired two-tailed Student's *t*-tests (two-group comparisons), or the one-way ANOVA followed by Dunnett's or Tukey's post hoc tests (comparisons between multiple groups). $p < 0.05$ was considered statistically significant.

RESULTS

Anti-myocardial Remodeling Effect of ARNI Is Superior to That of Valsartan

C57BL/6J male mice underwent permanent LCA ligation to induce MI. Importantly, TTC staining was performed 24–48 h after MI and showed that the mouse model of MI was successfully established with the infarcted areas appearing in white; of note, no infarcted areas were detected in sham-operated animals

TABLE 1 | Information of primers for RT-qPCR.

Gene name	Forward sequence (5′–3′)	Reverse sequence (5′–3′)
β-catenin	5'TTGTAGAAGCTGGTGGGATGC	5'AGTCGCTGCATCTGAAAGGT
sFRP-1	5'GCGAGTTTGCACTGAGGATG	5'GTTGTGGCTGAGGTTGTCCA
α-SMA	5'TTCGTGACTACTGCCGAGC	5'GTCAGGCAGTTCGTAGCTCT
GSK-3β	5'GAGCCACTGATTACACGTCCA	5'CCAACTGATCCACACCACTGT
TGF-β	5'AGCTGCGCTTGCAGAGATTA	5'AGCCCTGTATTCCGTCTCCT
ANP	5'CTCCGATAGATCTGCCCTCTTGAA	5'GGTACCGGAAGCTGTTGCAGCCTA
BNP	5'GCTCTTGAAGGACCAAGGCCTCAC	5'GATCCGATCCGGTCTATCTTGTGC

(**Figure 1A**). Additionally, the MI group showed a significantly increased heart size; however, interestingly, after the drug intervention, the heart size was observed to have decreased, especially in the ARNI group (**Figure 1B**). Furthermore, HE staining showed that ARNI improved the increase in the ventricular cross-sectional area after MI; at high magnification, we observed the texture of the myocardium in the infarcted area to be white gelatinous, while the texture becomes hard, like ground glass. Of note, the improvement after ARNI treatment was considerably greater than that observed after VAL treatment (**Figure 1C**). As expected, the ratio of heart weight to body weight in the MI group was higher than that in the sham group (**Figure 1D**); This ratio in the ARNI group was significantly lower than that in the VAL group. Moreover, there was no significant difference in the body weight among the four groups (**Figure 1D**). Finally, yet importantly, after the drug intervention, there was a downward trend in the systolic blood pressure (SBP) of mice, more obviously in VAL-treated animals, but without statistical relevance (**Figure 1E**).

ARNI Alleviates MI-Induced Cardiac Dysfunction

The serum NT-proBNP levels were significantly increased 5 weeks after MI in the MI group; of note, there was a significant difference upon treatment with ARNI and VAL, and the effect of ARNI was superior to that of VAL (**Figure 2A**). Meanwhile, qRT-PCR analysis revealed that the mRNA levels of ANP and BNP in the MI group were significantly increased, while ARNI treatment reversed this trend (**Figure 2B**). Echocardiography further showed that LVEF, FS, E/A, and E'/A' in the MI group were decreased compared to those in the sham group and that ARNI treatment significantly improved these metrics; of note, the difference was statistically significant compared with the metrics in the VAL group. Additionally, the LVEDd and LV mass were higher in the MI group than in the sham groups. However, compared with those in the VAL group, the LVEDd and LV mass in the ARNI group showed improvements (**Figure 2D**).

ARNI has Anti-fibrosis and Anti-Apoptotic Effects

Masson's trichrome and PicroSirius red staining of heart sections demonstrated that collagen deposition in the hearts of MI animals was worse than that observed in the sham group, as expected. Additionally, ARNI treatment prevented collagen deposition to a greater extent than VAL treatment (**Figures 3A,A1,B,B1**). We also examined cardiac expression of α-smooth muscle actin (α-SMA), a molecular signature for myofibroblast activation. The immunofluorescence results showed that α-SMA was strongly expressed in the infarct area, and the expression was significantly decreased after drug intervention as shown in **Figures 3C,C1**. The immunohistochemistry (IHC) results showed that the expression of collagen I and collagen III in and around the infarcted area was enhanced in the MI group and decreased in the ARNI group to a significantly greater extent than that observed in the VAL group (**Figures 3D,D1,E,E1**). The TUNEL assay showed that the apoptosis rate was also increased significantly in MI group (**Figures 3F,F1**); apoptosis was found to have decreased after drug intervention, especially for the ARNI group. Meanwhile, qRT-PCR indicated that the mRNA levels of genes encoding for α-SMA and TGF-β in MI animals were significantly increased, and that ARNI treatment reversed this trend; the effects were significantly superior in ARNI-treated animals than in VAL-treated animals (**Figures 3G,H**). Of note, no significant difference was detected in the expression of TGF-β between the VAL and MI groups.

Wnt/β-catenin Signaling Pathway Is Activated in Mice From the MI Group

Remarkably, western blot analysis showed that the expression of β-catenin and active β-catenin was increased 4 weeks after MI in mice (compared to the sham group). Interestingly, after 4 weeks of treatment with ARNI and VAL, the expression of β-catenin was inhibited; of note, the expression of β-catenin and active β-catenin in the ARNI group was significantly lower than that in the VAL and MI groups (**Figures 4A–C**). In contrast, the effects on GSK-3β and *p*-GSK-3β were the opposite (**Figures 4D–F**). Similarly, the IHC results for β-catenin and GSK-3β were also consistent with the above results (**Figures 4G–I**). Although qRT-PCR results for β-catenin and GSK-3β were also consistent with those stated above (**Figures 4J,K**), there was no significant difference in the expression of GSK-3β between the VAL and MI groups. Additionally, the expression of Dvl1 was also found to have increased after MI, and decreased after drug treatment, with ARNI outperforming VAL (**Figure.4L**).

ARNI Promotes the Expression of sFRP-1

Next, we investigated the expression of sFRP-1, which is found upstream of the Wnt signaling pathway. The

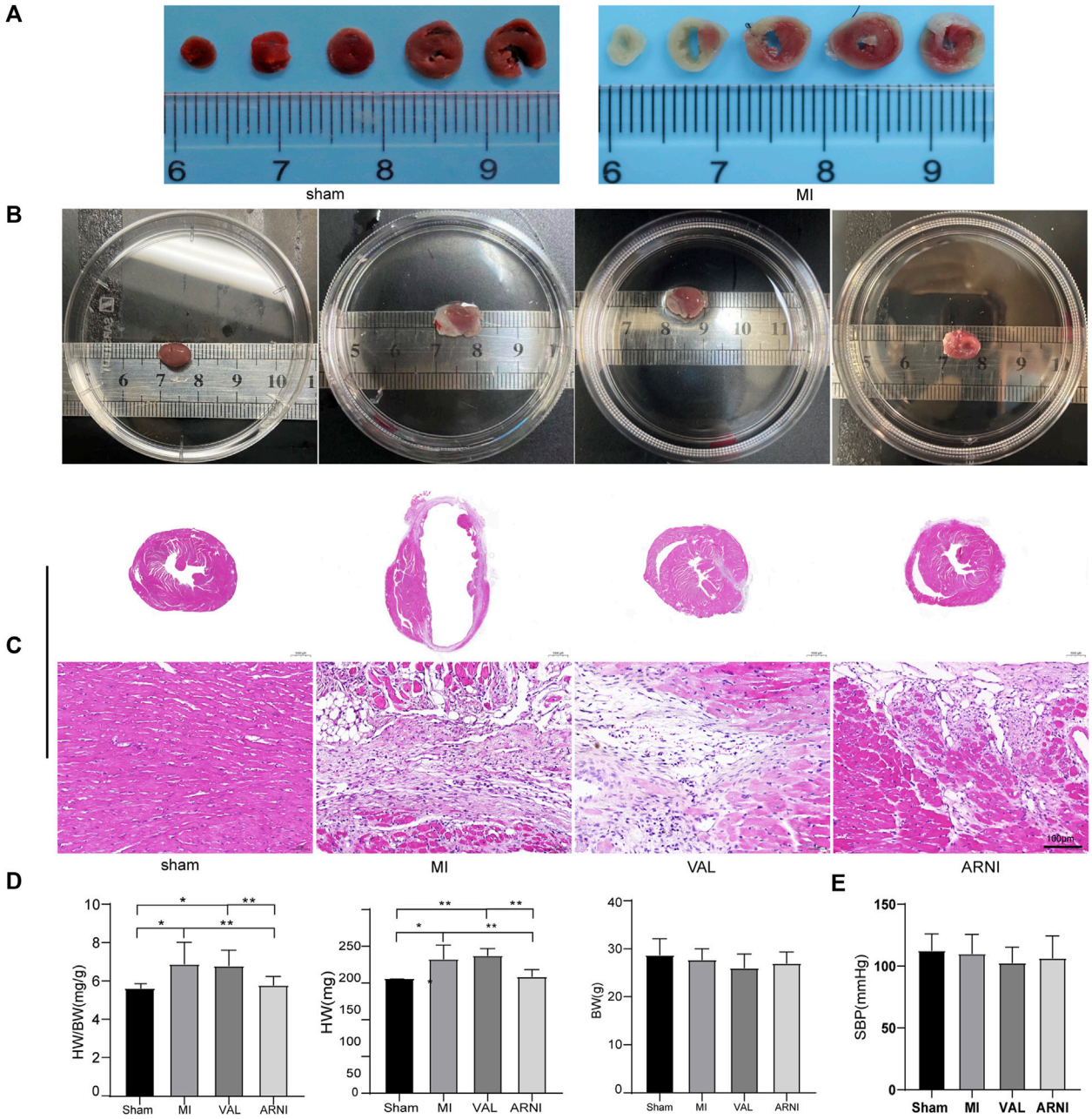

FIGURE 1 | TTC staining, heart size, and pathology in the four groups of mice. **(A)** TTC staining.**(B)** The heart gross morphological image. **(C)** H&E staining of Cross-sections of the hearts at the papillary muscle level and the infarct section (scale bar: 100 μm). **(D)** Quantitative analysis of the heart weight to body weight (HW/BW) ratio. **(E)** SBP-systolic blood pressure. Sham: sham-operated group; MI: myocardial infarction; VAL: valsartan intervention group; ARNI: Sacubitril/valsartan intervention group. Each group n = 7. $^{*}p < 0.01$,$^{**}p < 0.05$.

western blot results showed that the expression of sFRP-1 was increased in the MI group compared with that in the sham group. Remarkably, after drug treatment, the expression of sFRP-1 was increased more obvious; of note, the increase was observed to be higher in the ARNI group than in the VAL group (**Figures 5A,B**). Importantly, the IHC and qRT-PCR analyses yielded similar results; the expression of sFRP-1 was found to have significantly increased in the ARNI group (**Figures 5C–E**).

sFRP-1 Regulates the Wnt/β-Catenin Signaling Pathway *in vitro*

For further mechanistic insights, we obtained primary mouse fibroblasts according to the methods mentioned above and

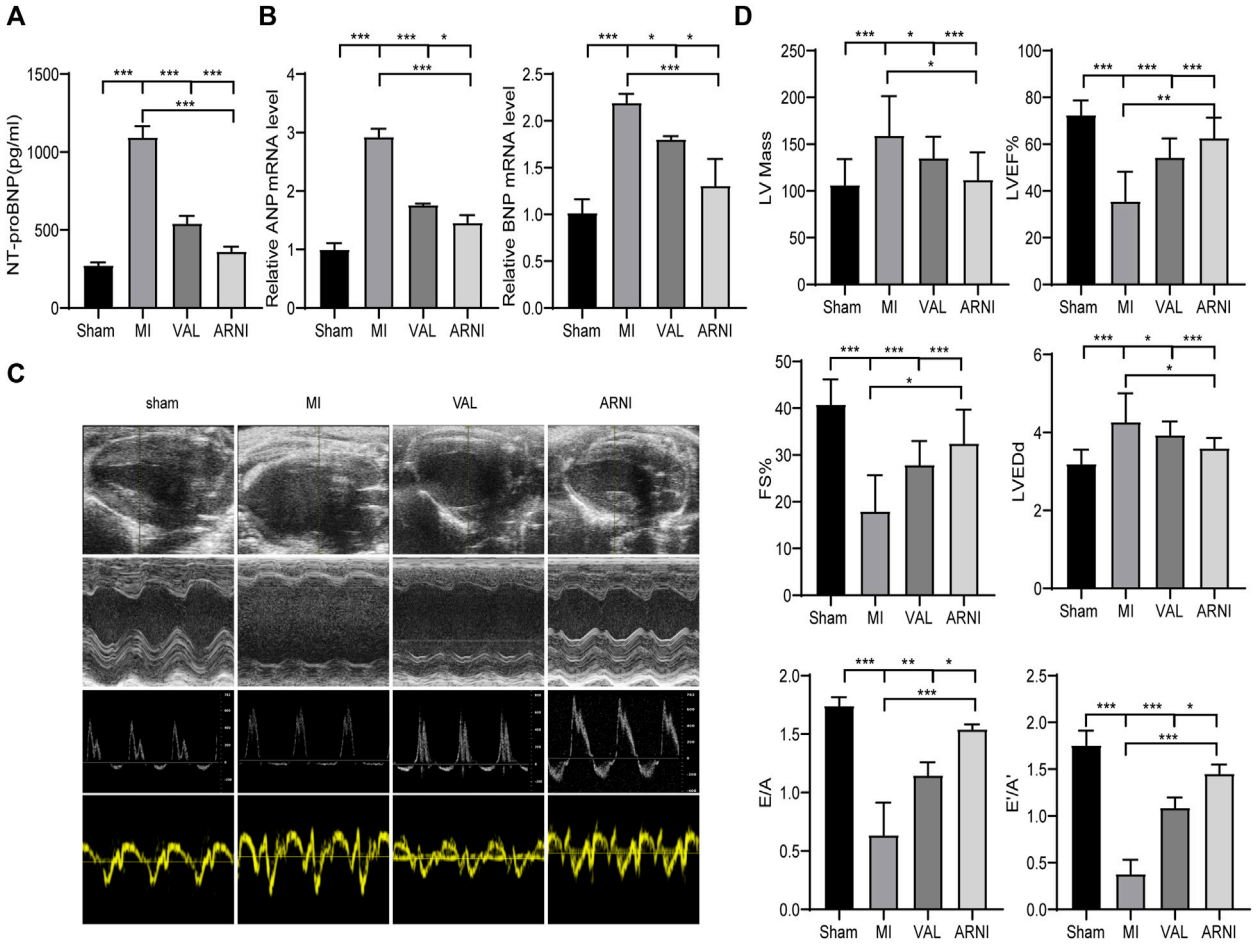

FIGURE 2 | ARNI alleviates cardiac dysfunction in mice with myocardial infarction. **(A)** Serum NT-proBNP concentration. **(B)** Relative mRNA fold changes of *ANP* and *BNP*.**(C)**. The 1st row:Representative 2D echocardiograms. The 2nd row: Representative M-mode echocardiograms. The 3rd row: Representative pulse-wave doppler echocardiograms of mitral inflow. The 4th row: Representative tissue doppler echocardiograms. **(D)** Left ventricular mass, LV ejection fraction (LVEF%), fractional shortening (FS), left ventricular end-diastolic dimension (LVEDd), early-to-late mitral flow (E/A), and diastolic velocity ratio (E'/A'). Each group n = 8.*$p < 0.01$,**$p < 0.05$, ***$p < 0.001$.

studied the effects of lcz696 and VAL on the Wnt/β-catenin signaling pathway as well as on the expression of sFRP-1. The western blot results indicated that β-catenin expression was significantly inhibited at 30 mmol/L lcz696 (**Figure 6A**). The qRT-PCR results showed that β-catenin expression was significantly inhibited with 30 μmol/L lcz696, while the expression of sFRP-1 was increased (**Figures 6G,H**). Of note, the qRT-PCR analysis showed that the expression of Dvl-1 was also the lowest at 30 μmol/L lcz696 (**Figure 6I**). Next, in order to further explore the role of sFRP-1, we used the sFRP-1 inhibitor way316606. Interestingly, western blot analysis revealed that the expression of β-catenin in way316606-treated cells (way316606^{+}) was higher than that in lcz696-treated cells and lower than that in AngII-treated cells, suggesting that the influence of lcz696 on β-catenin is related to the expression of sFRP-1 (**Figure 6B**). The results of qRT-PCR were once again consistent with these observations (**Figure 6J**). Additionally, qRT-PCR revealed that the expression of α-SMA and TGF-β was significantly increased in AngII-stimulated cells and decreased in lcz696-treated cells; furthermore, their expression in way316606-treated cells was higher than that in lcz696-treated cells (**Figure 6K,L**). In addition, western blot analysis revealed that the expression of collagen III in way316606-treated cells was higher than that in lcz696-treated cells and lower than that in AngII-treated cells (**Figure 6B**), suggesting that the sFRP-1 can alleviate collagen deposition in myocardial fibroblasts.

DISCUSSION

In this study, we show that the sFRP-1/Wnt/β-catenin axis plays a role in the prevention of myocardial fibrosis and improvement of myocardial remodeling in the context of ARNI treatment.

Studies have shown that ARNI has an inhibitory effect on fibrosis after MI, but the exact underlying mechanism is not entirely clear. Cardiac fibrosis is a common process in

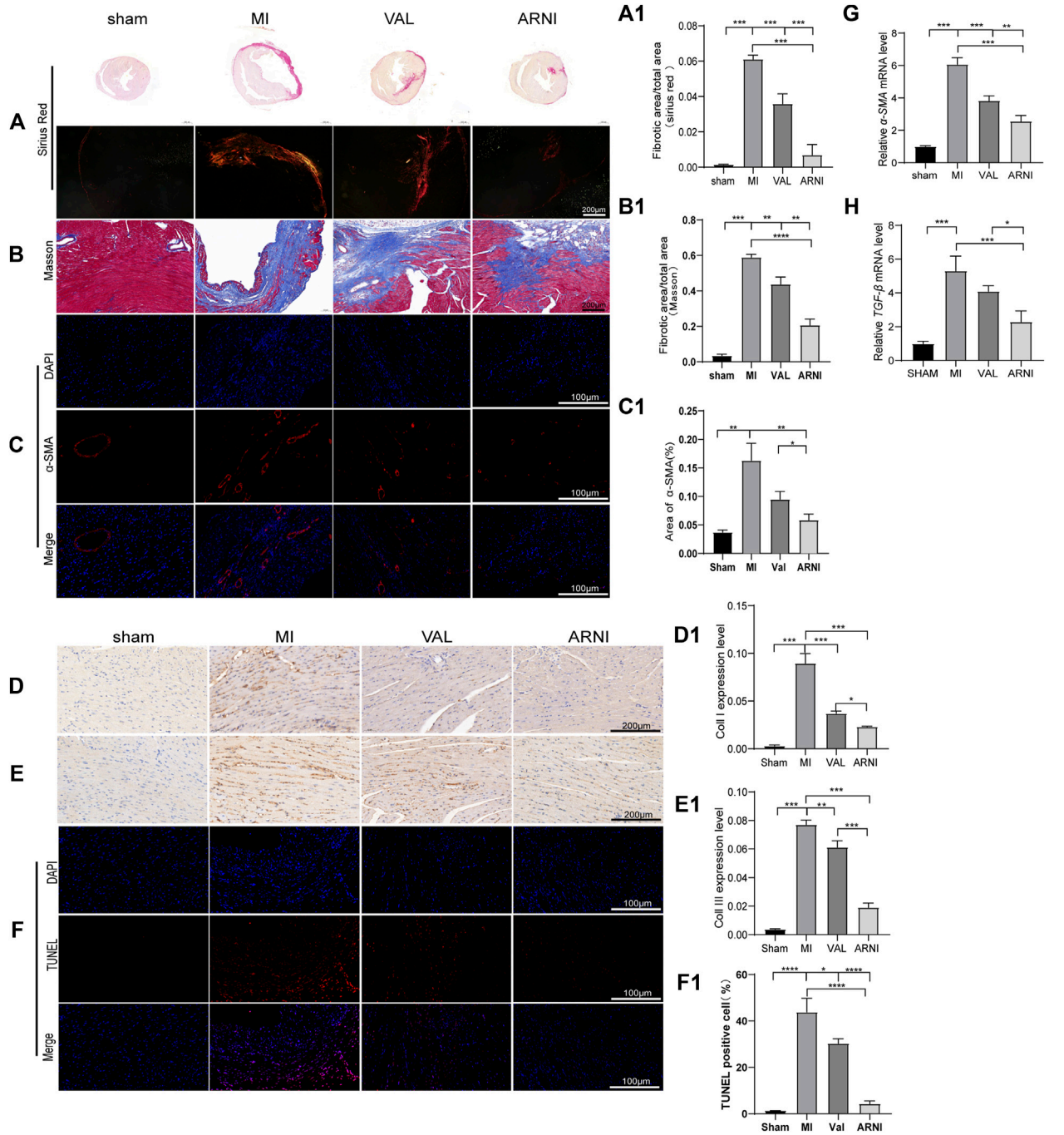

FIGURE 3 | Effects of ARNI on myocardial fibrosis in mice with MI. **(A)** Sirius Red staining of myocardium tissues (2nd row, scale bar = 100 μm). **(A1)** Quantitative analysis of myocardial fibrosis (Sirius Red staining). **(B)** Masson's trichrome staining of myocardium tissues (scale bar = 200 μm). **(B1)** Quantitative analysis of myocardial fibrosis (Masson's trichrome staining).**(C)** Immunofluorescence images of myofibroblasts derived from CFs. Red, α-SMA; Blue, nuclei. (scale bars = 100 μm). **(C1)** Quantitative analysis of α-SMA; **(D,D1,E,E1)** Immunostaining of collagen I and collagen III. **(F)** TUNEL staining of myocardium (scale bar = 100 μm). **(F1)**. Quantitative analysis of TUNEL positive cells. **(G,H)** Relative mRNA level of α-SMA and TGF-β.Each group n = 7. $^{*}p < 0.01$,$^{**}p < 0.05$, $^{***}p < 0.001$.

remodeling hearts after MI and is mediated by myofibroblast invasion and collagen deposition (van den Borne et al., 2010). In the present study, we successfully established a MI model in mice as revealed by TTC staining. Importantly, Masson's trichrome and PicroSirius Red staining showed that the degree of myocardial fibrosis was the highest in the MI group and was decreased in the ARNI- and VAL-treated groups. Von Lueder et al. found that ARNI could improve the LVEDd and LVEF after MI, reduce cardiac weight, and reduce myocardial fibrosis (von Lueder et al., 2015). We

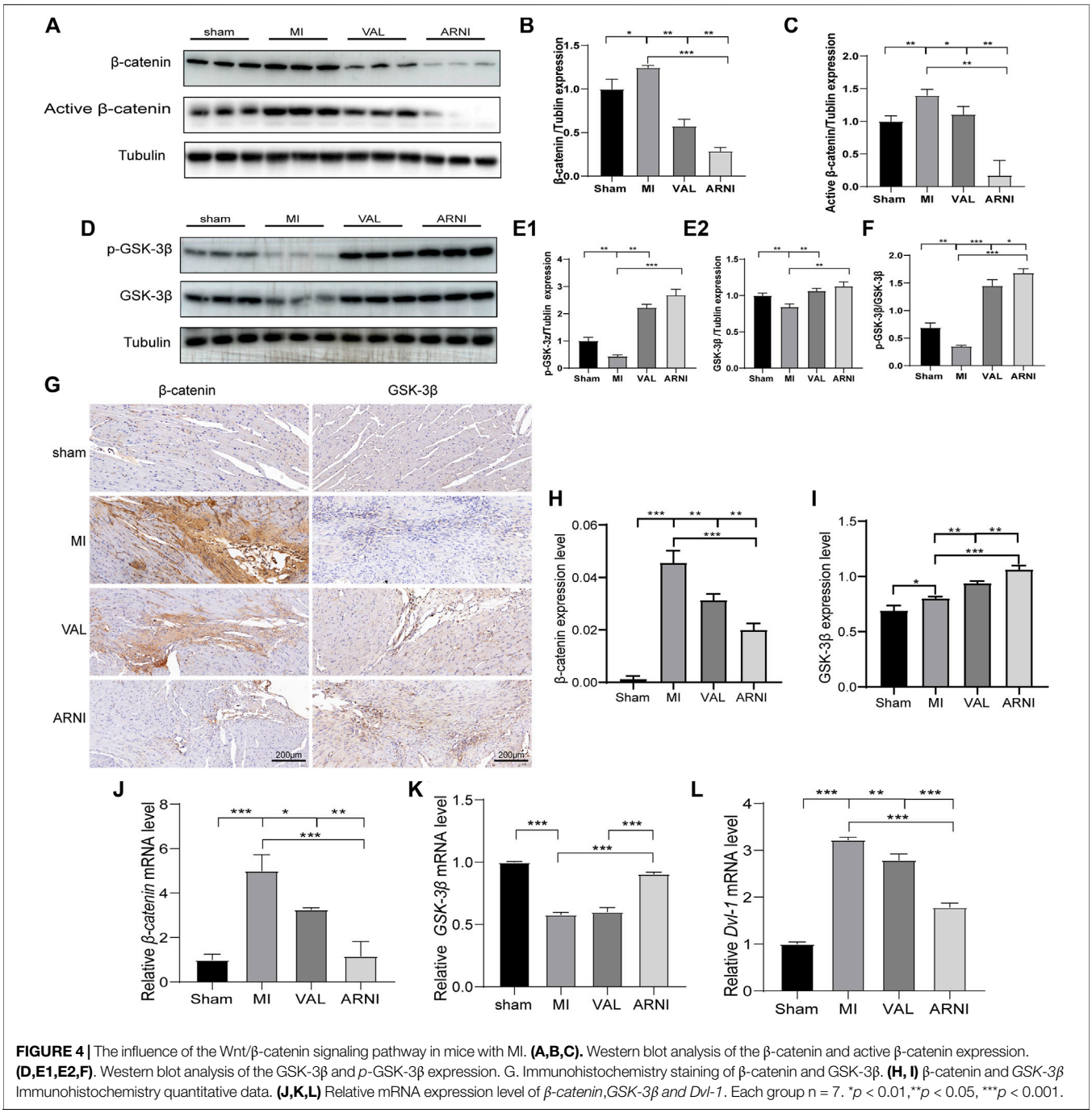

FIGURE 4 | The influence of the Wnt/β-catenin signaling pathway in mice with MI. **(A,B,C).** Western blot analysis of the β-catenin and active β-catenin expression. **(D,E1,E2,F)**. Western blot analysis of the GSK-3β and *p*-GSK-3β expression. G. Immunohistochemistry staining of β-catenin and GSK-3β. **(H, I)** β-catenin and *GSK-3β* Immunohistochemistry quantitative data. **(J,K,L)** Relative mRNA expression level of *β-catenin*,*GSK-3β and Dvl-1*. Each group n = 7. $^{*}p < 0.01$,$^{**}p < 0.05$, $^{***}p < 0.001$.

hypothesize that ARNI inhibits cardiac fibrosis and consequently prevents the development of cardiac hypertrophy.

ARNI was observed to show significant improvement over standard of care therapy in patients with class II, III, or IV heart failure and reduce the ejection fraction in the PARADIGM-HF trial (McMurray et al., 2014b). In the present study, we compared the changes in cardiac function after MI in four groups of mice and found that cardiac function was significantly reduced in the MI group and improved in the ARNI- and VAL-treated groups; the improvement in the ARNI group was more significant than that observed in the VAL group. We believe that the use of ARNI is advantageous over the use of a single RAAS blocker, which is supported by echocardiographic data, including the ejection fraction, LVIDd, and LV mass.

The Wnt signal transduction pathway is involved in myocardial repair after MI (Blankesteijn et al., 2000). (Schumann et al., 2000). Studies by Yue Z et al. showed that the connection between RAAS and Wnt/β-catenin might not be a one-way path; rather, it appears to be bidirectional and reciprocal. Therefore, RAAS activation and Wnt/β-catenin could form a

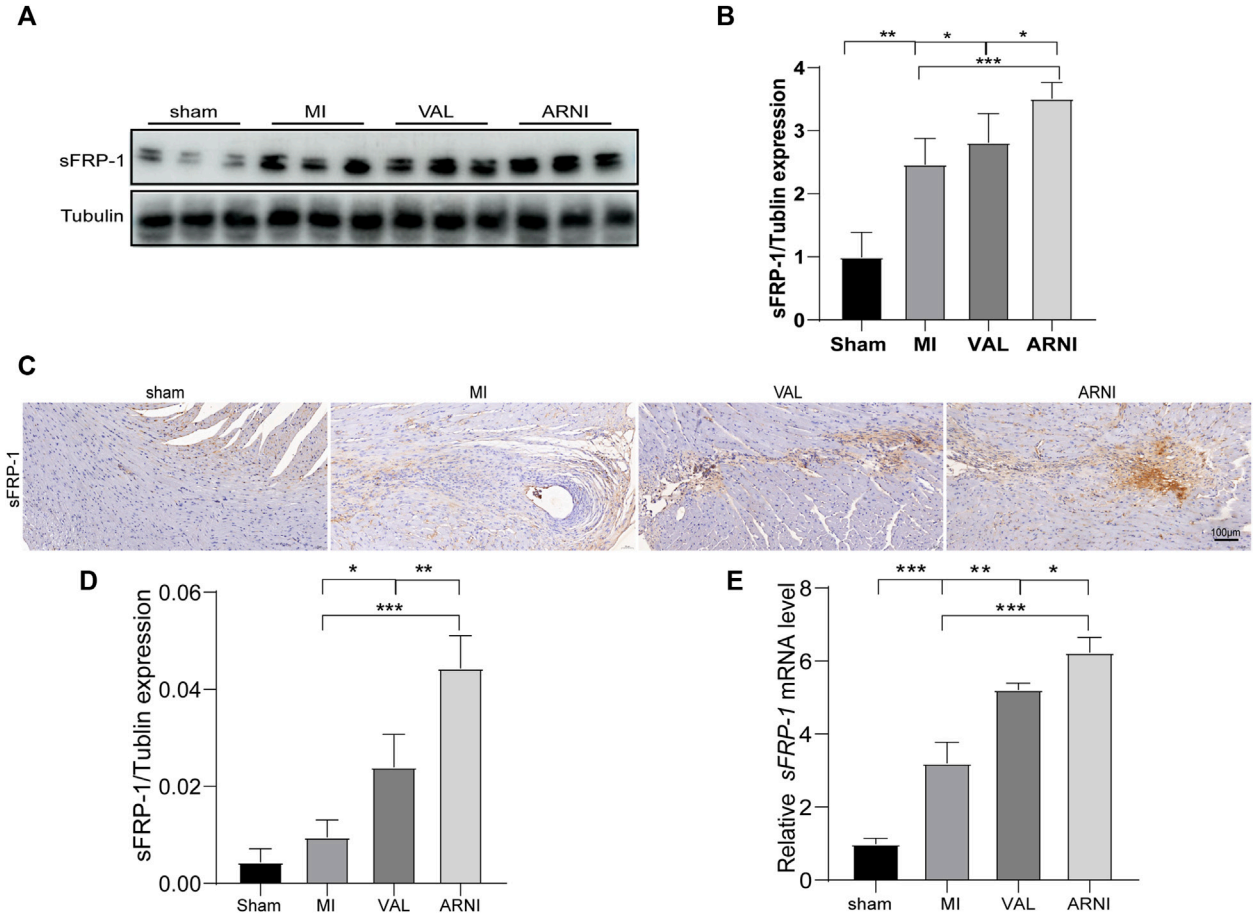

FIGURE 5 | The expression of sFRP-1 after ARNI and VAL intervention. **(A,B)** Western blot analysis of the expression of sFRP-1. **(C,D)** Immunohistochemistry staining of sFRP-1. **(E)** Relative mRNA expression level of sFRP-1. Each group n = 7.*p < 0.01,**p < 0.05, ***p < 0.001.

vicious cycle, leading to myocardial fibrosis; meanwhile, activation of β-catenin can stimulate the expression of ANP and BNP, which are markers for left ventricular dysfunction and cardiac injury (Zhao et al., 2018). We also assessed cardiac expression of ANP and BNP and found that ARNI can reduce the expression of ANP and BNP. Further, studies have shown that Wnt/β-catenin signaling in resident cardiac fibroblasts is required for excessive extracellular matrix gene expression and collagen deposition after cardiac remodeling (Xiang et al., 2017). The results of PicroSirius Red and Masson's trichrome, α-SMA immunofluorescence, and collagen I, III immunohistochemistry are consistent with this observation.

Under general physiological conditions, the Wnt/β-catenin signaling pathway is inactive, and β-catenin is phosphorylated by the GSK-3β degradation complex following phosphorylation, β-catenin is identified and degraded by the ubiquitin-mediated proteasomal degradation pathway, maintaining low levels of expression in the cytoplasm. The canonical Wnt signaling pathway is activated after MI (MacDonald et al., 2009), proteins from the Wnt family can bind to frizzled receptors. This causes an activation of the signal transduction molecule disheveled (Dvl) which, in turn, inhibits the (GSK-3β), the expression level of β-catenin increased. However, we found that the expression of p-GSK-3β was different from the results of previous studies (Gupte et al., 2018), which may be related to the time stage after myocardial infarction (Lal et al., 2014) or likely related different MI areas, such as MI and non-MI areas or maybe lcz696 likely regulating β-catenin and GSK-3β through two independent pathways, this will encourage us to explore further.

this enzyme is responsible for the phosphorylation of β-catenin (van Gijn, 2002). Inhibition of the Wnt signaling pathway can effectively reduce myocardial remodeling and improve cardiac function. In line with these studies, here, we found that the Wnt signaling pathway was activated in the context of MI and that the expression of β-catenin and Dvl-1 was increased. Of note, ARNI treatment prevented the activation of Wnt signaling.

Although studies have shown that inhibiting the Wnt pathway leads to cardioprotective effects in the context of MI in mice, blocking the Wnt signaling pathway has been shown to lead to an increased heart rupture rate (Barandon et al., 2003b). Barandon et al. established an acute MI model using transgenic mice overexpressing sFRP-1 and reported the inhibition of the Wnt

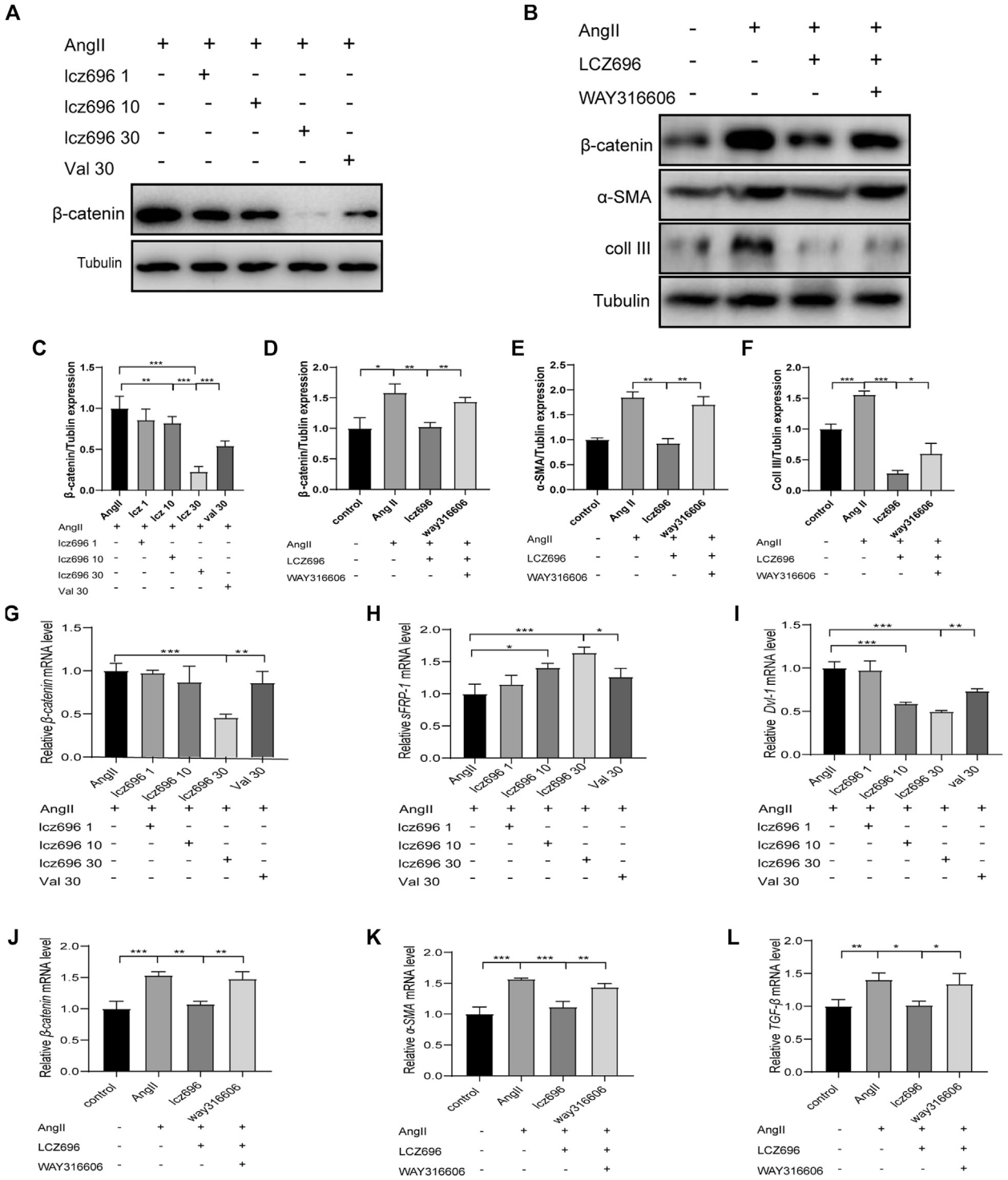

FIGURE 6 | Effects of sFRP-1 on myocardial fibrosis**. (A,C)**Western blot analysis of the β-catenin expression. **(B,D,E,F)**. Western blot analysis of the β-catenin, α-SMA and collagen III expression in the context of way316606 treatment. **(G,H,I).** Relative mRNA expression level of *β-catenin,sFRP-1* and *Dvl-1*.**(J,K,L)** Relative mRNA expression level of *β-catenin, α-SMA* and *TGF-β* in the context of way316606 treatment. Angiotensin II:100 nmol/L; lcz696 1 μmol/L; lcz696 10 μmol/L; lcz696 30 μmol/L; valsartan 30 μmol/L; way316606 2 μmol/L. The experiment was conducted at least 3 times independently,*$p < 0.01$,**$p < 0.05$, ***$p < 0.001$.

pathway after acute MI in mice as well as the consequent reduction in the MI area and rate of heart rupture; thus, sFRP-1 could control the healing process after MI (Alfaro et al., 2010). Therefore, the timely adoption of certain methods to overexpress sFRP-1 after MI can effectively improve the prognosis of MI. Of note, these protective effects are likely due to the inhibition of the over-activation of the Wnt/β-catenin pathway (Alfaro et al., 2010). (Barandon et al., 2011). One interesting finding of the present study is that ARNI could inhibit the activation of the Wnt/β-catenin pathway, and the expression of sFRP-1 was also increased *in vivo*. We speculated that the inhibition of the Wnt/β-catenin pathway by ARNI might be achieved through sFRP-1. To further verify our hypothesis, we stimulated myocardial fibroblasts with AngII *in vitro*, after pre-incubation with lcz696 and Val. Interestingly, the expression of β-catenin was the lowest when 30 μmol/L of ARNI was administered. Additionally, the inhibition of sFRP-1 led to an increased expression of β-catenin. These observations provide novel insights into the mechanism by which inhibition of the Wnt/β-catenin signaling pathway by ARNI might be achieved by influencing the expression of sFRP-1.

Although our study provides new insights into the mechanism of action of ARNI in myocardial fibrosis, the underlying molecular mechanisms are not well understood. Further investigation is required to explore the specific mechanism of the regulation of the Wnt/β-catenin signaling pathway by ARNI.

CONCLUSION

This study confirmed that the Wnt/β-catenin signaling pathway is activated in the context of MI. Importantly, we show that ARNI improves myocardial fibrosis, prevents myocardial remodeling, and inhibits the Wnt/β-catenin signaling pathway via the upregulation of sFRP-1 in the context of MI.

DATA AVAILABILITY STATEMENT

The datasets presented in this study can be found in online repositories. The names of the repository/repositories and accession number(s) can be found in the article/ Supplementary Material.

ETHICS STATEMENT

The animal study was reviewed and approved by the Animal Ethics Committee of Shandong University.

AUTHOR CONTRIBUTIONS

JL: Conceptualization, Methodology, Investigation, Writing-Original draft and Performed the experiments. XHZ: Software, Conceptualization, Visualization, Methodology. CZ: Data curation, Validation, Formal analysis. CMZ: Formal analysis, Visualizationk, Data curation. PB: Supervision, Project administration, Funding acquisition. All authors read and approved the final manuscript.

FUNDING

This work was supported by the State Key Program of National Natural Science Foundation of China 81530014; National Key R&D Plan of China 2017YFC1700502; National Natural Science Foundation for Young Scientists of China 81700366.

ACKNOWLEDGMENTS

We are thankful to Di Wang for technical contribution.

REFERENCES

Alfaro, M. P., Vincent, A., Saraswati, S., Thorne, C. A., Hong, C. C., Lee, E., et al. (2010). sFRP2 suppression of bone morphogenic protein (BMP) and Wnt signaling mediates mesenchymal stem cell (MSC) self-renewal promoting engraftment and myocardial repair. *J. Biol. Chem.* 285, 35645–35653. doi:10.1074/jbc.M110.135335

Barandon, L., Casassus, F., Leroux, L., Moreau, C., Allières, C., Lamazière, J. M., et al. (2011). Secreted frizzled-related protein-1 improves postinfarction scar formation through a modulation of inflammatory response. *Arterioscler Thromb. Vasc. Biol.* 31, e80–7. doi:10.1161/ATVBAHA.111.232280

Barandon, L., Couffinhal, T., Ezan, J., Dufourcq, P., Costet, P., Alzieu, P., et al. (2003). Reduction of Infarct Size and Prevention of Cardiac Rupture in Transgenic Mice Overexpressing FrzA. *Circulation* 108 (18), 2282–2289. doi:10.1161/01.CIR.0000093186.22847.4C

Barandon, L., Couffinhal, T., Ezan, J., Dufourcq, P., Costet, P., and Alzieu, P. (2003). Reductionof infarctsize and prevention of cardiac rupture in transgenic mice overexpressing FrzA. *Circulation* 108, 2282–2289. doi:10.1038/s41401-018-0060-4

Barandon, L., Dufourcq, P., Costet, P., Moreau, C., Allières, C., Daret, D., et al. (2005). Involvement of FrzA/sFRP-1 and the Wnt/frizzled pathway in ischemic preconditioning. *Circ. Res.* 96, 1299–1306. doi:10.1161/01.RES.0000171895.06914.2c

Blankesteijn, W. M., van Gijn, M. E., Essers-Janssen, Y. P., Daemen, M. J., and Smits, J. F. (2000). β-Catenin, an inducer of uncontrolled cell proliferation and migration in malignancies,is localized in the cytoplasm of vascular endothelium during neovascularization after myocardial infarction. *Am. J. Pathol.* 157, 877–883. doi:10.1056/NEJMoa1409077

Burke, R. M., Lighthouse, J. K., Mickelsen, D. M., and Small, E. M., Sacubitril/Valsartan Decreases Cardiac Fibrosis in Left Ventricle Pressure Overload by Restoring PKG Signaling in Cardiac Fibroblasts, 2019. 12(4) e005565.

Campbell, D. J. (2017). Long-term neprilysin inhibition - implications for ARNIs. *Circ. Heart Fail.* 14 (3), 171–186. doi:10.1161/CIRCHEARTFAILURE.118.005565

Chen, L., Wu, Q., Guo, F., Xia, B., and Zuo, J. (2004). Expression of Dishevelled-1 in wound healing after acute myocardial infarction: possible involvement in myofibroblast proliferation and migration. *J. Cel Mol Med* 8, 257–264. doi:10.1111/j.1582-4934.2004.tb00281.x

Eid, R. A., Khalil, M. A., Alkhateeb, M. A., Eleawa, S. M., Zaki, M. S. A., El-Kott, A. F., et al. (2020). Exendin-4 Attenuates Remodeling in the Remote Myocardium of Rats after an Acute Myocardial Infarction by Activating β-Arrestin-2, Protein Phosphatase 2A, and Glycogen Synthase Kinase-3 and Inhibiting β-Catenin. *Cardiovasc. Drugs Ther.* doi:10.1007/s10557-020-07006-9

Fu, W. B., Wang, W. E., and Zeng, C. Y. (2019). Wnt signaling pathways in myocardial infarction and the therapeutic effects of Wnt pathway inhibitors. *Acta Pharmacol. Sin* 40 (1), 9–12.

Gao, E., Lei, Y. H., Shang, X., Huang, Z. M., Zuo, L., Biucher, M., et al. (2010). A Novel and Efficient Model of Coronary Artery Ligation and Myocardial Infarction in the Mouse. *Circ. Res.* 107 (12), 1445–1453. doi:10.1177/1535370219861283

Ge, Q., Zhao, L., Ren, X.-M., Ye, P., and Hu, Z.-Y. (2019). LCZ696, an angiotensin receptor-neprilysin inhibitor, ameliorates diabetic cardiomyopathy by inhibiting inflammation, oxidative stress and apoptosis. *Exp. Biol. Med. (Maywood)* 244, 1028–1039.

Gupte, M., Tumuluru, S., Sui, J. Y., Singh, A. P., Umbarkar, P., Parikh, S. S., et al. (2018). Cardiomyocyte-specific deletion of GSK-3β leads to cardiac dysfunction in a diet induced obesity model. *Int. J. Cardiol.* 259, 145–152.

Kobayashi, K., Luo, M., Zhang, Y., Wilkes, D. C., Ge, G., Grieskamp, T., et al. (2009). Secreted Frizzled-related protein 2 is a procollagen C proteinase enhancer with a role in fibrosis associated with myocardial infarction. *Nat. Cel Biol* 11, 46–55. doi:10.1038/ncb1811

Lal, H., Ahmad, F., Zhou, J., Yu, J. E., Vagnozzi, R. J., Guo, Y., et al. (2014). Cardiac Fibroblast Glycogen Synthase Kinase-3β Regulates Ventricular Remodeling and Dysfunction in Ischemic Heart. *Circulation* 130 (5), 419–430. doi:10.1161/CIRCULATIONAHA.113.008364

Liu, M., Yin, L., Li, W., Hu, J., Wang, H., Ye, B., et al. (2019). C1q/TNF-related protein-9 promotes macrophage polarization and improves cardiac dysfunction after myocardial infarction. *J. Cel. Physiol.* 234, 18731–18747. doi:10.1002/jcp.2851310.1002/jcp.28513

MacDonald, B. T., Tamai, K., and He, X. (2009). Wnt/beta-catenin signaling: components, mechanisms, and diseases. *Dev. Cel* 17 (1), 9–26.

McMurray, J. J., Packer, M., Desai, A. S., Gong, J., Lefkowitz, M. P., Rizkala, A. R., et al. (2014). Angiotensin-neprilysin inhibition versus enalapril in heart failure. *N. Engl. J. Med.* 371, 993–1004.

McMurray, J. J. V., Packer, M., Desai, A. S., Gong, J., Lefkowitz, M. P., Rizkala, A. R., et al. (2014). Angiotensin-Neprilysin Inhibition versus Enalapril in Heart Failure. *N. Engl. J. Med.* 371 (11), 993–1004. doi:10.1056/nejmoa1409077

Mizutani, M., Wu, J. C., and Nusse, R. (2016). Fibrosis of the Neonatal Mouse Heart after Cryoinjury Is Accompanied by Wnt Signaling Activation and Epicardial-to-Mesenchymal Transition. *J. Am. Heart Assoc.* 5, e002457. doi:10.1161/JAHA.115.00245710.1161/JAHA.115.002457

Mozaffarian, D., Mozaffarian, D., Benjamin, E. J., Go, A. S., Arnett, D. K., Blaha, M. J., et al. (2016). Heart Disease and Stroke Statistics-2016 Update: A Report from the American Heart Association. *Circulation* 133, e38–360. doi:10.1161/CIR.0000000000000350

Palevski, D., Levin-Kotler, L. P., Kain, D., Naftali-Shani, N., Landa, N., Ben-Mordechai, T., et al. (2017). Loss of Macrophage Wnt Secretion Improves Remodeling and Function after Myocardial Infarction in Mice. *J. Am. Heart Assoc.* 6 (1), e004387. doi:10.1161/JAHA.116.004387

Ponikowski, P., Voors, A. A., Anker, S. D., Bueno, H., Cleland, J. G., Coats, A. J., et al. (2016). 2016 ESC Guidelines for the diagnosis and treatment of acute and chronic heart failure: The Task Force for the diagnosis and treatment of acute and chronic heart failure of the European Society of Cardiology (ESC). Developed with the special contribution of the Heart Failure Association (HFA) of the ESC. *Eur. J. Heart Fail.* 18, 891–975. doi:10.1002/ejhf.592

Schumann, H., Holtz, J., Zerkowski, H. R., and Hatzfeld, M. (2000). Expression of secreted frizzled related proteins 3 and 4 in human ventricular myocardium correlates with apoptosis related gene expression. *Cardiovasc. Res.* 45, 720–728. doi:10.1016/s0008-6363(99)00376-4

Sklepkiewicz, P., Shiomi, T., Kaur, R., Sun, J., Kwon, S., Mercer, B., et al. (2015). Loss of Secreted Frizzled-Related Protein-1 Leads to Deterioration of Cardiac Function in Mice and Plays a Role in Human Cardiomyopathy. *Circ. Heart Fail.* 8 (2), 362–372. doi:10.1161/circheartfailure.114.001274

Tao, J., Chen, B. D., Ma, Y. T., Yang, Y. N., Li, X. M., Ma, X., et al. (2015). FrzA gene protects cardiomyocytes from H2O2-induced oxidative stress through restraining the Wnt/Frizzled pathway. *Lipids Health Dis.* 14 (1), 90. doi:10.1186/s12944-015-0088-0

van den Borne, S. W., Diez, J., Blankesteijn, W. M., Verjans, J., Hofstra, L., and Narula, J. (2010). Myocardial remodeling after infarction: the role of myofibroblasts. *Nat. Rev. Cardiol.* 7, 30–37. doi:10.1038/nrcardio.2009.199

van Gijn, M. E. (2002). The wnt-frizzled cascade in cardiovascular disease. *Cardiovasc. Res.* 55 (1), 16–24.

von Lueder, T. G. (2015). Angiotensin Receptor Neprilysin Inhibitor LCZ696 Attenuates Cardiac Remodeling and Dysfunction after Myocardial Infarction by Reducing Cardiac Fibrosis and Hypertrophy. *Circ. Heart Fail.* 8 (1), 71–78.

von Lueder, T. G., Wang, B. H., Kompa, A. R., Huang, L., Webb, R., Jordaan, P., et al. (2015). Angiotensin Receptor Neprilysin Inhibitor LCZ696 Attenuates Cardiac Remodeling and Dysfunction after Myocardial Infarction by Reducing Cardiac Fibrosis and Hypertrophy. *Circ. Heart Fail.* 8 (1), 71–78. doi:10.1161/circheartfailure.114.001785

Voors, A. A., Dorhout, B., and van der Meer, P. (2013). The potential role of valsartan+AHU377 (LCZ696) in the treatment of heart failure. *Expert Opin. Investig. Drugs* 22, 1041–1047.

Xia, Y., Chen, Z., Chen, A., Dong, M. Z., Hu, K., Yang, X., et al. (2017). LCZ696 improves cardiac function via alleviating Drp1-mediated mitochondrial dysfunction in mice with doxorubicin-induced dilated cardiomyopathy. *J. Mol. Cel Cardiol* 108, 138–148. doi:10.1016/j.yjmcc.2017.06.003

Xiang, F. L., Fang, M., and Yutzey, K. E. (2017). Loss of β-catenin in resident cardiac fibroblasts attenuates fibrosis induced by pressure overload in mice. *Nat. Commun.* 8 (1), 712. doi:10.1038/s41467-017-00840-w.30.MacDonald

Zhao, Y., Wang, C., Wang, C., Hong, X., Miao, J., Liao, Y., et al. (2018). An essential role for Wnt/β-catenin signaling in mediating hypertensive heart disease. *Sci. Rep.* 8 (1), 8996. doi:10.1038/s41598-018-27064-2.29.Xiang

Zile, M. R., O'Meara, E., Claggett, B., Prescott, M. F., Solomon, S. D., Swedberg, K., et al. (2019). Effects of Sacubitril/Valsartan on Biomarkers of Extracellular Matrix Regulation in Patients with HFrEF. *J. Am. Coll. Cardiol.* 73 (7), 795–806. doi:10.1016/j.jacc.2018.11.042

Conflict of Interest: The authors declare that the research was conducted in the absence of any commercial or financial relationships that could be construed as a potential conflict of interest.

Publisher's Note: All claims expressed in this article are solely those of the authors and do not necessarily represent those of their affiliated organizations, or those of the publisher, the editors and the reviewers. Any product that may be evaluated in this article, or claim that may be made by its manufacturer, is not guaranteed or endorsed by the publisher.

frontiers in Pharmacology

ORIGINAL RESEARCH
published: 10 September 2021
doi: 10.3389/fphar.2021.729568

Effects of Trandolapril on Structural, Contractile and Electrophysiological Remodeling in Experimental Volume Overload Heart Failure

*Dagmar Jarkovská[1,2], Matúš Miklovič[3,4], Jitka Švíglerová[1,2], Luděk Červenka[3,4], Petra Škaroupková[3], Vojtěch Melenovský[5] and Milan Štengl[1,2]**

[1]Department of Physiology, Faculty of Medicine in Pilsen, Charles University, Pilsen, Czechia, [2]Biomedical Center, Faculty of Medicine in Pilsen, Charles University, Pilsen, Czechia, [3]Center for Experimental Medicine, Institute for Clinical and Experimental Medicine, Prague, Czechia, [4]Department of Pathophysiology, 2nd Faculty of Medicine, Charles University, Prague, Czechia, [5]Department of Cardiology, Institute for Clinical and Experimental Medicine, Prague, Czechia

Chronic volume overload induces multiple cardiac remodeling processes that finally result in eccentric cardiac hypertrophy and heart failure. We have hypothesized that chronic angiotensin-converting enzyme (ACE) inhibition by trandolapril might affect various remodeling processes differentially, thus allowing their dissociation. Cardiac remodeling due to chronic volume overload and the effects of trandolapril were investigated in rats with an aortocaval fistula (ACF rats). The aortocaval shunt was created using a needle technique and progression of cardiac remodeling to heart failure was followed for 24 weeks. In ACF rats, pronounced eccentric cardiac hypertrophy and contractile and proarrhythmic electrical remodeling were associated with increased mortality. Trandolapril substantially reduced the electrical proarrhythmic remodeling and mortality, whereas the effect on cardiac hypertrophy was less pronounced and significant eccentric hypertrophy was preserved. Effective suppression of electrical proarrhythmic remodeling and mortality but not hypertrophy indicates that the beneficial therapeutic effects of ACE inhibitor trandolapril in volume overload heart failure might be dissociated from pure antihypertrophic effects.

Keywords: cardiac remodeling, volume overload, aortocaval fistula, rat, renin-angiotensin-aldosterone system, trandolapril

OPEN ACCESS

Edited by:
Helene Tronchere, Institut National de la Santé et de la Recherche Médicale (INSERM), France

Reviewed by:
Ahmed F. El-Yazbi, Alexandria University, Egypt
Oscar Casis, Universidad del País Vasco UPV/EHU, Spain

****Correspondence:***
Milan Štengl
milan.stengl@lfp.cuni.cz

Specialty section:
This article was submitted to Cardiovascular and Smooth Muscle Pharmacology, a section of the journal Frontiers in Pharmacology

Received: *23 June 2021*
Accepted: *31 August 2021*
Published: *10 September 2021*

Citation:
Jarkovská D, Miklovič M, Švíglerová J, Červenka L, Škaroupková P, Melenovský V and Štengl M (2021) Effects of Trandolapril on Structural, Contractile and Electrophysiological Remodeling in Experimental Volume Overload Heart Failure. Front. Pharmacol. 12:729568. doi: 10.3389/fphar.2021.729568

INTRODUCTION

Heart failure (HF) is a complex clinical syndrome characterized by cardiac dysfunction, i.e., the inability to maintain sufficient cardiac output, and myocardial structural abnormalities including hypertrophy and dilated cardiomyopathy. It is considered an epidemic disease in the modern world, affecting approximately 1–2% of the adult population and its prevalence is increasing (Savarese and Lund, 2017). HF is a multifactorial and systemic disease; the most common etiologies are ischemic heart disease, hypertension, and diabetes (Lloyd-Jones et al., 2002). HF activates a variety of structural, neurohumoral, cellular, and molecular mechanisms, which compensate for the decrease in mean arterial pressure due to reduced cardiac output (Kemp and Conte, 2012). These compensatory responses comprise the Frank-Starling Law, mainly in the early stages of HF (Westerhof and O'Rourke, 1995), stimulation of the sympathetic nervous system with release of

catecholamines (Chaggar et al., 2009), activation of the renin-angiotensin-aldosterone-system (RAAS) (Ruzicka et al., 1993; Ruzicka et al., 1995; Rea and Dunlap, 2008), ventricular remodeling (Schirone et al., 2017), and the release of many neurohormones with vasoactive effects (Kim and Januzzi, 2011). Despite the early beneficial effects, long-term sympathetic and RAAS activations result in maladaptive ventricular remodeling with deleterious effects on cardiac function and accelerated progression of HF (Lee and Tkacs, 2008; Triposkiadis et al., 2009). The significant role of RAAS in HF progression is also supported by a number of beneficial effects of drugs affecting this signaling pathway such as ACE inhibitors, angiotensin receptor blockers and mineralocorticoid receptor antagonists (Orsborne et al., 2017).

Rats with chronic volume overload due to aortocaval fistula (ACF rats) represent a well-characterized, reproducible and simple model of heart failure (Abassi et al., 2011). This model was adapted from dogs to rats in the early 1970s (Stumpe et al., 1973; Hatt et al., 1979; Hatt et al., 1980) and simplified by the needle procedure in the early 1990s (Garcia and Diebold, 1990). The model reproduces several characteristic features of human heart failure, e.g. gradual development from asymptomatic into decompensated phase, cardiac hypertrophy and dilatation as well as myocardial remodeling (Liu et al., 1991a; Liu et al., 1991b), elevated cardiac filling pressures, diminished effective cardiac output (despite elevated total cardiac output in ACF rats), neurohumoral activation and altered calcium handling (Flaim et al., 1979; Lee and Tkacs, 2008; Abassi et al., 2011). Special features distinct from those of pressure overload and infarction models include a lack of fibrosis and inflammation as well as the activation of different signaling pathways (Ruzicka et al., 1994; Toischer et al., 2010). Cardiac hypertrophy is often associated with increased susceptibility to ventricular arrhythmias and sudden cardiac death due to electrical remodeling with action potential prolongation, altered electrotonic coupling among the cells, slower conduction, and dispersion of refractoriness (Hill, 2003).

In this study we have hypothesized that multiple remodeling processes due to volume overload might be affected differentially by chronic ACE inhibition possibly allowing their dissociation. The objectives were to describe volume overload-induced structural, contractile and electrophysiological cardiac remodeling and to analyze the effects of chronic trandolapril administration on remodeling processes as well as on overall mortality.

MATERIALS AND METHODS

Animal handling was in accordance with the European Directive for the Protection of Vertebrate Animals Used for Experimental and Other Scientific Purposes (86/609/EU). The experiments were approved by the Committee for Experiments on Animals of the Charles University Faculty of Medicine in Pilsen and by the Ministry of Education, Youth and Sports of the Czech Republic (Protocol No. MZ-5809/2015-OZV-30.0-5.2.15). In this study, 62 Hannover Sprague-Dawley male rats (8 weeks old) were used. The animals were divided into three groups: sham-operated rats (sham surgery and placebo treatment), ACF rats (aortocaval fistula and placebo treatment), and ACF rats with trandolapril (aortocaval fistula and trandolapril treatment). The drug treatment started 4 weeks after the surgery and continued for 20 weeks. Experimental time points of 4 weeks (start of trandolapril treatment) and 24 weeks (*in vivo* and *in vitro* analyses) after surgery were chosen based on previous studies and our experience with the model. The time point of 4 weeks after surgery represents the compensatory stage with eccentric dilation, moderately impaired pump function and minimal mortality (Brower et al., 1996; Brower and Janicki, 2001; Ryan et al., 2007), in which reverse cardiac remodeling can be induced by therapeutic intervention (Hutchinson et al., 2011; Brower et al., 2015). The time point of 24 weeks after surgery was chosen as the end point, at which overt congestive heart failure should be developed in most animals (Brower and Janicki, 2001) and the mortality still allows a systematic analysis of cardiac function (Oliver-Dussault et al., 2010; Melenovsky et al., 2012). Trandolapril was administered in drinking water, 6 mg/L (Gopten; Abbot, Prague, Czech Republic). The dosing was based on previous studies (Červenka et al., 2015a; Červenka et al., 2015b), in which the effective suppression of angiotensin II plasma and tissue levels was demonstrated. In the placebo groups, the animals were given tap water.

Surgery

Prior to the surgery the animals were anaesthetized using ketamine and midazolam applied intraperitoneally (Calypsol, Gedeon Richter, Hungary, 160 mg/kg and Dormicum, Roche, France, 160 mg/kg). The aortocaval fistula was created as described previously (Garcia and Diebold, 1990). The abdominal aorta was pierced into the inferior vena cava by an 18-gauge needle (1.2 mm in diameter). A bulldog vascular clamp was placed across the caudal aorta, the needle was removed, and an acrylamide tissue glue (Histoacryl, B.Braun AG, Germany) was applied at the puncture point. After 30 s, the clamp was removed and the aortocaval shunt was checked visually by vena cava pulsation. The sham-operated rats underwent only opening and closing of the abdominal cavity, without the aortocaval fistula procedure. As post-operative analgesia, meloxicam (1–2 mg/kg/day SC) was given for 2–3 days.

In Vivo Experiments

Cardiac examination was performed 24 weeks after the surgery on anaesthetized animals (50 mg/kg of ketamine and 5 mg/kg of midazolam i.p.). Electrocardiography (ECG) was measured as previously (Sedmera et al., 2016) (sham-operated rats, $n = 13$; ACF rats, $n = 10$; and ACF rats with trandolapril, $n = 9$). In brief, four ECG leads were recorded using FE 132 Bioamp and Powerlab 8 (ADInstuments, Ltd., Australia) at a sampling rate of 1 kHz. Offline analyses of 200 consecutive beats in the lead with the least noise from each recording was performed in LabChart Pro 7 (ADInstruments, Ltd.). The beats chosen by the software classifier as good ones were averaged and the program measured the RR intervals, PR intervals, QRS intervals, and QT intervals

automatically. The QTc intervals were determined using Bazett's formula normalized to the average RR interval [QTc = QT/(RR/f)$^{1/2}$, f = 160 ms], (Kmecova and Klimas, 2010).

Echocardiography (sham-operated rats, n = 15; ACF rats; n = 15, and ACF rats with trandolapril, n = 15) was performed with a 10 MHz probe (Vivid System 5, GE, United States). The aortic blood pressure (sham-operated rats, n = 13; ACF rats, n = 14; and ACF rats with trandolapril, n = 14) was measured using Powerlab 8 (ADInstruments Ltd.) and a 2F micro-manometer catheter (Millar Instruments, TX, United States) put into the aorta and left ventricle via the carotid artery. The offline analysis was made in LabChart Pro 7 (ADInstruments Ltd.) (Melenovsky et al., 2018).

In Vitro Experiments

The animals were sacrificed by cervical dislocation 24 weeks after the surgery. The hearts were excised, weighed, and used either for multicellular (sham-operated rats, n = 12; ACF rats, n = 10; and ACF rats with trandolapril, n = 10) or for cellular (8 cells/3 rats in each group) experiments. The multicellular experiments included measurements of atrial electrical activity in isolated atria and of contraction force and membrane potential in ventricular trabeculae from the left ventricles. The spontaneous atrial activity was recorded in a warm oxygenated (37°C) experimental chamber filled with Tyrode solution (in mmol/L: NaCl 137, KCl 4.5, $MgCl_2$ 1, $CaCl_2$ 2, glucose 10, and HEPES 5; pH was adjusted to 7.4 with NaOH; all chemicals were purchased from Sigma-Aldrich, Czech Republic) using Biopac System (Biopac Systems Inc., Santa Barbara, CA, United States). After a 5-min stabilization period, norepinephrine was added to the bath solution to increase the concentration every 3 min (10^{-8}, 10^{-7}, 10^{-6}, 10^{-5}, and 10^{-4} mol/L). Analysis of the acquired signal was performed offline using Biopac Student Lab PRO 3.7.2 (Biopac Systems Inc., Santa Barbara, CA, United States). Values of the heart rate obtained from this analysis were normalized to the heart rate in the control solution (Tyrode solution without norepinephrine).The ventricular preparations (trabeculae isolated from the left ventricle) were placed into a measurement chamber perfused with oxygenated warm (37°C) Tyrode solution (in mmol/L: NaCl 137, KCl 4.5, $MgCl_2$ 1, $CaCl_2$ 2, glucose 10, and HEPES 5; the pH was adjusted to 7.4 with NaOH; all chemicals were purchased from Sigma-Aldrich, Czech Republic) and stimulated at various frequencies (0.5, 1, 2, 3, and 5 Hz; Pulsemaster Multi-Channel Stimulator A300, World Precision Instruments, Inc., FL, United States). Contraction force was measured by an isometric force transducer (model F30; Hugo Sachs Electronik, Harvard Apparatus, GmBH, Germany) and membrane potential was measured using glass microelectrodes filled with 3M KCl (resistance >20 MΩ; Microelectrode Puller P-1000, Sutter Instruments, CA, United States). Action potential duration at 75% repolarization and maximal contraction force were measured offline in 10 consecutive beats by in-house software made in MATLAB 2014b (MathWorks Inc., MA, United States). These results were averaged and used for statistical analysis.

The ventricular cardiomyocytes were isolated by enzymatic dissociation. After excision of the heart, the aorta was cannulated and the heart was mounted to a constant-pressure Langendorff apparatus, where it was perfused with warm (37°C) oxygenated solution: 1) 3 min Ca^{2+}-free Tyrode solution; 2) 12 min 0.5 mmol/L Ca^{2+} Tyrode solution with collagenase A (1 g/L, Sigma-Aldrich) and bovine serum albumin (0.5 g/L, Sigma-Aldrich); 3) 3 min Ca^{2+}-free Tyrode solution. The digested ventricular tissue was cut into cubic pieces (1 mm^3), mechanically agitated and the debris filtered. The Ca^{2+} concentration in the solution with cardiomyocytes was gradually (1 µmol/L, 5 µmol/L, 10 µmol/L, 0.1 mmol/L) increased up to 0.2 mmol/L. Calcium transients and sarcomeric contractions were measured by Ionoptix HyperSwitch Myocyte Calcium and Contractility System (IonOptix LLC, CA, United States) with the Sarclen sarcomere length acquisition module. The cardiomyocytes were incubated in 1 mmol/L Fura-2-AM solution (Molecular Probes, Invitrogen, MA, United States) dissolved in dimethyl sulfoxide (Sigma-Aldrich) for 20 min in 2 mmol/L Ca^{2+} Tyrode solution. After the incubation, the cells were washed with 2 mmol/L Ca^{2+} Tyrode solution repeatedly. During the measurement, the cardiomyocytes were placed in an experimental chamber perfused with warm (37°C) 2 mmol/L Ca^{2+} Tyrode solution and stimulated with the MyoPacer Field Stimulator (IonOptix LLC, CA, United States) at various frequencies (0.5, 1, 2, 3, and 5 Hz). Offline analysis of the calcium transients and the sarcomeric length was realized in IonWizard 6.5 (IonOptix LLC, CA, United States).

Statistical Analysis

The results of the experiments (presented as mean ± SD) were checked for normality distribution using the Shapiro-Wilk test and outliers were excluded by the Grubbs test. The boxplots show mean (dot), median (horizontal line), SD (box) and max-min (whiskers). The comparisons were made with a one-way ANOVA test followed by a post hoc Tukey test to determine possible significant differences between the experimental groups. The two-way mixed-design ANOVA (with stimulation frequency as a repeated-measures factor and experimental groups as a non-repeated-measures factor), followed by a post hoc Tukey test was used to analyze the results of *in vitro* experiments. Survival analysis was performed with the Kaplan-Meier estimator. The incidence of spontaneous activity in ventricular cardiomyocytes was compared by Fisher's exact test between experimental groups; $p < 0.05$ was considered statistically significant. The whole statistical analysis described above was performed in OriginPro 2019 (OriginLab Corporation, Northampton, MA, United States).

RESULTS

In ACF rats, the administration of trandolapril significantly improved the survival rate (**Figure 1A**) to values similar to sham-operated animals (24 weeks after surgery survived 100% of sham-operated animals, 52% of ACF rats, and 86% of ACF rats with trandolapril). Chronic volume overload in ACF rats induced the development of cardiac hypertrophy in both left and right ventricles (**Figures 1B–D**). The hypertrophy was slightly

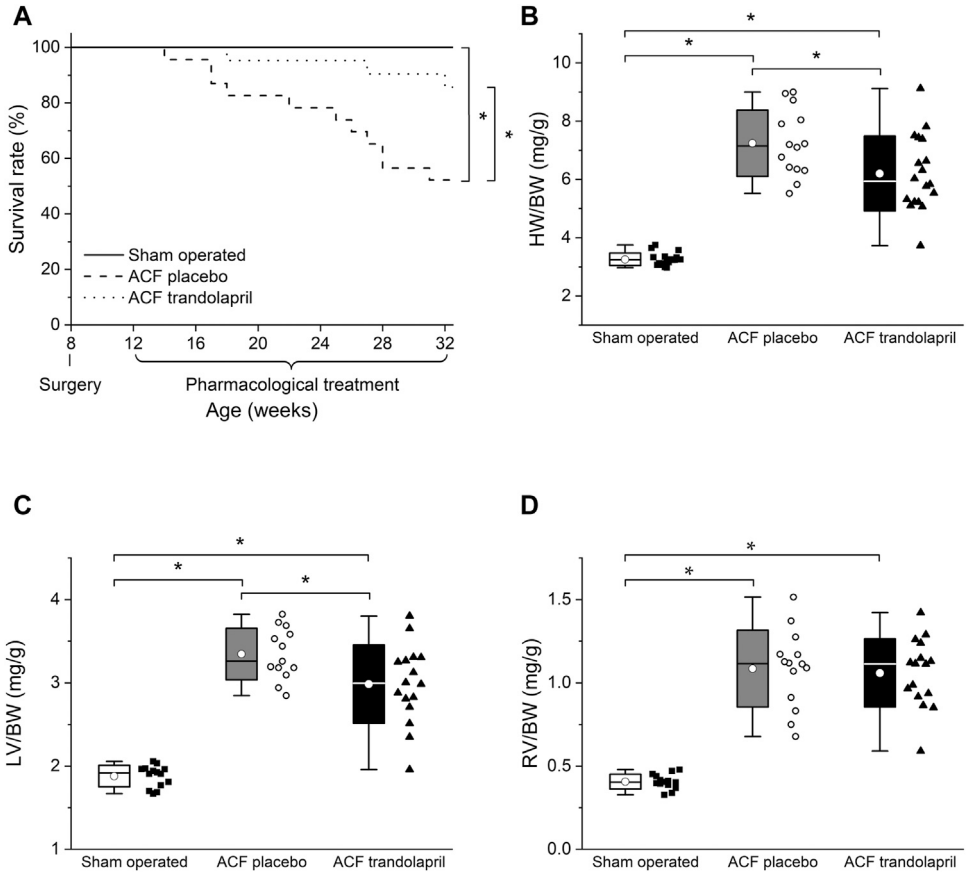

FIGURE 1 | Survival and heart weights. **(A)** Survival rates in sham-operated rats (n = 18), ACF rats (n = 23) and ACF rats with trandolaprl (n = 21). **(B)** Heart weight to body weight ratios in sham-operated rats (n = 12), ACF rats (n = 10) and ACF rats with trandolapril (n = 10). **(C)** Left ventricle weight to body weight ratios in sham-operated rats (n = 12), ACF rats (n = 10) and ACF rats with trandolapril (n = 10). **(D)** Right ventricle weight to body weight ratios in sham-operated rats (n = 12), ACF rats (n = 10) and ACF rats with trandolapril (n = 10). *$p < 0.05$.

attenuated by trandolapril in the left ventricle (**Figure 1C**; left ventricle weight to body weight ratio of 1.88 ± 0.13 mg/g in sham-operated rats, of 3.35 ± 0.31 mg/g in ACF rats, and of 2.98 ± 0.47 mg/g in ACF rats with trandolapril), but not in the right ventricle (**Figure 1D**; right ventricle weight to body weight ratio of 0.41 ± 0.04 mg/g in sham-operated rats, of 1.09 ± 0.23 mg/g in ACF rats, and of 1.06 ± 0.21 mg/g in ACF rats with trandolapril).

Electrocardiographic analysis revealed similar heart rates, PR and QTc intervals in all three experimental groups (**Figures 2A–D**). The QRS interval was significantly prolonged in ACF rats; this effect was suppressed by the administration of trandolapril (**Figure 2E**; QRS interval of 29 ± 4 ms in sham-operated rats, of 38 ± 11 ms in ACF rats, and of 26 ± 2 ms in ACF rats with trandolapril).

Echocardiographic measurements showed a significant reduction of left ventricular fractional shortening in ACF rats, which was partially reversed by trandolapril (**Figure 3A**). The left ventricular diameters and volumes were markedly increased in ACF rats, but significantly less in ACF rats treated with trandolapril (**Figures 3B,C**; **Table 1**). Left ventricular posterior wall and septal thickness was decreased in ACF rats and trandolapril did not affect it (**Table 1**). Systemic vascular resistance was substantially reduced in ACF rats and remained low in the presence of trandolapril (**Table 1**). Cardiac output was increased in ACF rats regardless of trandolapril treatment (**Table 1**). Mean arterial (aortic) blood pressure was decreased only in ACF rats treated with trandolapril (**Figure 3D**), due to a decrease in both systolic and diastolic blood pressures (**Table 1**).The lung/body weight ratio was increased in ACF rats as well as in ACF rats with trandolapril, whereas the liver/body weight ratio was not influenced by either intervention (**Table 1**).

In isolated atria, the norepinephrine-induced increase in heart rate was significantly reduced in ACF rats, and treatment with trandolapril did not affect it (**Figure 4A**; heart rate increased by 96 ± 35% in sham-operated rats, by 36 ± 17% in ACF rats, and by 43 ± 15% in ACF rats with trandolapril at norepinephrine concentration of 10^{-5} mol/L). In left ventricle isolated trabeculae, the contraction force was similar in all three groups regardless of stimulation frequency (**Figure 4B**). Action potential duration was significantly prolonged in ACF rats at all stimulation frequencies (1–5 Hz) and treatment with trandolapril

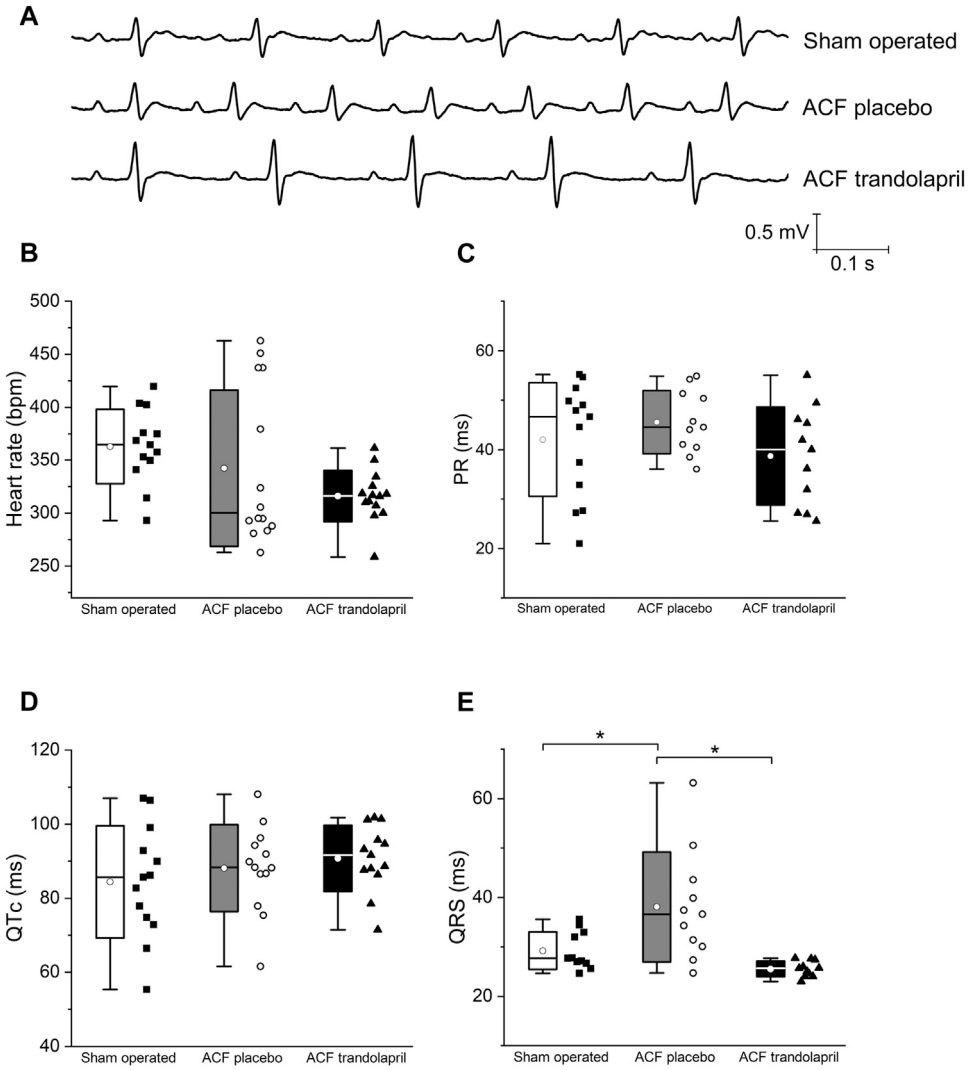

FIGURE 2 | Electrocardiographic intervals. **(A)** Representative ECG tracings in a sham-operated rat, an ACF rat, and an ACF rat with trandolapril. **(B)** Heart rates in sham-operated rats (n = 13), ACF rats (n = 10) and ACF rats with trandolapril (n = 9). **(C)** PR intervals in sham-operated rats (n = 13), ACF rats (n = 10) and ACF rats with trandolapril (n = 9). **(D)** QTc intervals in sham-operated rats (n = 13), ACF rats (n = 10) and ACF rats with trandolapril (n = 9). **(E)** QRS intervals in sham-operated rats (n = 13), ACF rats (n = 10) and ACF rats with trandolapril (n = 9). *p < 0.05.

suppressed the prolongation (**Figures 4C,D**; APD_{75} of 47 ± 11 ms in sham-operated rats, of 107 ± 20 ms in ACF rats, and of 69 ± 24 ms in ACF rats with trandolapril at stimulation frequency of 0.5 Hz). Similar results were obtained also for right ventricle papillary muscles (not shown).

Baseline Fura-2 fluorescence ratios that reflect intracellular Ca^{2+} concentration in isolated ventricular myocytes at rest were higher in cells from ACF rats, both treated and untreated with trandolapril (**Figure 5A**; baseline fluorescence ratio of 0.45 ± 0.05 in sham-operated rats, of 0.53 ± 0.06 in ACF rats, and of 0.56 ± 0.06 ms in ACF rats with trandolapril at stimulation frequency of 0.5 Hz). Ca^{2+} transient amplitudes of Fura-2 fluorescence ratios were not significantly different (**Figure 5B**). The intracellular Ca^{2+} levels corresponded well with sarcomeric lengths, which were at baseline the highest in myocytes from sham-operated rats (**Figure 5C**; baseline sarcomeric length of 1.79 ± 0.04 μm in sham-operated rats, of 1.74 ± 0.05 μm in ACF rats, and of 1.72 ± 0.02 μm in ACF rats with trandolapril at stimulation frequency of 0.5 Hz) and the contraction shortenings were similar in all experimental groups (not shown). In isolated ventricular myocytes, spontaneous activity was observed. The incidence of spontaneous activity was increased in myocytes from ACF rats and this increase was suppressed by trandolapril treatment, both during period of regular pacing (spontaneous activity developed in 8 out of 18 sham myocytes, in 12 out of 12 ACF myocytes and in 4 out of 12 ACF+trandolapril myocytes) and period of recovery after fast pacing (spontaneous activity developed in 1 out of 18 sham myocytes, in 10 out of 12 ACF myocytes and in 0 out of 12 ACF+trandolapril myocytes; **Figure 5D**).

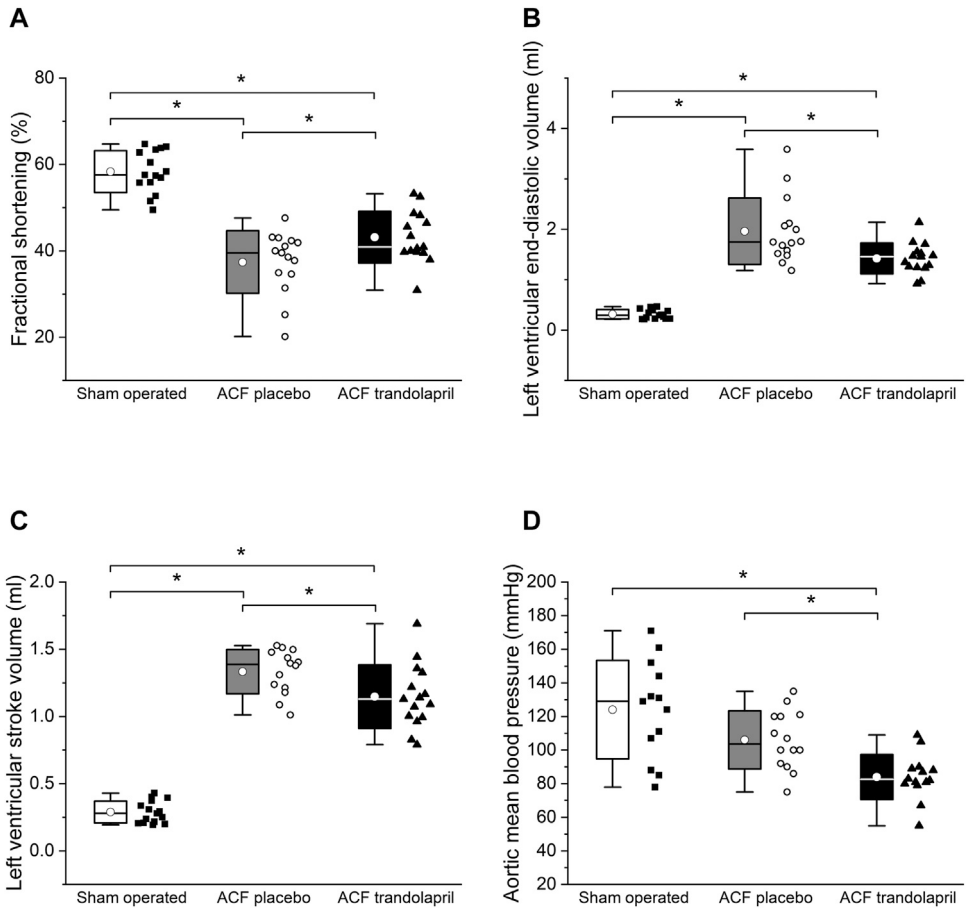

FIGURE 3 | Hemodynamics by echocardiography. **(A)** Left ventricular fractional shortening in sham-operated rats (n = 15), ACF rats (n = 15) and ACF rats with trandolapril (n = 15). **(B)** Left ventricular end-diastolic volume in sham-operated rats (n = 15), ACF rats (n = 15) and ACF rats with trandolapril (n = 15). **(C)** Left ventricular stroke volume in sham-operated rats (n = 15), ACF rats (n = 15) and ACF rats with trandolapril (n = 15). **(D)** Mean arterial (aortic) blood pressure in sham-operated rats (n = 13), ACF rats (n = 14) and ACF rats with trandolapril (n = 14). *$p < 0.05$.

TABLE 1 | Echocardiography.

Parameter	Sham operated	ACF placebo	ACF trandolapril
End-diastolic left ventricular internal diameter (mm)	6.73 ± 0.65	12.39 ± 1.29*	11.19 ± 0.8*,#
End-systolic left ventricular internal diameter (mm)	2.81 ± 0.51	7.82 ± 1.67*	6.38 ± 0.93*,#
End-diastolic interventricular septal thickness (mm)	2.41 ± 0.24	1.84 ± 0.18*	1.86 ± 0.28*
Left ventricular posterior wall thickness (mm)	2.68 ± 0.29	2.13 ± 0.22*	1.93 ± 0.22*
Systemic vascular resistance (dyn·s/cm^5)	1730 ± 426	349 ± 76*	290 ± 72*
Left ventricular cardiac output/body weight (mL/min/g)	0.23 ± 0.05	0.83 ± 0.11*	0.83 ± 0.15*
Aortic systolic blood pressure (mmHg)	138 ± 31	130 ± 22	102 ± 13*,#
Aortic diastolic blood pressure (mmHg)	109 ± 28	83 ± 15*	66 ± 13*
Lung weight/body weight (mg/g)	4.13 ± 1.14	5.18 ± 1.00*	5.51 ± 1.21*
Liver weight/body weight (mg/g)	35.7 ± 5.3	29.5 ± 3.8	30.6 ± 8.1

*Significantly different from sham operated, $p < 0.05$.
#Significantly different from ACF placebo, $p < 0.05$.

DISCUSSION

Chronic volume overload due to aortocaval fistula led to pronounced cardiac hypertrophy (both left and right ventricles) and increased mortality. Trandolapril substantially reduced the mortality; the effect on cardiac hypertrophy, however, was less pronounced and significant hypertrophy was preserved in ACF rats with trandolapril treatment. Echocardiography revealed decreased fractional shortening in ACF rats, which was only moderately and incompletely

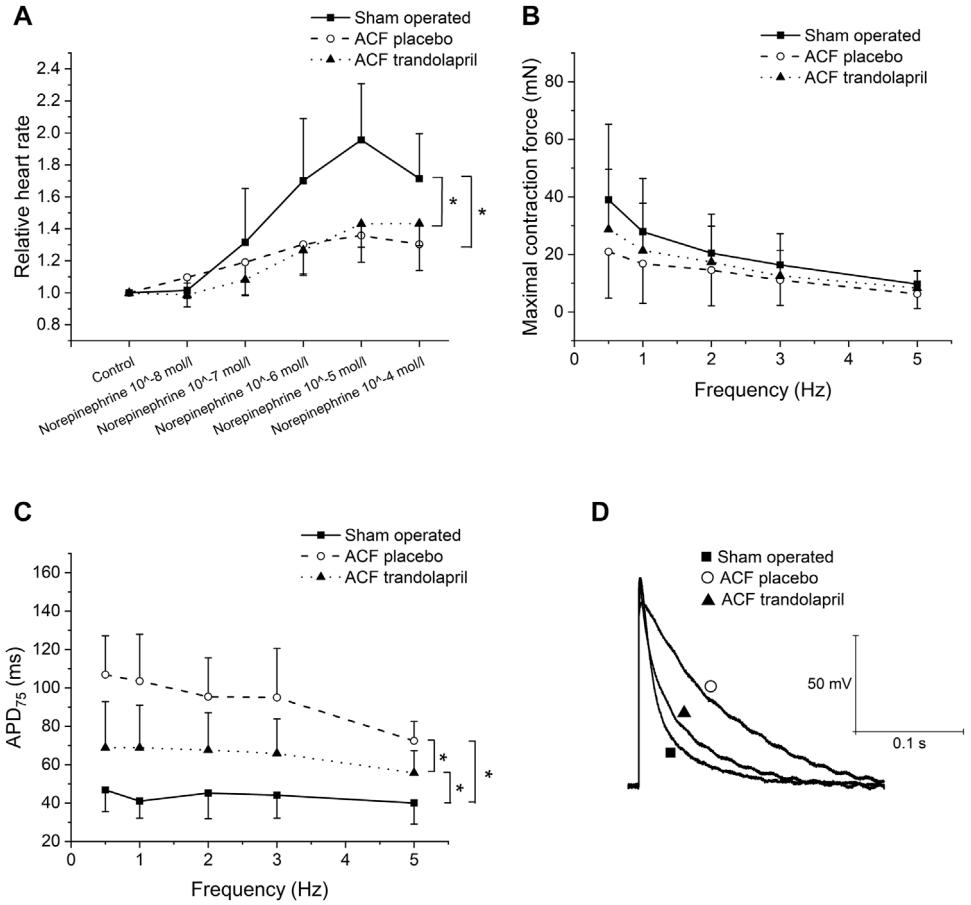

FIGURE 4 | Isolated cardiac tissue. **(A)** Effect of norepinephrine on spontaneous activity of isolated atria from sham-operated rats (n = 12), ACF rats (n = 10) and ACF rats with trandolapril (n = 10). **(B)** Contraction force in left ventricle trabeculae of sham-operated rats (n = 12), ACF rats (n = 10) and ACF rats with trandolapril (n = 10). **(C)** Action potential duration at 75% repolarization (APD_{75}) in left ventricle trabeculae of sham-operated rats (n = 12), ACF rats (n = 10) and ACF rats with trandolapril (n = 10). **(D)** Representative cellular action potentials in left ventricle trabeculae of a sham-operated rat, an ACF rat, and an ACF rat with trandolapril at stimulation frequency of 1 Hz. *p < 0.05.

reversed by trandolapril. *Ex vivo* experiments in isolated cardiac tissues (trabeculae) and ventricular myocytes did not show any significant contractile remodeling, similar to a previous study (Ryan et al., 2007). Several proarrhythmic electrophysiological alterations that developed in ACF rats, including the widening of the QRS complex, prolongation of APD, and increased spontaneous activity of cardiac myocytes, were suppressed by trandolapril treatment. All in all, chronic volume overload was associated with pronounced structural, contractile, and electrophysiological cardiac remodeling, which probably contributed to the increased mortality in ACF rats. Effective suppression of electrophysiological proarrhythmic changes, as well as of mortality, by trandolapril might suggest a significant contribution of arrhythmic deaths to the overall mortality of ACF rats.

In heart failure, defective Ca^{2+} homeostasis, together with electrical remodeling, contributes to enhanced susceptibility to cardiac arrhythmias and arrhythmia-induced sudden death (Luo and Anderson, 2013). Impaired Ca^{2+} handling in failing hearts due to altered expression and/or function of multiple proteins and signaling pathways results in decreased Ca^{2+} transients and elevated diastolic intracellular Ca^{2+} levels (Lou et al., 2012). Electrical remodeling involves changes in various ionic currents leading to prolongation of action potential duration and potential arrhythmogenesis (Cutler et al., 2011). The electrical remodeling and Ca^{2+} homeostasis are closely interconnected through a number of Ca^{2+}-dependent signaling pathways (e.g. Ca^{2+}- and calmodulin-dependent protein kinase II, CaMKII), with intracellular Ca^{2+} emerging as a central player in maladaptive remodeling and arrhythmogenesis (Luo and Anderson, 2013). In ACF rats, diastolic (baseline) intracellular Ca^{2+} levels were increased and action potentials were significantly prolonged. These alterations could contribute to proarrhythmic substrate and/or trigger, as evidenced by increased spontaneous activity in isolated ventricular myocytes. Increased susceptibility to ventricular arrhythmias in ACF rats with a high frequency of ventricular ectopic beats and bursts of ventricular tachycardia degenerating into lethal ventricular fibrillation was also demonstrated in an earlier study (Benes et al., 2011). Since trandolapril suppressed both the manifestations of

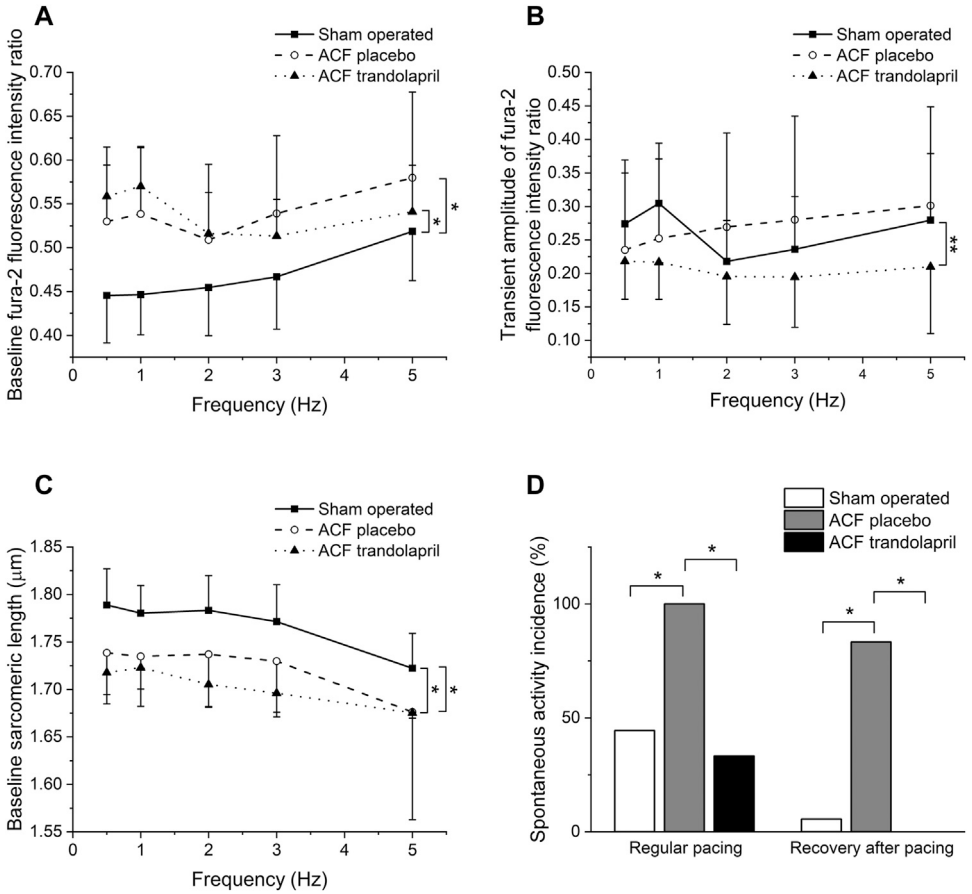

FIGURE 5 | Intracellular Ca^{2+} and sarcomeric length in isolated ventricular myocytes. **(A)** Baseline Fura-2 fluorescence ratios in isolated ventricular myocytes from sham-operated rats (n = 8), ACF rats (n = 8) and ACF rats with trandolapril (n = 8). **(B)** Transient amplitudes of Fura-2 fluorescence ratios in isolated ventricular myocytes from sham-operated rats (n = 8), ACF rats (n = 8) and ACF rats with trandolapril (n = 8). **(C)** Baseline sarcomeric length in isolated ventricular myocytes from sham-operated rats (n = 8), ACF rats (n = 8) and ACF rats with trandolapril (n = 8). **(D)** Incidence of spontaneous activity in isolated ventricular myocytes from sham-operated rats, ACF rats and ACF rats with trandolapril during regular pacing and during recovery after fast (5 Hz) pacing. *p < 0.05.

proarrhythmic substrate (action potential duration prolongation, spontaneous activity, wide QRS complex) and mortality, it is tempting to speculate that arrhythmic deaths contribute significantly to overall mortality and that trandolapril might prevent them through inhibiting proarrhythmic remodeling.

The aortocaval shunt led to a pronounced reduction of total systemic vascular resistance and an increased cardiac output as reported earlier (Liu et al., 1991a; Liu et al., 1991b). The increased cardiac output was due to an increase in stroke volume, the heart rate was not affected. The aortic systolic blood pressure was not changed in ACF rats, whereas the aortic diastolic blood pressure was reduced, again consistent with previous report (Liu et al., 1991b). Increased dimensions of left ventricle, both end-systolic and end-diastolic, with slightly reduced wall thickness, document development of an eccentric hypertrophy in ACF rats. Collectively, these findings support the concept that the chronic volume overload triggers, through increased wall stress and neurohumoral activation, compensatory biventricular hypertrophy, which eventually deteriorates into heart failure (Kehat and Molkentin, 2010). The hemodynamic load, however, is different for the right and left ventricles: whereas in the left ventricle pure volume overload is present, the right ventricle faces a mixed pressure and volume overload, leading to a distinct pattern of activation of cardiac growth factors (Modesti et al., 2004). Differential mechanisms of the left *vs.* right ventricular hypertrophy are also supported by the selective antihypertrophic effect of trandolapril in the left ventricle only (this study). The different sensitivity of ventricles to the antihypertrophic effect of trandolapril might be due to different signaling pathways activated in either ventricle (Modesti et al., 2004) and/or to the differential effects of trandolapril on systemic and pulmonary circulation. In agreement with the latter hypothesis, in a clinical study chronic trandolapril administration was found to reduce mean arterial systemic blood pressure (as shown in our study), but not to influence pulmonary artery pressure (van der Ent et al., 1998).

Multiple beneficial effects of trandolapril have been demonstrated. The antihypertensive effects are based on decreased levels of angiotensin II, catecholamines, and vascular remodeling. In patients with left ventricular systolic dysfunction

due to myocardial infarction, trandolapril decreased the mortality rate, incidence of atrial fibrillation, risk of sudden death, and development of severe heart failure (Diaz and Ducharme, 2008). Similar to clinical studies, multiple vascular and cardiac effects of trandolapril were also demonstrated in animal models (Fornes et al., 1992; Koffi et al., 1998; Tanonaka et al., 2001). The relationships between various levels of cardiac remodeling and trandolapril effects, however, remain unclear. In healthy guinea pig isolated hearts, electrophysiological effects of ACE inhibition were shown; the effects, however, were not substantial enough to produce either antiarrhythmic or proarrhythmic effects (Gilat et al., 1998). In middle-aged spontaneously hypertensive rats, the relationships between structural and electrical remodeling and trandolapril treatment were investigated (Chevalier et al., 1995). The structural remodeling was defined in terms of hypertrophy and fibrosis, with the electrical proarrhythmic remodeling as prevalence of premature ventricular beats. Based on a correspondence analysis, a strong correlation between hypertrophy, fibrosis, and ventricular premature beats was found only for severe hypertrophy; for moderate hypertrophy, the correlation disappeared. This indicates that the electrical remodeling is not always linked to structural remodeling, and additional causal factors (e.g., Ca^{2+} homeostasis) must be taken into account. The results obtained in ACF rats support this view of rather independent structural (hypertrophy) and functional (electrical proarrhythmic) remodeling (at least in the early stages of heart failure), although the hypertrophic phenotype of ACF rats did not include excessive fibrosis (Benes et al., 2011). Whereas the hypertrophy was preserved (only slightly affected) in ACF rats treated with trandolapril, the electrical proarrhythmic remodeling and mortality were almost completely suppressed. It should be realized, however, that only surviving rats were analyzed in tissue and cellular experiments and therefore the most advanced stages of heart failure (i.e., non-survivors) probably were not included. In a study on the long-term outcome of the volume overload rat model, 28% of the animals were found to die without previous heart failure signs, probably due to arrhythmia-related death (Melenovsky et al., 2012).

Besides direct cardiac effects, the vascular effects of trandolapril could also contribute to better ventricular-vascular coupling and improved cardiac function. Reduction of elevated blood pressure by ACE inhibitors including trandolapril was reported to decrease arterial stiffness and pulse wave velocity (Topouchian et al., 1999; Ichihara et al., 2003; Meani et al., 2018), which was associated with a significant regression of cardiac hypertrophy. Nevertheless, preserved cardiac hypertrophy and the absence of hypertension in our model rather argue against this mechanism, although the slight decrease in LV/BW ratio might be attributed to the aortic pressure difference between ACF rats and ACF rats with trandolapril.

After initial beneficial effects of sympathetic stimulation, the chronic activation of adrenergic signaling pathways in heart failure leads to multiple detrimental changes that decrease responsiveness to the adrenergic signaling and impair Ca^{2+} handling (Lou et al., 2012). This was manifested in our study by a significantly lower norepinephrine-induced heart rate elevation *in vitro* in the ACF groups. Similarly, in a porcine volume-overload ACF model the decreased heart rate responsiveness to adrenergic stimulation was described *in vivo* together with increased norepinephrine plasma levels, decreased myocardial norepinephrine content, number of β1-adrenergic receptors, cAMP production, and cardiac G_s-protein (Hammond et al., 1992). In ACF rats, elevated norepinephrine plasma levels with depletion of cardiac norepinephrine stores due to sympathetic denervation were described (Willenbrock et al., 1997; Kristen et al., 2006). An inverse relation between the abundance of sympathetic marker tyrosin hydroxylase and left ventricular hypertrophy severity and/or degree of congestion also suggests a blunted β-adrenergic signaling in this model (Sedmera et al., 2016).

An analysis of interactions of volume overload and of trandolapril on several levels of biological complexity showed some apparent discrepancies. Although an *in vivo* electrocardiogram did not show any significant differences in QT/QTc intervals between the experimental groups, the action potential durations were markedly prolonged in ACF rats. The absence of differences in cardiac repolarization *in vivo* was probably due to relatively high heart rates and complex regulatory mechanisms present *in vivo*. Removal of these superimposed control mechanisms unmasked the intrinsic repolarization differences that reflect a lower repolarization reserve in the hearts of ACF rats and consequently a higher propensity of cardiac myocytes to triggered activity (Varró and Baczkó, 2011). Furthermore, a significant *in vivo* prolongation of QTc interval in ACF rats was shown in a recent study (Wang et al., 2019), in which, however, the duration of volume overload period was shorter (12 weeks *vs.* 24 weeks in our study) and anesthesia was different (chloral hydrate *vs.* ketamine/midazolam in our study) compared to our study. The wide QRS complexes indicate impaired spreading of cardiac excitation in ACF rats, probably due to connexin 43 downregulation and hypophosphorylation (Sedmera et al., 2016). Reduction of echocardiographic fractional shortening in ACF rats was not translated to a corresponding decrease in the contraction force of multicellular preparations or sarcomeric shortening of isolated myocytes. This discrepancy could be related to changes in chamber geometry, differential preload/afterload conditions, and again to the absence of *in vivo* regulatory mechanisms in cellular experiments. Blunted sympathetic regulation (Willenbrock et al., 1997; Kristen et al., 2006; Sedmera et al., 2016) could contribute to the reduced *in vivo* fractional shortening. Furthermore, cellular remodeling might be heterogeneous with transmural, regional, and interventricular differences, as suggested by some discrepant results of our and previous studies (Ryan et al., 2007; Guggilam et al., 2013).

From a clinical point of view, it should be emphasized that volume overload represents a proarrhythmic condition. In a large cohort of patients with isolated mitral valve prolapse, ventricular arrhythmias were frequent although rarely severe. Nevertheless, for arrhythmic mitral valve prolapse, long-term severe arrhythmia was independently associated with notable excess mortality and reduced event-free survival (Essayagh et al., 2020). Similarly, in a porcine model of pulmonary regurgitation and

volume overload, increased incidence of inducible ventricular and atrial arrhythmias was found (Zeltser et al., 2005). Our study indicates that the proarrhythmic remodeling and arrhythmic event risk associated with volume overload can be reduced by angiotensin-converting enzyme inhibitors regardless of their anti-hypertrophic effects. To the best of our knowledge, such a combination of several proarrhythmic factors in volume overload and their regression by ACE inhibitors, together with a reduction of mortality despite preserved hypertrophy, was never shown; this sheds light on the unclear beneficial effects of ACE inhibitors in conditions of volume-overload heart failure. In general, the beneficial effects of ACE inhibitors in heart failure were associated with antihypertrophic effects and attenuation of ventricle enlargement in a number of both experimental and clinical studies (Pfeffer et al., 1992; St John Sutton et al., 1994; Brower et al., 2015). However, in pure volume overload conditions, the effects of ACE inhibitors remain unclear: Although, in rats with aortic regurgitation, ACE inhibitors reduced left ventricle hypertrophy and improved survival (Arsenault et al., 2013), they failed to attenuate left ventricle remodeling in dogs with mitral regurgitation (Dell'italia et al., 1997; Perry et al., 2002) and rats with aortocaval fistula (Ryan et al., 2007). Inconsistent results have also been obtained in patients with aortic insufficiency (Mahajerin et al., 2007). In this context, the evidence of reduced mortality and regression of proarrhythmic electrophysiological remodeling despite the preservation of substantial hypertrophy is novel and suggests the dissociation of antiarrhythmic and antihypertrophic effects of ACE inhibitors in volume overload.

Study Limitations

Although several manifestations of proarrhythmic electrophysiological remodeling were demonstrated in this study, life-threatening ventricular arrhythmias were not documented in our experimental design. Previous studies documented lethal ventricular arrhythmias in ACF rats (Benes et al., 2011) and a significant incidence of arrhythmia-related deaths was suggested (Melenovsky et al., 2012). Telemetric studies that would allow long-term and repeated ECG monitoring, and recording of arrhythmic events will be necessary for understanding mechanisms of arrhythmia initiation and perpetuation in this rat model.

Detailed analyses of both upstream and downstream elements of relevant signaling pathways and remodeling targets were beyond the scope of this study. Proteomic and transcriptomic analysis of hearts from ACF rats revealed the differential expression of 66 myocardial proteins and 851 differentially expressed mRNAs (Petrak et al., 2011), which testifies to the complexity of such a task. Patch-clamp investigations of ionic currents showed a reduction in potassium currents I_K and I_{K1} in hypertrophied cardiomyocytes from ACF rats (Alvin Z. V. et al., 2011). L-type calcium current (I_{CaL}) was shown to be either decreased (Alvin Z. et al., 2011) or unchanged (Ding et al., 2008). For major calcium transporters, the downregulation of SERCA2 and ryanodine receptor proteins was reported (Ding et al., 2008; Petrak et al., 2011). In another study, an unchanged protein expression of SERCA2 was found, together with reduced protein expression of phospholamban and Na/Ca^{2+} exchanger (Harris et al., 2007). Collectively, these changes in ionic currents and calcium transporters correspond with our findings and might underlie them.

Trandolapril was administered in drinking water. Although the effective suppression of angiotensin II plasma and tissue levels with such administration and dosing was demonstrated (Červenka et al., 2015a; Červenka et al., 2015b), the variable intake of drinking water could contribute to the observed variability of some results.

Only male rats were used for the study, to decrease the gender-related heterogeneity of the results. The higher susceptibility of male hearts to ventricular remodeling induced by chronic volume overload was demonstrated in an earlier study (Gardner et al., 2002).

CONCLUSION

Chronic volume overload due to aortocaval fistula induced pronounced structural, contractile, and electrophysiological cardiac remodeling, which resulted in increased mortality. The effective suppression of electrical proarrhythmic remodeling and mortality, but not hypertrophy, indicates that the therapeutic effects of the ACE inhibitor trandolapril in volume-overload heart failure might be dissociated from the purely antihypertrophic effects.

DATA AVAILABILITY STATEMENT

The raw data supporting the conclusions of this article will be made available by the authors, without undue reservation.

ETHICS STATEMENT

The animal study was reviewed and approved by Committee for Experiments on Animals of the Charles University Faculty of Medicine in Pilsen, Pilsen, Czech Republic.

AUTHOR CONTRIBUTIONS

Conceptualization, MŠ, VM, and LČ; methodology, DJ, MM, JŠ, and PŠ; investigation, DJ, MM, JŠ, LČ, PŠ, VM, and MŠ; resources, MŠ, VM, and LČ; writing and editing, DJ, MM, JŠ, LČ, PŠ, VM, and MŠ. All authors have read and agreed to the submitted version of the manuscript.

FUNDING

This research was funded by Charles University (Progres Q39) and by the Ministry of Health of the Czech Republic grant no. NU20-02-00052 awarded to LČ and VM.

REFERENCES

Abassi, Z., Goltsman, I., Karram, T., Winaver, J., Hoffman, A., Abassi, Z., et al. (2011). Aortocaval Fistula in Rat: a Unique Model of Volume-Overload Congestive Heart Failure and Cardiac Hypertrophy. *J. Biomed. Biotechnol.* 2011, 729497. doi:10.1155/2011/729497

Alvin, Z., Laurence, G. G., Coleman, B. R., Zhao, A., Hajj-Moussa, M., and Haddad, G. E. (2011a). Regulation of L-type Inward Calcium Channel Activity by Captopril and Angiotensin II via the Phosphatidyl Inositol 3-kinase Pathway in Cardiomyocytes from Volume-Overload Hypertrophied Rat Hearts. *Can. J. Physiol. Pharmacol.* 89, 206–215. doi:10.1139/Y11-011

Alvin, Z. V., Laurence, G. G., Coleman, B. R., Zhao, A., Hajj-Moussa, M., and Haddad, G. E. (2011b). Regulation of the Instantaneous Inward Rectifier and the Delayed Outward Rectifier Potassium Channels by Captopril and Angiotensin II via the Phosphoinositide-3 Kinase Pathway in Volume-Overload-Induced Hypertrophied Cardiac Myocytes. *Med. Sci. Monit.* 17, BR165–72. doi:10.12659/msm.881843

Arsenault, M., Zendaoui, A., Roussel, E., Drolet, M. C., Dhahri, W., Grenier, A., et al. (2013). Angiotensin II-Converting Enzyme Inhibition Improves Survival, Ventricular Remodeling, and Myocardial Energetics in Experimental Aortic Regurgitation. *Circ. Heart Fail.* 6, 1021–1028. doi:10.1161/CIRCHEARTFAILURE.112.000045

Benes, J., Melenovsky, V., Skaroupkova, P., Pospisilova, J., Petrak, J., Cervenka, L., et al. (2011). Myocardial Morphological Characteristics and Proarrhythmic Substrate in the Rat Model of Heart Failure Due to Chronic Volume Overload. *Anat. Rec. (Hoboken)* 294, 102–111. doi:10.1002/ar.21280

Brower, G. L., Henegar, J. R., and Janicki, J. S. (1996). Temporal Evaluation of Left Ventricular Remodeling and Function in Rats with Chronic Volume Overload. *Am. J. Physiol.* 271, H2071–H2078. doi:10.1152/ajpheart.1996.271.5.H2071

Brower, G. L., and Janicki, J. S. (2001). Contribution of Ventricular Remodeling to Pathogenesis of Heart Failure in Rats. *Am. J. Physiol. Heart Circ. Physiol.* 280, H674–H683. doi:10.1152/ajpheart.2001.280.2.H674

Brower, G. L., Levick, S. P., and Janicki, J. S. (2015). Differential Effects of Prevention and Reversal Treatment with Lisinopril on Left Ventricular Remodelling in a Rat Model of Heart Failure. *Heart Lung Circ.* 24, 919–924. doi:10.1016/j.hlc.2015.02.023

Červenka, L., Melenovský, V., Husková, Z., Škaroupková, P., Nishiyama, A., and Sadowski, J. (2015a). Inhibition of Soluble Epoxide Hydrolase Counteracts the Development of Renal Dysfunction and Progression of Congestive Heart Failure in Ren-2 Transgenic Hypertensive Rats with Aorto-Caval Fistula. *Clin. Exp. Pharmacol. Physiol.* 42, 795–807. doi:10.1111/1440-1681.12419

Červenka, L., Melenovský, V., Husková, Z., Sporková, A., Bürgelová, M., Škaroupková, P., et al. (2015b). Inhibition of Soluble Epoxide Hydrolase Does Not Improve the Course of Congestive Heart Failure and the Development of Renal Dysfunction in Rats with Volume Overload Induced by Aorto-Caval Fistula. *Physiol. Res.* 64, 857–873. doi:10.33549/physiolres.932977

Chaggar, P. S., Malkin, C. J., Shaw, S. M., Williams, S. G., and Channer, K. S. (2009). Neuroendocrine Effects on the Heart and Targets for Therapeutic Manipulation in Heart Failure. *Cardiovasc. Ther.* 27, 187–193. doi:10.1111/j.1755-5922.2009.00094.x

Chevalier, B., Heudes, D., Heymes, C., Basset, A., Dakhli, T., Bansard, Y., et al. (1995). Trandolapril Decreases Prevalence of Ventricular Ectopic Activity in Middle-Aged SHR. *Circulation* 92, 1947–1953. doi:10.1161/01.cir.92.7.1947

Cutler, M. J., Jeyaraj, D., and Rosenbaum, D. S. (2011). Cardiac Electrical Remodeling in Health and Disease. *Trends Pharmacol. Sci.* 32, 174–180. doi:10.1016/j.tips.2010.12.001

Dell'italia, L. J., Balcells, E., Meng, Q. C., Su, X., Schultz, D., Bishop, S. P., et al. (1997). Volume-overload Cardiac Hypertrophy Is Unaffected by ACE Inhibitor Treatment in Dogs. *Am. J. Physiol.* 273, H961–H970. doi:10.1152/ajpheart.1997.273.2.H961

Diaz, A., and Ducharme, A. (2008). Update on the Use of Trandolapril in the Management of Cardiovascular Disorders. *Vasc. Health Risk Manag.* 4, 1147–1158. doi:10.2147/vhrm.s3467

Ding, Y. F., Brower, G. L., Zhong, Q., Murray, D., Holland, M., Janicki, J. S., et al. (2008). Defective Intracellular Ca2+ Homeostasis Contributes to Myocyte Dysfunction During Ventricular Remodelling Induced by Chronic Volume Overload in Rats. *Clin. Exp. Pharmacol. Physiol.* 35, 827–835. doi:10.1111/j.1440-1681.2008.04923.x

Essayagh, B., Sabbag, A., Antoine, C., Benfari, G., Yang, L. T., Maalouf, J., et al. (2020). Presentation and Outcome of Arrhythmic Mitral Valve Prolapse. *J. Am. Coll. Cardiol.* 76, 637–649. doi:10.1016/j.jacc.2020.06.029

Flaim, S. F., Minteer, W. J., Nellis, S. H., and Clark, D. P. (1979). Chronic Arteriovenous Shunt: Evaluation of a Model for Heart Failure in Rat. *Am. J. Physiol.* 236, H698–H704. doi:10.1152/ajpheart.1979.236.5.H698

Fornes, P., Richer, C., Pussard, E., Heudes, D., Domergue, V., and Giudicelli, J. F. (1992). Beneficial Effects of Trandolapril on Experimentally Induced Congestive Heart Failure in Rats. *Am. J. Cardiol.* 70, 43D–51D. doi:10.1016/0002-9149(92)90271-y

Garcia, R., and Diebold, S. (1990). Simple, Rapid, and Effective Method of Producing Aortocaval Shunts in the Rat. *Cardiovasc. Res.* 24, 430–432. doi:10.1093/cvr/24.5.430

Gardner, J. D., Brower, G. L., and Janicki, J. S. (2002). Gender Differences in Cardiac Remodeling Secondary to Chronic Volume Overload. *J. Card. Fail.* 8, 101–107. doi:10.1054/jcaf.2002.32195

Gilat, E., Girouard, S. D., Pastore, J. M., Laurita, K. R., and Rosenbaum, D. S. (1998). Angiotensin-converting Enzyme Inhibition Produces Electrophysiologic but Not Antiarrhythmic Effects in the Intact Heart. *J. Cardiovasc. Pharmacol.* 31, 734–740. doi:10.1097/00005344-199805000-00012

Guggilam, A., Hutchinson, K. R., West, T. A., Kelly, A. P., Galantowicz, M. L., Davidoff, A. J., et al. (2013). *In Vivo* and *In Vitro* Cardiac Responses to Beta-Adrenergic Stimulation in Volume-Overload Heart Failure. *J. Mol. Cel Cardiol* 57, 47–58. doi:10.1016/j.yjmcc.2012.11.013

Hammond, H. K., Roth, D. A., Insel, P. A., Ford, C. E., White, F. C., Maisel, A. S., et al. (1992). Myocardial Beta-Adrenergic Receptor Expression and Signal Transduction after Chronic Volume-Overload Hypertrophy and Circulatory Congestion. *Circulation* 85, 269–280. doi:10.1161/01.CIR.85.1.269

Harris, G. S., Lust, R. M., and Katwa, L. C. (2007). Hemodynamic Effects of Chronic Urotensin II Administration in Animals with and without Aorto-Caval Fistula. *Peptides* 28, 1483–1489. doi:10.1016/j.peptides.2007.04.018

Hatt, P. Y., Rakusan, K., Gastineau, P., Laplace, M., and Cluzeaud, F. (1980). Aorto-caval Fistula in the Rat. An Experimental Model of Heart Volume Overloading. *Basic Res. Cardiol.* 75, 105–108. doi:10.1007/BF02001401

Hatt, P. Y., Rakusan, K., Gastineau, P., and Laplace, M. (1979). Morphometry and Ultrastructure of Heart Hypertrophy Induced by Chronic Volume Overload (Aorto-caval Fistula in the Rat). *J. Mol. Cel Cardiol* 11, 989–998. doi:10.1016/0022-2828(79)90390-0

Hill, J. A. (2003). Electrical Remodeling in Cardiac Hypertrophy. *Trends Cardiovasc. Med.* 13, 316–322. doi:10.1016/j.tcm.2003.08.002

Hutchinson, K. R., Guggilam, A., Cismowski, M. J., Galantowicz, M. L., West, T. A., Stewart, J. A., Jr., et al. (2011). Temporal Pattern of Left Ventricular Structural and Functional Remodeling Following Reversal of Volume Overload Heart Failure. *J. Appl. Physiol.* 111 (6), 1778–1788. doi:10.1152/japplphysiol.00691.2011

Ichihara, A., Hayashi, M., Koura, Y., Tada, Y., Hirota, N., and Saruta, T. (2003). Long-term Effects of Intensive Blood-Pressure Lowering on Arterial wall Stiffness in Hypertensive Patients. *Am. J. Hypertens.* 16, 959–965. doi:10.1016/s0895-7061(03)01004-5

Kehat, I., and Molkentin, J. D. (2010). Molecular Pathways Underlying Cardiac Remodeling during Pathophysiological Stimulation. *Circulation* 122, 2727–2735. doi:10.1161/CIRCULATIONAHA.110.942268

Kemp, C. D., and Conte, J. V. (2012). The Pathophysiology of Heart Failure. *Cardiovasc. Pathol.* 21, 365–371. doi:10.1016/j.carpath.2011.11.007

Kim, H. N., and Januzzi, J. L. (2011). Natriuretic Peptide Testing in Heart Failure. *Circulation* 123, 2015–2019. doi:10.1161/CIRCULATIONAHA.110.9795009

Kmecova, J., and Klimas, J. (2010). Heart Rate Correction of the QT Duration in Rats. *Eur. J. Pharmacol.* 641, 187–192. doi:10.1016/j.ejphar.2010.05.038

Koffi, I., Lacolley, P., Kirchengaast, M., Pomiès, J. P., Laurent, S., and Benetos, A. (1998). Prevention of Arterial Structural Alterations with Verapamil and Trandolapril and Consequences for Mechanical Properties in Spontaneously

Hypertensive Rats. *Eur. J. Pharmacol.* 361, 51–60. doi:10.1016/s0014-2999(98)00691-8

Kristen, A. V., Kreusser, M. M., Lehmann, L., Kinscherf, R., Katus, H. A., Haass, M., et al. (2006). Preserved Norepinephrine Reuptake but Reduced Sympathetic Nerve Endings in Hypertrophic Volume-Overloaded Rat Hearts. *J. Card. Fail.* 12, 577–583. doi:10.1016/j.cardfail.2006.05.006

Lee, C. S., and Tkacs, N. C. (2008). Current Concepts of Neurohormonal Activation in Heart Failure: Mediators and Mechanisms. *AACN Adv. Crit. Care* 19, 364–367. doi:10.1097/01.AACN.0000340718.93742.c4

Liu, Z., Hilbelink, D. R., Crockett, W. B., and Gerdes, A. M. (1991a). Regional Changes in Hemodynamics and Cardiac Myocyte Size in Rats with Aortocaval Fistulas. 1. Developing and Established Hypertrophy. *Circ. Res.* 69, 52–58. doi:10.1161/01.res.69.1.52

Liu, Z., Hilbelink, D. R., and Gerdes, A. M. (1991b). Regional Changes in Hemodynamics and Cardiac Myocyte Size in Rats with Aortocaval Fistulas. 2. Long-Term Effects. *Circ. Res.* 69, 59–65. doi:10.1161/01.res.69.1.59

Lloyd-Jones, D. M., Larson, M. G., Leip, E. P., Beiser, A., D'Agostino, R. B., Kannel, W. B., et al. (2002). Lifetime Risk for Developing Congestive Heart Failure: the Framingham Heart Study. *Circulation* 106, 3068–3072. doi:10.1161/01.cir.0000039105.49749.6f

Lou, Q., Janardhan, A., and Efimov, I. R. (2012). Remodeling of Calcium Handling in Human Heart Failure. *Adv. Exp. Med. Biol.* 740, 1145–1174. doi:10.1007/978-94-007-2888-2_52

Luo, M., and Anderson, M. E. (2013). Mechanisms of Altered Ca^{2+} Handling in Heart Failure. *Circ. Res.* 113, 690–708. doi:10.1161/CIRCRESAHA.113.301651

Mahajerin, A., Gurm, H. S., Tsai, T. T., Chan, P. S., and Nallamothu, B. K. (2007). Vasodilator Therapy in Patients with Aortic Insufficiency: a Systematic Review. *Am. Heart J.* 153, 454–461. doi:10.1016/j.ahj.2007.01.006

Meani, P., Maloberti, A., Sormani, P., Colombo, G., Giupponi, L., Stucchi, M., et al. (2018). Determinants of Carotid-Femoral Pulse Wave Velocity Progression in Hypertensive Patients over a 3.7 Years Follow-Up. *Blood Press.* 27, 32–40. doi:10.1080/08037051.2017.1378069

Melenovsky, V., Cervenka, L., Viklicky, O., Franekova, J., Havlenova, T., Behounek, M., et al. (2018). Kidney Response to Heart Failure: Proteomic Analysis of Cardiorenal Syndrome. *Kidney Blood Press. Res.* 43, 1437–1450. doi:10.1159/000493657

Melenovsky, V., Skaroupkova, P., Benes, J., Torresova, V., Kopkan, L., and Cervenka, L. (2012). The Course of Heart Failure Development and Mortality in Rats with Volume Overload Due to Aorto-Caval Fistula. *Kidney Blood Press. Res.* 35, 167–173. doi:10.1159/000331562

Modesti, P. A., Vanni, S., Bertolozzi, I., Cecioni, I., Lumachi, C., Perna, A. M., et al. (2004). Different Growth Factor Activation in the Right and Left Ventricles in Experimental Volume Overload. *Hypertension* 43, 101–108. doi:10.1161/01.HYP.0000104720.76179.18

Oliver-Dussault, C., Ascah, A., Marcil, M., Matas, J., Picard, S., Pibarot, P., et al. (2010). Early Predictors of Cardiac Decompensation in Experimental Volume Overload. *Mol. Cel Biochem* 338, 271–282. doi:10.1007/s11010-009-0361-5

Orsborne, C., Chaggar, P. S., Shaw, S. M., and Williams, S. G. (2017). The Renin-Angiotensin-Aldosterone System in Heart Failure for the Non-specialist: the Past, the Present and the Future. *Postgrad. Med. J.* 93, 29–37. doi:10.1136/postgradmedj-2016-134045

Perry, G. J., Wei, C. C., Hankes, G. H., Dillon, S. R., Rynders, P., Mukherjee, R., et al. (2002). Angiotensin II Receptor Blockade Does Not Improve Left Ventricular Function and Remodeling in Subacute Mitral Regurgitation in the Dog. *J. Am. Coll. Cardiol.* 39, 1374–1379. doi:10.1016/s0735-1097(02)01763-1

Petrak, J., Pospisilova, J., Sedinova, M., Jedelsky, P., Lorkova, L., Vit, O., et al. (2011). Proteomic and Transcriptomic Analysis of Heart Failure Due to Volume Overload in a Rat Aorto-Caval Fistula Model Provides Support for New Potential Therapeutic Targets - Monoamine Oxidase A and Transglutaminase 2. *Proteome Sci.* 9, 69. doi:10.1186/1477-5956-9-69

Pfeffer, M. A., Braunwald, E., Moyé, L. A., Basta, L., Brown, E. J., Cuddy, T. E., et al. (1992). Effect of Captopril on Mortality and Morbidity in Patients with Left Ventricular Dysfunction after Myocardial Infarction. Results of the Survival and Ventricular Enlargement Trial. The SAVE Investigators. *N. Engl. J. Med.* 327, 669–677. doi:10.1056/NEJM199209033271001

Rea, M. E., and Dunlap, M. E. (2008). Renal Hemodynamics in Heart Failure: Implications for Treatment. *Curr. Opin. Nephrol. Hypertens.* 17, 87–92. doi:10.1097/MNH.0b013e3282f357da

Ruzicka, M., Keeley, F. W., and Leenen, F. H. (1994). The Renin-Angiotensin System and Volume Overload-Induced Changes in Cardiac Collagen and Elastin. *Circulation* 90, 1989–1996. doi:10.1161/01.cir.90.4.1989

Ruzicka, M., Skarda, V., and Leenen, F. H. (1995). Effects of ACE Inhibitors on Circulating versus Cardiac Angiotensin II in Volume Overload-Induced Cardiac Hypertrophy in Rats. *Circulation* 92, 3568–3573. doi:10.1161/01.cir.92.12.3568

Ruzicka, M., Yuan, B., Harmsen, E., and Leenen, F. H. (1993). The Renin-Angiotensin System and Volume Overload-Induced Cardiac Hypertrophy in Rats. Effects of Angiotensin Converting Enzyme Inhibitor versus Angiotensin II Receptor Blocker. *Circulation* 87, 921–930. doi:10.1161/01.cir.87.3.921

Ryan, T. D., Rothstein, E. C., Aban, I., Tallaj, J. A., Husain, A., Lucchesi, P. A., et al. (2007). Left Ventricular Eccentric Remodeling and Matrix Loss Are Mediated by Bradykinin and Precede Cardiomyocyte Elongation in Rats with Volume Overload. *J. Am. Coll. Cardiol.* 49, 811–821. doi:10.1016/j.jacc.2006.06.083

Savarese, G., and Lund, L. H. (2017). Global Public Health Burden of Heart Failure. *Card. Fail. Rev.* 3, 7–11. doi:10.15420/cfr.2016:25:2

Schirone, L., Forte, M., Palmerio, S., Yee, D., Nocella, C., Angelini, F., et al. (2017). A Review of the Molecular Mechanisms Underlying the Development and Progression of Cardiac Remodeling. *Oxidative Med. Cell Longevity* 2017, 1–16. doi:10.1155/2017/3920195

Sedmera, D., Neckar, J., Benes, J., Pospisilova, J., Petrak, J., Sedlacek, K., et al. (2016). Changes in Myocardial Composition and Conduction Properties in Rat Heart Failure Model Induced by Chronic Volume Overload. *Front. Physiol.* 7, 367. doi:10.3389/fphys.2016.00367

St John Sutton, M. M., Pfeffer, M. A., Plappert, T., Rouleau, J. L., Moyé, L. A., Dagenais, G. R., et al. (1994). Quantitative Two-Dimensional Echocardiographic Measurements Are Major Predictors of Adverse Cardiovascular Events after Acute Myocardial Infarction. The Protective Effects of Captopril. *Circulation* 89, 68–75. doi:10.1161/01.cir.89.1.68

Stumpe, K. O., Sölle, H., Klein, H., and Krück, F. (1973). Mechanism of Sodium and Water Retention in Rats with Experimental Heart Failure. *Kidney Int.* 4, 309–317. doi:10.1038/ki.1973.122

Tanonaka, K., Toga, W., Yoshida, H., Furuhama, K., and Takeo, S. (2001). Effect of Long-Term Treatment with Trandolapril on Hsp72 and Hsp73 Induction of the Failing Heart Following Myocardial Infarction. *Br. J. Pharmacol.* 134, 969–976. doi:10.1038/sj.bjp.0704323

Toischer, K., Rokita, A. G., Unsöld, B., Zhu, W., Kararigas, G., Sossalla, S., et al. (2010). Differential Cardiac Remodeling in Preload versus Afterload. *Circulation* 122, 993–1003. doi:10.1161/CIRCULATIONAHA.110.943431

Topouchian, J., Asmar, R., Sayegh, F., Rudnicki, A., Benetos, A., Bacri, A. M., et al. (1999). Changes in Arterial Structure and Function under Trandolapril-Verapamil Combination in Hypertension. *Stroke* 30, 1056–1064. doi:10.1161/01.str.30.5.1056

Triposkiadis, F., Karayannis, G., Giamouzis, G., Skoularigis, J., Louridas, G., and Butler, J. (2009). The Sympathetic Nervous System in Heart Failure Physiology, Pathophysiology, and Clinical Implications. *J. Am. Coll. Cardiol.* 54, 1747–1762. doi:10.1016/j.jacc.2009.05.015

van der Ent, M., Remme, W. J., de Leeuw, P. W., and Bartels, G. L. (1998). Renal Hemodynamic Effects in Patients with Moderate to Severe Heart Failure during Chronic Treatment with Trandolapril. *Cardiovasc. Drugs Ther.* 12, 395–403. doi:10.1023/a:1007729002821

Varró, A., and Baczkó, I. (2011). Cardiac Ventricular Repolarization reserve: a Principle for Understanding Drug-Related Proarrhythmic Risk. *Br. J. Pharmacol.* 164, 14–36. doi:10.1111/j.1476-5381.2011.01367.x

Wang, X., Zhuo, X., Gao, J., Liu, H., Lin, F., and Ma, A. (2019). Neuregulin-1beta Partially Improves Cardiac Function in Volume-Overload Heart Failure Through Regulation of Abnormal Calcium Handling. *Front Pharmacol* 10, 616–36. doi:10.3389/fphar.2019.00616

Westerhof, N., and O'Rourke, M. F. (1995). Haemodynamic Basis for the Development of Left Ventricular Failure in Systolic Hypertension and for its Logical Therapy. *J. Hypertens.* 13, 943–952. doi:10.1097/00004872-199509000-00002

Willenbrock, R., Stauss, H., Scheuermann, M., Osterziel, K. J., Unger, T., and Dietz, R. (1997). Effect of Chronic Volume Overload on Baroreflex Control of Heart Rate and Sympathetic Nerve Activity. *Am. J. Physiol.* 273, H2580–H2585. doi:10.1152/ajpheart.1997.273.6.H2580

Zeltser, I., Gaynor, J. W., Petko, M., Myung, R. J., Birbach, M., Waibel, R., et al. (2005). The Roles of Chronic Pressure and Volume Overload States in Induction of Arrhythmias: an Animal Model of Physiologic Sequelae after Repair of Tetralogy of Fallot. *J. Thorac. Cardiovasc. Surg.* 130, 1542–1548. doi:10.1016/j.jtcvs.2005.08.034

Conflict of Interest: The authors declare that the research was conducted in the absence of any commercial or financial relationships that could be construed as a potential conflict of interest.

Publisher's Note: All claims expressed in this article are solely those of the authors and do not necessarily represent those of their affiliated organizations, or those of the publisher, the editors and the reviewers. Any product that may be evaluated in this article, or claim that may be made by its manufacturer, is not guaranteed or endorsed by the publisher.

frontiers in Pharmacology

ORIGINAL RESEARCH
published: 28 October 2021
doi: 10.3389/fphar.2021.739615

Quercetin Attenuates Cardiac Hypertrophy by Inhibiting Mitochondrial Dysfunction Through SIRT3/PARP-1 Pathway

Wen-Jing Chen[1,2], *Yan Cheng*[2], *Wen Li*[3], *Xiao-Kang Dong*[2], *Jian-liang Wei*[2], *Chuan-Hua Yang*[2]* *and Yue-Hua Jiang*[4]*

[1]First Clinical Medical College, Shandong University of Traditional Chinese Medicine, Jinan, China, [2]Cardiovascular Department, Affiliated Hospital of Shandong University of Traditional Chinese Medicine, Jinan, China, [3]College of Traditional Chinese Medicine, Shandong University of Traditional Chinese Medicine, Jinan, China, [4]Central Laboratory, Affiliated Hospital of Shandong University of Traditional Chinese Medicine, Jinan, China

OPEN ACCESS

Edited by:
Antonio Lax,
University of Murcia, Spain

Reviewed by:
Srinivas Sriramula,
The Brody School of Medicine at East Carolina University, United States
Bing Shen,
Anhui Medical University, China
Suowen Xu,
University of Science and Technology of China, China

***Correspondence:**
Chuan-Hua Yang
yang_chuanhua@hotmail.com
Yue-Hua Jiang
jiang_yuehua@hotmail.com

Specialty section:
This article was submitted to Cardiovascular and Smooth Muscle Pharmacology, a section of the journal Frontiers in Pharmacology

Received: 11 July 2021
Accepted: 15 October 2021
Published: 28 October 2021

Citation:
Chen W-J, Cheng Y, Li W, Dong X-K, Wei J-l, Yang C-H and Jiang Y-H (2021) Quercetin Attenuates Cardiac Hypertrophy by Inhibiting Mitochondrial Dysfunction Through SIRT3/PARP-1 Pathway. Front. Pharmacol. 12:739615. doi: 10.3389/fphar.2021.739615

Cardiac hypertrophy is an important characteristic in the development of hypertensive heart disease. Mitochondrial dysfunction plays an important role in the pathology of cardiac hypertrophy. Recent studies have shown that sirtuin 3 (SIRT3)/poly (ADP-ribose) polymerase-1 (PARP-1) pathway modulation inhibits cardiac hypertrophy. Quercetin, a natural flavonol agent, has been reported to attenuate cardiac hypertrophy. However, the molecular mechanism is not completely elucidated. In this study, we aimed to explore the mechanism underlying the protective effect of quercetin on cardiac hypertrophy. Spontaneously hypertensive rats (SHRs) were treated with quercetin (20 mg/kg/d) for 8 weeks to evaluate the effects of quercetin on blood pressure and cardiac hypertrophy. Additionally, the mitochondrial protective effect of quercetin was assessed in H9c2 cells treated with Ang II. SHRs displayed aggravated cardiac hypertrophy and fibrosis, which were attenuated by quercetin treatment. Quercetin also improved cardiac function, reduced mitochondrial superoxide and protected mitochondrial structure *in vivo*. *In vitro*, Ang II increased the mRNA level of hypertrophic markers including atrial natriuretic factor (ANF) and β-myosin heavy chain (β-MHC), whereas quercetin ameliorated this hypertrophic response. Moreover, quercetin prevented mitochondrial function against Ang II induction. Importantly, mitochondrial protection and PARP-1 inhibition by quercetin were partly abolished after SIRT3 knockdown. Our results suggested that quercetin protected mitochondrial function by modulating SIRT3/PARP-1 pathway, contributing to the inhibition of cardiac hypertrophy.

Keywords: quercetin, mitochondrial function, Sirtuin3, poly (ADP-ribose) polymerase-1, cardiac hypertrophy

INTRODUCTION

Cardiac hypertrophy is a crucial characteristic of hypertensive heart disease that mainly involves cardiomyocyte hypertrophy in the early stage. Even though this may be a compensatory response initially to maintain function and efficiency in response to pressure overload, persistent increase in hypertrophy ultimately leads to ventricular dilatation and heart failure (Nakamura and Sadoshima, 2018). Therefore, ameliorating cardiac hypertrophy is the emphasis of clinical hypertension treatment.

Mitochondrial function, including reactive oxygen species (ROS) generation and detoxification, energy metabolism, mitochondrial biogenesis, mitophagy and dynamics, plays a vital role in maintaining cellular homeostasis of cardiomyocytes (Nunnari and Suomalainen, 2012). In recent years, mitochondrial dysfunction has emerged as one of the main pathogenic mechanisms underlying the development of cardiac hypertrophy (McDermott-Roe et al., 2011; Facundo et al., 2017). Reduced energy production and increased oxidative stress, as the main consequences of mitochondrial dysfunction, result in cardiomyocyte death and fibrosis, leading to progress of maladaptive hypertrophy (Forte et al., 2019). These findings suggest that modulating mitochondrial function may be considered a valid therapeutic strategy in cardiac hypertrophy (Manolis et al., 2021).

Sirtuins (SIRTs) are a family of nicotinamide adenine dinucleotide $(NAD)^+$–dependent deacetylases that consists of seven members (SIRT1—SIRT7) closely related to glucose/lipid metabolism, cell survival, energy metabolism, and NDA repair (Park et al., 2013). Among them, sirtuin 3 (SIRT3), localized in the mitochondrial matrix, regulates biological function of mitochondria as a vital stress-responsive protein deacetylase. In response to oxidative stress, SIRT3 is stimulated to deacetylate and activate superoxide dismutase (SOD2), leading to mitochondrial ROS clearance (Chen et al., 2011). The role of SIRT3 in cardiac hypertrophy has been widely examined both *in vivo* and *in vitro*. Recent studies demonstrate that SIRT3 knockout mice spontaneously develop myocardial fibrosis (Palomer et al., 2020), while SIRT3 overexpression partially attenuates the cardiac hypertrophic response by regulating the expression of antioxidant genes (Xiong et al., 2019) and mitochondrial function (Xu M. et al., 2019).

Poly (ADP-ribose) polymerases (PARPs) is a enzyme family composed of 17 members that can be activated by DNA damage. Poly (ADP-ribose) polymerase-1 (PARP-1), as the most abundant and ubiquitous member of the family, accounts for most of the PARP activity (Ryu et al., 2015). PARP-1 plays a crucial role in the physiological cellular functions such as DNA repair, transcription, bioenergetics, mtDNA maintenance, cell death and mitophagy (Kadam et al., 2020), using NAD^+ as a substrate to transfer ADP-ribose units from NAD^+ to form ADP-ribose polymers (PAR) (Hassa and Hottiger, 2008). Several studies have suggested that PARP-1 is closely associated with the development of cardiac hypertrophy. PARP-1 activity is significantly increased in diabetic cardiomyopathy (Waldman et al., 2018). In addition, treatment with the PARP-1 inhibitor AG-690/11026014 (6014) effectively prevents cardiomyocyte hypertrophy induced by Ang II (Feng et al., 2017). Importantly, a recent study reveals that SIRT3 interacts directly with PARP-1 and exerts protective effects against cardiomyocyte hypertrophy by deacetylating PARP-1 and inhibiting PARP-1 activity (Feng et al., 2020). Therefore, SIRT3/PARP-1 pathway regulation may represent a promising tool for improving mitochondrial function and treating cardiac hypertrophy.

Quercetin is a natural flavonol drug with many biological and health-promoting effects, including anti-inflammatory (Karuppagounder et al., 2016), antioxidant (Xu D. et al., 2019), antiatherosclerotic (Hung et al., 2015), antihypertensive (Elbarbry et al., 2020), anticancer (Reyes-Farias and Carrasco-Pozo, 2019), and anti-Alzheimer (Ebrahimpour et al., 2020) properties. In recent years, several studies have reported that quercetin protects against cardiac hypertrophy both *in vivo* and *in vitro* (Goncharov et al., 2016; Chen et al., 2018; Wang et al., 2020). Our previous study found that quercetin not only increases SIRT1 expression in aorta of $ApoE^{-/-}$ mice but also decreases cellular apoptosis and ROS generation in ox-LDL-induced cellular senescence (Jiang et al., 2020). However, the molecular mechanism by which quercetin attenuates cardiac hypertrophy remains unclear.

The purpose of this study was to confirm that quercetin alleviated cardiac hypertrophy, focusing on the SIRT3/PARP-1 pathway both in spontaneously hypertensive rats (SHRs) and H9c2 cells.

MATERIALS AND METHODS

Animals

Fifteen-week-old male SHRs (n = 16, weighing 280–320 g) and age/sex-matched Wistar-Kyoto (WKY) rats (n = 8, weighing 290–330 g) were obtained from Vital River Laboratory Animal Technology (Certificate: SCXK (Jing) 2016-0006, Beijing, China). The zoological study was performed in the Animal Experimental Center of the Affiliated Hospital of Shandong University of Traditional Chinese Medicine (Shandong, China) at controlled temperature (21 ± 1°C). The study was approved by the Animal Ethics Committee of the Affiliated Hospital of Shandong University of Traditional Chinese Medicine (Jinan, China), and the ethics approval number is AWE-2019-021.

After acclimatization for 1 week, 16 SHRs were randomly divided into the SHR (SHR, n = 8) and quercetin (Que, n = 8) groups; eight WKY rats were used as the normal control group (WKY, n = 8). According to a research and our previous study, intragastrical administration of quercetin at a dose of 20 mg/kg/d for 8–12 weeks prevented cardiac hypertrophy in established cardiac hypertrophic rat model and alleviated atherosclerotic lesion in $ApoE^{-/-}$ mice, respectively (Chen et al., 2018; Jiang et al., 2020). Therefore, in this study, Rats in the quercetin group were administered 20 mg/kg/d quercetin (Meilun Biotechnology, Dalian, China) intragastrically, while the other two groups received the same volume of saline intragastrically for 8 weeks.

Blood Pressure Measurement

Systolic blood pressure (SBP) and diastolic blood pressure (DBP) were measured by the tail-cuff method with Mouse and Rat Tail Cuff Blood Pressure Systems (MRBP-10, IITC Life Science, United States) before and after treatment every 2 weeks. Rats were placed on a heated platform (35°C) for 10 min to keep them warm before measurement. The measurements were repeated three times for each rat at each time point, with the mean value recorded.

Echocardiography

Eight weeks after treatment, rats were anesthetized and their chests were shaved with a depilatory agent. Transthoracic

echocardiography was performed using a Veterinary Ultrasonic system Ultrasound Scanner (M5 Vet, Mindray, Guangdong, China). Left ventricular structure and function were assessed by measuring left ventricular end-diastolic internal diameter (LVIDd), left ventricular end-diastolic posterior wall thickness (LVPWd), end-diastolic interventricular septal thickness (IVSd), left ventricular end-systolic internal diameter (LVIDs), left ventricular ejection fraction (LVEF) and left ventricular fractional shortening (LVFS) *via* two-dimensional and M-mode echocardiography.

Histopathological Examination

After echocardiography, the heart was quickly extracted. The heart and body weights of each rat were recorded. Heart tissues were collected, fixed with 4% formaldehyde for 48 h at room temperature, embedded in paraffin, and sectioned at 5 μm. Sections were stained with hematoxylin and eosin (H&E) and Masson's trichrome using standard protocols to assess general histology and interstitial fibrosis. In order to determine the cardiomyocyte cross-sectional area, heart sections were deparaffinized, rehydrated, and processed for antigen retrieval with EDTA antigen retrieval solution (Servicebio, G1206, Wuhan, China). Afer washes, sections were incubated with diluted wheat germ agglutinin (WGA) solution (Sigma-Aldrich, L4895, United States) at 37°C in the dark for 30 min, and then incubated with DAPI (Servicebio, G1012, Wuhan, China) at room temperature for 10 min. Following spontaneous fluorescence quenching, slides were mounted with anti-fade mounting medium. Images were captured using fluorescent microscope (Nikon, ECLIPSE C1, Japan). Four images were taken from four different rats in each group. The quantification of collagen volume fraction and cardiomyocyte cross-sectional area were analysed using Image-Pro Plus 6.0 software (Media Cybernetics, United States).

Transmission Electron Microscopy

The mitochondrial ultrastructure was observed by TEM. Fresh cardiac tissues were cut into 1–3 mm blocks, fixed with 2% glutaraldehyde at 4°C overnight. After dehydration, resin penetration and embedding, the ultrathin sections were stained with 2% uranium acetate-saturated alcohol solution. Ultrastructural images were captured with a TEM (JEOL-1200, Japan).

Mitochondrial Superoxide Measurement

Mitochondrial superoxide production was measured by MitoSOX™ Red mitochondrial superoxide indicator (Thermo Fisher (China), M36008, Shanghai, China) according to the manufacturer's instructions. Freshly prepared frozen heart sections were incubated with 5 μM MitoSOX™ reagent working solution for 10 min at 37°C protected from light. Images were captured using fluorescence microscope (Nikon, Japan) with excitation and emission at 514 and 585 nm, respectively. Four images were taken from four different rats in each group. ImageJ (National Institutes of Health, Bethesda, Maryland, United States) was employed to analyze the relative levels of mitochondrial superoxide in the heart.

Total Superoxide Dismutase, Malondialdehyde and Glutathione Peroxidase Assays

Blood samples were obtained from the inferior vena cava, and serum was obtained by centrifugation. Serum T-SOD, MDA and GSH-PX amounts were detected with the T-SOD assay (Jiancheng Biological Engineering Institute, A001-1, Nanjing, China), MDA assay (Jiancheng Biological Engineering Institute, A003-1) and GSH-PX assay (Jiancheng Biological Engineering Institute, A005-1) kits, respectively, according to the manufacturer's instructions.

Cell Culture

Immortalized rat myoblast H9c2 cells were purchased from Procell Life Science and Technology (Wuhan, China). H9c2 cells were cultured in DMEM (Procell) supplemented with 10% fetal bovine serum (Procell) and 1% penicillin/streptomycin (Procell) at 37°C in a humidified environment with 5% CO_2. H9c2 cells cultured in DMEM were treated with 0.5, 1, and 2 μM quercetin, respectively. One hour after quercetin treatment, cells were treated with the hypertrophic agonist angiotensin II (Ang II; Solarbio, Beijing, China) at 0.1 μM. All cells were incubated for an additional 24 h before analysis.

MTT Assay

Viability of H9c2 was determined by MTT assay. 20 μl MTT (5 mg/ml) was added to cultured cells in 96-well plate to incubated at 37°C for 4 h. Medium was replaced with 150 μl DMSO to dissolve the formazan crystals. Subsequently, the absorbance was measured using microplate reader (Thermo Scientific, Multiskan GO, United States) with wave length at 562 nm.

Cell Transfection

A small interfering RNA targeting SIRT3 (siRNA-SIRT3) and siRNA-NC were designed and synthesized by GenePharma (Shanghai, China). H9c2 cells were cultured in six-well plates (3×10^5 cells/well) with Opti-MEM (Thermo Fisher [China], Shanghai, China) overnight before transfection to ensure 80% cell confluence. Diluted Lipofectamine 3,000 (Thermo Fisher [China], Shanghai, China) and diluted siRNA were mixed, and incubated at room temperature for 20 min before adding to the corresponding plates. H9c2 cells were cultured at 37°C for 48 h, followed by western blot detection of transfection efficiency.

Detection of Mitochondrial Membrane Potential (ΔΨm)

Mitochondrial membrane potential was detected using a fluorescence tetraethylbenzimidazolylcarbocyanine iodide (JC-1) assay kit (Beyotime, C2006, Shanghai, China). Collected H9c2 cells were incubated with JC-1 staining mixture at 37°C for 20 min and washed with JC-1 staining buffer twice. ΔΨm was analyzed on a flow cytometer (BD Accuri C6 Plus, United States) with excitation and emission at 485 and 590 nm, respectively. The aggregate/monomer (red/green fluorescence) ratio was used to measure mitochondrial membrane depolarization.

Determination of Intracellular ATP Levels

Intracellular ATP levels were determined with an intracellular ATP assay kit (Beyotime, S0026, Shanghai, China) following the manufacturer's instructions. H9c2 cells were lysed and centrifuged at 4°C for 10 min, and the resulting supernatant was used for further analysis. ATP detection reagent was added to each sample, and luminescence (RLU) was subsequently measured on a microplate reader (Bio-TEK, Synergy HTX, Vermont, United States). Finally, ATP levels were calculated according to a standard curve.

Quantitative Real-Time PCR (q-PCR)

Total RNA was extracted from cultured H9c2 cells with TRIzol reagent (Invitrogen, Carlsbad, CA, United States) following the manufacturer's protocol. Then, cDNA was synthesized and amplified by PCR with a Transcriptor Reverse Transcriptase kit (Roche, Basel, Switzerland). The mRNA levels of target genes were measured with ChamQ SYBR qPCR Master Mix (Vazyme, Nanjing, China) on the LightCyler 480 system (Roche, Basel, Switzerland). Glyceraldehyde 3-phosphate dehydrogenase (GAPDH) expression was used for normalization. The primers are listed in **Supplementary Table S1**.

Western Blot

The concentration of total protein extracted from heart tissues and H9c2 cells were assessed with the BCA Protein assay kit (Cwbio, Jiangsu, China) and adjusted to 20 μg/μl. Then, 30 μg total protein per samples was separated by 12% sodium dodecyl sulfate polyacrylamide gel electrophoresis (SDS-PAGE) and subsequently transferred onto PVDF membranes. After blocking, the PVDF membranes were incubated with primary antibodies (Anti-Collagen I Rabbit pAb, GB11022, 1:1,000, Servicebio, Wuhan, China; Anti-alpha smooth muscle Actin Rabbit pAb, GB11044, 1:1,000, Servicebio, Wuhan, China; Anti-SIRT3 Rabbit pAb, GB11354, 1:1,000, Servicebio, Wuhan, China; PARP1 Rabbit pAb, A0942, 1:1,000, Abclonal, Wuhan, China; Anti-PAR mouse pAb, ab14459, 1:1,000, Abcam, Cambridge, United Kingdom) at 4°C overnight. After a washing step, the blots were incubated with horseradish peroxidase-conjugated goat anti-rabbit IgG or goat anti-mouse IgG (1:5,000) at room temperature for 2 h. Finally, immunoreactive bands were quantified by ImageJ (National Institutes of Health, Bethesda, Maryland, United States). GAPDH expression was used for normalization. Western blot was performed in three biological replicates.

NAD^+ Measurement

The level of NAD^+ in H9c2 cells was determined using NAD^+/NADH assay kit (Beyotime, S0175, Shanghai, China) with WST-8 according to the manufacturer's instructions. In brief, 1×10^6 cells were collected and lysed with 200 ul cold lysis buffffer to obtain sample. Afer reagent preparation, alcohol dehydrogenase working solution was added to 20 ul sample, and the suspension was incubated at 37°C for 10 min to obtain total NAD and NADH, respectively. Based on the relationship between NADH and the absorbance value measured at 450 nm, a standard curve was generated. Subsequently, the total NAD and NADH concentration were estimated according to the standard curve, and NAD^+ concentration was calculated by subtracting NADH from total NAD.

Statistical Analysis

Statistical analysis was performed using SPSS 26.0. Data are mean ± standard deviation (SD). Statistical differences among groups were determined by one-way analysis of variance (ANOVA) followed by least significant difference-*t* test (LSD-*t*). Differences were considered statistically significant at $p < 0.05$.

RESULTS

Quercetin Decreases Blood Pressure in SHRs

As shown in **Figures 1A,B**, SHRs had significantly higher SBP and DBP at each time point compared with WKY rats, and SBP and DBP levels were homogenous among SHRs before treatment. As expected, from the second week of treatment, both SBP and DBP in SHRs were significantly decreased by quercetin, suggesting an anti-hypertensive effect for quercetin.

Quercetin Attenuates Cardiac Hypertrophy in SHRs

Next, we evaluated the efficacy of quercetin to attenuate cardiac hypertrophy in SHRs. As shown in **Figure 2A**, heart weight to body weight ratio (HW/BW) was higher in SHRs than WKY rats, which was related to increased LVPWd and IVSd, and decreased LVIDd in SHRs as revealed by the M-mode echocardiography. Whereas these pathological phenotype were significantly prevented in quercetin-treated rats (**Figures 2B,C**). In addition, SHRs developed increased LVEF and LVFS, which were also reversed to normal levels by quercetin administration (**Figures 2D,E**). Moreover, histological analysis showed elevated collagen volume fraction and cardiomyocyte cross-sectional area in SHRs compared with WKY rats, accompanied by increased collagen I and α-smooth muscle actin (α-SMA). However, quercetin treatment rescued these changes (**Figures 2F–J**). Since previous studies suggested a protective role of SIRT3 in cardiac hypertrophy (Pillai et al., 2015), we assessed SIRT3 levels in rats by western blot. SIRT3 levels were markedly reduced in SHRs, but significantly increased by quercetin treatment (**Figures 2K,L**). These results demonstrated that quercetin might attenuate cardiac hypertrophy by activating SIRT3-mediated signaling pathway *in vivo*.

Quercetin Improves Mitochondrial Structure and Inhibits Oxidative Stress in SHRs

Previous data demonstrated a close link between mitochondrial dysfunction and pressure overload-induced cardiac hypertrophy (Kumar et al., 2019). In order to assess the effect of quercetin on

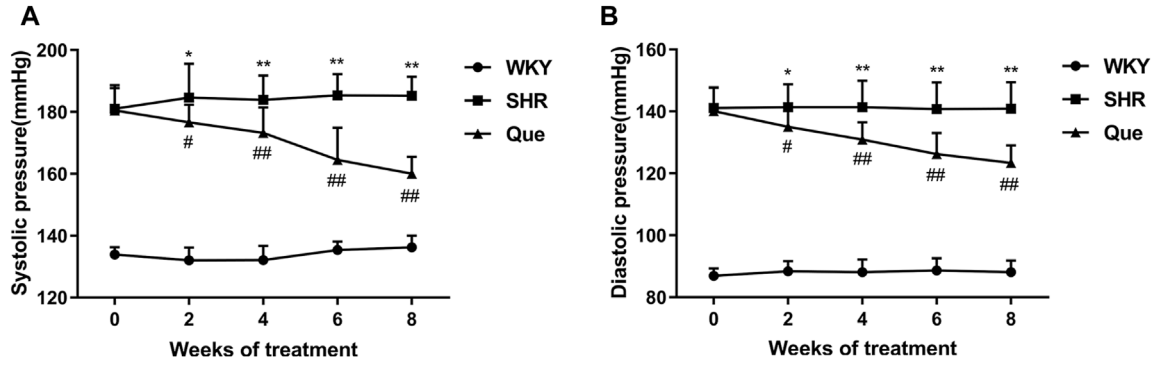

FIGURE 1 | Quercetin decreases systolic blood pressure (SBP) and diastolic blood pressure (DBP) in spontaneously hypertensive rats (SHRs). **(A)** SBP in different rat groups at each time point (n = 8). **(B)** DBP in different rat groups at each time point (n = 8). Data are mean ± SD. $^{*}p < 0.05$, $^{**}p < 0.01$ *vs* WKY group; $^{\#}p < 0.05$, $^{\#\#}p < 0.01$ *vs* SHR group.

mitochondrial integrity and function in SHRs, we observed mitochondrial ultrastructure using TEM. Mitochondria in the hearts of WKY rats had regular morphology, with abundant cristae. Meanwhile, SHRs hearts showed defective mitochondrial organization, as indicated by swollen mitochondria with distorted cristae, even accompanied by mitochondrial membrane damage. However, quercetin treatment rescued these ultrastructure changes, with a relatively improved mitochondrial phenotype (**Figure 3A**). Based on the mitochondrial function in ROS generation, we detected mitochondrial superoxide with MitoSOX™ Red staining. As shown in **Figure 3B**, superoxide generation was significant increased in SHRs, which was decreased by quercetin treatment. In agreement, oxidative stress was exacerbated as determined by increased MDA and decreased T-SOD and GSH-PX in SHRs, whereas quercetin treatment significantly ameliorated oxidative stress (**Figure 3C**). These data confirmed that quercetin alleviated mitochondrial damage and oxidative stress *in vivo*.

Quercetin Inhibits Ang II-Induced Hypertrophic Response in H9c2 Cells and Protects Mitochondrial Function *in Vitro*

Before evaluating anti-hypertrophic effects of quercetin *in vivo*, we tested the cytotoxicity of quercetin by MTT assay. The MTT results showed that Ang II reduced viability of H9c2 cells by 46% compared with the control, while no significant reduction in cell viability was observed after quercetin intervention, indicating that there were no cytotoxic effects (**Figure 4A**). Subsequently, we investigated the hypertrophic response in Ang II-induced H9c2 cells by using hypertrophic markers, including atrial natriuretic factor (ANF) and β-myosin heavy chain (β-MHC), as indicators of cardiomyocyte hypertrophy. As shown in **Figures 4B,C**, Ang II-induced H9c2 cells showed increased mRNA levels of ANF and β-MHC compared with control cells, which were markedly reduced after quercetin treatment in a dose dependent manner.

To get further support for the protective effect of quercetin on mitochondrial function, we measured ΔΨm using JC-1. As shown in **Figure 4D**, the aggregate/monomer (red/green fluorescence intensity) ratio represented mitochondrial membrane potential depolarization. Quercetin attenuated mitochondrial membrane potential depolarization and restored the decreased ΔΨm in Ang II-induced H9c2 cells in a dose dependent manner (**Figure 4E**). Moreover, SIRT3 expression was decreased by Ang II, whereas quercetin significantly restored SIRT3 levels, especially in the high-dose group (**Figures 4F,G**). Therefore, 2 μM quercetin was chosen as the optimal dose for subsequent experiments. These data confirmed that quercetin inhibited the cardiac hypertrophic response and protected mitochondrial function *in vitro*, likely *via* SIRT3 activation.

Quercetin Protects Mitochondrial Function *via* SIRT3/PARP-1 Pathway

Due to the vital roles of SIRT3 in cardiac mitochondrial dysfunction and oxidative stress (Wei et al., 2017), we focused on SIRT3-mediated pathway in quercetin pharmacology using siRNA-SIRT3 to knock down SIRT3. In this study, western blot showed that SIRT3 was effectively knocked down after siRNA transfection (**Figures 5A,B**). As shown in **Figures 5C,D**, Ang II induced mitochondrial membrane depolarization and altered the mitochondrial membrane potential in H9c2 cells, which was markedly reversed by quercetin treatment. However, these effects were partly abolished in siRNA-SIRT3 cells but not in siRNA-NC cells. Similar effects were found in the ATP assay (**Figure 5E**). Since SIRT3 is an NAD^+-dependent enzyme, its activity is dependent on NAD^+ level, thus we examined the NAD^+ level in H9c2 cells. As shown in **Figure 5F**, quercetin alleviated Ang II-induced NAD^+ level decrease, which was markedly reduced after SIRT3 knockdown. These results suggested the involvement of SIRT3 activation in quercetin pharmacology in mitochondrial protection.

PARP-1 is an important effector suppressed by SIRT3 overexpression in hypertrophic cardiomyocytes (Feng et al., 2020), its activity is represented by PAR expression. In the present study, quercetin dramatically inhibited PARP-1 and PAR upregulation in Ang II-induced H9c2 cells, whereas this effect was reduced after SIRT3 knockdown (**Figures 5G–J**).

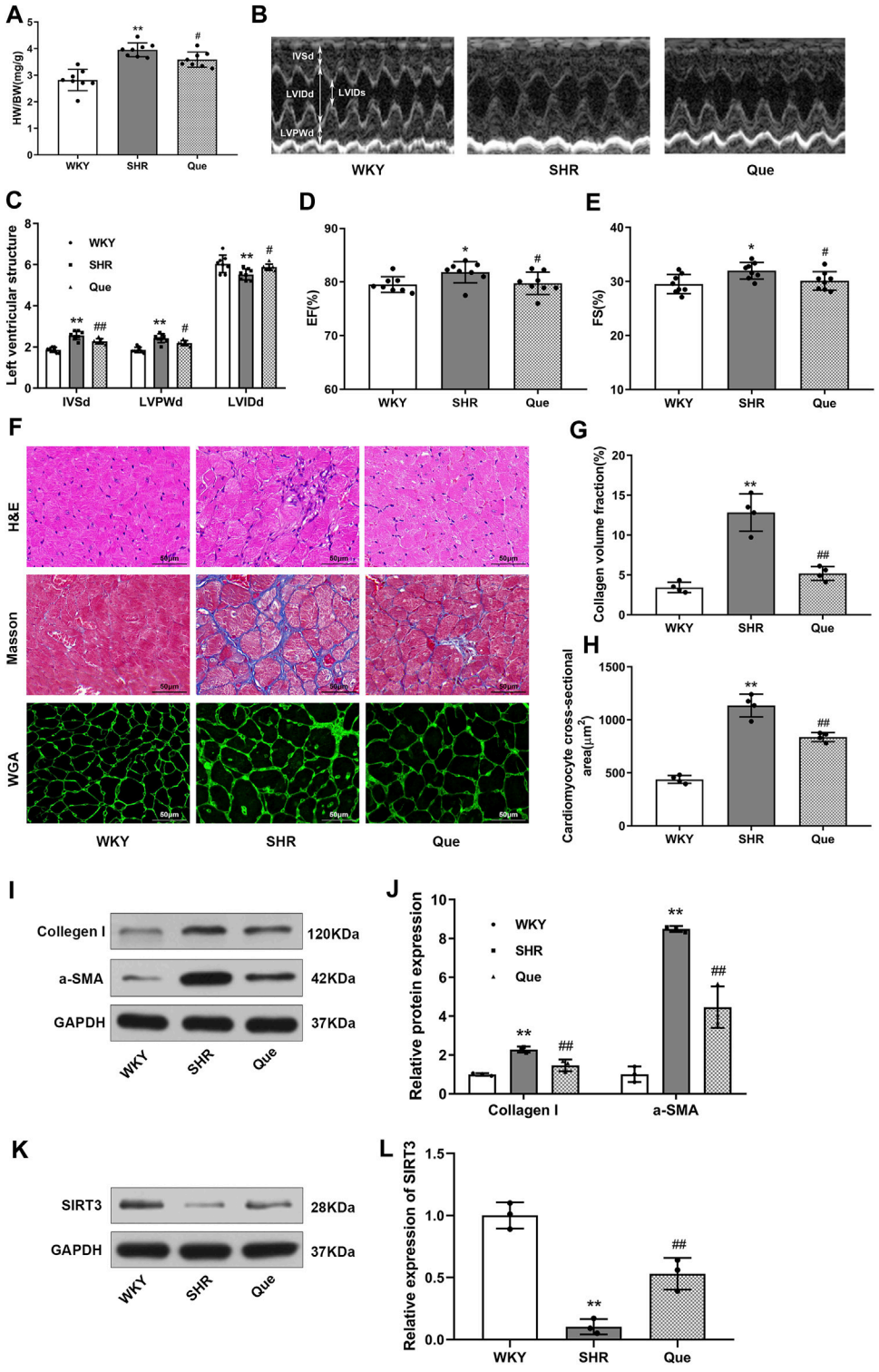

FIGURE 2 | Quercetin attenuates cardiac hypertrophy in SHRs. **(A)** Heart weight to body weight ratios (HW/BW, n = 8). **(B)** Representative M-mode echocardiograms in WKY rats and SHRs. **(C–E)** Quantitative analysis of end-diastolic interventricular septal thickness (IVSd), left ventricular end-diastolic posterior wall thickness (LVPWd), left ventricular end-diastolic internal diameter (LVIDd), left ventricular ejection fraction (LVEF) and left ventricular fractional shortening (LVFS) (n = 8). **(F)** Representative histological images of the myocardium. In detail, hematoxylin and eosin (H&E) staining, Masson's trichrome staining, and wheat germ agglutinin (WGA) staining in hearts from WKY rats and SHRs. Scale bar = 50 μm. **(G)** Quantitative analysis of collagen volume fraction (n = 4). **(H)** Quantitative analysis of cardiomyocyte cross-sectional area (n = 4). **(I,J)** Representative blots of collagen I and α-smooth muscle actin (α-SMA), and densitometric quantification after normalization to GAPDH levels (n = 3). Data are mean ± SD. $^{*}p < 0.05$, $^{**}p < 0.01$ *vs* WKY group; $^{\#}p < 0.05$, $^{\#\#}p < 0.01$ *vs* SHR group.

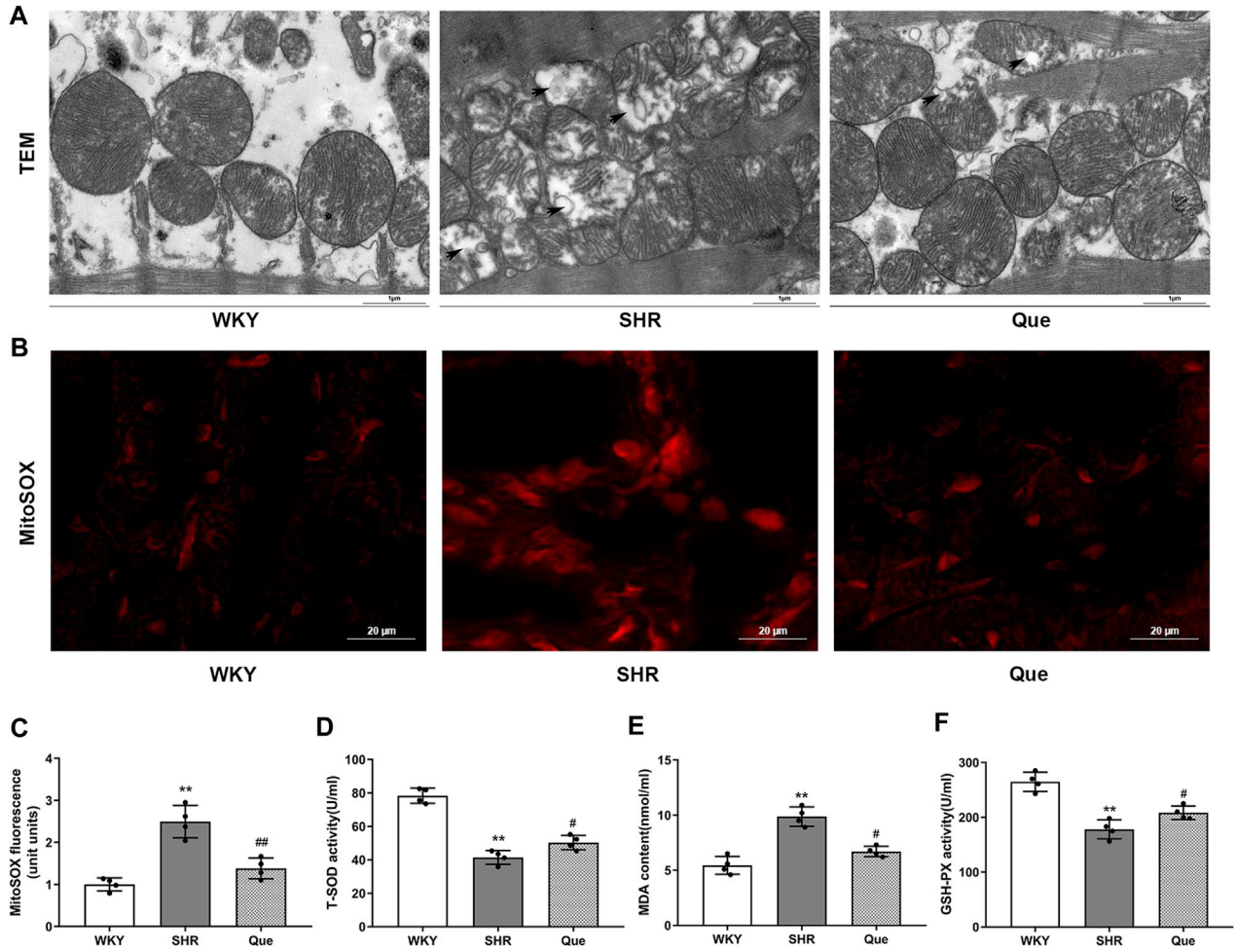

FIGURE 3 | Quercetin improves mitochondrial structure and inhibits oxidative stress in SHRs. **(A)** Representative transmission electron microscopy (TEM) images of mitochondria in hearts from WKY rats and SHRs. Scale bar = 1 μm. **(B)** Representative microphotographs of MitoSOX staining in hearts from WKY rats and SHRs. Scale bar = 20 μm. **(C)** Quantitative analysis of the relative levels of mitochondrial superoxide in hearts from WKY rats and SHRs (n = 4). **(D–F)** Quantification of Total Superoxide dismutase (T-SOD), Malondialdehyde (MDA) and Glutathione peroxidase (GSH-PX) levels (n = 4). Data are mean ± SD. $^{*}p < 0.05$, $^{**}p < 0.01$ *vs* WKY group; $^{\#}p < 0.05$, $^{\#\#}p < 0.01$ *vs* SHR group.

Taken together, these findings demonstrated that quercetin played a protective role in mitochondrial function by regulating SIRT3/PARP-1 signaling pathway.

DISCUSSION

In the present study, quercetin demonstrated a beneficial effect in attenuating cardiac hypertrophy in SHRs and Ang II-induced hypertrophic response in H9c2 cells, which was concomitant with improved mitochondrial function as well as increased SIRT3 expression both *in vivo* and *in vitro*. The pharmacology of quercetin was studied *via* SIRT3-knockdown by siRNA. The protective effect of quercetin against mitochondrial dysfunction was overtly blocked after SIRT3 knockdown, which was accompanied by PAR upregulation, suggesting that activation of SIRT3/PARP-1 signaling pathway might be the target of quercetin in improving mitochondrial function and attenuating cardiac hypertrophy.

Mitochondria play central roles in the regulation of cellular metabolism responsible for ATP production, ROS generation and detoxification, which are considered to be vital for the maintenance of cellular homeostasis in cardiomyocytes with high-energy demand (Jusic and Devaux, 2020). Accumulating evidence reveals a close relationship between mitochondrial dysfunction and cardiac hypertrophy. During the development of cardiac hypertrophy, the activities of ATP synthase and mitochondrial oxidative phosphorylation complex are decreased, leading to impaired ATP production (Pham et al., 2014). Additionally, in Dahl salt-sensitive rats, hypertensive cardiac hypertrophy and fibrosis are suppressed by mdivi1, an inhibitor of Drp1, *via* reduction of excessive ROS production, which is also associated with improved mitochondrial dynamics (Hasan et al., 2018). Moreover, a recent study demonstrated that

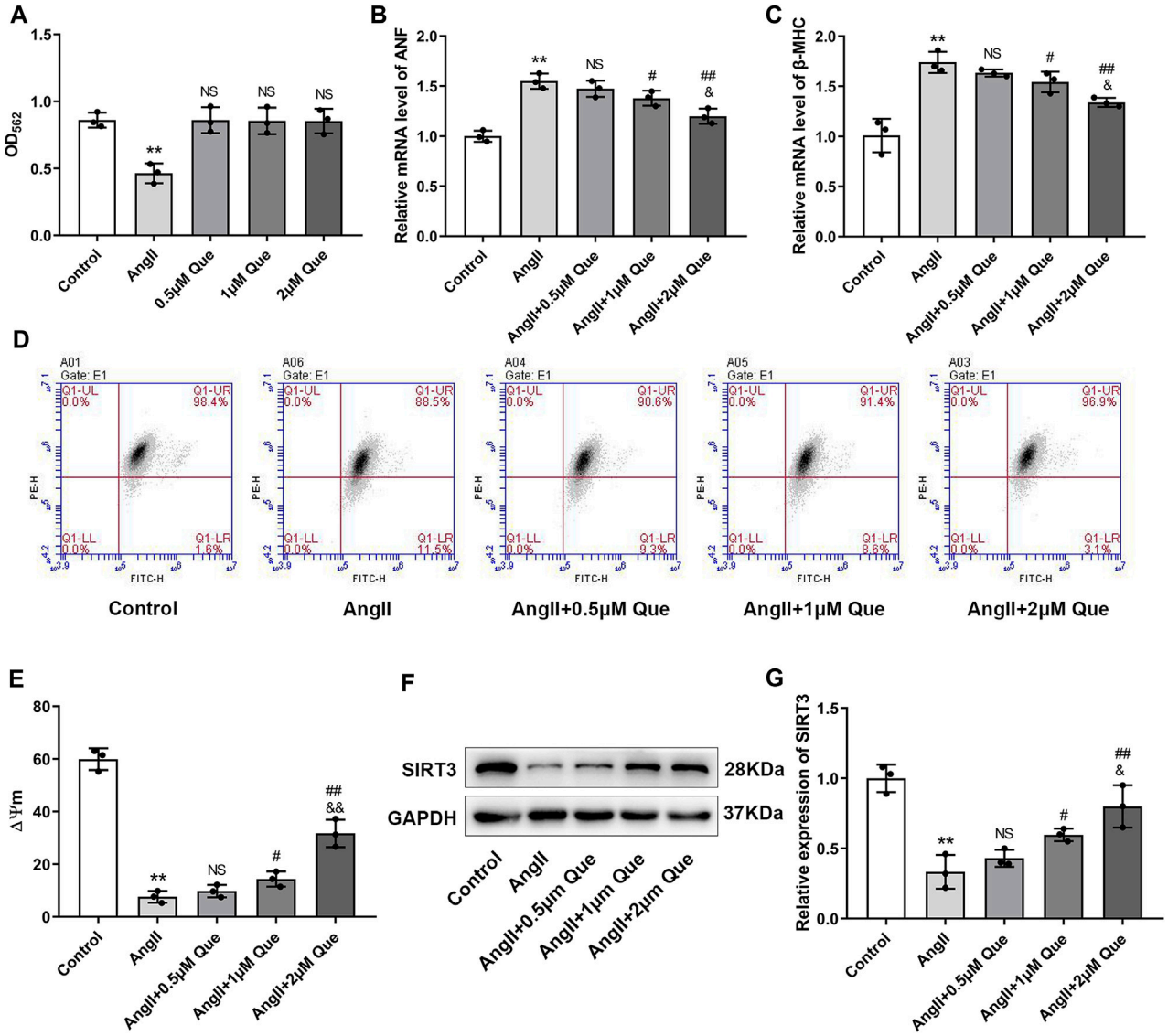

FIGURE 4 | Quercetin inhibits Ang II-induced hypertrophic response in H9c2 cells and protects mitochondrial function *in vitro*. **(A)** Quantitative analysis of viability in H9c2 cells (n = 3). **(B,C)** Atrial natriuretic factor (ANF) and β-myosin heavy chain (β-MHC) mRNA levels determined by q-PCR (n = 3). **(D)** Mitochondrial membrane potential (ΔΨm) measurement with the JC-1 probe. **(E)** Quantification of ΔΨm by the aggregate/monomer ratio (n = 3). **(F,G)** Representative blots of the SIRT3 protein and densitometric quantification after normalization to GAPDH levels (n = 3). Data are mean ± SD. $^{*}p < 0.05$, $^{**}p < 0.01$ *vs* control group; $^{\#}p < 0.05$, $^{\#\#}p < 0.01$ *vs* Ang II group; $^{NS}P > 0.05$ *vs* control/Ang II group; $^{\&}p < 0.05$, $^{\&\&}p < 0.01$ *vs* Ang II + 1 μm Que group.

diabetic cardiomyopathy in mice shows a reduced IP3-stimulated Ca^{2+} transfer to mitochondria, associated with decreased mitochondrial bioenergetics, indicating disruption of reticulum-mitochondria Ca^{2+} transfer leads to mitochondrial dysfunction in diabetic cardiomyopathy (Dia et al., 2020). Consistent with previous studies, impaired mitochondrial function was found in SHRs and Ang II-induced H9c2 cells in this study.

Quercetin, one of the most distributed bioflavonoids, is widely present in a variety of vegetables and fruits. A growing number of studies have reported beneficial effects for quercetin in cardiovascular disease, cancer, metabolic syndrome, Alzheimer's disease, and nervous system disorders (Ebrahimpour et al., 2020; Hosseini et al., 2021). In the present study, quercetin decreased blood pressure and cardiac hypertrophy, including cardiomyocyte hypertrophy and cardiac fibrosis as revealed by changed left ventricular structure and enhanced collagen I and α-SMA, *in vivo*. Interestingly, EF and FS in SHRs still increased instead of decreasing, indicating that the heart pathology was still at the hypertrophic stage but not reflecting heart failure. It is possible that quercetin might restore the excessive systolic function of the heart by preventing pressure overload (Chen et al., 2018), but the underlying mechanism needs further investigation. Ang II, the

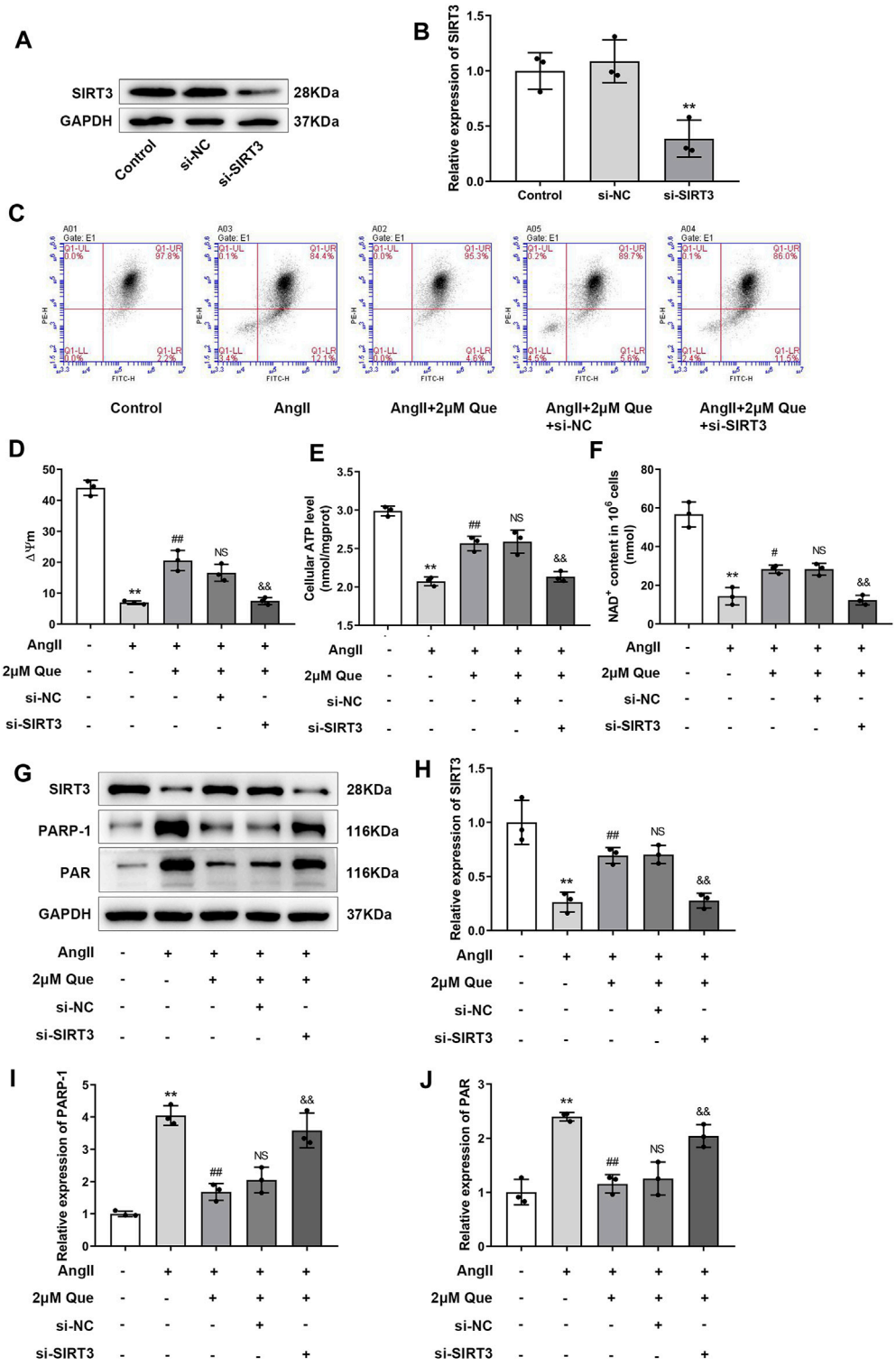

FIGURE 5 | Quercetin protects mitochondrial function *via* SIRT3/PARP-1 pathway. **(A,B)** Representative blots of siRNA-SIRT3-mediated transfection efficiency and densitometric quantification after normalization to GAPDH levels (n = 3). **(C)** ΔΨm measurement with the JC-1 probe. **(D)** Quantification of ΔΨm by the aggregate/monomer ratios (n = 3). **(E)** Quantification of cellular ATP levels with the intracellular ATP Assay Kit (n = 3). **(F)** Introcellular levels of nicotinamide adenine dinucleotide (NAD^+) determined by NAD^+/NADH assay kit (n = 3). **(G–J)** Representative blots of SIRT3, PARP-1 and PAR, and densitometric quantification after normalization to GAPDH levels (n = 3). Data are mean ± SD. $^*p < 0.05$, $^{**}p < 0.01$ *vs* control group; $^{\#}p < 0.05$, $^{\#\#}p < 0.01$ *vs* Ang II group; $^{NS}P > 0.05$ *vs* Ang II + 2 μm Que group; $^{\&}p < 0.05$, $^{\&\&}p < 0.01$ *vs* Ang II + 2 μm Que group.

key component of renin-angiotensin system (RAS), plays a vital role in mediating hypertension (Hall, 1991) and cardiac hypertrophy (Sadoshima et al., 1993). During RAS activation, Ang II binds to its specific receptors such as Ang II type-1 receptor (AT1R), which stimulates aldosterone synthesis and release, involving in the pathogenesis of hypertension and cardiac remodeling (Borghi and Rossi, 2015). Thus, Ang II is widely used to establish the cardiac hypertrophic model. ANF and β-MHC, common biomarkers of cardiac hypertrophy, have been used to investigate hypertrophic effects in clinical studies and animal experiments (Liu et al., 2018; Fulgencio-Covián et al., 2020). The results of the *in vitro* experiment showed that Ang II induction led to the increase of ANF and β-MHC at the mRNA level, while quercetin decreased Ang II-induced ANF and β-MHC upregulation. We speculates that RAS inhibition maybe involved in the anti-hypertrophic effect of quercetin. In addition, it is well known that estrogen is a vital regulator in the pathology of hypertension. A recent evidence has revealed that quercetin could bind to type-2 estrogen receptor at a low dose (10 mg/kg/d) intake (Shahzad et al., 2014). Another research confirms that quercetin exerts cardioprotective effects against estrogen receptor α (ERα)-deficiency-induced cardiac dysfunction (Wang et al., 2021). These evidences indicate a close relationship between quercetin and estrogen. In view of this, further study is needed to investigate the involvement of estrogen in the anti-hypertensive effect of quercetin using female rats.

Quercetin has been proven to protect mice cardiac mitochondria against oxidative stress, since quercetin restores mitochondrial GSH levels and elevates Mn-SOD activity (Ballmann et al., 2015). Moreover, quercetin interacts directly with the mitochondrial membrane and the components of the mitochondrial electron transport chain, affecting ATP production (Qiu et al., 2018; Ryu et al., 2019). Since mitochondrial superoxide is the predominant ROS in mitochondria, and excessive mitochdrial ROS production leads to an overwhelmed antioxidant system and oxidative stress (Munro and Treberg, 2017). Thus we evaluated the anti-oxidant effcts of quercetin by measuring mitochondrial superoxide. In this study, quercetin protected cardiac mitochondria against morphological impairment as well as increased mitochondrial superoxide and oxidative stress in SHRs. In addition, membrane potential disruption and ATP collapse caused by Ang II in cultured H9c2 cells were also rescued by quercetin, indicating that quercetin improves mitochondrial function by alleviating oxidative stress and restoring ATP production.

SIRT3, one of the most prominent deacetylases, is mainly found in the mitochondrial matrix, playing a vital role in the mitochondrial metabolism and homeostasis by modulating the acetylation levels of its substrates, thus protecting mitochondria from functional disorders. Accumulating evidence reveals a close link between SIRT3 and human diseases, including age-related diseases, cancer, cardiovascular diseases and metabolic diseases (Zhang et al., 2020). Among them, the role of SIRT3 in cardiac hypertrophy has attracted considerable attention. A previous study showed that SIRT3 deficiency impairs mitochondrial function and accelerates hypertensive cardiac remodeling through mitochondrial oxidative stress (Wei et al., 2017). Another study reported that SIRT3 attenuates diabetic cardiomyopathy by regulating p53 acetylation and TIGAR expression (Li et al., 2021). PARP-1 is involved in the pathological mechanism of cardiac hypertrophy and heart failure. It was reported that PARP-1 expression is significantly elevated in the onset and progression of cardiac hypertrophy (Pillai et al., 2005). In addition, the PARP-1 inhibitor AG-690/11026014 (6,014) improves Ang II-induced cardiac remodeling and function in mice. Moreover, another PARP-1 inhibitor, L-2286, can not only prevent the development of left ventricular hypertrophy in SHRs, but also modulate mitochondrial dynamics and biogenesis, indicating that PARP-1 may be a therapeutic target in hypertensive cardiac hypertrophy.

In the current study, both SIRT3 expression and NAD^+ content were decreased in Ang II-induced H9c2 cells, indicating that Ang II stimulated hypertrophic response partly through inhibiting SIRT3 activity. But these changes were reversed after quercetin treatment. To further investigate the role of SIRT3 in quercetin pharmacology, SIRT3 was knocked down using small interfering RNA (siRNA). Normal and siRNA H9c2 cells were treated with Ang II with or without quercetin. We found that after SIRT3 knockdown, the downregulation effect of quercetin on PARP-1 activity was partly abolished. Meanwhile, mitochondrial protection by quercetin (oxidative stress and ATP production) was blocked after SIRT3 knockdown. These results suggested that quercetin protects mitochondrial function by modulating SIRT3/PARP-1 signaling pathway, which is involved in the prevention of cardiac hypertrophy.

In summary, the present study provides evidence that quercetin ameliorates cardiac hypertrophy by protecting mitochondrial structure and function in SHRs and Ang II-induced H9c2 cells, involving the SIRT3/PARP-1 pathway. These findings provide a potentially mechanic insight into quercetin-mediated attenuation of cardiac hypertrophy.

LIMITATION

Although we evaluated mitochondrial function using ΔΨm and ATP production *in vitro*, the biological process of mitochondrial function is complicated, and there are several other assays for assessing mitochondrial function. Thus, the pharmacological mechanisms of quercetin's effects on mitochondrial function and cardiac hypertrophy deserve further investigation. Futhermore, we used Ang II as a stimuli to trigger the hypertrophic response *in vitro*, but we didn't detect the expression of RAS in Ang II-induced H9c2 cells. This issue should be further studied in our future work.

DATA AVAILABILITY STATEMENT

The raw data supporting the conclusions of this article will be made available by the authors, without undue reservation.

ETHICS STATEMENT

The animal study was reviewed and approved by the Animal Ethics Committee of Affiliated Hospital of Shandong University of Traditional Chinese Medicine (Jinan, China).

AUTHOR CONTRIBUTIONS

C-HY and Y-HJ designed the experiment, W-JC performed zoology experiments, contributed to animal care, and drafted the manuscript, WL and J-LW performed cytology experiments, YC and X-KD collected samples and analyzed data, C-HY and Y-HJ revised the manuscript. All authors reviewed and approved the final manuscript.

FUNDING

This study was supported by the Taishan Scholar Project of Shandong Province (NO. 2018-35), Jinan City Project of Science-Technology and Development (NO. 202019150) and Shandong Province Science-Technology and Development Project of Traditional Chinese Medicine (NO. 2019-0085).

SUPPLEMENTARY MATERIAL

The Supplementary Material for this article can be found online at: https://www.frontiersin.org/articles/10.3389/fphar.2021.739615/full#supplementary-material

REFERENCES

Ballmann, C., Hollinger, K., Selsby, J. T., Amin, R., and Quindry, J. C. (2015). Histological and Biochemical Outcomes of Cardiac Pathology in Mdx Mice with Dietary Quercetin Enrichment. *Exp. Physiol.* 100 (1), 12–22. doi:10.1113/expphysiol.2014.083360

Borghi, C., Rossi, F., and Rossi, F. (2015). Role of the Renin-Angiotensin-Aldosterone System and its Pharmacological Inhibitors in Cardiovascular Diseases: Complex and Critical Issues. *High Blood Press. Cardiovasc. Prev.* 22 (4), 429–444. doi:10.1007/s40292-015-0120-5

Chen, K., Rekep, M., Wei, W., Wu, Q., Xue, Q., Li, S., et al. (2018). Quercetin Prevents *In Vivo* and *In Vitro* Myocardial Hypertrophy through the Proteasome-GSK-3 Pathway. *Cardiovasc. Drugs Ther.* 32 (1), 5–21. doi:10.1007/s10557-018-6771-4

Chen, Y., Zhang, J., Lin, Y., Lei, Q., Guan, K. L., Zhao, S., et al. (2011). Tumour Suppressor SIRT3 Deacetylates and Activates Manganese Superoxide Dismutase to Scavenge ROS. *EMBO Rep.* 12 (6), 534–541. doi:10.1038/embor.2011.65

Dia, M., Gomez, L., Thibault, H., Tessier, N., Leon, C., Chouabe, C., et al. (2020). Reduced Reticulum-Mitochondria Ca2+ Transfer Is an Early and Reversible Trigger of Mitochondrial Dysfunctions in Diabetic Cardiomyopathy. *Basic Res. Cardiol.* 115 (6), 74. doi:10.1007/s00395-020-00835-7

Ebrahimpour, S., Zakeri, M., and Esmaeili, A. (2020). Crosstalk between Obesity, Diabetes, and Alzheimer's Disease: Introducing Quercetin as an Effective Triple Herbal Medicine. *Ageing Res. Rev.* 62, 101095. doi:10.1016/j.arr.2020.101095

Elbarbry, F., Abdelkawy, K., Moshirian, N., and Abdel-Megied, A. M. (2020). The Antihypertensive Effect of Quercetin in Young Spontaneously Hypertensive Rats; Role of Arachidonic Acid Metabolism. *Int. J. Mol. Sci.* 21 (18), 6554. doi:10.3390/ijms21186554

Facundo, H. D. T. F., Brainard, R. E., Caldas, F. R. L., and Lucas, A. M. B. (2017). Mitochondria and Cardiac Hypertrophy. *Adv. Exp. Med. Biol.* 982, 203–226. doi:10.1007/978-3-319-55330-6_11

Feng, G. S., Zhu, C. G., Li, Z. M., Wang, P. X., Huang, Y., Liu, M., et al. (2017). Synthesis of the Novel PARP-1 Inhibitor AG-690/11026014 and its Protective Effects on Angiotensin II-Induced Mouse Cardiac Remodeling. *Acta Pharmacol. Sin* 38 (5), 638–650. doi:10.1038/aps.2016.159

Feng, X., Wang, Y., Chen, W., Xu, S., Li, L., Geng, Y., et al. (2020). SIRT3 Inhibits Cardiac Hypertrophy by Regulating PARP-1 Activity. *Aging (Albany NY)* 12 (5), 4178–4192. doi:10.18632/aging.102862

Forte, M., Palmerio, S., Bianchi, F., Volpe, M., and Rubattu, S. (2019). Mitochondrial Complex I Deficiency and Cardiovascular Diseases: Current Evidence and Future Directions. *J. Mol. Med. (Berl)* 97 (5), 579–591. doi:10.1007/s00109-019-01771-3

Fulgencio-Covián, A., Alonso-Barroso, E., Guenzel, A. J., Rivera-Barahona, A., Ugarte, M., Pérez, B., et al. (2020). Pathogenic Implications of Dysregulated miRNAs in Propionic Acidemia Related Cardiomyopathy. *Transl Res.* 218, 43–56. doi:10.1016/j.trsl.2019.12.004

Goncharov, S., Portnichenko, G., Tumanovska, L., Goshovska, Y., and Dosenko, V. (2016). Quercetin Prevents Cardiac Hypertrophy, Fibrosis and Lipidosis in Spontaneously Hypertensive Rats and Inhibits Proteasomal Activity. *Acta Physiol.* 217, 36–37.

Hall, J. E. (1991). Control of Blood Pressure by the Renin-Angiotensin-Aldosterone System. *Clin. Cardiol.* 14 (8 Suppl. 4), IV6-5–IV51-25. doi:10.1002/clc.4960141802

Hasan, P., Saotome, M., Ikoma, T., Iguchi, K., Kawasaki, H., Iwashita, T., et al. (2018). Mitochondrial Fission Protein, Dynamin-Related Protein 1, Contributes to the Promotion of Hypertensive Cardiac Hypertrophy and Fibrosis in Dahl-Salt Sensitive Rats. *J. Mol. Cell Cardiol* 121, 103–106. doi:10.1016/j.yjmcc.2018.07.004

Hassa, P. O., and Hottiger, M. O. (2008). The Diverse Biological Roles of Mammalian PARPS, a Small but Powerful Family of Poly-ADP-Ribose Polymerases. *Front. Biosci.* 13, 3046–3082. doi:10.2741/2909

Hosseini, A., Razavi, B. M., Banach, M., and Hosseinzadeh, H. (2021). Quercetin and Metabolic Syndrome: A Review. *Phytotherapy Res.* doi:10.1002/ptr.7144

Hung, C. H., Chan, S. H., Chu, P. M., and Tsai, K. L. (2015). Quercetin Is a Potent Anti-atherosclerotic Compound by Activation of SIRT1 Signaling under oxLDL Stimulation. *Mol. Nutr. Food Res.* 59 (10), 1905–1917. doi:10.1002/mnfr.201500144

Jiang, Y. H., Jiang, L. Y., Wang, Y. C., Ma, D. F., and Li, X. (2020). Quercetin Attenuates Atherosclerosis via Modulating Oxidized LDL-Induced Endothelial Cellular Senescence. *Front. Pharmacol.* 11, 512. doi:10.3389/fphar.2020.00512

Jusic, A., and Devaux, Y. (2020). Mitochondrial Noncoding RNA-Regulatory Network in Cardiovascular Disease. *Basic Res. Cardiol.* 115 (3), 23. doi:10.1007/s00395-020-0783-5

Kadam, A., Jubin, T., Roychowdhury, R., and Begum, R. (2020). Role of PARP-1 in Mitochondrial Homeostasis. *Biochim. Biophys. Acta Gen. Subj* 1864 (10), 129669. doi:10.1016/j.bbagen.2020.129669

Karuppagounder, V., Arumugam, S., Thandavarayan, R. A., Sreedhar, R., Giridharan, V. V., and Watanabe, K. (2016). Molecular Targets of Quercetin with Anti-inflammatory Properties in Atopic Dermatitis. *Drug Discov. Today* 21 (4), 632–639. doi:10.1016/j.drudis.2016.02.011

Kumar, V., A, A. K., Sanawar, R., Jaleel, A., Santhosh Kumar, T. R., and Kartha, C. C. (2019). Chronic Pressure Overload Results in Deficiency of Mitochondrial Membrane Transporter ABCB7 Which Contributes to Iron Overload, Mitochondrial Dysfunction, Metabolic Shift and Worsens Cardiac Function. *Sci. Rep.* 9 (1), 13170. doi:10.1038/s41598-019-49666-0

Li, L., Zeng, H., He, X., and Chen, J. X. (2021). Sirtuin 3 Alleviates Diabetic Cardiomyopathy by Regulating TIGAR and Cardiomyocyte Metabolism. *J. Am. Heart Assoc.* 10 (5), e018913. doi:10.1161/jaha.120.018913

Liu, B. L., Cheng, M., Hu, S., Wang, S., Wang, L., Tu, X., et al. (2018). Overexpression of miR-142-3p Improves Mitochondrial Function in Cardiac Hypertrophy. *Biomed. Pharmacother.* 108, 1347–1356. doi:10.1016/j.biopha.2018.09.146

Manolis, A. S., Manolis, A. A., Manolis, T. A., Apostolaki, N. E., Apostolopoulos, E. J., Melita, H., et al. (2021). Mitochondrial Dysfunction in Cardiovascular

Disease: Current Status of Translational Research/clinical and Therapeutic Implications. *Med. Res. Rev.* 41 (1), 275–313. doi:10.1002/med.21732

McDermott-Roe, C., Ye, J., Ahmed, R., Sun, X. M., Serafín, A., Ware, J., et al. (2011). Endonuclease G Is a Novel Determinant of Cardiac Hypertrophy and Mitochondrial Function. *Nature* 478 (7367), 114–118. doi:10.1038/nature10490

Munro, D., and Treberg, J. R. (2017). A Radical Shift in Perspective: Mitochondria as Regulators of Reactive Oxygen Species. *J. Exp. Biol.* 220 (Pt 7), 1170–1180. doi:10.1242/jeb.132142

Nakamura, M., and Sadoshima, J. (2018). Mechanisms of Physiological and Pathological Cardiac Hypertrophy. *Nat. Rev. Cardiol.* 15 (7), 387–407. doi:10.1038/s41569-018-0007-y

Nunnari, J., and Suomalainen, A. (2012). Mitochondria: in Sickness and in Health. *Cell* 148 (6), 1145–1159. doi:10.1016/j.cell.2012.02.035

Palomer, X., Román-Azcona, M. S., Pizarro-Delgado, J., Planavila, A., Villarroya, F., Valenzuela-Alcaraz, B., et al. (2020). SIRT3-mediated Inhibition of FOS through Histone H3 Deacetylation Prevents Cardiac Fibrosis and Inflammation. *Signal. Transduct Target. Ther.* 5 (1), 14. doi:10.1038/s41392-020-0114-1

Park, S., Mori, R., and Shimokawa, I. (2013). Do sirtuins Promote Mammalian Longevity? A Critical Review on its Relevance to the Longevity Effect Induced by Calorie Restriction. *Mol. Cell* 35 (6), 474–480. doi:10.1007/s10059-013-0130-x

Pham, T., Loiselle, D., Power, A., and Hickey, A. J. (2014). Mitochondrial Inefficiencies and Anoxic ATP Hydrolysis Capacities in Diabetic Rat Heart. *Am. J. Physiol. Cell Physiol* 307 (6), C499–C507. doi:10.1152/ajpcell.00006.2014

Pillai, J. B., Russell, H. M., Raman, J., Jeevanandam, V., and Gupta, M. P. (2005). Increased Expression of poly(ADP-Ribose) Polymerase-1 Contributes to Caspase-independent Myocyte Cell Death during Heart Failure. *Am. J. Physiol. Heart Circ. Physiol.* 288 (2), H486–H496. doi:10.1152/ajpheart.00437.2004

Pillai, V. B., Samant, S., Sundaresan, N. R., Raghuraman, H., Kim, G., Bonner, M. Y., et al. (2015). Honokiol Blocks and Reverses Cardiac Hypertrophy in Mice by Activating Mitochondrial Sirt3. *Nat. Commun.* 6, 6656. doi:10.1038/ncomms7656

Qiu, L., Luo, Y., and Chen, X. (2018). Quercetin Attenuates Mitochondrial Dysfunction and Biogenesis via Upregulated AMPK/SIRT1 Signaling Pathway in OA Rats. *Biomed. Pharmacother.* 103, 1585–1591. doi:10.1016/j.biopha.2018.05.003

Reyes-Farias, M., and Carrasco-Pozo, C. (2019). The Anti-cancer Effect of Quercetin: Molecular Implications in Cancer Metabolism. *Int. J. Mol. Sci.* 20 (13), 3177. doi:10.3390/ijms20133177

Ryu, K. W., Kim, D. S., and Kraus, W. L. (2015). New Facets in the Regulation of Gene Expression by ADP-Ribosylation and poly(ADP-Ribose) Polymerases. *Chem. Rev.* 115 (6), 2453–2481. doi:10.1021/cr5004248

Ryu, S., Park, S., Lim, W., and Song, G. (2019). Quercetin Augments Apoptosis of Canine Osteosarcoma Cells by Disrupting Mitochondria Membrane Potential and Regulating PKB and MAPK Signal Transduction. *J. Cell Biochem* 120 (10), 17449–17458. doi:10.1002/jcb.29009

Sadoshima, J., Xu, Y., Slayter, H. S., and Izumo, S. (1993). Autocrine Release of Angiotensin II Mediates Stretch-Induced Hypertrophy of Cardiac Myocytes *In Vitro*. *Cell* 75 (5), 977–984. doi:10.1016/0092-8674(93)90541-w

Shahzad, H., Giribabu, N., Muniandy, S., and Salleh, N. (2014). Quercetin Induces Morphological and Proliferative Changes of Rat's Uteri under Estrogen and Progesterone Influences. *Int. J. Clin. Exp. Pathol.* 7 (9), 5484–5494.

Waldman, M., Nudelman, V., Shainberg, A., Abraham, N. G., Kornwoski, R., Aravot, D., et al. (2018). PARP-1 Inhibition Protects the Diabetic Heart through Activation of SIRT1-PGC-1α axis. *Exp. Cell Res* 373 (1-2), 112–118. doi:10.1016/j.yexcr.2018.10.003

Wang, G., Li, Y., Lei, C., Lei, X., Zhu, X., Yang, L., et al. (2021). Quercetin Exerts Antidepressant and Cardioprotective Effects in Estrogen Receptor α-deficient Female Mice via BDNF-AKT/ERK1/2 Signaling. *J. Steroid Biochem. Mol. Biol.* 206, 105795. doi:10.1016/j.jsbmb.2020.105795

Wang, L., Tan, A., An, X., Xia, Y., and Xie, Y. (2020). Quercetin Dihydrate Inhibition of Cardiac Fibrosis Induced by Angiotensin II *In Vivo* and *In Vitro*. *Biomed. Pharmacother.* 127, 110205. doi:10.1016/j.biopha.2020.110205

Wei, T., Huang, G., Gao, J., Huang, C., Sun, M., Wu, J., et al. (2017). Sirtuin 3 Deficiency Accelerates Hypertensive Cardiac Remodeling by Impairing Angiogenesis. *J. Am. Heart Assoc.* 6 (8), e006114. doi:10.1161/jaha.117.006114

Xiong, S., Sun, H. J., Cao, L., Zhu, M., Liu, T., Wu, Z., et al. (2019). Stimulation of Na+/K+-ATPase with an Antibody against its 4th Extracellular Region Attenuates Angiotensin II-Induced H9c2 Cardiomyocyte Hypertrophy via an AMPK/SIRT3/PPARγ Signaling Pathway. *Oxid Med. Cell Longev* 2019, 4616034. doi:10.1155/2019/4616034

Xu, D., Hu, M. J., Wang, Y. Q., and Cui, Y. L. (2019a). Antioxidant Activities of Quercetin and its Complexes for Medicinal Application. *Molecules* 24 (6), 1123. doi:10.3390/molecules24061123

Xu, M., Xue, R. Q., Lu, Y., Yong, S. Y., Wu, Q., Cui, Y. L., et al. (2019b). Choline Ameliorates Cardiac Hypertrophy by Regulating Metabolic Remodelling and UPRmt through SIRT3-AMPK Pathway. *Cardiovasc. Res.* 115 (3), 530–545. doi:10.1093/cvr/cvy217

Zhang, J., Xiang, H., Liu, J., Chen, Y., He, R. R., and Liu, B. (2020). Mitochondrial Sirtuin 3: New Emerging Biological Function and Therapeutic Target. *Theranostics* 10 (18), 8315–8342. doi:10.7150/thno.45922

Conflict of Interest: The authors declare that the research was conducted in the absence of any commercial or financial relationships that could be construed as a potential conflict of interest.

Publisher's Note: All claims expressed in this article are solely those of the authors and do not necessarily represent those of their affiliated organizations, or those of the publisher, the editors and the reviewers. Any product that may be evaluated in this article, or claim that may be made by its manufacturer, is not guaranteed or endorsed by the publisher.

frontiers in Pharmacology

ORIGINAL RESEARCH
published: 05 November 2021
doi: 10.3389/fphar.2021.731609

G Protein–Coupled Estrogen Receptor 30 Reduces Transverse Aortic Constriction–Induced Myocardial Fibrosis in Aged Female Mice by Inhibiting the ERK1/2 -MMP-9 Signaling Pathway

Xiaowu Wang†, Jipeng Ma†, Shuaishuai Zhang†, Zilin Li, Ziwei Hong, Liqing Jiang, Weixun Duan and Jincheng Liu**

Department of Cardiovascular Surgery, Xijing Hospital, Fourth Military Medical University, Xi'an, China

The incidence of cardiovascular diseases was significantly increased in postmenopausal women. The protection of estrogen in the cardiovascular system has been further reported for decades. Although menopausal hormone therapy has been used in many clinical trials, the debatable results indicate that the studies for elucidating the precise molecular mechanism are urgently required. G protein–coupled estrogen receptor 30 (GPR30) is a membrane receptor of estrogen and displays protective roles in diverse cardiovascular diseases. Previous studies have revealed that ERK1/2-mediated MMP-9 signaling was involved in ischemic heart diseases. However, the role of ERK1/2-mediated MMP-9 signaling in the protection of GPR30 against cardiac hypertrophy in aged female mice has not been investigated. Our present study demonstrated that GPR30 overexpression and its agonist G1 co-administration reduced transverse aortic constriction–induced myocardial fibrosis and preserved cardiac function in aged female mice. MMP-9 expression was markedly increased *via* ERK1/2 phosphorylation in transverse aortic constriction–injured myocardium of aged female mice. Further results showed that GPR30/G1 activation decreased MMP-9 expression *via* ERK1/2 inhibition, which further reduced TGF-β1 expression. Inhibition of the ERK1/2 signaling pathway by its inhibitor PD98059 suppressed the induction of the cardiomyocyte MMP-9 level caused by the GRP30 antagonist G15 and inhibited TGF-β1 expression in cardiac fibroblast *in vitro*. In summary, our results from *in vivo* and *in vitro* studies indicated that GPR30 activation inhibited myocardial fibrosis and preserved cardiac function *via* inhibiting ERK-mediated MMP-9 expression. Thus, the present study may provide the novel drug targets for prevention and treatment of cardiac pathological hypertrophy in postmenopausal women.

Keywords: G protein–coupled estrogen receptor 30 (GPR30), transverse aortic constriction, MMP-9, aged female, cardiac fibrosis

OPEN ACCESS

Edited by:
Helene Tronchere, Institut National de la Santé et de la Recherche Médicale (INSERM), France

Reviewed by:
Michael A. Hill, University of Missouri, United States
Carlos Alonso Escudero, University of the Bío-Bío, Chile

****Correspondence:***
Jincheng Liu
liujch@fmmu.edu.cn
Weixun Duan
duanweixun@126.com

†These authors have contributed equally to this work

Specialty section:
This article was submitted to Cardiovascular and Smooth Muscle Pharmacology, a section of the journal Frontiers in Pharmacology

Received: *27 June 2021*
Accepted: *30 September 2021*
Published: *05 November 2021*

Citation:
Wang X, Ma J, Zhang S, Li Z, Hong Z, Jiang L, Duan W and Liu J (2021) G Protein–Coupled Estrogen Receptor 30 Reduces Transverse Aortic Constriction–Induced Myocardial Fibrosis in Aged Female Mice by Inhibiting the ERK1/2 -MMP-9 Signaling Pathway. Front. Pharmacol. 12:731609. doi: 10.3389/fphar.2021.731609

INTRODUCTION

Cardiovascular disease is the leading cause of death worldwide, which accounts for 17.3 million death each year (Mendis et al., 2011; Laslett et al., 2012). Clinical studies revealed that the incidence of cardiovascular diseases was much lower in premenopausal women than in age-matched men (Iorga et al., 2017), whereas women at age of 50 years have high cardiovascular risk as compared to men at age of 70 years (Lloyd-Jones et al., 2006). These studies strongly indicate that estrogen and its receptor-mediated signaling pathways may play a cardioprotective role in diverse cardiovascular diseases in postmenopausal women (Aryan et al., 2020). Furthermore, a clinical statistical analysis showed that patients who had bilateral oophorectomy were associated with double risk of coronary heart disease, as compared with age-matched premenopausal women (Parker et al., 2009). Although accumulating evidence suggested the increased cardiovascular risk after menopause, menopausal hormone therapy (MHT) for prevention and treatment of cardiovascular diseases is still controversial (Schierbeck et al., 2012; Boardman et al., 2015; Manson et al., 2020). Thus, elucidating the underlying molecular mechanisms may identify the potential drug targets for treating cardiovascular diseases in postmenopausal women.

G protein–coupled receptor 30 (GPR30), also designated as G protein–coupled estrogen receptor (GPER), is a seven-transmembrane protein and a novel estrogen receptor, besides the two classic nuclear receptors ERα and ERβ. Previous studies have demonstrated that GPR30 is widely expressed and participates in multiple biological functions including glucose tolerance, bone growth, and blood pressure regulation (Chagin & Sävendahl, 2007; Hazell et al., 2009; Lindsey et al., 2009; Mårtensson et al., 2009; Groban et al., 2019). It was further revealed that GPR30 activation protected neurons from ischemia-induced injury through autophagy regulation (Wang et al., 2020). GPR30 preserved neuronal survival in a cerebral ischemia mouse model induced by cardiac arrest and cardiopulmonary resuscitation (Kosaka et al., 2012). In particular, our previous data showed that GPR30 protected the heart against myocardial infarction and diabetes-induced cardiac dysfunction in the female ovariectomized murine model (Wang et al., 2018; Wang et al., 2019). However, the role of GPR30 in the hypertrophied heart of aged female mice needs further investigation.

MMP-9 belongs to matrix metalloproteinase superfamily and can maintain extracellular matrix homeostasis *via* matrix metalloprotein degradation (Radosinska et al., 2017). It thus exacerbated cardiac fibrosis and inhibited angiogenesis following myocardial infarction since extracellular matrix remodeling was a key pathological feature of ischemia cardiac injury (Ducharme et al., 2000; Lindsey et al., 2006). However, whether GPR30 activation could regulate MMP-9 expression was still unclear. Therefore, the present study was designed to investigate the role of GPR30, and its downstream signaling pathway focusing on MMP-9–mediated fibrosis in transverse aortic constriction (TAC)–induced cardiac hypertrophy of aged female mice.

MATERIALS AND METHODS

Reagents

GPR30 (ab37742), vimentin (ab92547), cardiac troponin I (ab47003), TGF-β1 (ab27969), and MMP-9 38,898) were purchased from Abcam. ERK 4,695) and *p*-ERK (4,370) were purchased from Cell Signaling Technology. GAPDH was obtained from Santa Cruz Biotechnology (Santa Cruz, CA, United States). The rabbit anti-goat, goat anti-rabbit, and goat anti-mouse secondary antibodies were purchased from the Zhongshan Company (Beijing, China). The MMP-9 ELISA kit was purchased from Elabscience Bioengineering Institute (Wuhan, China). GPR30 agonist G1 (10,008,933) and GPR30 antagonist G15 14,673) were purchased from Cayman Chemical (Ann Arbor, MI, United States). The ERK inhibitor PD98059 (HY-12028) and DOX (HY-15142) were purchased from MCE. AAV-GPR30 was purchased from the GeneChem Company (Shanghai, China). DAPI was obtained from Roche Molecular Biochemicals (Bayer, Mannheim, Germany). The ECL reagent was purchased from Millipore (Billerica, MA, United States).

Experimental Animals

Female C57BL/6 mice (20–25 g, 18 months old, obtained from the Experimental Animal Center of Fourth Military Medical University) were housed in individual cages under a 12:12-h light/dark cycle (light on 06:00) at 22–24 °C and fed with regular pellet diet *ad libitum*. The subjects in this study were mice which were raised and used in experiments in accordance with the Guide for the Care and Use of Laboratory Animals of the Chinese Animal Welfare Committee.

In vivo Experimental Design and Treatment

All animal experiments were approved by the Institutional Animal Care and Use Committee of Fourth Military Medical University. The *in vivo* experiments were designed to investigate the influence of the estrogen receptor GPR30 on the cardiac function and myocardial fibrosis in hypertrophied aged female mice. Mice were randomly divided into the following four experimental groups: 1) aged female mice (AG group), 2) the AG + GPR30/G1 group, 3) the AG/TAC group, and 4) the AG/TAC + GPR30/G1 group. Mice were subjected to a tail intravenous injection of 5×10^{10} adeno-associated virus genome particles carrying GPR30 in the AG + GPR30/G1 group and the AG/TAC + GPR30/G1 group, while the equal amount of empty adeno-associated virus was injected in the AG group and the AG/TAC group. Briefly, awake mice were placed in a special device to avoid the movement of mice for tail vein injection. Then the tail of the mouse was wiped with a 75% ethanol cotton ball, followed by a tail vein injection with the volume of 50 μl. Mice in the AG/TAC group and the AG/TAC + GPR30/G1 group underwent TAC operation after 3 weeks, while those in the AG group and the AG + GPR30/G1 group were underwent sham operation. Following the surgery, the AG + GPR30/G1 group and the AG/TAC + GPR30/G1 group were injected intraperitoneally with G1 each day with a dose of 35 μg/kg body weight. The cardiac function of the mouse from

each group was assessed at the time of fourth and eighth weeks following the operation.

Transverse Aortic Constriction Surgery Protocol

TAC surgery was performed to establish cardiac hypertrophy in the mouse model, as previously described (Wang et al., 2013). Briefly, mice were anesthetized in an induction chamber with 1–2% isoflurane mixed with pure oxygen (0.5–1.0 l/min), which were then intubated endotracheally and connected to a ventilator (Minivent Type 845, Hugo Sachs Electronic, March, Germany, 100–120/min 0.15-ml tidal volume). Median thoracotomy was performed to expose the aortic arch, which was then constricted using a 7–0 silk suture tied firmly with a 27-gauge needle between the carotid arteries. The needle was immediately removed, and the chest was closed and sutured. Sham-operated mice underwent the same operation procedure, except for the ligation of aortic arch. After the surgery, mice were placed on a 38°C insulation blanket to keep warm and were observed carefully until they were free to move around.

Echocardiography

The ultrasound technicians were not informed of the protocol of the study and the details of the animal groups to ensure unbiased reporting. After the mouse was anesthetized with 1–2% isoflurane, the left front chest hair of the mouse was removed. Transthoracic ultrasonography was performed using a VisualSonics 2,100 echocardiograph (FUJIFILM VisualSonics, Toronto, ON, Canada), and a 30-MHz transducer was used to obtain the images in both parasternal long axis and short axis of the left ventricle. The indexes that can be detected through echocardiography included ejection fraction (EF)% and fraction shortening (FS)% (indicating the cardiac function), interventricular septal thickness at end diastole (IVSd), and left ventricular posterior wall thickness at end diastole (LVPWd) (indicating the thickness of ventricular wall). The aforementioned parameters were calculated by Vevo Lab 3.1.0 software (FUJIFILM VisualSonics. Toronto, ON, Canada).

Heart Weight, Body Weight, and Histological Examination

After completion of the experiments, mice were euthanized, and their hearts were harvested. The heart weight (HW) and body weight (BW) were recorded. From these data, the HW/BW ratios were calculated.

Hearts of mice used for morphological observation were fixed in 4% paraformaldehyde for 72 h, embedded in paraffin, and cut into 5-μm sections. Histomorphology was evaluated by hematoxylin and eosin (H&E) staining. Myocardial fibrosis was evaluated by Masson Staining, and the cell cross-sectional area was evaluated by wheat germ agglutinin (WGA) staining.

Neonatal Rat Cardiomyocytes and Neonatal Rat Cardiac Fibroblasts Culture and Treatment

Newborn Sprague–Dawley (SD) rats were obtained from the Experimental Animal Center of the Fourth Military Medical University. Isolation and culture of neonatal rat cardiomyocytes (NRCMs) and neonatal rat cardiac fibroblasts (NRCFs) were performed, as described previously (Zhai et al., 2017). Briefly, the heart was harvested from newborn SD rats and cut into small pieces. The small pieces of myocardium were digested in phosphate-buffered saline (PBS) solution containing 1% collagenase I (Sigma V900891, Sigma-Aldrich, St. Louis, MO, United States). After passing through the sieve to remove tissue fragments, the cells were culture for 2 h in a CO_2 incubator. The non-adherent NRCMs were transferred to another culture flask or confocal dish, and the remaining adherent cells are mostly NRCFs. NRCMs were plated at a density of 5×10^5 cells per ml and were cultured in the serum containing culture medium DME/F-12 (Gibco, Carlsbad, CA, United States), 10% new bovine serum (Gibco, Carlsbad, CA, United States), penicillin (100 U/ml), streptomycin (100 U/ml), and bromodeoxyuridine (BrdU) (0.1 mM) for 48 h at 37 °C with 5% CO_2. After culturing for 24 h, NRCFs were plated at a density of 5×10^5 cells/ml and cultured in the same medium as NRCMs.

In vitro experiments are designed to investigate the expression of *p*-ERK1/2, ERK1/2, and MMP-9 in primary cultured cardiomyocytes in the Dox + Ang II state (simulating the aging pressure-overload stress) by the GPR30 agonist G1/antagonist G15 and the changes in the content of MMP-9 in the culture medium of each group. After the intervention of G1 or G15, the effects of the culture supernatant on cardiomyocytes and the subsequent different treatments on the expression of TGF-β1 of cardiac fibroblast were examined. The neonatal rat cardiomyocytes were isolated and divided into five groups. The cell without any treatment was considered as the control group (CON group). The cells in the Dox group were treated with 0.1 μM Dox for 24 h to mimic cell senescence, while the cells in the Dox + Ang II group were treated with 0.1 μM Dox combined with 0.1 μM Ang II for 24 h (Spallarossa et al., 2009). Cardiomyocytes were then treated with GPR30 agonist 10 nM G1 or GPR30 antagonist 1 μM G15 for 24 h in the indicated groups. For inhibition of ERK1/2 by its inhibitor, cells were first treated with 10 μM PD98059 for 24 h. The culture medium following diverse treatments was then transferred to cardiac fibroblast for 24-h treatment to examine the interaction between cardiomyocytes and fibroblast.

Immunofluorescence Staining

The immunofluorescence staining experiments were performed with myocardium or isolated cells from neonatal hearts. NRCM- or NRCF-covered confocal dishes were washed with PBS following diverse treatments and then fixed with 4% paraformaldehyde at 4°C for 30 min. The tissues or cells were then treated with 0.05% Triton X-100 for permeabilization and were incubated with 1% bovine serum albumin, followed by incubation with primary antibodies targeting GPR30 (1:250), MMP-9 (1:800), *p*-ERK (1:800), TGF-β1 (1:200), vimentin (1:250), or troponin I (1:100) overnight at 4°C. Then cells were incubated with secondary antibodies for 2 h at room temperature. Nuclear staining was performed with DAPI. Tissue slides and cell slides were examined with an Olympus FV1000 laser confocal microscope (Olympus, Japan). ImageJ software was used to

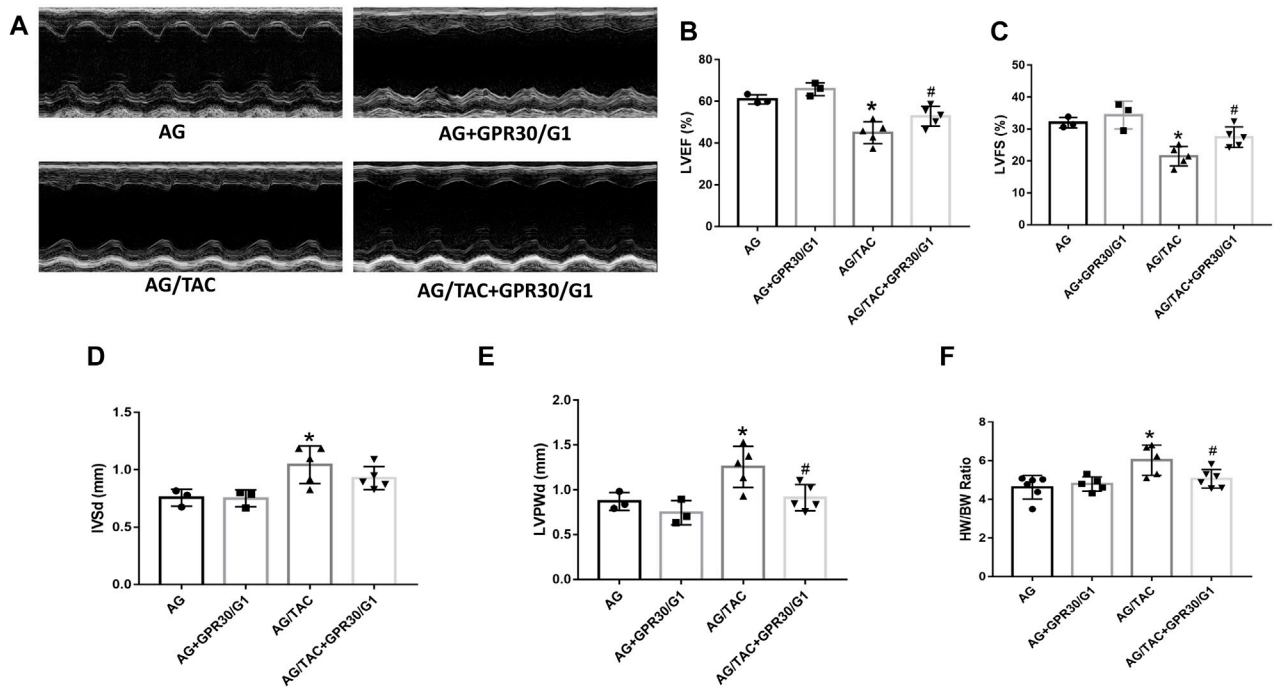

FIGURE 1 | Effects of GPR30 activation on cardiac function four weeks after TAC surgery in aged female mice. Mouse underwent TAC surgery three weeks after tail vein injection of GPR30 adeno-associated virus, and M-mode echocardiography was performed four weeks thereafter. **(A)** Representative M-mode images by echocardiography. **(B)** LVEF. **(C)** LVFS. **(D)** IVSd. **(E)** LVPWd. **(F)** HW/BW ratio. The results were expressed as mean ± S.E.M, $n = 3–6$, $^*p < 0.05$ compared with the AG group. $\#p < 0.05$ compared with the AG/TAC group.

quantify the fluorescence of tissue slides and cell slides in each group.

Western Blot Analysis

As previously described, protein samples from myocardium and cells were extracted using a RIPA buffer with a protease inhibitor and a phosphatase inhibitor, separated by 8–12% SDS-PAGE, and transferred to a polyvinylidene fluoride membrane (Millipore). Membranes were blocked in Tris-buffered saline with 0.1% Tween containing 5% non-fat milk for 2 h at room temperature, followed by incubation with primary antibodies targeting GPR30 (1:1,000), MMP-9 (1:1,000), *p*-ERK (1:1,000), or TGF-β1 (1:1,000) overnight at 4°C. Then the membranes were incubated with the corresponding secondary horseradish peroxidase–conjugated antibodies (1:5,000) for 2 h at room temperature. The blots were visualized using enhanced chemiluminescence reagent (Millipore). GAPDH was determined as an internal loading control. The density of each band was quantified using Image Lab software (Bio-Rad Laboratories, United States).

Determination of MMP-9

The levels of MMP-9 in the culture supernatant of NRCMs in different treatment groups were determined with ELISA kits (Elabscience Bioengineering Institute, China), following the manufacture's instruction.

Statistical Analysis

All values were presented as mean ± S.E.M, and all statistical tests were performed using GraphPad Prism software (version 7.0, GraphPad Software Inc, San Diego, CA, United States). The normality of the distribution was assessed using the Shapiro–Wilk test. The statistical analysis among multiple groups was performed using one-way ANOVA followed by Bonferroni multiple comparisons test. A value of $p < 0.05$ was considered statistically significant.

RESULTS

Effects of GPR30 on Cardiac Function and HW/BW in Aged Female Mice Surgery at the Fourth Week After Transverse Aortic Constriction Surgery

This *in vivo* study tried to elucidate the effects of GPR30 activation on cardiac hypertrophy in aged female mice. To fully activate GPR30, the GPR30-specific agonist G1 and GPR30 adeno-associated virus were used. M-mode echocardiography results of different groups are shown in **Figure 1**. The LVEF and LVFS in the AG/TAC group were worsened than those in the AG group, whereas those in the AG/TAC + GPR30/G1 group were partially recovered compared to those in the AG/TAC group (**Figures 1B,C**). For cardiac

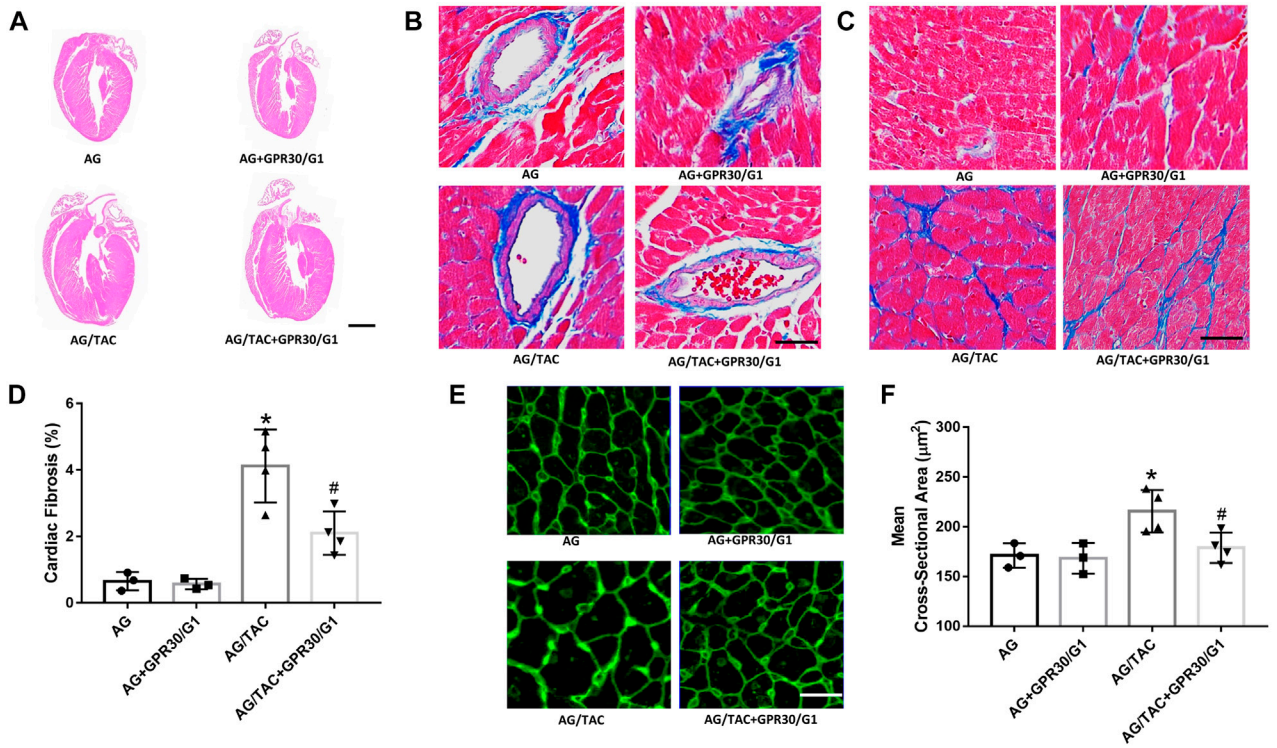

FIGURE 2 | Effects of cardiac fibrosis and morphology four weeks after myocardial TAC surgery in aged female mice. **(A)** Cardiac HE staining (bar = 0.5 mm). **(B–C)** Cardiac Masson trichrome staining (bar = 100 μm). **(D)** Cardiac fibrosis ratio. **(E)** WGA staining (bar = 100 μm). **(F)** Mean cross-sectional area of cardiomyocytes. The results are expressed as mean ± S.E.M, n = 3–4. *p < 0.05 compared with the AG group. #p < 0.05 compared with the AG/TAC group.

hypertrophy, compared to the AG group, IVSd and LVPWd were significantly enlarged in the AG/TAC group, while the LVPWd in the AG/TAC + GPR30/G1 group was reduced compared to that in the AG/TAC group (**Figures 1D,E**). The HW/BW ratio of the AG/TAC group was significantly increased compared to that of the AG group, while this ratio was inhibited in the AG/TAC + GPR30/G1 group (**Figure 1F**). These results together indicated that cardiac function of aged female mice was impaired at the fourth week after TAC surgery, while GPR30/G1 administration could partially recover cardiac function in aged female mice following TAC, showing a cardioprotective effect.

Effects of GPR30/G1 Treatment on Cardiac Fibrosis of Aged Female Mice at Fourth Week After Transverse Aortic Constriction Surgery

The hallmarks of cardiac remodeling caused by pressure overload are changes in the myocardial cell size, ventricular wall thickness, and myocardial fibrosis. HE staining, Masson staining, and WAG staining were used to observe the effect of GPR30 activation on myocardial remodeling caused by pressure overload at the fourth week after TAC surgery. HE staining showed that the ventricular wall thickness was increased in the AG/TAC group compared to the AG group, while the reduction trend of ventricular wall thickness was observed in the AG/TAC + GPR30/G1 group, which was consistent with our echocardiographic data and the HW/BW ratio. The results of Masson staining (**Figures 2B,C**) showed that myocardial fibrosis of the heart tissue in the AG/TAC group was significantly elevated compared to the AG group at the fourth week after TAC surgery. GPR30/G1 treatment for 4-week intervention inhibited cardiac fibrosis in the AG/TAC + GPR30/G1 group (**Figure 2D**). WAG staining results further showed (**Figure 2E**) that the size of cardiomyocytes in heart tissue in the AG/TAC group was significantly increased compared to the AG group. However, it was significantly reduced after 4-week GPR30/G1 intervention in the AG/TAC + GPR30/G1 group (**Figure 2F**).

Effects of GPR30/G1 Treatment on Cardiac Function of Aged Female Mice at Eighth Week After TAC Surgery

To further assess the long-term effects of GPR30 activation on cardiac hypertrophy in aged female mice, cardiac function and fibrosis were examined in 8 weeks post TAC surgery. The results showed that cardiac LVEF and LVFS in the AG/TAC group further deteriorated compared to those in the AG group, whereas those indices in the AG/TAC + GPR30/G1 group were significantly recovered compared to those in the AG/TAC group (**Figures 3B,C**). The IVSd and LVPWd in the AG/TAC group were significantly enlarged compared to those in the AG

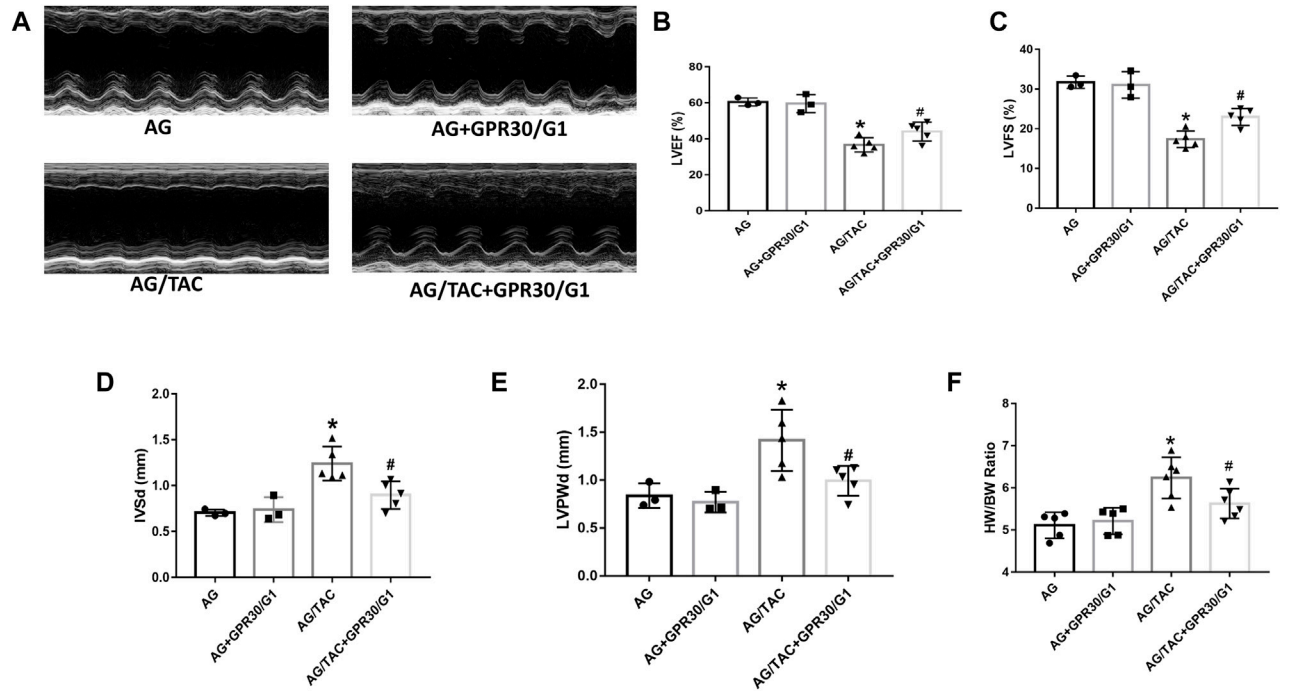

FIGURE 3 | Effects of cardiac function eight weeks after myocardial TAC surgery in aged female mice. Mouse underwent TAC surgery three weeks after tail vein injection of GPR30 adeno-associated virus, and M-mode echocardiography was performed eight weeks thereafter. **(A)** Representative M-mode images by echocardiography. **(B)** LVEF. **(C)** LVFS. **(D)** IVSd. **(E)** LVPWd. **(F)** HW/BW ratio. The results are expressed as mean ± S.E.M, $n = 3–6$, $^{*}p < 0.05$ compared with the AG group. $\#p < 0.05$ compared with the AG/TAC group.

group, whereas those in the AG/TAC + GPR30/G1 group were significantly lower than those in the AG/TAC group (**Figures 3D,E**). The HW/BW ratio of AG/TAC group was significantly elevated compared to the AG group, while this ratio was greatly decreased in the AG/TAC + GPR30/G1 group (**Figure 3F**). All these data indicated that the heart function of mice was worsened at the eighth week following TAC surgery, and GPR30/G1 treatment could partially inhibit cardiac damage in the long term in response to pressure overload.

GPR30/G1 Co-Administration Reduced Cardiac Fibrosis After 8 Weeks of Transverse Aortic Constriction Surgery

HE staining, Masson staining, and WAG staining were employed to investigate the effects of GPR30 on cardiac remodeling caused by pressure load after 8 weeks of TAC surgery. The results of Masson staining (**Figures 4B,C**) showed that myocardial fibrosis in the AG + TAC group was aggravated at the eighth week after TAC surgery compared to the AG group. GPR30/G1 intervention for 8 weeks attenuated cardiac fibrosis in the AG/TAC + GPR30/G1 group (**Figure 4D**). In order to further confirm whether GPR30/G1 treatment could reduce the cardiac hypertrophy response caused by pressure overload at the time of the eighth week post-TAC surgery, the cross-sectional cell area of cardiac tissue was determined by WGA staining (**Figures 4E,F**). The average cross-sectional area of cardiac tissue at the time point of the eighth week after TAC surgery in the AG/TAC group was enlarged, while the average myocardial cross-sectional cell area in the AG/TAC + GPR30/G1 group was mitigated following 8 weeks of GPR30/G1 intervention. However, myocardial fibrosis was comparable between the AG group and the AG + GPR30/G1 group.

Effects of GPR30 Agonist G1 Co-Administration for 8 Weeks on the Expression of GPR30, *p*-ERK, ERK, MMP-9, and TGF-β1 Proteins in Myocardial Tissue of Aged Female Mice in Response to Pressure Overload

Western blot results revealed that continuous intraperitoneal injection of GPR30 agonist G1 for 8 weeks combined with GPR30 overexpression affected the expressions of GPR30, *p*-ERK, ERK, MMP-9, and TGF-β1 proteins in the myocardium of aged TAC mice (**Figure 5A**). GPR30/G1 significantly increased the expression of GPR30 in the myocardial tissue of the AG + GPR30/G1 group and the AG/TAC + GPR30/G1 group (**Figure 5B**). Following TAC surgery, the ratio of *p*-ERK1/2 to ERK1/2 in the myocardial tissue of the AG/TAC group increased significantly, while GPR30/G1 can significantly reduce the ratio of *p*-ERK1/2 to ERK1/2 in the myocardial tissue compared to the AG/TAC group (**Figure 5C**). The expression of MMP-9 in the myocardial tissue of the AG/TAC group was significantly increased, which was significantly decreased by GPR30/G1 treatment (**Figure 5D**).

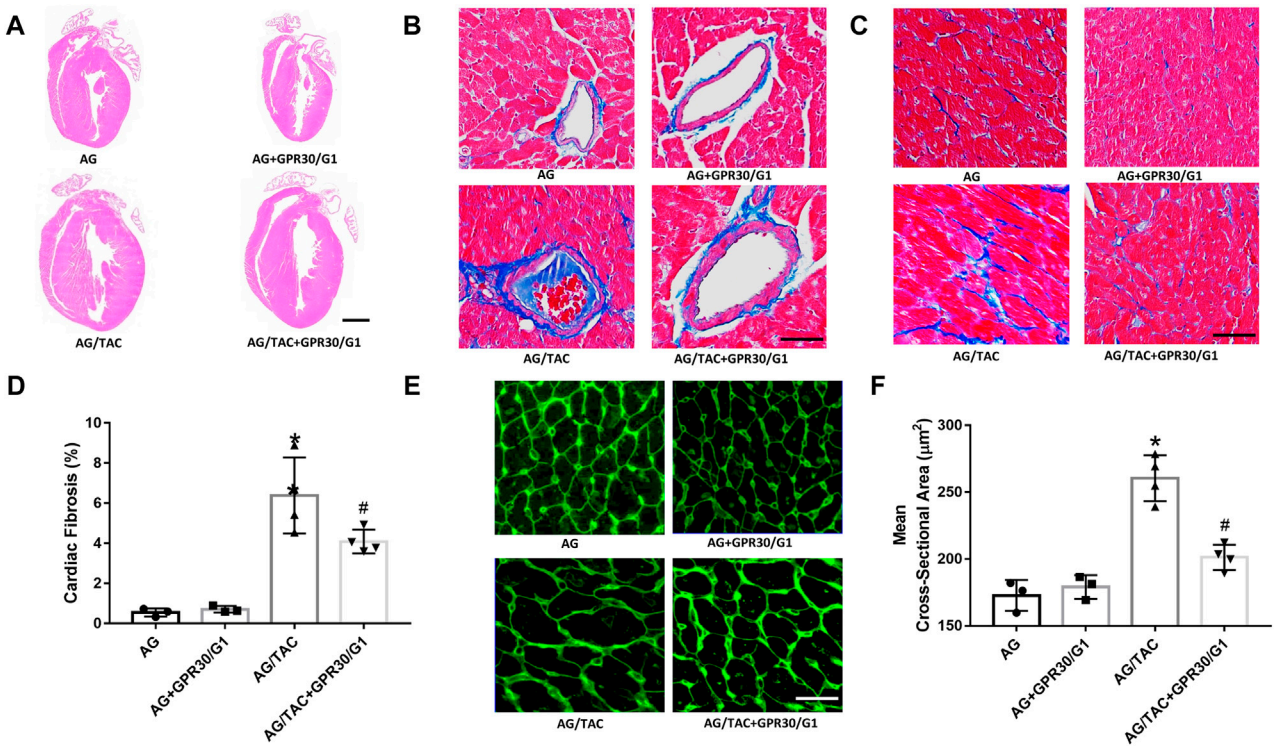

FIGURE 4 | Effects of cardiac fibrosis and morphology eight weeks after myocardial TAC surgery in aged female mice. **(A)** Cardiac HE staining (bar = 0.5 mm). **(B–C)** Cardiac Masson trichrome staining (bar = 100 μm). **(D)** Cardiac fibrosis ratio. **(E)** WGA staining (bar = 100 μm). **(F)** Mean cross-sectional area of cardiomyocytes. The results are expressed as mean ± S.E.M, n = 3–4. *p < 0.05 compared with the AG group. #p < 0.05 compared with the AG/TAC group.

Meanwhile, the reduction of TGF-β1 expression in myocardium was observed in the AG/TAC + GPR30/G1 group compared to that in the AG/TAC group (**Figure 5E**).

The results of immunofluorescent staining revealed that GPR30/G1 significantly elevated the expressions of GPR30 in the TAC-injured myocardium of aged female mice (**Figures 5F–H**). Furthermore, compared with AG, the expression of MMP-9 in the myocardial tissue of the AG/TAC group was significantly increased, while GPR30/G1 intervention decreased the expression of MMP-9 significantly (**Figures 5F–H**).

As shown in **Figure 5 I-K**, the expression of TGF-β1 was increased in the AG/TAC group following pressure overload, while GRP30/G1 treatment greatly inhibited the TGF-β1 protein level. Our *in vivo* results showed that GPR30/G1 activation may be associated with the reduction of TGF-β1 and myocardial fibrosis, which may be related with ERK-regulated MMP-9 expression.

Effects of GPR30 Agonist G1 on the Expressions of *p*-ERK1/2, ERK1/2, and MMP-9 in the Simulated Senescent Cardiomyocytes as well as on the Expression of TGF-β1 in Cardiac Fibroblasts

Primary cultured cardiomyocytes express troponin but not vimentin, and fibroblasts express vimentin but not troponin, which is consistent with the description of cardiomyocytes and cardiac fibroblasts (**Figure 6A**). Dox and Ang II greatly enhanced the phosphorylated ERK1/2 in cardiomyocytes, while G1 treatment significantly reduced the ratio of *p*-ERK1/2 to ERK1/2 in the Dox group and the Dox + Ang II group (**Figure 6 B** and **C**). Furthermore, MMP-9 expression assessed by Western blot and ELISA was significantly inhibited by G1 treatment, which was significantly induced by addition of Dox + Ang II (**Figure 6 B**, **D**, and **E**). Following these treatments, TGF-β1 expression was increased in the Dox + Ang II group, while G1 treatment decreased the expression of TGF-β1 (**Figure 6 F** and **G**).

Effects of GPR30 Antagonist G15 and ERK Inhibitor PD98059 on the Expressions of *p*-ERK1/2, ERK1/2, and MMP-9 in the Simulated Aged Cardiomyocytes as well as on the Expression of TGF-β1 in Cardiac Fibroblasts

The results from Western blot showed that G15 treatment upregulated phosphorylated ERK1/2 and MMP-9 expression compared to the Dox + Ang II group, while PD98059 could reverse the effects of G15 addition, as evidenced by the reduction of phosphorylated ERK1/2 and MMP-9 expression (**Figures 7A–D**). The data from ELISA also showed that G15 elevated

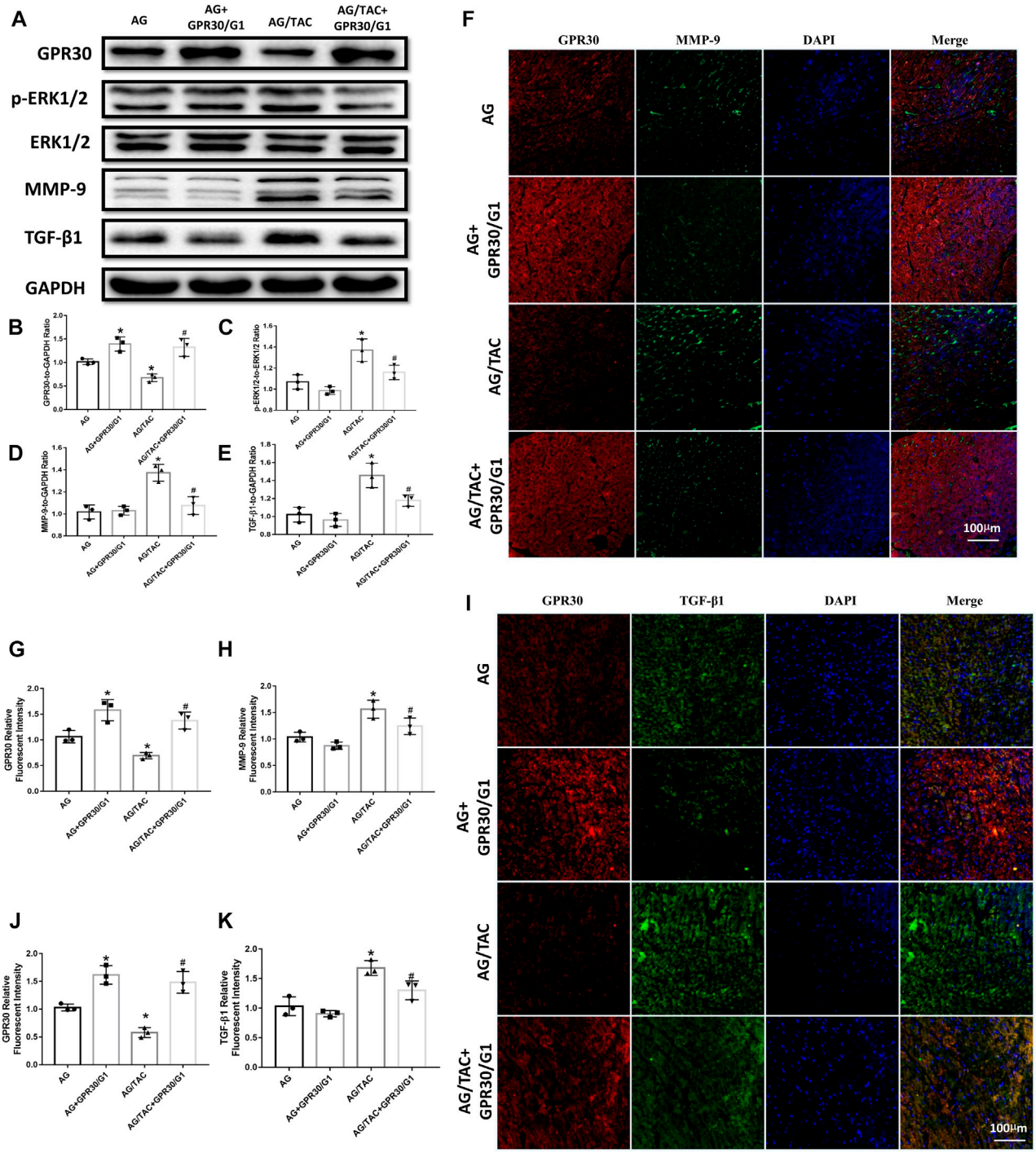

FIGURE 5 | Effects of 8-week GPR30/G1 treatment on the protein expression levels of GPR30, *p*-ERK1/2, ERK1/2, MMP-9, and TGF-β1 in mice subjected to TAC. **(A)** Representative images of the Western blot. **(B)** GPR30 protein level. **(C)** *p*-ERK1/2 to ERK1/2 protein level. **(D)** MMP-9 protein level. **(E)** TGF-β1 protein level. **(F)** Representative confocal microscopy images of myocardial tissue stained with GPR30, MMP-9, and DAPI. Red fluorescence for GPR30 expression. Green fluorescence for MMP-9 expression. Blue fluorescence for nuclei of total cells (bar = 100 μm). **(G)** IFC intensity of GPR30. **(H)** IFC intensity of MMP-9. **(I)** Representative confocal microscopy images of myocardial tissue stained with GPR30, TGF-β1, and DAPI. Red fluorescence for GPR30 expression. Green fluorescence for TGF-β1 expression. Blue fluorescence for nuclei of total cells (bar = 100 μm). **(J)** IFC intensity of GPR30. **(K)** IFC intensity of TGF-β1. The results are expressed as mean ± S.E.M, $n = 3$. *$p <$ 0.05 compared with the AG group. #$p < 0.05$ compared with the AG/TAC group.

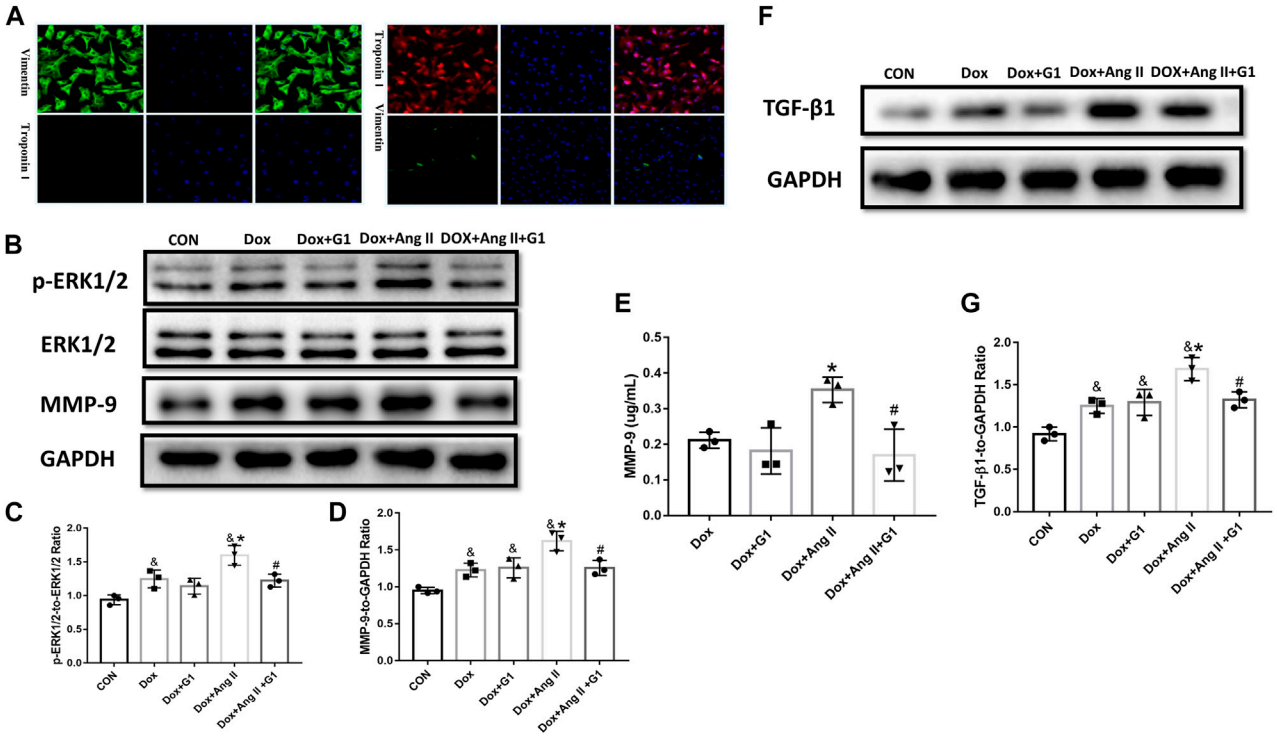

FIGURE 6 | Effects of GPR30 agonist G1 on the expression of *p*-ERK1/2, ERK1/2, and MMP-9 protein in DOX/Ang II-treated cardiomyocytes and on the expression of TGF-β1 in cardiac fibroblast. **(A)** Primary CFs express vimentin and are negative for troponin, which is consistent with the characteristics of primary cultured cardiac fibroblasts. **(B)** Representative images of Western blot. **(C)** *p*-ERK1/2 to ERK1/2. **(D)** MMP-9 expression. **(E)** The content of MMP-9 in the culture medium of cardiomyocytes. **(F)** Representative images of Western blot. **(G)** TGF-β1 expression. The results were expressed as mean ± S.E.M, $n = 3$. $^{*}p < 0.05$ compared with the Dox group, $\#p < 0.05$ compared with the Dox + Ang II group.

MMP-9 expression of cell culture medium, while this could be reversed by PD98059 treatment (**Figure 7E**). Moreover, TGF-β1 expression was increased in the Dox + Ang II + G15 group, while PD98059 treatment decreased the expression of TGF-β1 (**Figure 7 F** and **G**).

DISCUSSION

With the use of ovariectomized rodent models, we have previously explored the function of GPR30 in pathological condition such as myocardial infarction and diabetes-induced myocardial injury (Wang et al., 2018; Wang et al., 2019). Here, we further investigated the effects of GPR30 activation on TAC-induced cardiac hypertrophy of aged female mice. The novel finding of the present study was that GPR30 activation could reduce TAC-induced cardiac fibrosis through downregulation of the MMP-9 level, which may provide the potential therapeutic targets for the treatment of pathological cardiac hypertrophy in postmenopausal women.

Since the incidence of cardiovascular diseases differs significantly between men and women, the protection of estrogen in the cardiovascular system has been proposed and reported for decades (Mendelsohn & Karas, 1999). Especially, the observation of higher risk of cardiovascular diseases with the lower estradiol level among postmenopausal women further emphasized the vital function of estrogen for the cardiovascular system. Thus, several studies including observational research and clinical trials were conducted to evaluate the effects of estrogen supplement on the incidence of cardiovascular diseases of postmenopausal women (Barrett-Connor & Bush, 1991; Rossouw et al., 2002). Although the results from Nurses' Health Study showed the benefits of estrogen use to decrease both the incidence of coronary heart diseases and the mortality from cardiovascular diseases in menopause women (Stampfer et al., 1991), the reduction of morbidity of cardiovascular diseases by estrogen supplement was not observed in the Framingham Heart Study (Wilson et al., 1985). Therefore, not only double-blind, randomized controlled trials are required to further validate the previous study but also well-designed animal studies should be conducted to reveal the precise molecular mechanisms to better explain these contradictory clinical data.

Estrogen receptors play important roles to mediate multiple biological functions of estrogen. Till date, GPR30 is the only membrane receptor of estrogen that protects the heart from diverse pathological injuries (Mizukami, 2010; Feldman & Limbird, 2017). A previous study showed that the activation of GPR30 by its agonist G1 improved cardiac diastolic function and reduced cardiac fibrosis in ovariectomized female mRen2.Lewis

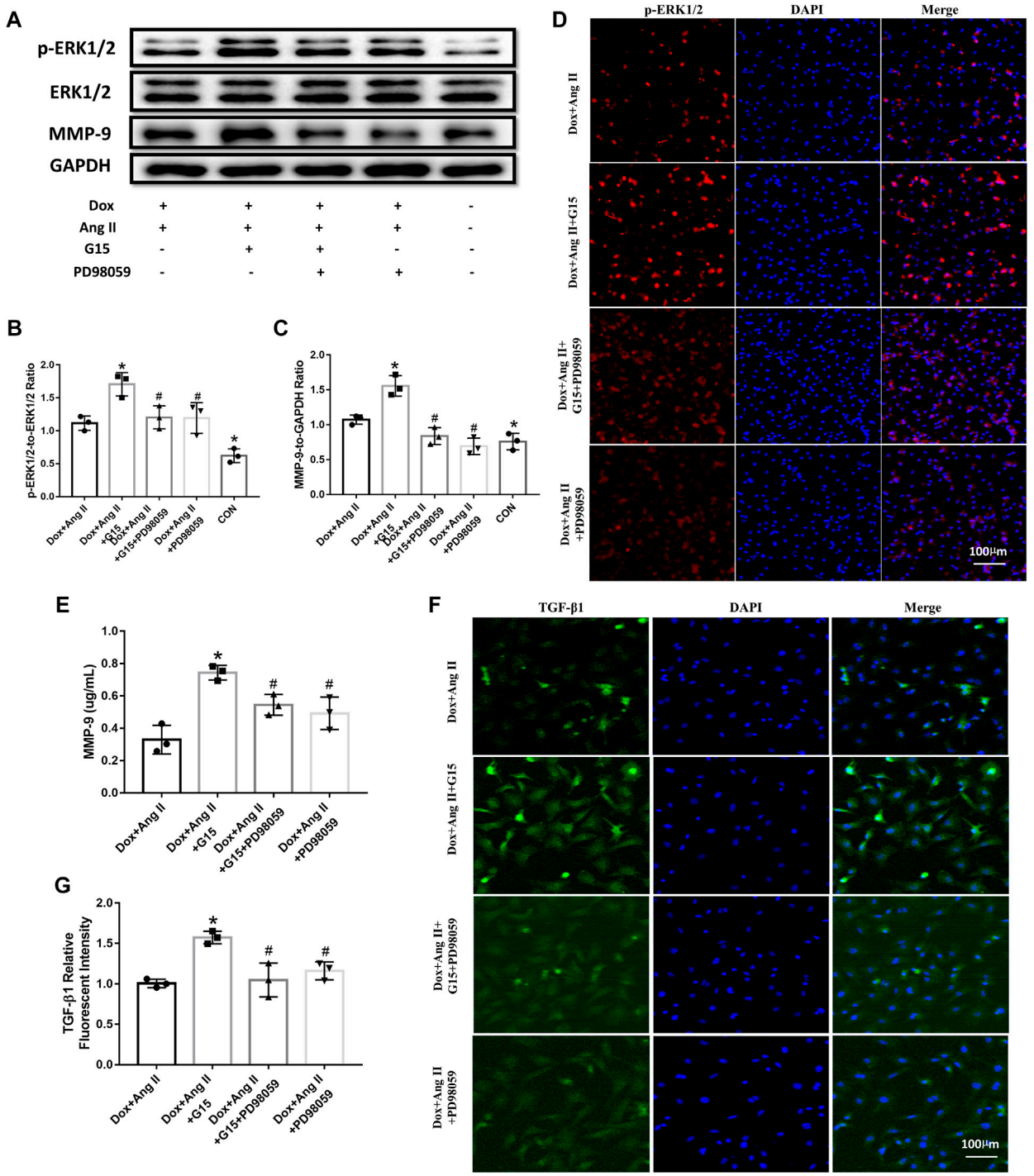

FIGURE 7 | Effects of GPR30 antagonist G15 on *p*-ERK1/2, ERK1/2, and MMP-9 in cardiomyocytes, and the effect on the expression of TGF-β1 in fibroblasts. **(A)** Representative blots of Western blot. **(B)** *p*-ERK1/2 to ERK1/2. **(C)** MMP-9 expression. **(D)** Representative confocal microscopy images of primary cultured cardiomyocytes stained with *p*-ERK and DAPI. Red fluorescence for *p*-ERK expression. Blue fluorescence for nuclei of total cardiomyocytes (bar = 100 μm). **(E)** The content of MMP-9 in the culture medium of cardiomyocytes. **(F)** Representative confocal microscopy images of primary cultured cardiomyocytes stained with TGF-β1 and DAPI. Red fluorescence for TGF-β1 expression. Blue fluorescence for nuclei of total cardiac fibroblasts (bar = 100 μm). **(G)** TGF-β1 expression. *$p < 0.05$ compared with the Dox + Ang II group. #$p < 0.05$ compared with the Dox + Ang II+G15 group.

rats (Wang et al., 2012). Moreover, G1 administration attenuated ischemic cardiac injury by using a Langendorff rat model in a gender-independent manner (Deschamps & Murphy, 2009). Our present study employed the aged hypertrophied hearts of female mice to show that LVEF and LVFS in aged female mice were worsened and IVSd and LVPWd were partially recovered at the fourth week post-TAC surgery. The Masson staining revealed that cardiac fibrosis was exacerbated, and the cross-sectional area of cardiomyocytes was further enlarged. Moreover, these indices were aggravated at the eighth week post-TAC. Our results also showed that GPR30 activation could partially recover LVEF and LVFS, inhibit IVSd and LVPWd, and mitigate the fibrotic area of cardiac tissues at both four and eight weeks following TAC surgery. Taken together, these results clearly indicated that activation of GPR30 could partially protect the cardiac function and attenuate cardiac fibrosis in aged female hypertrophied hearts.

Furthermore, the underlying molecular mechanism of GPR30 activation on cardiac fibrosis was further clarified. The present data showed that cardiac fibrotic areas at both myocardial interstitial tissue and the perivascular space were decreased following GPR30 overexpression and G1 administration evidenced by Masson staining. The phosphorylated ERK1/2 was upregulated in response to pressure overload induced by TAC, which as a member of MAPK superfamily has been shown to contribute to pathogenesis of cardiac hypertrophy (Braz et al., 2002; Lorenz et al., 2009). Our data further revealed that GPR30 activation and G1 treatment could inhibit ERK1/2 phosphorylation in aged hypertrophied hearts *in vivo*. These results indicated that this reduction of cardiac fibrosis was associated with suppressed ERK1/2 signaling. Meanwhile, the reduction of MMP-9 in myocardium was observed following GPR30/G1 treatments. The components of the myocardial extracellular matrix were regulated by the balance of numerous matrix metalloproteinases including MMP-9, and the disruption of this balance can cause cardiac fibrosis (Fan et al., 2012). It was reported that MMP-9 expression was induced *via* ERK1/2 signaling in H9c2 cells challenged by lipopolysaccharides (Cheng et al., 2009). Mice lacking MMP-9 have better cardiac function and less left ventricular remodeling than the wild type in response to pressure overload (Heymans et al., 2005), which indicated that MMP-9 inhibitors may preserve cardiac function in pathological hypertrophy. Our results also revealed that MMP-9 expression was increased following TAC surgery in aged female mice hearts, while GPR30 activation could partially inhibit MMP-9 expression. Furthermore, the fibrotic marker protein TGF-β1 was significantly upregulated following TAC surgery in aged female mice hearts, while GPR30/G1 treatment greatly reduced TGF-β1 expression, implying the inhibition of myocardial fibrosis by GPR30 activation. The *in vitro* study showed that G1 treatment decreased angiotensin II and doxorubicin-induced MMP-9 expression in neonatal cardiomyocytes. The MMP-9 level in the supernatant of the cardiomyocyte culture was increased following angiotensin II and doxorubicin treatment, which was reduced by G1 treatment. Furthermore, addition of GPR30 antagonist G15 could elevate ERK1/2 phosphorylation and MMP-9 expression, which can be reversed by ERK1/2 inhibitor PD98059. By adding the culture medium from cardiomyocytes to fibroblasts, the TGF-β1 expression of fibroblasts was increased in the medium, which was treated by angiotensin II and doxorubicin, while the TGF-β1 expression of fibroblast was inhibited in the medium which was treated by G1. Taken together, these results favored the notion that GRP30 activation inhibited MMP-9 expression *via* ERK1/2 signaling to at least partially preserve cardiac function and inhibited myocardial fibrosis in aged female hypertrophied hearts.

Although the ovariectomized female mouse is a powerful model for studying the effects of estrogen use, aging is a more complex pathological process, instead of bilateral oophorectomy. Thus, in order to fully mimic the pathological condition of postmenopausal women, mice at the age of 18 months were used in this study. Second, despite overexpression of GPR30 by adeno-associated virus delivery in our study, we further intraperitoneally injected the agonist G1 to thoroughly activate GPR30. While our present study clarified the vital role of GPR30 activation in aged hypertrophied female hearts, there are some limitations, which can be improved in further studies. In this study, we used GPR30 adeno-associated virus to overexpress GPR30. But GPR30 knockout or transgenic mice should be used in future studies, the result of which may provide valid evidence. Second, we only observed cardiac hypertrophy and cardiac function till 8 weeks post-TAC surgery. The long-term results may indicate the potential beneficial or detrimental effects of GPR30 activation.

In summary, this study demonstrated that GPR30 and G1 co-administration reduced TAC-induced cardiac fibrosis and preserved cardiac contractile function in aged female hearts. These effects were attributed to GPR30 activation and the subsequent inhibition of ERK1/2-mediated MMP-9 expression. By using an *in vitro* model, the importance of ERK1/2 in mediating GPR30 protection against TAC-induced cardiac fibrosis was verified by ERK1/2 signaling inhibitor PD98059. Collectively, our results presented the new potential drug for the treatment of cardiac pathological hypertrophy in postmenopausal women.

DATA AVAILABILITY STATEMENT

The raw data supporting the conclusion of this article will be made available by the authors, without undue reservation.

ETHICS STATEMENT

The animal study was reviewed and approved by the Experimental Animal Center in the Fourth Military Medical University.

AUTHOR CONTRIBUTIONS

JL and WD conceived and designed the research; XW, JM, SZ, and ZH performed the experiments; ZH and LJ analyzed the data;

ZL, XW, and JM established the animal models; and XW, JM, and JL wrote, revised, and checked the manuscript. All authors have reviewed the contents of the manuscript, validated the accuracy of the data, and approved the submitted manuscript.

ACKNOWLEDGMENTS

This study was supported by grants from the National Natural Science Foundation of China (82070264, 82070503), the Natural Science Foundation of the Shaanxi Province (2019 PT-24), and the Subject Boosting Project of Xijing Hospital (XJZT19Z04, XJZT19X13).

SUPPLEMENTARY MATERIAL

The Supplementary Material for this article can be found online at: https://www.frontiersin.org/articles/10.3389/fphar.2021.731609/full#supplementary-material

REFERENCES

Aryan, L., Younessi, D., Zargari, M., Banerjee, S., Agopian, J., Rahman, S., et al. (2020). The Role of Estrogen Receptors in Cardiovascular Disease. *Int. J. Mol. Sci.* 21 (12). doi:10.3390/ijms21124314

Barrett-Connor, E., and Bush, T. L. (1991). Estrogen and Coronary Heart Disease in Women. *Jama* 265 (14), 1861–1867. doi:10.1001/jama.1991.03460140089033

Boardman, H. M., Hartley, L., Eisinga, A., Main, C., Roqué i Figuls, M., Bonfill Cosp, X., et al. (2015). Hormone Therapy for Preventing Cardiovascular Disease in post-menopausal Women. *Cochrane Database Syst. Rev.* (3), CD002229. doi:10.1002/14651858.CD002229.pub4

Braz, J. C., Bueno, O. F., De Windt, L. J., and Molkentin, J. D. (2002). PKC Alpha Regulates the Hypertrophic Growth of Cardiomyocytes through Extracellular Signal-Regulated Kinase1/2 (ERK1/2). *J. Cel Biol* 156 (5), 905–919. doi:10.1083/jcb.200108062

Chagin, A. S., and Sävendahl, L. (2007). GPR30 Estrogen Receptor Expression in the Growth Plate Declines as Puberty Progresses. *J. Clin. Endocrinol. Metab.* 92 (12), 4873–4877. doi:10.1210/jc.2007-0814

Cheng, Y. C., Chen, L. M., Chang, M. H., Chen, W. K., Tsai, F. J., Tsai, C. H., et al. (2009). Lipopolysaccharide Upregulates uPA, MMP-2 and MMP-9 via ERK1/2 Signaling in H9c2 Cardiomyoblast Cells. *Mol. Cel Biochem* 325 (1-2), 15–23. doi:10.1007/s11010-008-0016-y

Deschamps, A. M., and Murphy, E. (2009). Activation of a Novel Estrogen Receptor, GPER, Is Cardioprotective in Male and Female Rats. *Am. J. Physiol. Heart Circ. Physiol.* 297 (5), H1806–H1813. doi:10.1152/ajpheart.00283.2009

Ducharme, A., Frantz, S., Aikawa, M., Rabkin, E., Lindsey, M., Rohde, L. E., et al. (2000). Targeted Deletion of Matrix Metalloproteinase-9 Attenuates Left Ventricular Enlargement and Collagen Accumulation after Experimental Myocardial Infarction. *J. Clin. Invest.* 106 (1), 55–62. doi:10.1172/JCI8768

Fan, D., Takawale, A., Lee, J., and Kassiri, Z. (2012). Cardiac Fibroblasts, Fibrosis and Extracellular Matrix Remodeling in Heart Disease. *Fibrogenesis Tissue Repair* 5 (1), 15. doi:10.1186/1755-1536-5-15

Feldman, R. D., and Limbird, L. E. (2017). GPER (GPR30): A Nongenomic Receptor (GPCR) for Steroid Hormones with Implications for Cardiovascular Disease and Cancer. *Annu. Rev. Pharmacol. Toxicol.* 57, 567–584. doi:10.1146/annurev-pharmtox-010716-104651

Groban, L., Tran, Q. K., Ferrario, C. M., Sun, X., Cheng, C. P., Kitzman, D. W., et al. (2019). Female Heart Health: Is GPER the Missing Link? *Front. Endocrinol. (Lausanne)* 10, 919. doi:10.3389/fendo.2019.00919

Hazell, G. G., Yao, S. T., Roper, J. A., Prossnitz, E. R., O'Carroll, A. M., and Lolait, S. J. (2009). Localisation of GPR30, a Novel G Protein-Coupled Oestrogen Receptor, Suggests Multiple Functions in Rodent Brain and Peripheral Tissues. *J. Endocrinol.* 202 (2), 223–236. doi:10.1677/JOE-09-0066

Heymans, S., Lupu, F., Terclavers, S., Vanwetswinkel, B., Herbert, J. M., Baker, A., et al. (2005). Loss or Inhibition of uPA or MMP-9 Attenuates LV Remodeling and Dysfunction after Acute Pressure Overload in Mice. *Am. J. Pathol.* 166 (1), 15–25. doi:10.1016/S0002-9440(10)62228-6

Iorga, A., Cunningham, C. M., Moazeni, S., Ruffenach, G., Umar, S., and Eghbali, M. (2017). The Protective Role of Estrogen and Estrogen Receptors in Cardiovascular Disease and the Controversial Use of Estrogen Therapy. *Biol. Sex. Differ.* 8 (1), 33. doi:10.1186/s13293-017-0152-8

Kosaka, Y., Quillinan, N., Bond, C., Traystman, R., Hurn, P., and Herson, P. (2012). GPER1/GPR30 Activation Improves Neuronal Survival Following Global Cerebral Ischemia Induced by Cardiac Arrest in Mice. *Transl Stroke Res.* 3 (4), 500–507. doi:10.1007/s12975-012-0211-8

Laslett, L. J., Alagona, P., Jr., Clark, B. A., 3rd, Drozda, J. P., Jr., Saldivar, F., Wilson, S. R., et al. (2012). The Worldwide Environment of Cardiovascular Disease: Prevalence, Diagnosis, Therapy, and Policy Issues: a Report from the American College of Cardiology. *J. Am. Coll. Cardiol.* 60 (25 Suppl. l), S1–S49. doi:10.1016/j.jacc.2012.11.002

Lindsey, M. L., Escobar, G. P., Dobrucki, L. W., Goshorn, D. K., Bouges, S., Mingoia, J. T., et al. (2006). Matrix Metalloproteinase-9 Gene Deletion Facilitates Angiogenesis after Myocardial Infarction. *Am. J. Physiol. Heart Circ. Physiol.* 290 (1), H232–H239. doi:10.1152/ajpheart.00457.2005

Lindsey, S. H., Cohen, J. A., Brosnihan, K. B., Gallagher, P. E., and Chappell, M. C. (2009). Chronic Treatment with the G Protein-Coupled Receptor 30 Agonist G-1 Decreases Blood Pressure in Ovariectomized mRen2.Lewis Rats. *Endocrinology* 150 (8), 3753–3758. doi:10.1210/en.2008-1664

Lloyd-Jones, D. M., Leip, E. P., Larson, M. G., D'Agostino, R. B., Beiser, A., Wilson, P. W., et al. (2006). Prediction of Lifetime Risk for Cardiovascular Disease by Risk Factor burden at 50 Years of Age. *Circulation* 113 (6), 791–798. doi:10.1161/CIRCULATIONAHA.105.548206

Lorenz, K., Schmitt, J. P., Schmitteckert, E. M., and Lohse, M. J. (2009). A New Type of ERK1/2 Autophosphorylation Causes Cardiac Hypertrophy. *Nat. Med.* 15 (1), 75–83. doi:10.1038/nm.1893

Manson, J. E., Bassuk, S. S., Kaunitz, A. M., and Pinkerton, J. V. (2020). The Women's Health Initiative Trials of Menopausal Hormone Therapy: Lessons Learned. *Menopause* 27 (8), 918–928. doi:10.1097/GME.0000000000001553

Mårtensson, U. E., Salehi, S. A., Windahl, S., Gomez, M. F., Swärd, K., Daszkiewicz-Nilsson, J., et al. (2009). Deletion of the G Protein-Coupled Receptor 30 Impairs Glucose Tolerance, Reduces Bone Growth, Increases Blood Pressure, and Eliminates Estradiol-Stimulated Insulin Release in Female Mice. *Endocrinology* 150 (2), 687–698. doi:10.1210/en.2008-0623

Mendelsohn, M. E., and Karas, R. H. (1999). The Protective Effects of Estrogen on the Cardiovascular System. *N. Engl. J. Med.* 340 (23), 1801–1811. doi:10.1056/NEJM199906103402306

Mendis, S., Puska, P., and Norrving, B. (2011). *Global Atlas on Cardiovascular Disease Prevention and Control*. Geneva, Switzerland: World Health Organization.

Mizukami, Y. (2010). *In Vivo* functions of GPR30/GPER-1, a Membrane Receptor for Estrogen: from Discovery to Functions *In Vivo*. *Endocr. J.* 57 (2), 101–107. doi:10.1507/endocrj.k09e-332

Parker, W. H., Jacoby, V., Shoupe, D., and Rocca, W. (2009). Effect of Bilateral Oophorectomy on Women's Long-Term Health. *Womens Health (Lond)* 5 (5), 565–576. doi:10.2217/whe.09.42

Radosinska, J., Barancik, M., and Vrbjar, N. (2017). Heart Failure and Role of Circulating MMP-2 and MMP-9. *Panminerva Med.* 59 (3), 241–253. doi:10.23736/S0031-0808.17.03321-3

Rossouw, J. E., Anderson, G. L., Prentice, R. L., LaCroix, A. Z., Kooperberg, C., Stefanick, M. L., et al. (2002). Risks and Benefits of Estrogen Plus Progestin in Healthy Postmenopausal Women: Principal Results from the Women's Health Initiative Randomized Controlled Trial. *Jama* 288 (3), 321–333. doi:10.1001/jama.288.3.321

Schierbeck, L. L., Rejnmark, L., Tofteng, C. L., Stilgren, L., Eiken, P., Mosekilde, L., et al. (2012). Effect of Hormone Replacement Therapy on Cardiovascular Events in Recently Postmenopausal Women: Randomised Trial. *Bmj* 345, e6409. doi:10.1136/bmj.e6409

Spallarossa, P., Altieri, P., Aloi, C., Garibaldi, S., Barisione, C., Ghigliotti, G., et al. (2009). Doxorubicin Induces Senescence or Apoptosis in Rat Neonatal Cardiomyocytes by Regulating the Expression Levels of the Telomere Binding Factors 1 and 2. *Am. J. Physiol. Heart Circ. Physiol.* 297 (6), H2169–H2181. doi:10.1152/ajpheart.00068.2009

Stampfer, M. J., Colditz, G. A., Willett, W. C., Manson, J. E., Rosner, B., Speizer, F. E., et al. (1991). Postmenopausal Estrogen Therapy and Cardiovascular Disease. Ten-Year Follow-Up from the Nurses' Health Study. *N. Engl. J. Med.* 325 (11), 756–762. doi:10.1056/NEJM199109123251102

Wang, H., Jessup, J. A., Lin, M. S., Chagas, C., Lindsey, S. H., and Groban, L. (2012). Activation of GPR30 Attenuates Diastolic Dysfunction and Left Ventricle Remodelling in Oophorectomized mRen2.Lewis Rats. *Cardiovasc. Res.* 94 (1), 96–104. doi:10.1093/cvr/cvs090

Wang, J., Gao, E., Chan, T. O., Zhang, X. Q., Song, J., Shang, X., et al. (2013). Induced Overexpression of Na(+)/Ca(2+) Exchanger Does Not Aggravate Myocardial Dysfunction Induced by Transverse Aortic Constriction. *J. Card. Fail.* 19 (1), 60–70. doi:10.1016/j.cardfail.2012.11.003

Wang, X., Lu, L., Tan, Y., Jiang, L., Zhao, M., Gao, E., et al. (2019). GPR 30 Reduces Myocardial Infarct Area and Fibrosis in Female Ovariectomized Mice by Activating the PI3K/AKT Pathway. *Life Sci.* 226, 22–32. doi:10.1016/j.lfs.2019.03.049

Wang, X., Tan, Y., Xu, B., Lu, L., Zhao, M., Ma, J., et al. (2018). GPR30 Attenuates Myocardial Fibrosis in Diabetic Ovariectomized Female Rats: Role of iNOS Signaling. *DNA Cel Biol* 37 (10), 821–830. doi:10.1089/dna.2018.4208

Wang, X. S., Yue, J., Hu, L. N., Tian, Z., Zhang, K., Yang, L., et al. (2020). Activation of G Protein-Coupled Receptor 30 Protects Neurons by Regulating Autophagy in Astrocytes. *Glia* 68 (1), 27–43. doi:10.1002/glia.23697

Wilson, P. W., Garrison, R. J., and Castelli, W. P. (1985). Postmenopausal Estrogen Use, Cigarette Smoking, and Cardiovascular Morbidity in Women over 50. The Framingham Study. *N. Engl. J. Med.* 313 (17), 1038–1043. doi:10.1056/NEJM198510243131702

Zhai, M., Liu, Z., Zhang, B., Jing, L., Li, B., Li, K., et al. (2017). Melatonin Protects against the Pathological Cardiac Hypertrophy Induced by Transverse Aortic Constriction through Activating PGC-1β: *In Vivo* and *In Vitro* Studies. *J. Pineal Res.* 63 (3). doi:10.1111/jpi.12433

Conflict of Interest: The authors declare that the research was conducted in the absence of any commercial or financial relationships that could be construed as a potential conflict of interest.

Publisher's Note: All claims expressed in this article are solely those of the authors and do not necessarily represent those of their affiliated organizations, or those of the publisher, the editors, and the reviewers. Any product that may be evaluated in this article, or claim that may be made by its manufacturer, is not guaranteed or endorsed by the publisher.

frontiers in Pharmacology

ORIGINAL RESEARCH
published: 17 November 2021
doi: 10.3389/fphar.2021.716884

Knockout of AMPKα2 Blocked the Protection of Sestrin2 Overexpression Against Cardiac Hypertrophy Induced by Pressure Overload

*Nan Zhang[1,2,3†], Hai-Han Liao[1,2,3†], Hong Feng[4], Shan-Qi Mou[1,2,3], Wen-Jing Li[1,2,3], Xiahenazi Aiyasiding[1,2,3], Zheng Lin[1,2,3], Wen Ding[1,2,3], Zi-Ying Zhou[1,2,3], Han Yan[2], Si Chen[2,3] and Qi-Zhu Tang[1,2,3]**

[1]Department of Cardiology, Renmin Hospital of Wuhan University, Wuhan, China, [2]Cardiovascular Research Institute of Wuhan University, Wuhan, China, [3]Hubei Key Laboratory of Metabolic and Chronic Diseases, Wuhan, China, [4]Department of Geriatrics, Renmin Hospital of Wuhan University, Wuhan, China

OPEN ACCESS

Edited by:
Helene Tronchere,
Institut National de la Santé et de la Recherche Médicale (INSERM), France

Reviewed by:
Dharmani Devi Murugan,
University of Malaya, Malaysia
Brian Sansbury,
University of Louisville, United States

***Correspondence:**
Qi-Zhu Tang
qztang@whu.edu.cn

†These authors have contributed equally to this work

Specialty section:
This article was submitted to Cardiovascular and Smooth Muscle Pharmacology, a section of the journal Frontiers in Pharmacology

Received: 29 May 2021
Accepted: 13 October 2021
Published: 17 November 2021

Citation:
Zhang N, Liao H-H, Feng H, Mou S-Q, Li W-J, Aiyasiding X, Lin Z, Ding W, Zhou Z-Y, Yan H, Chen S and Tang Q-Z (2021) Knockout of AMPKα2 Blocked the Protection of Sestrin2 Overexpression Against Cardiac Hypertrophy Induced by Pressure Overload. Front. Pharmacol. 12:716884. doi: 10.3389/fphar.2021.716884

Objectives: Sestrin2 (Sesn2) has been demonstrated to be a cysteine sulfinyl reductase and protects cells from multiple stress insults, including hypoxia, endoplasmic reticulum stress, and oxidative stress. However, the roles and mechanisms of Sesn2 in pressure overload-induced mouse cardiac hypertrophy have not been clearly clarified. This study intended to investigate whether sestrin2 (Sesn2) overexpression could prevent pressure overload-induced cardiac hypertrophy via an AMPKα2 dependent pathway through conditional knockout of AMPKα2.

Methods and results: Sesn2 expression was significantly increased in mice hearts at 2 and 4 weeks after aortic banding (AB) surgery, but decreased to 60–70% of the baseline at 8 weeks. Sesn2 overexpression (at 3, 6, and 9 folds) showed little cardiac genetic toxicity in transgenic mice. Cardiac dysfunctions induced by pressure overload were attenuated by cardiomyocyte-specific Sesn2 overexpression when measured by echocardiography and hemodynamic analysis. Results of HE and PSR staining showed that Sesn2 overexpression significantly alleviated cardiac hypertrophy and fibrosis in mice hearts induced by pressure overload. Meanwhile, adenovirus-mediated-Sesn2 overexpression markedly suppressed angiotensin II-induced neonatal rat cardiomyocyte hypertrophy *in vitro*. Mechanistically, Sesn2 overexpression increased AMPKα2 phosphorylation but inhibited mTORC1 phosphorylation. The cardiac protections of Sesn2 overexpression were also *via* regulating oxidative stress by enhancing Nrf2/HO-1 signaling, restoring SOD activity, and suppressing NADPH activity. Particularly, we first proved the vital role of AMPKα2 in the regulation of Sesn2 with AMPKα2 knockout (AMPKα2-/-) mice and Sesn2 transgenic mice crossed with AMPKα2-/-, since Sesn2 overexpression failed to improve cardiac function, inhibit cardiac hypertrophy and fibrosis, and attenuate oxidative stress after AMPKα2 knockout.

Conclusion: This study uniquely revealed that Sesn2 overexpression showed little genetic toxicity in mice hearts and inhibited mTORC1 activation and oxidative stress to protect against pressure overload-induced cardiac hypertrophy in an

AMPKα2 dependent pathway. Thus, interventions through promoting Sesn2 expression might be a potential strategy for treating pathological cardiac hypertrophy and heart failure.

Keywords: Sestrin2, cardiac hypertrophy, fibrosis, AMPKα, oxidative stress

1 INTRODUCTION

Cardiac pathological hypertrophy represents a common initial stage for a variety of heart diseases caused by pathological stimuli such as hypertension-associated pressure overload, myocardial infarction-related injuries, excess neurohormonal activation, and inflammatory stimuli (Yildiz et al., 2020). Sustained pathological hypertrophy causes fetal gene re-expression, enlarged cardiomyocyte area, malignant interstitial fibrosis, and dysregulation of signaling pathways, which finally lead to heart failure. Moreover, the occurrence of heart failure means high morbidity and mortality (Murphy et al., 2020). Treatment at the initial stage of cardiac hypertrophy might block and even regress the development and progress of heart failure (Yildiz et al., 2020). However, the molecular mechanisms underlying pathological hypertrophy remain to be fully clarified.

The mechanisms involved in cardiac hypertrophy are intricated and continuous efforts have been paid to elucidate the pathways (Bauml and Underwood, 2010; Khatibzadeh et al., 2013). Among these, the AMP-activated protein kinase α (AMPKα) mammalian target of rapamycin (mTOR) pathway plays a central role in coordinating the complex signaling events (Haque and Wang, 2017; Zhang et al., 2018b). AMPK is a critical sensor and regulator of cellular energy status and exerts important functions in the intracellular adaptation to energy stress (Qi and Young, 2015). Deficiency of AMPKα or inhibiting its activity could exaggerate pathological cardiac hypertrophy, but activating AMPKα by genetic or pharmaceutical strategies could alleviate cardiac hypertrophy and improve cardiac function via suppressing excessive protein synthesis in cardiomyocytes (Ma et al., 2016; Zhang et al., 2018b). Besides, previous reports have closely correlated the AMPKα/mTOR pathway with the hypertrophic response by inhibiting oxidative stress and apoptosis (Shaw, 2009). However, some different upstream signaling and molecular mechanisms could activate or inactivate AMPKα activity depending on different pathophysiological contexts. Therefore, it is necessary to elucidate the precise mechanisms of upstream regulating molecules in different pathophysiological conditions (Qi and Young, 2015).

Sestrin2 (Sesn2), a member of the Sestrin (Sesn) family, also known as the product of hypoxia-inducible gene 95 (Hi95), is a stress-induced protein with a molecular weight of 55 kDa. Previous studies demonstrated that Sesn2 participated in various diseases by regulating apoptosis, oxidative stress, and toxicity (Kim et al., 2015c; Pasha et al., 2017; Sun et al., 2020). Sesn2 can also attenuate degenerative processes induced by aging and diabetes via depressing reactive oxygen species (ROS) accumulation and mTORC1 activation (Kim et al., 2015a). Sesn2 could exert a protective role in dopaminergic cells by maintaining autophagy activity via activating AMPK (Hou et al., 2015). However, the effects and underlying mechanisms of Sesn2 in adult mouse cardiac hypertrophy have not been clearly illustrated. Therefore, this study intends to investigate the role and mechanisms of Sesn2 in cardiac hypertrophy with Sesn2 transgenic and AMPKα2 knockout mice by establishing a pressure overload-induced cardiac hypertrophy model via aortic banding (AB) surgery.

2 MATERIALS AND METHODS

2.1 Reagents

Ang II was purchased from ENZO (ALX-151-039-M025); collagenase and trypsin were purchased from Gibco (Grand Island, NY, United States); the BCA protein assay kit was bought from Pierce (Rockford, United States); and 2,7-dichlorofluorescindiacetate (DCFH-DA) was obtained from the Bioengineering Institute (Nanjing, China). The following primary antibodies were obtained from Cell Signaling Technology (CST, United States): glyceraldehyde-3-phosphate dehydrogenase (GAPDH) (#2118), p-mTORC1 (#2971), T-mTORC1 (#2983), α-actinin (#69758S), P-p70 S6 kinase (Thr389) (#9234P), T-p70 S6 kinase (#2708), P-JNK (T183/Y185) (#4668P),T-JNK (#9258), P-p44/42 MAPK (Erk1/2) (Thr202/Tyr204) (#4370P), T-ERK (#4695), P-p38 (#4511P), p38 MAPK (#9212P), T-TAK1 (#5206), P-TAK1 (#4508), T-AKT (#4691), P-AKT (#4060), acetyl-CoA carboxylase antibody (#3676), and P-acetyl-CoA carboxylase antibody (#3661S). ABCAM provided the following primary antibodies: Anti-AMPKα2 (ab3760), p-AMPKα2 (S491, ab109402), anti-SOD1 (ab16831), anti-SOD2 (ab38155), Nrf2 (ab15323), 4-hydroxynonenal (ab46545), sarcomeric α-actinin (ab68167), heme oxygenase1 (ab-13243), and NOX2/gp91phox (ab129068). The Sesn2 antibody was acquired from Proteintech (no. 10795-1-AP). Antibodies were used at 1:1,000 dilutions for Western blotting. The secondary antibodies were obtained from LI-COR Biosciences (Lincoln, United States).

2.2 Animals and Treatments

All animal procedures were performed following the Guidelines for the Care and Use of Laboratory Animals published by the United States National Institutes of Health (NIH Publication, revised 2011) and approved by the Animal Care and Use Committee of Renmin Hospital of Wuhan University (Protocol No. 00013274).

Sesn2 conditional manipulated transgenic mice were established according to the published protocol as shown in **Supplementary Figure S1** (Deng et al., 2017; Larson and Baker, 2019; Luo et al., 2020). In brief, the CMV promoter followed by the loxP-STOP-loxP cassette was engineered to establish transgenic mice for temporal and spatial controlling

of Sesn2 expression. The transgenic mice were then bred with a tamoxifen-inducible Cre mouse to obtain an inducible specific expression of Sesn2 in the cardiomyocyte after treating with tamoxifen, which was injected into the abdomen for 7 consecutive days at a dose of 20 mg/kg/d.

The AMPKα2 knockout (AMPKα2-/-) mice were described in our previous study (Deng et al., 2013). Sesn2 transgenic mice were crossed with AMPKα2-/- to test whether the protective role of Sesn2 was via activating AMPKα2. All mice used in this study (male, aged 8–10 weeks, weighing 23.5–27.5 g) were housed under specific-pathogen-free conditions with food and water available ad libitum. Transgenic mice and littermates were subjected to aortic banding (AB) or sham surgery to establish pressure overload-induced cardiac hypertrophy animal models.

2.3 Aortic Banding Surgery

AB surgery was performed according to our previously published surgical protocol (Liao et al., 2019). In brief, sodium pentobarbital (50 mg/kg) with intraperitoneal injection was used to anesthetize the mice. After the loss of pain stimulation reflex in mice, mice were put on a thermostatic heating pad. After the open of the left side of the chest, the thoracic aorta was exposed by blunt dissection, and the descending thoracic aorta was ligated against a 27 G needle with a 7-0 silk suture. After quickly removing the 27 G needle, the descending thoracic aorta was narrowed about 70%. The sham surgery group was performed with the same operation as described in the AB surgery process but without ligating the descending thoracic aorta. Vascular ultrasound was performed to examine the AB surgery after 1 week of AB operation. Mice with unsuccessful surgery were removed from experimental groups.

2.4 Cardiomyocyte Cultures

Neonatal rat cardiomyocytes (NRCMs) were isolated as previously described (Liao et al., 2019). In brief, we sacrificed the neonatal Sprague-Dawley rats (1–3 days old), cut the ventricles into pieces, and digested them with 0.125% trypsin and 0.1% collagenase type II. Then, we centrifuged the harvested cells and resuspended the sediment in 15% fetal bovine serum (FBS, GIBCO). The serum was supplemented with 100 U/ml penicillin/100 mg/ml streptomycin in case of infection and 0.1 mmol/L bromodeoxyuridine (BrdU) to inhibit the proliferation of cardiac fibroblasts. After culture at 37°C in an incubator containing 5% CO_2 for 90 min, non-myocytes were removed and the suspended medium which consists of cardiomyocytes was seeded into 6-well culture plates.

After culture for 48 h, the cells were starved by changing the culture medium to serum-free DMEM/F12 for 6 h. Then, the cells were incubated and infected with adenoviruses of Sesn2 (Ad-Sesn2) or a similar adenovirus vector expressing the GFP protein (Ad-GFP) for 24 h. Subsequently, the infected cardiomyocytes were stimulated with Ang II (1 nM) for 24 h to induce cardiomyocyte hypertrophy. The hypertrophic phenotype was evaluated and the markers of the AMPKα/mTOR pathway were detected by RT-PCR and Western blotting. To further investigate the precise molecular mechanism of Sesn2 in cardiac hypertrophy, Ad-shAMPKα silencing AMPKα was used to further clarify the role of AMPKα in the protective role of Sesn2 in cardiac hypertrophy in NRCMs *in vitro*.

2.5 Echocardiography and Hemodynamics Measurements

Four weeks after AB or sham surgery, cardiac functions of mice were evaluated by echocardiography and hemodynamics as described previously (Ma et al., 2019). In brief, mice were anesthetized by inhaling 1.5% isoflurane. Mylab 30CV (Esaote S.P.A, Genoa, Italy) equipped with a 10-MHz linear array ultrasound transducer was used to examine mouse cardiac functions. The end-systolic and end-diastolic diameter of left ventricle (LVEDs and LVEDd) was measured in a parasternal short-axis view at the end of systole or diastole phase. The LV ejection fraction (EF) and fraction shortening (FS) were calculated according to LVEDs and LVEDd.

For hemodynamic measurements, a microtip catheter transducer (SPR-839, Millar Instruments, Houston, TX, United States) was inserted into the left ventricle through the right carotid artery of mice after anesthetization. The Millar Pressure-Volume System (MPVS-400, Millar Instruments) was used to record the continuous signals for the following analysis. The data were processed by PVAN data analysis software to analyze parameters, including the end-diastolic pressure (EDP), end-systolic pressure (ESP), maximal rate of pressure development (dp/dt max), and minimal rate of pressure decay (dp/dt min). After cardiac function analysis, the mice were sacrificed by decapitation. The body weight (BW), heart weight (HW), tibia length (TL), and lung weight (LW) were recorded. Then the hearts were quickly harvested and randomly divided into pathological staining and molecular analysis groups respectively. Hearts were arrested in diastole with 10% KCL, and preserved in 10% formalin for histological analysis and immunohistochemistry. Heart samples were preserved at −80°C for RT-PCR and Western blotting.

2.6 Histological Analysis

Mice hearts were fixed in 10% formalin for 12 h, and then were dehydrated and embedded in paraffin for cutting into 4–5 μm thick sections. The sections were stained with hematoxylin-eosin (HE) to evaluate the cross-section area (CSA) or stained with picrosirius red (PSR) to evaluate the fibrosis volume as described in our published protocol (Liao et al., 2019). After visualizing and taking photos under an optical microscope, Image Pro-Plus (version 6.0) was used to trace the outline of single cardiomyocyte to obtain cell surface area and collagen deposition area in the left ventricle for evaluating cardiac hypertrophy and fibrosis.

2.7 Immunohistochemistry

Immunohistochemistry was performed according to our published protocol (Wu et al., 2019). In brief, after deparaffinization and rehydration, sections were put into a 1X citrate unmasking solution for 10 min at a sub-boiling temperature (98°C). Then the sections were cooled at room

TABLE 1 | Sequences for the primers used in the qRT-PCR experiments.

Gene species	Forward (5′-3′)	Reverse (5′-3′)
Sesn2-M	AGCAGAGCTGGTTTAGTGAACCG	GACAAACCACAACTAGAATGCAGTG
ANP-M	ATTGACAGGATTGGAGCCCAG	TCAAGCAGAATCGACTGCCTT
BNP-M	TTTGGGCTGTAACGCACTGA	CACTTCAAAGGTGGTCCCAGA
αMHC-M	AGGTGGACCTGATCATGGAG	ATACCGGAGATCATGCAAGC
βMHC-M	CCGAGTCCCAGGTCAACAA	CTTCACGGGCACCCTTGGA
Collagen I-M	AGCACGTCTGGTTTGGAGAG	GACATTAGGCGCAGGAAGGT
Collagen III-M	TGACTGTCCCACGTAAGCAC	GAGGGCCATAGCTGAACTGA
CTGF-M	AGACCTGTGCCTGCCATTAC	ACGCCATGTCTCCGTACATC
Fibronectin-M	GACCCTTACACGGTTTCCCA	AAGCACTGGCATGTGAGCTT
αSMA-M	CCAGCCATCTTTCATTGGGAT	ACAGGACGTTGTTAGCATAGAG
GAPDH-M	ACTCCACTCACGGCAAATTC	TCTCCATGGTGGTGAAGACA
Sesn2-H	TGCTTAATGGTGTGAGGCGT	GGCAATGTGACCAGCAAAGG
ANP-R	CGGTACCGAAGATAACAGCCA	TCACCACCTCTCAGTGGCAA
βMHC-R	AGTGAAGAGCCTCCAGAGTTTG	GTTGATGAGGCTGGTGTTCTGG
Collagen I-R	GAGAGAGCATGACCGATGGATT	TGGACATTAGGCGCAGGAA
Collagen III-R	AAGGGCAGGGAACAACTGAT	GTGAAGCAGGGTGAGAAGAAAC
CTGF-R	AGACACATTTGGCCCTGACC	TCTTAGAACAGGCGCTCCAC
Fibronectin-R	GGATCCCCTCCCAGAGAAGT	GGGTGTGGAAGGGTAACCAG
αSMA-R	CATCACCAACTGGGACGACA	TCCGTTAGCAAGGTCGGATG
GAPDH-R	GACATGCCGCCTGGAGAAAC	AGCCCAGGATGCCCTTTAGT

M, mouse; R: rat; H, human.

temperature for 30 min. After incubation in 3% H2O2 for 10 min, sections were blocked for 1 h in a blocking solution (1X TBST/5% Normal Goat Serum) before incubation with 4-hydroxynonenal (4-HNE) overnight at 4°C. The next day, after incubation with a GTVisionTM+/HRP reagent (GK500610A, Gene tech, China), a DAB substrate kit (GK600710, Gene tech, China) was used to detect the positive area under an optical microscope for 1–10 min. After counterstaining sections with hematoxylin, we mounted sections with coverslips and took photos under an optical microscope. Image Pro-Plus (version 6.0) was used to analyze images.

2.8 Immunofluorescence Staining

Immunofluorescence staining was performed according to our published protocol (Zhang et al., 2018a). In brief, NRCMs were cultured on coverslips. After giving the corresponding treatment as described in the figure legends, NRCMs were washed three times with PBS, fixed with 4% paraformaldehyde, and then permeabilized with 0.2% Triton X-100. After blocking with 10% goat serum, NRCMs were incubated with a primary antibody of α-actinin (1:100) overnight at 4°C. The next day, after discarding the primary antibody, NRCMs were incubated with Alexa Fluor® 488-conjugated goat anti-rabbit IgG for 1 h at 37°C. Slow Fade Gold antifade reagent with DAPI (Sigma-Aldrich) was used to stain the cell nucleus. Fluorescence images were captured by a special OLYMPUS DX51 fluorescence microscope (Tokyo, Japan) in dark conditions and were analyzed by Image-Pro Plus 6.0 software.

2.9 Detection of Oxidative Stress

Commercial kits (Beyotime Biotechnology, China) were used to detect the activity of SOD (Cu/Zn-SOD and Mn-SOD Assay Kit with WST-8, S0103) and NADPH oxidase (NADP+/NADPH Assay Kit with WST-8, S0179) and the malondialdehyde (MDA) (Lipid Peroxidation MDA Assay Kit, S0131S) content in fresh heart tissue (80–120 mg) according to the manufacturer's instructions.

2.10 Measurements of ROS

The DCFH-DA probe (S0033S, Beyotime Biotechnology, China) was used to examine the intracellular ROS level according to the manufacturer's instructions and our published protocol (Zhang et al., 2020). In brief, NRCMs were incubated with DCFH-DA for 2 h at 37°C, and then the cells were washed with PBS three times in the dark. Photos were taken using an Olympus IX53 fluorescence microscope. Image Pro-Plus (version 6.0) was used to analyze images.

2.11 RNA Isolation and Quantitative Real-Time PCR

Total RNA from the left ventricle or cultured cardiomyocytes was extracted with Trizol as previously described (Liao et al., 2019). The Transcriptor First Strand cDNA Synthesis Kit (Roche, Basel, Switzerland) was used to reverse-transcribed 2 μg of RNA into cDNA. Light Cycler 480 SYBR Green 1 Master Mix (04887352001, Roche, United States) was used to perform real-time PCR. The primers used in this study were shown in **Table 1**. GAPDH was used as an internal control.

2.12 Western Blotting Analysis

Total proteins were extracted according to published protocols (Liao et al., 2019). In brief, heart tissue or NRCMs was lysed in RIPA lysis buffer. The protein concentration was measured by using the BCA Protein Assay Kit (23227, Thermo Scientific, China). Protein lysates were electrophoresed in different concentrations of SDS-PAGE (8, 10, and 12%), and then transferred onto PVDF membranes. After blocking the membranes with 5% BSA for 1 h, the blots were incubated

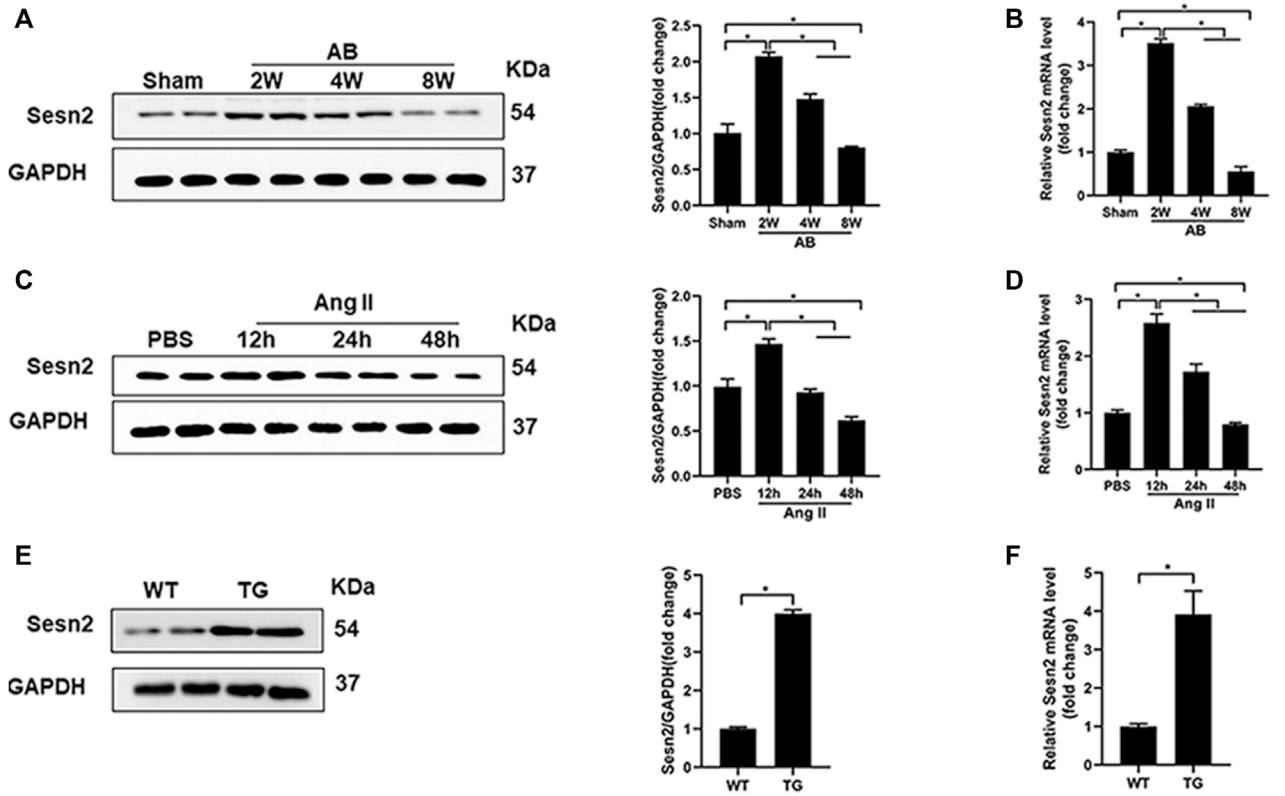

FIGURE 1 | The expression of Sesn2 in hypertrophic hearts and Ang II-induced cardiomyocytes. **(A)** Representative immunoblots and quantitative results of Sesn2 protein expression in mice hearts at 2, 4, and 8 weeks after AB surgery ($n = 6$). **(B)** qPCR analysis of the mRNA levels of Sesn2 at 2, 4, and 8 weeks after AB surgery ($n = 6$). **(C)** Representative Western blots and statistical analysis of Sesn2 expression in NRCMs at 12, 24, and 48 h after Ang II treatment ($n = 6$). **(D)** Sesn2 mRNA expression levels in NRCMs treated with or without Ang II stimulation ($n = 6$). **(E)** Representative Western blots and statistical analysis of Sesn2 expression in the hearts of WT and TG mice, respectively ($n = 6$). **(F)** Sesn2 mRNA expression in WT and TG mice hearts ($n = 6$). The data were expressed as the mean ± SD.*$p < 0.05$ *vs.* indicated group. One-way analysis of variance (ANOVA) followed by Tukey post hoc tests were used for significance analysis.

with primary antibodies overnight at 4°C. The next day, blots were incubated with secondary antibodies at room temperature for 1 h. All blots were visualized using ChemiDoc TM XRS + (Bio-Rad). The blots were quantified and analyzed by using Image Lab software.

2.13 Statistical Analysis

All of the data in our study were expressed as Mean ± SD (standard deviation). Cell experiments were repeated three times independently. The experiments and analysis were blinded whenever it need. SPSS 22.0 software was used to data analysis. One-way analysis of variance (ANOVA) and Tukey post hoc tests were used for multi-group comparisons. $p < 0.05$ was considered statistically significant.

3 RESULTS

3.1 The Expression of Sesn2 in Hypertrophic Hearts and Cardiomyocytes

As shown in **Figures 1A,B**, results of Western blotting and RT-PCR exhibited that Sesn2 expression was significantly upregulated in mice hearts 2 and 4 weeks after AB surgery compared to the sham-operated group, while the expression level reduced to 60–70% of the baseline after 8 weeks of AB surgery. In isolated NRCMs, angiotensin II (Ang II 1 μM) treatment caused a significant upregulation of Sesn2 at 12 h compared to the PBS treatment group both at protein and mRNA level. However, Ang II treatment for 48 h significantly decreased Sesn2 expression compared to the PBS treatment group (**Figures 1C,D**). These results implied that Sesn2 might take part in regulating pathological cardiac hypertrophy. To evaluate the role of Sesn2 in cardiac hypertrophy, transgenic mice (TG) were constructed for human Sesn2 specific overexpression in the cardiomyocytes (**Supplementary Figure S1**). The human Sesn2 was successfully overexpressed in the hearts of TG (**Figures 1E,F**). The TG mice and their wild-type (WT) littermates were used for the following experiments.

3.2 Sesn2 Overexpression in Cardiomyocytes Alleviated Pressure Overload Induced Cardiac Dysfunction

Echocardiography was performed to examine mouse cardiac function among different groups (**Figure 2A**). There was no

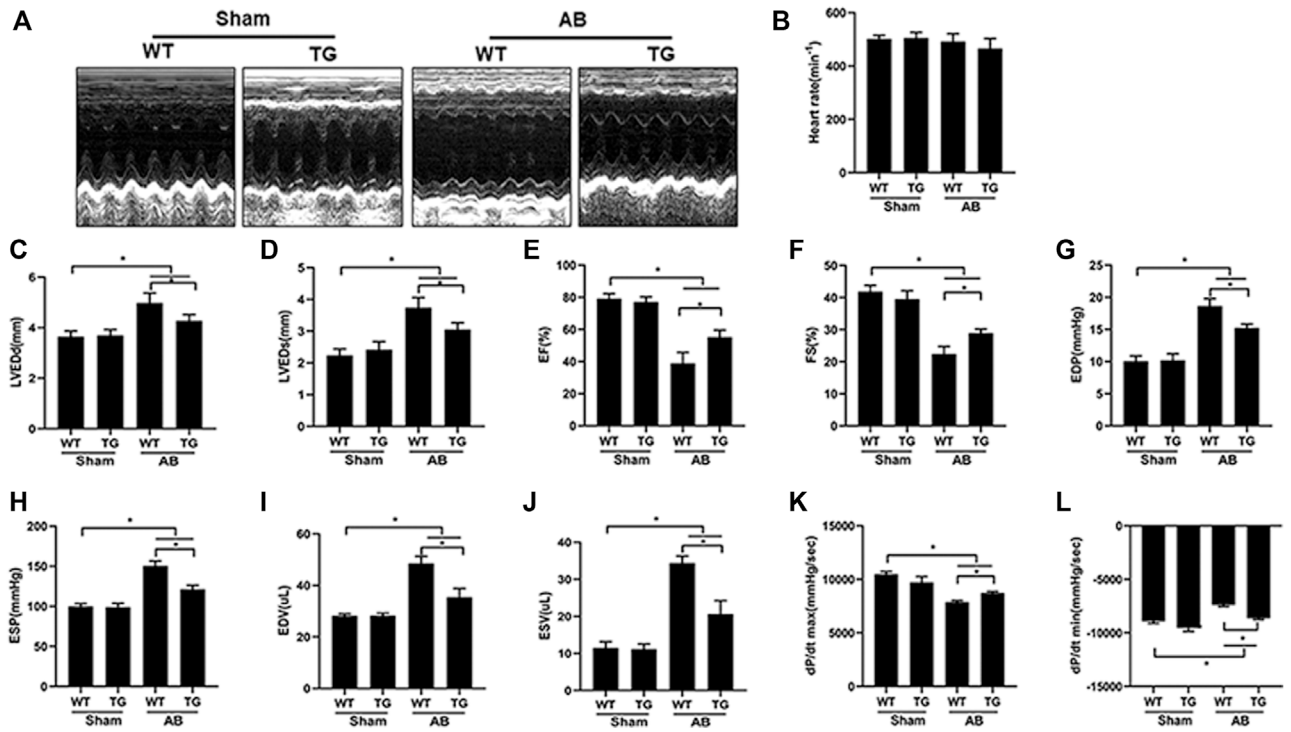

FIGURE 2 | Cardiomyocyte-specific overexpression of Sesn2 attenuated pressure overload-induced cardiac dysfunction. **(A)** Representative echocardiographic images in each group ($n = 6$). Echocardiography and pressure-volume loop were performed to evaluate mouse cardiac function at 8 weeks after AB surgery ($n = 6$). **(B)** heart rate (HR), **(C)** left ventricular end diastolic diameter (LVEDd), **(D)** left ventricular end systolic diameter (LVEDs), **(E)** left ventricular ejection fraction (EF), **(F)** LV fraction shortening (FS), **(G)** end diastolic pressure (EDP), **(H)** end systolic pressure (ESP), **(I)** end diastolic volume (EDV), **(J)** end systolic volume (ESV), **(K)** left ventricular maximal rate of pressure rise (dp/dt max), **(L)** left ventricular maximal rate of pressure decay (dp/dt min). Data were presented as the mean ± SD. *$p < 0.05$ vs indicated group. One-way analysis of variance (ANOVA) followed by Tukey post hoc tests were used for significance analysis.

difference in heart rate among all groups (**Figure 2B**). Four weeks of pressure overload caused a marked increase in parameters, including left ventricular end-diastolic diameter (LVEDd) (**Figure 2C**), left ventricular end-systolic diameter (LVEDs) (**Figure 2D**), end diastolic pressure (EDP) (**Figure 2G**), end systolic pressure (ESP) (**Figure 2H**), end diastolic volume (EDV) (**Figure 2I**), and end systolic volume (ESV) (**Figure 2J**), but significantly decreased left ventricular ejection fraction (EF) (**Figure 2E**) and left ventricular fraction shortening (FS) (**Figure 2F**) in the WT + AB group, compared to WT + sham group. However, Sesn2 overexpression markedly alleviated cardiac dysfunction induced by pressure overload, as evidenced by preserved LVEF and FS, decreased LVEDd, LVEDs, EDP, ESP, EDV, and ESV in the TG + AB group compared to the WT + AB group. Pressure volume loop analysis was used to further assess the mouse cardiac function. Pressure overload caused a significant decrease in maximal left ventricular pressure rising rate (dp/dt max) and the rate of left ventricle diastolic pressure change (dp/dt min) in the WT + AB group compared to the WT + sham group (**Figures 2K,L**). Similarly, Sesn2 overexpression significantly restored the dp/dt max and dp/dt min in the TG + AB group compared to the WT + AB group (**Figures 2K,L**), which confirmed again the protective role of Sesn 2 in cardiac dysfunction caused by pressure overload.

3.3 Sesn2 Overexpression Improved Pressure Overload-Induced Cardiac Hypertrophy and Fibrosis in Mice

Pressure overload significantly induced mouse heart hypertrophy, as shown by the increased cardiomyocyte surface area (CSA) in the WT + AB group compared to the WT + sham group. Sesn2 overexpression inhibited cardiac hypertrophy, since it decreased CSA in the TG + AB group compared to the WT + AB group (**Figures 3A,B**). Congruously, the heart weight/body weight (HW/BW) (**Figure 3C**), heart weight/tibia length (HW/TL) (**Figure 3D**), and lung weight/body weight (LW/BW) (**Figure 3E**) were significantly increased in the WT + AB group compared to the WT + sham group. Sesn2 overexpression significantly decreased HW/BW, HW/TL, and HW/BW in the TG + AB group compared to the WT + AB group (**Figures 3C–E**). The hypertrophic markers, including atrial natriuretic peptide (ANP) (**Figure 3F**), B-type natriuretic peptide (BNP) (**Figure 3G**), and β-MHC (**Figure 3I**), were significantly upregulated in the WT + AB group compared to

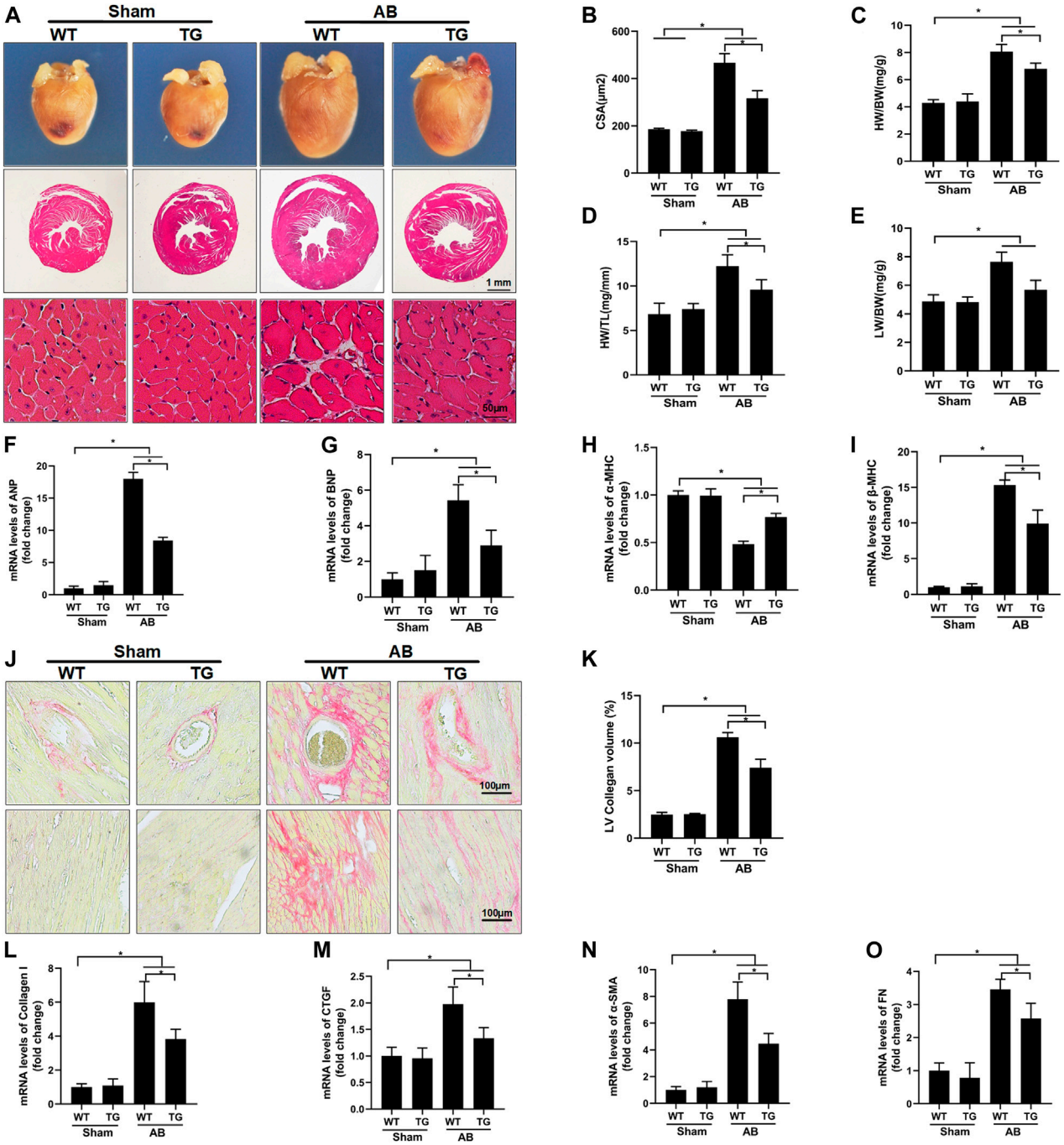

FIGURE 3 | Sesn2 overexpression alleviated pressure overload-induced hypertrophy and fibrosis in mice. **(A)** Representative images of gross hearts and HE staining in the indicated groups (n = 6). **(B)** Quantification of the cross-sectional area (CSA) of cardiomyocytes in the indicated mice ($n \geq 100$ left ventricular cells). Statistical results of the **(C)** HW/BW, **(D)** HW/TL **(E)** and LW/BW of mice at 8 weeks after AB surgery(n = 9). Cardiac mRNA levels of. **(F)** ANP, **(G)** BNP, **(H)** α-MHC, and **(I)** β-MHC. **(J)** Picrosirius red (PSR) staining of histological sections of left ventricles (n = 6), **(K)** quantitative results of the left ventricular collagen volume ($n \geq 25$ fields). L-O The mRNA levels of **(L)** Collagen I, **(M)** CTGF, **(N)** α-SMA, and **(O)** FN. ANP: atrial natriuretic peptide; BNP, brain natriuretic peptide; α-MHC, α-myosin heavy chain; β-MHC, β-myosin heavy chain; HW, heart weight; BW, body weight; TL, tibia length; HE, hematoxylin and eosin; CTGF, connective tissue growth factor; FN, fibronectin; αSMA, alpha-smooth muscle actin (αSMA). The data were expressed as the mean ± SD. *$p < 0.05$ *vs.* indicated group. One-way analysis of variance (ANOVA) followed by Tukey post hoc tests were used for significance analysis.

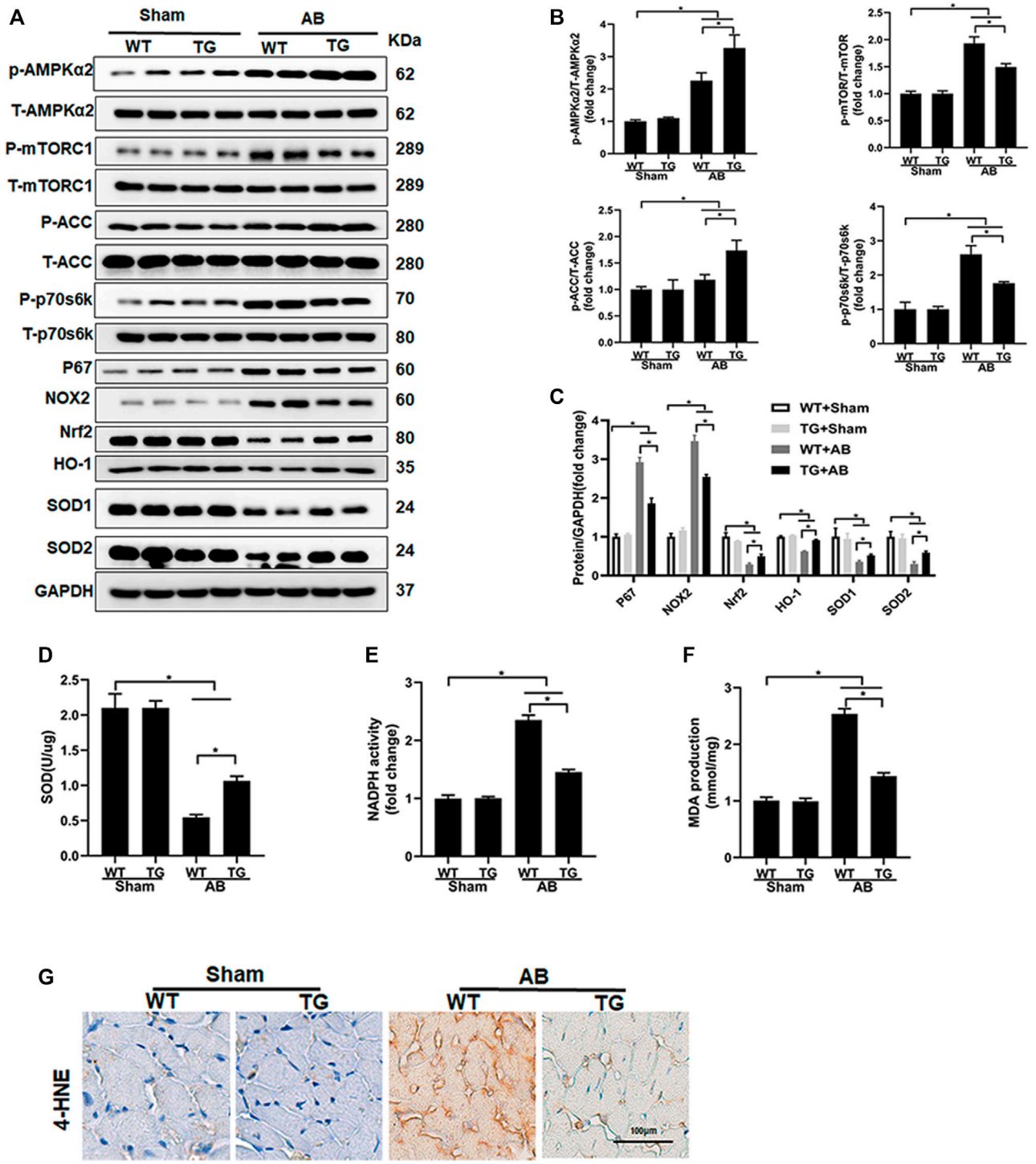

FIGURE 4 | Sesn2 overexpression activated the AMPKα2 pathway and suppressed oxidative stress. **(A)** Representative Western blots of the phosphorylated and total protein expression of AMPKα2, mTORC1, ACC, P70s6k, P67, NOX2, Nrf2, HO-1, SOD1, and SOD2 at 8 weeks after AB surgery ($n = 6$). **(B,C)** Quantification of the proteins. **(D)** Examination of SOD activity ($n = 6$), **(E)** Examination of NADPH activity ($n = 6$), **(F)** Examination of MDA accumulation ($n = 6$). **(G)**. Immunohistochemical staining for 4-hydroxynonenal (4-HNE). $^*p < 0.05$ *vs.* indicated group. One-way analysis of variance (ANOVA) followed by Tukey post hoc tests were used for significance analysis.

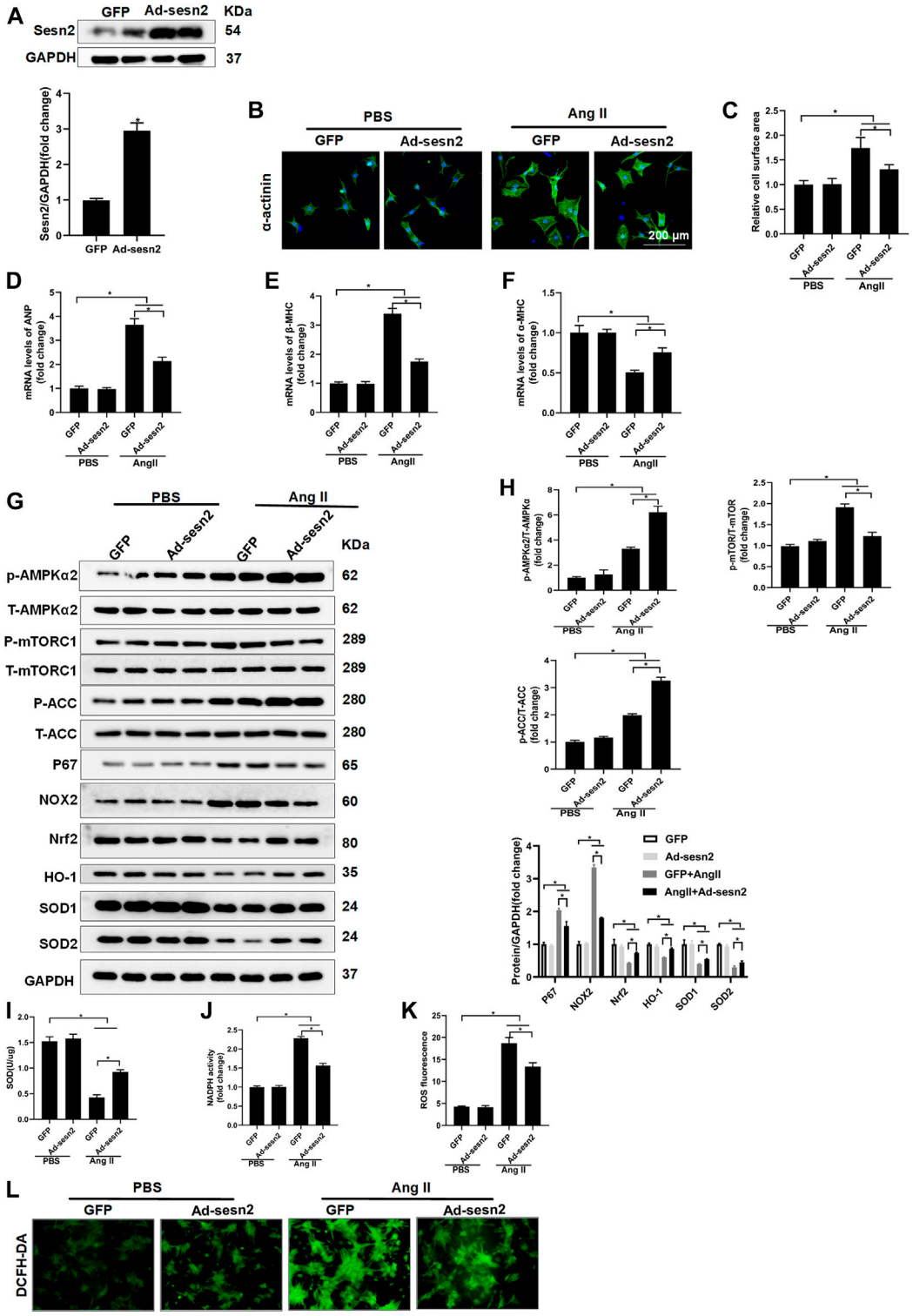

FIGURE 5 | Sesn2 overexpression alleviates Ang II- induced cardiomyocyte hypertrophy *in* vitro. NRCMs were transfected with adenovirus (Ad)-Sesn2 or Ad-GFP for 24 h, and then treated with Ang II for another 48 h. **(A)** Examination of Sesn2 overexpression in cardiomyocytes (n = 6). **(B,C)** Representative images of α-actinin staining and statistical results of cell surface area (n > 50 cells per group). mRNA expression of **(D)** ANP, **(E)** α-MHC and **(F)** β-MHC. **(G)** Representative Western blots of the phosphorylated and total proteins of AMPKα2, mTORC1, ACC, P67, NOX2, Nrf2, HO-1, SOD1, and SOD2 in NRCMs transfected with Ad-Sesn2 or Ad-GFP for

(*Continued*)

FIGURE 5 | 24 h and treated with Ang II for 48 h ($n = 6$). **(H)** Quantitative results of the Western blotting analysis. Examination of **(I)** SOD and **(J)** NADPH activities transfected with Ad-Sesn2 or Ad-GFP for 24 h and treated with Ang II for 48 h ($n = 6$). **(K,L)** DCFH-DA staining and ROS calculation in NRCMs transfected with Ad-Sesn2 or Ad-GFP and treated with Ang II for 48 h ($n = 6$). NRCM: neonatal rat cardiomyocytes. DCFH-DA: DCFH-DA; 2′,7′-dichlorodihydrofluorescein diacetate. The data were expressed as the mean ± SD from 3 independent experiments. $^*p < 0.05$ *vs.* indicated group. One-way analysis of variance (ANOVA) followed by Tukey post hoc tests were used for significance analysis.

the WT + sham group. However, Sesn2 overexpression significantly depressed the mRNA expression of these hypertrophic markers in the TG + AB group compared to the WT + AB group (**Figures 3F,G,I**). Besides, pressure overload caused a significant decrease of α-MHC in the WT + AB group compared to the WT + sham group, but Sesn2 overexpression obviously reversed the α-MHC expression in the TG + AB group compared to the WT + AB group (**Figure 3H**). Taken together, these data exhibited that Sesn2 overexpression protected against pressure overload-induced cardiac hypertrophy.

Cardiac fibrosis is an integrated process of pathological cardiac hypertrophy. PSR staining revealed that pressure overload induced significant fibrosis around the perivascular and in the interstitium of the mouse heart in the WT + AB group compared to the WT + sham group, but Sesn2 overexpression markedly mitigated cardiac fibrosis in the TG + AB group compared to the WT + AB group (**Figures 3J,K**). Moreover, the fibrosis associated markers, including collagen I (**Figure 3L**), connective tissue growth factor (CTGF) (**Figure 3M**), alpha-smooth muscle actin (α-SMA) (**Figure 3N**), and fibronectin (FN) (**Figure 3O**), were significantly upregulated in the WT + AB group compared to the WT + sham group. However, Sesn2 overexpression depressed the expression of these fibrosis-associated markers in the TG + AB group compared to the WT + AB group (**Figures 3L–O**). Therefore, cardiac fibrosis caused by pressure overload could also be ameliorated by Sesn2.

3.4 Sesn2 Overexpression Activated the AMPKα2 Signaling Pathway and Suppressed Oxidative Stress

In previous studies, Sesn2 has been suggested to regulate the MAPK, AKT, AMPKα, and oxidative stress-associated signaling pathways, all of which have been implicated in the regulation of pathological cardiac hypertrophy. Our data presented that Sesn2 overexpression seemed not to regulate the MAPK and AKT signaling pathway (**Supplementary Figures S2A,B**). However, AMPKα2 and ACC phosphorylation was significantly enhanced by Sesn2 overexpression in the TG + AB group compared to the WT + AB group. Meanwhile, mTORC1, and p70s6k phosphorylation was significantly inhibited in the TG + AB group compared to the WT + AB group (**Figures 4A,B**).

We also detected the oxidative stress-associated signaling pathway and oxidative stress status among different groups. The pro-oxidative stress markers, including p67 and NOX2, and the anti-oxidative stress proteins, including Nrf2, HO-1, SOD1, and SOD2 were significantly upregulated and downregulated in the WT + AB group compared to the WT + sham group, respectively (**Figure 4A**). Sesn2 overexpression markedly suppressed the expression of p67 and NOX2, and restored the expression of Nrf2, HO-1, SOD1, and SOD2 in the TG + AB group compared to the WT + AB group (**Figures 4A,C**). SOD catalyzes the conversion of superoxide radicals into hydrogen peroxide and oxygen, which could prevent cells from ROS-associated damage. The SOD activity was significantly decreased but the NADPH activity was markedly increased in the WT + AB group compared to the WT + sham group, which could be restored by Sesn2 overexpression in the TG + AB group compared to the WT + AB group (**Figures 4D,E**). Finally, the products of oxidative stress, including MDA and 4-hydroxynonenal (4-HNE), were significantly accumulated in the WT + AB group compared to the WT + sham group, which could be markedly inhibited by Sesn2 overexpression in the TG + AB group compared to the WT + AB group (**Figures 4F,G**).

3.5 Sesn2 Inhibited Cardiomyocyte Hypertrophy *in vitro*

NRCMs were isolated and transfected with adenovirus for Sesn2 (Ad-Sesn2) overexpression in order to investigate the role of Sesn2 in Ang II-induced cardiomyocyte hypertrophy. As shown in **Figure 5A**, Sesn2 was successfully overexpressed in the NRCMs. Ang II treatment for 48 h successfully induced cardiomyocyte hypertrophy *in vitro*, as evidenced by significantly enlarged cardiomyocyte surface area (**Figures 5B,C**), markedly increased expression of ANP and β-MHC, and dramatically decreased α-MHC in the GFP + Ang II group compared to the GFP + PBS group. In accordance with results from experiments *in vivo*, the Sesn2 overexpression significantly inhibited cardiomyocyte hypertrophy, suppressed mRNA expression of ANP and β-MHC, and restored mRNA expression of α-MHC in the Ad-Sesn2 + Ang II group compared to the GFP + Ang II group (**Figures 5D–F**).

Sesn2 overexpression significantly promoted the phosphorylation of AMPKα2 and ACC, and decreased mTORC1 phosphorylation in NRCMs treated with Ang II (**Figures 5G,H**). The expression of Nrf2, HO-1, SOD1, and SOD2 was obviously restored but the expression of p67 and NOX2 was reduced in the AngII + Ad-Sesn2 group compared to the Ang II + GFP group (**Figures 5G,H**). Besides, the activity of SOD was significantly reduced while the activity of NADPH was significantly increased in the Ang II + GFP group compared to the PBS + GFP group. However, Sesn2 overexpression successfully inhibited Ang II-induced increase in NADPH activity but enhanced the SOD activity (**Figures 5I,J**). In addition, we detected the ROS production in each group and found that Sesn2 overexpression dramatically inhibited ROS over-production induced by Ang II (**Figures 5K,L**).

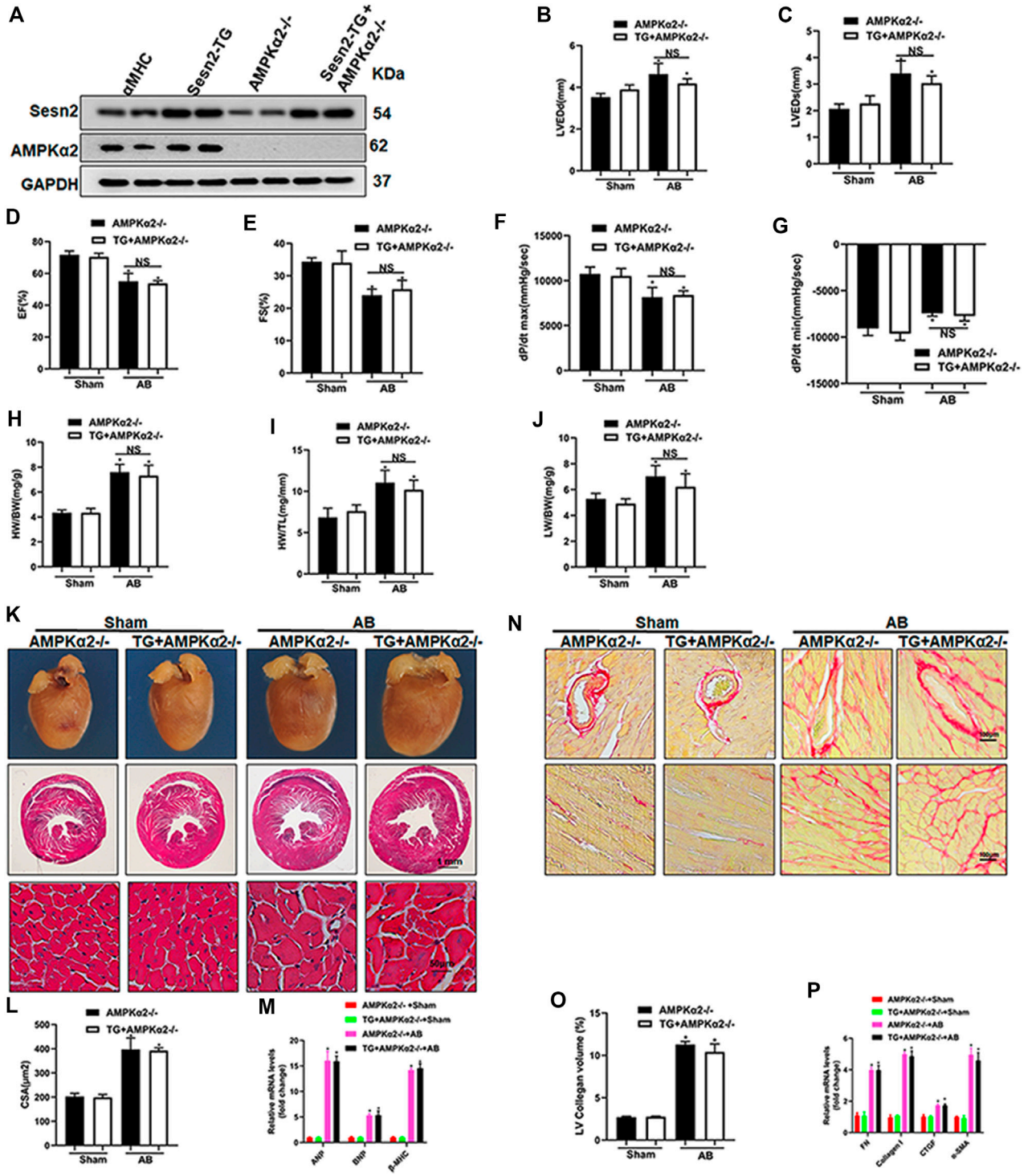

FIGURE 6 | Sesn2 overexpression could not protect against cardiac remodeling in AMPKα2 knockout mice. **(A)** Representative Western blots of Sesn2 and AMPKα2 ($n = 6$). Echocardiography and pressure-volume loop parameters detected mouse cardiac function at 8 weeks after sham or AB surgery ($n = 6$): **(B)** LVEDd, **(C)** LVEDs, **(D)** EF, **(E)** FS, **(F)** dp/dtmax and **(G)** dp/dtmin. The ratios of **(H)** HW/BW, **(I)** HW/TL and **(J)** LW/BW at 8 weeks after sham or AB surgery ($n = 9$). **(K)** Representative images of gross hearts and HE-stained heart sections ($n = 6$). **(L)** Quantitative measurements of cell surface area (CSA) of cardiomyocytes ($n = 60$) ($n \geq 100$ left ventricular cells). **(M)** RT-PCR detected ANP, BNP and βMHC mRNA expression ($n = 6$). **(N)** Representative images of PSR staining ($n = 6$). **(O)** Quantitative results of the left ventricular collagen volume ($n = 6$). **(P)** RT-PCR detected FN, Collagen I, CTGF, and α-SMA mRNA expression. The data were expressed as the mean ± SD. $^*p < 0.05$ *vs.* indicated group. One-way analysis of variance (ANOVA) followed by Tukey post hoc tests were used for significance analysis.

3.6 Sesn2 Overexpression Failed to Protect Against Cardiac Dysfunction and Cardiac Hypertrophy in AMPKα2 Knockout Mice

To further determine whether the cardiac protective effect of Sesn2 overexpression was dependent on AMPKα2 signaling pathway, we crossed the cardiac-specific overexpression of Sesn2 mice (Sesn2-TG) with AMPKα2 knockout mice (AMPKα2-/-) to construct Sesn2-TG + AMPKα2-/- mice. As shown in **Figure 6A**, Western blotting analysis was performed to examine the expression of Sesn2 and AMPKα2 in Sesn2-TG + AMPKα2-/- mice. Pressure overload caused mouse cardiac dysfunction, as evidenced by significantly increased LVEDd and LVEDs and decreased EF and FS in the AMPKα2-/- + AB group compared to the AMPKα2-/- + sham group (**Figures 6B–E**). However, no significant difference on these parameters could be detected between the Sesn2-TG + AMPKα2-/- + AB group and the AMPKα2-/- + AB group (**Figures 6B–E**). Pressure volume-loop analysis also showed that pressure overload could significantly disturb the dp/dt max and dp/dt min (**Figures 6F,G**) in the AMPKα2-/- + AB group compared to the AMPKα2-/- + sham group, but no significant difference could be detected on dp/dt max and dp/dt min between the Sesn2-TG + AMPKα2-/- + AB group and the AMPKα2-/- + AB group. These data show that Sesn2 overexpression failed to prevent mouse cardiac dysfunction in AMPKα2-/- mice.

Parameters including HW/BW, HW/TL, and LW/BW increased in the AMPKα2-/- + AB group compared to the AMPKα2-/- + sham group, while there was no significant difference on these parameters between the Sesn2-TG + AMPKα2-/- + AB group and the AMPKα2-/- + AB group (**Figures 6H–J**). HE staining exhibited pressure overload induced increased cardiomyocyte surface area, which could not be inhibited by Sesn2 overexpression in AMPKα2-/- mice (**Figures 6K,L**). Meanwhile, the mRNA expression of ANP, BNP, and β-MHC in AMPKα2-/- + AB group was increased when compared to the AMPKα2-/- + sham group, but Sesn2 overexpression showed little effect on ANP, BNP, and β-MHC expression in the Sesn2-TG + AMPKα2-/- + AB group compared to the AMPKα2-/- + AB group (**Figure 6M**).

In addition, PSR staining showed that pressure overload induced significant fibrosis in interstitium and peri-vascular heart tissue, which could not be inhibited by Sesn2 overexpression in AMPKα2-/-mouse (**Figures 6N,O**). Similarly, the mRNA expression of fibrosis markers, including FN, collagen I, CTGF, and α-SMA, were significantly increased in the AMPKα2-/- + AB group compared to the AMPKα2-/- + sham group. However, Sesn2 overexpression failed to block the increase of FN, Collagen I, CTGF, and α-SMA expression in AMPKα2 subjected to AB surgery (**Figure 6P**). To sum up, these data showed that AMPKα2 deficiency completely abrogated the protective effects of Sesn2 overexpression. Furthermore, in AMPKα2-/- mice, Sesn2 overexpression could not inhibit Nox2 or p67 expression and restore Nrf2, HO-1, SOD1, and SOD2 expression (**Supplement Figures S3A,B**).

3.7 Ang II-Induced Hypertrophy and Oxidative Stress Could Not Be Prevented by Sesn2 Overexpression After AMPKα2 Silence in NRCMs

NRCMs were transfected with Ad-Sesn2 or Ad-shAMPKα2 to over-express Sesn2 and silence AMPKα2 respectively, as shown in **Supplement Figures S4A,B**. The phosphorylation of AMPKα2 was downregulated by about 90%, and Sesn2 was enhanced about 3.5 fold compared with the control group. Ang II treatment significantly increased the cell surface of NRCMs and promoted mRNA expression of ANP and β-MHC (**Supplement Figures S4C–S4F**). There was no significant difference on CSA and mRNA expression of ANP and β-MHC between the Ang II + Ad-Sesn2 + Ad-shAMPKα2 group and the Ang II + Ad-shAMPKα2 group (**Supplement Figures S4C–S4F**). Moreover, Ang II treatment caused a significant accumulation of ROS, which could not be inhibited by Sesn2 overexpression in NRCMs after AMPKα2 silence (**Supplement Figure S4G**). Finally, we also presented that Ang II treatment decreased SOD activity and enhanced NADPH activity in the Ang II + Ad-shAMPKα2 group compared to the Ad-shAMPKα2 group. However, Sesn2 overexpression showed no effects on regulating SOD and NADPH activity in NRCMs after AMPKα2 silence (**Supplement Figures S4H,I**).

4 DISCUSSION

We firstly demonstrated that Sesn2 expression was upregulated at 2 weeks and decreased to 60% of the baseline at 8 weeks after AB surgery. A previous study indicated that Sesn2 was significantly downregulated at the end of 10 weeks after transverse aortic constriction surgery (Du et al., 2019). These studies implied that Sesn2 might take part in regulating pressure overload-induced pathological cardiac hypertrophy. We established a transgenic (TG) mouse for specifically overexpressing Sesn2 in cardiomyocytes by crossing with a transgenic mouse with α-MHC mediated Cre expression. The TG mouse subjected to aortic banding surgery revealed that Sesn2 overexpression prevented mice hearts from pressure overload-induced cardiac dysfunction, hypertrophy, and fibrosis. The underlying mechanisms might be at least partly through activating AMPKα2, inhibiting mTORC1/p70s6k signaling pathway, and suppressing excessive oxidative stress *via* restoring Nrf2/HO-1 and depressing NOX and NAPDH activity. These mechanisms could also be confirmed in Ang II treated NRCMs *in vitro*. Moreover, this study demonstrated that Sesn2 overexpression failed to protect against pressure overload-induced pathological hypertrophy in AMPKα2-/- mouse and NRCMs with AMPKα2 silence. Thus, this study firstly demonstrated that transgenic Sesn2 overexpression negatively regulated cardiac hypertrophy and combating oxidative stress, which was dependent on AMPKα2 regulation.

AMPK is a heterotrimeric protein containing a catalytic subunit (α) and two regulatory subunits (β and γ) (Zaha and Young, 2012). The α subunit has two isoforms (α1 and α2)

encoded by different genes and the α2 isoform mainly exists in cardiomyocytes (Zaha and Young, 2012). AMPK functions as the hub protein of regulating fatty acid oxidation (FAO) in the cardiomyocytes by supplying ATP (Zuurbier et al., 2020). AMPK activation could phosphorylate and depress the activity of both isoforms of acetyl-CoA carboxylase (AAC1/ACC2), which suppresses the conversion of acetyl-CoA to malonyl-CoA (Zuurbier et al., 2020). Malonyl-CoA is a rate-limiting enzyme for FAO (Zuurbier et al., 2020), and the accumulation of malonyl-CoA could inhibit fatty acid uptake of mitochondria by inhibiting CPT1 activity and result in FAO inhibition (Zuurbier et al., 2020). Activating AMPKα2 has been suggested to promote FAO for alleviating pathological hypertrophy (Zuurbier et al., 2020). Besides, multiple hypertrophic stimuli, including pressure overload, β-adrenergic stimulation, angiotensin II and IGF-1, could cause mTORC1 hyperphosphorylation, and lead to exaggerated pathological cardiac hypertrophy (Sciarretta et al., 2018). Inhibiting mTORC1 activity by activating AMPKα2 could effectively protect against cardiac hypertrophy induced by various pro-hypertrophic stimuli (Sciarretta et al., 2018). However, AMPKα2 deletion caused malignant activation of the mTORC1 signaling pathway, resulting in exacerbated cardiac hypertrophy and dysfunction (Zhang et al., 2008). Direct inhibition and indirect inhibition by AMPKα2 activation of mTORC1 significantly mitigated cardiac hypertrophy (Zhang et al., 2008). These studies clearly indicated that mTORC1 inhibition through activating AMPKα2 might be a potential strategy for protecting against pressure overload or neurohumoral factors induced pathological cardiac hypertrophy. Discovering new targets for regulating AMPK/mTOR signaling pathway might efficiently inhibit the development and progress of cardiac hypertrophy and heart failure.

Previous studies found that genotoxic stress could induce p53-dependent Sesn2 upregulation. Upregulated Sesn2 interacted with TSC1:TSC2 and AMPKα for activating AMPKα phosphorylation, which led to the inhibition of mTROC1 signaling (Budanov and Karin, 2008). Sesn2 deficiency exaggerated hyper-nutrition and obesity-associated insulin resistance and hepato-steatosis through chronic activation of mTORC1-p70/S6K signaling, which could be effectively reversed by metformin treatment via activating AMPKα (Lee et al., 2012). Sesn2 overexpression mitigated rotenone-induced α-synuclein accumulation and caspase 3 activation via enhancing AMPK-dependent autophagy in dopaminergic cells (Hou et al., 2015). Lee et al. reported that loss of drosophila sestrin (dSesn) resulted in age-associated cardiac malfunction, which could be prevented by pharmacological activation of AMPK or inhibition of mTOR (Lee et al., 2010). These studies presented that Sesn2 inhibited mTORC1 activity via an AMPK-dependent pathway.

Some other studies also presented that Sesn2 inhibited mTORC1 phosphorylation via an AMPK-independent pathway. Park HW et al. demonstrated that Sesn2 expression could be induced by an endoplasmic reticulum (ER) stress-activated transcription factor in the liver (Park et al., 2014). Once induced, Sesn2 could depress protein synthesis by inhibiting mTORC1 through an AMPK-independent manner (Park et al., 2014). Parmigiani A et al. demonstrated that Sesn2 could inhibit mTORC1 activation via the interaction with GTPase-activating protein activity toward Rags 2 (GATOR2) instead of an AMPK-dependent mechanism (Parmigiani et al., 2014; Kim et al., 2015b). Lately, Nanhu Quan et al. reported that Sesn2 deficiency exaggerated pressure overload or age-induced mouse cardiac hypertrophy and dysfunction (Quan et al., 2020), and adeno-associated virus 9-mediated Sesn2 overexpression in the mouse heart could attenuate these changes *via* interacting with GATOR2 and thus inhibiting mTORC1 activity (Quan et al., 2020). Therefore, these studies showed that Sesn2 might regulate mTORC1 activation through an AMPK-independent but GATOR2-dependent pathway. However, relying on AMPKα2-/- mice, our study firstly demonstrated that the inhibition of Sens2 on mTORC1/p70s6k activation was via an AMPK-dependent manner in pressure overload-induced pathological cardiac hypertrophy, because Sesn2 overexpression could not depress mTORC1/p70s6K signaling pathway in AMPKα2-/- mouse heart.

Besides the AMPK/mTORC1 pathway, Sesn2 has been suggested to regulate signals involved in oxidative stress in various diseases. Sesn2 expression was significantly elevated in peripheral nerves after injuries. Sesn2 knockout mice presented extraordinarily augmented late-phase neuropathic pain behavior because of excessive ROS accumulation (Kallenborn-Gerhardt et al., 2013). The analysis of the crystal structure of human Sesn2 demonstrated that a structure of helix-turn-helix oxidoreductase motif locating at the N-terminal domain inhibited ROS production (Kim et al., 2015a). Forced expression of Sesn2 could induce keap1 degradation via a p62-dependent pathway, resulting in upregulation of Nrf2 activity, thus protect the mouse liver from acute stimulation of lipogenesis-associated oxidative damage (Bae et al., 2013). Sesn2 has also been suggested to regulate intracellular ROS via regenerating hyperoxidized peroxiredoxins in renal proximal tubule cells (Yang et al., 2014). Contrarily, Sesn2-knockdown in renal proximal tubule cells significantly decreased hyperoxidized peroxiredoxin production and resulted in ROS accumulation (Yang et al., 2014). These studies indicated that Sesn2 could exert evident anti-oxidant effects in various diseases. Our study demonstrated that Sesn2 overexpression could attenuate oxidative stress in pathological cardiac hypertrophy via increasing Nrf2/HO-1 signaling pathway and SOD activity but decreasing the production of MDA, p67, and 4-HEN and depressing NADPH activity. What's more, this study first found that Sesn2 overexpression failed to exert its antioxidant function in AMPKα2-/- mice.

Theoretically, there are three possibilities to explain this phenomenon. Firstly, Sesn2-dependent AMPK activation and mTORC1 inhibition could be essential for maintaining basal autophagy, which could help organism get rid of dysfunctional mitochondria by preventing electron leak and excessive ROS production (Packer, 2020). Lee et al. demonstrated that dSesn deletion in Drosophila could cause mitochondrial dysfunction and ROS production in skeletal muscle and heart. However,

pharmacological mTORC1 inhibitors could completely mitigate excessive ROS production in dSesn deficient muscle. Moreover, the mutant of dSesn in its antioxidant domain remained to suppress ROS accumulation by its ability to depress mTORC1 activity. These studies indicated that the antioxidant property of sestrin might be associated with its regulation on mTORC1. Secondly, some studies have also indicated that activated AMPK could promote Nrf2 expression to enhance antioxidant functions in various animal disease models (Fischhuber et al., 2020; Huang et al., 2020). Moreover, Manuel et al. (Matzinger et al., 2020) demonstrated that AMPKα1 directly phosphorylated Nrf2 at serine 374, 408, and 433 to determine the extent of transactivation of Nrf2-regulated downstream genes (Matzinger et al., 2020). Zhou et al. (Li et al., 2020) exhibited that sulforaphane (SFN) treatment protected against type-2-diabetes-induced renal lipotoxicity through AMPKα2-mediated Nrf2 activation and the beneficial effects of SFN were lost in AMPKα2-/- mice (Li et al., 2020). These studies indicated that AMPKα2 activation could promote Nrf2 mediated antioxidant function. Thirdly, AMPK has also been suggested to regulate NADPH oxidase activity. In high glucose-treated podocytes, AMPK inactivation led to upregulation of Nox4 and enhancement of NADPH oxidase and thus resulted in podocyte apoptosis (Eid et al., 2010). Pharmacologic activation of AMPK significantly depressed Nox4 expression and alleviated oxidative stress (Eid et al., 2010). Assaad AE et al. (Eid et al., 2013) further demonstrated that Sesn2 mediated AMPK activation alleviated HG-induced fibronectin synthesis via blocking Nox4-dependent ROS and peroxynitrite production in glomerular mesangial cells (Eid et al., 2013). Our study also demonstrated that Sesn2 overexpression could suppress Nox4 expression in hypertrophic mouse hearts. Therefore, previous published studies support our finding that Sesn2 overexpression in cardiomyocytes could no longer depress oxidative stress in AMPKα2-/- mice hearts. The regulation of AMPK-mTORC1 signaling pathway by Sesn2 might be more potent than other anti-oxidants in depressing ROS overproduction in pathological cardiac hypertrophy.

5 CONCLUSION

This study first demonstrated that Sesn2 overexpression (at 3, 6, and 9 folds) showed no genetic toxicity in transgenic mice hearts. Sesn2 overexpression could mitigate pressure overload-induced cardiac hypertrophy *in vivo* and Ang II-induced NRCMs hypertrophy *in vitro via* activating AMPKα2, depressing ACC1/mTORC1 signaling, and oxidative stress, as well as restoring Nrf2/HO-1 signaling. We also showed that Sesn2 mediated AMPKα2 activation might be the key point for its activity in preventing excessive ROS accumulation and restoring Nrf2/HO-1 signaling. Strategies on regulating Sesn2 expression by genetic or pharmacologic means might be effective for preventing pathological cardiac hypertrophy and heart failure.

DATA AVAILABILITY STATEMENT

The original contributions presented in the study are included in the article/**Supplementary Materials**, further inquiries can be directed to the corresponding author.

ETHICS STATEMENT

The animal study was reviewed and approved by the Animal Care and Use Committee of Renmin Hospital of Wuhan University.

AUTHOR CONTRIBUTIONS

Q-ZT designed, supervised, and revised this study. NZ and H-HL analyzed data, prepared draft, and completed the cellular experiments. HF, S-QM, and W-JL managed animal, performed aortic banding surgery, and completed oxidative stress associated examination. XA and ZL performed echocardiography and pressure-volume loop analysis. WD and Z-YZ performed Western blots and RT-PCR analysis. HY and SC performed histopathological and immunofluorescence staining.

FUNDING

This work was supported by the National Natural Science Foundation (No. 81470402, 81530012), the National Key R&D Program of China (No. 2018YFC1311300), the Development Center for Medical Science and Technology National Health and Family Planning Commission of the People's Republic of China (The prevention and control project of cardiovascular disease, No. 2016ZX-008-01), the Fundamental Research Funds for the Central Universities (No. 2042018kf1032), and the Science and Technology Planning Projects of Wuhan (No. 2018061005132295).

SUPPLEMENTARY MATERIAL

The Supplementary Material for this article can be found online at: https://www.frontiersin.org/articles/10.3389/fphar.2021.716884/full#supplementary-material

REFERENCES

Bae, S. H., Sung, S. H., Oh, S. Y., Lim, J. M., Lee, S. K., Park, Y. N., et al. (2013). Sestrins Activate Nrf2 by Promoting P62-dependent Autophagic Degradation of Keap1 and Prevent Oxidative Liver Damage. *Cell Metab* 17, 73–84. doi:10.1016/j.cmet.2012.12.002

Bauml, M. A., and Underwood, D. A. (2010). Left Ventricular Hypertrophy: an Overlooked Cardiovascular Risk Factor. *Cleve Clin. J. Med.* 77, 381–387. doi:10.3949/ccjm.77a.09158

Budanov, A. V., and Karin, M. (2008). p53 Target Genes Sestrin1 and Sestrin2 Connect Genotoxic Stress and mTOR Signaling. *Cell* 134, 451–460. doi:10.1016/j.cell.2008.06.028

Deng, W., Zong, J., Bian, Z., Zhou, H., Yuan, Y., Zhang, R., et al. (2013). Indole-3-carbinol Protects against Pressure Overload Induced Cardiac Remodeling via Activating AMPK-α. *Mol. Nutr. Food Res.* 57, 1680–1687. doi:10.1002/mnfr.201300012

Deng, K. Q., Li, J., She, Z. G., Gong, J., Cheng, W. L., Gong, F. H., et al. (2017). Restoration of Circulating MFGE8 (Milk Fat Globule-EGF Factor 8) Attenuates Cardiac Hypertrophy through Inhibition of Akt Pathway. *Hypertension* 70, 770–779. doi:10.1161/HYPERTENSIONAHA.117.09465

Du, J. X., Wu, J. Z., Li, Z., Zhang, C., Shi, M. T., Zhao, J., et al. (2019). Pentamethylquercetin Protects against Cardiac Remodeling via Activation of Sestrin2. *Biochem. Biophys. Res. Commun.* 512, 412–420. doi:10.1016/j.bbrc.2019.03.031

Eid, A. A., Ford, B. M., Block, K., Kasinath, B. S., Gorin, Y., Ghosh-Choudhury, G., et al. (2010). AMP-activated Protein Kinase (AMPK) Negatively Regulates Nox4-dependent Activation of P53 and Epithelial Cell Apoptosis in Diabetes. *J. Biol. Chem.* 285, 37503–37512. doi:10.1074/jbc.M110.136796

Eid, A. A., Lee, D. Y., Roman, L. J., Khazim, K., and Gorin, Y. (2013). Sestrin 2 and AMPK Connect Hyperglycemia to Nox4-dependent Endothelial Nitric Oxide Synthase Uncoupling and Matrix Protein Expression. *Mol. Cel Biol* 33, 3439–3460. doi:10.1128/MCB.00217-13

Fischhuber, K., Matzinger, M., and Heiss, E. H. (2020). AMPK Enhances Transcription of Selected Nrf2 Target Genes via Negative Regulation of Bach1. *Front Cel Dev Biol* 8, 628. doi:10.3389/fcell.2020.00628

Haque, Z. K., and Wang, D. Z. (2017). How Cardiomyocytes Sense Pathophysiological Stresses for Cardiac Remodeling. *Cell Mol Life Sci* 74, 983–1000. doi:10.1007/s00018-016-2373-0

Hou, Y. S., Guan, J. J., Xu, H. D., Wu, F., Sheng, R., and Qin, Z. H. (2015). Sestrin2 Protects Dopaminergic Cells against Rotenone Toxicity through AMPK-dependent Autophagy Activation. *Mol. Cel Biol* 35, 2740–2751. doi:10.1128/MCB.00285-15

Huang, X. T., Liu, W., Zhou, Y., Sun, M., Yang, H. H., Zhang, C. Y., et al. (2020). Galectin-1 Ameliorates Lipopolysaccharide-Induced Acute Lung Injury via AMPK-Nrf2 Pathway in Mice. *Free Radic. Biol. Med.* 146, 222–233. doi:10.1016/j.freeradbiomed.2019.11.011

Kallenborn-Gerhardt, W., Lu, R., Syhr, K. M., Heidler, J., Von Melchner, H., Geisslinger, G., et al. (2013). Antioxidant Activity of Sestrin 2 Controls Neuropathic Pain after Peripheral Nerve Injury. *Antioxid. Redox Signal.* 19, 2013–2023. doi:10.1089/ars.2012.4958

Khatibzadeh, S., Farzadfar, F., Oliver, J., Ezzati, M., and Moran, A. (2013). Worldwide Risk Factors for Heart Failure: a Systematic Review and Pooled Analysis. *Int. J. Cardiol.* 168, 1186–1194. doi:10.1016/j.ijcard.2012.11.065

Kim, H., An, S., Ro, S. H., Teixeira, F., Park, G. J., Kim, C., et al. (2015a). Janus-faced Sestrin2 Controls ROS and mTOR Signalling through Two Separate Functional Domains. *Nat. Commun.* 6, 10025. doi:10.1038/ncomms10025

Kim, J. S., Ro, S. H., Kim, M., Park, H. W., Semple, I. A., Park, H., et al. (2015b). Sestrin2 Inhibits mTORC1 through Modulation of GATOR Complexes. *Sci. Rep.* 5, 9502. doi:10.1038/srep09502

Kim, K. M., Yang, J. H., Shin, S. M., Cho, I. J., and Ki, S. H. (2015c). Sestrin2: A Promising Therapeutic Target for Liver Diseases. *Biol. Pharm. Bull.* 38, 966–970. doi:10.1248/bpb.b15-00228

Larson, J. D., and Baker, S. J. (2019). Engineering Inducible Knock-In Mice to Model Oncogenic Brain Tumor Mutations from Endogenous Loci. *Methods Mol. Biol.* 1869, 207–230. doi:10.1007/978-1-4939-8805-1_18

Lee, J. H., Budanov, A. V., Park, E. J., Birse, R., Kim, T. E., Perkins, G. A., et al. (2010). Sestrin as a Feedback Inhibitor of TOR that Prevents Age-Related Pathologies. *Science* 327, 1223–1228. doi:10.1126/science.1182228

Lee, J. H., Budanov, A. V., Talukdar, S., Park, E. J., Park, H. L., Park, H. W., et al. (2012). Maintenance of Metabolic Homeostasis by Sestrin2 and Sestrin3. *Cel Metab* 16, 311–321. doi:10.1016/j.cmet.2012.08.004

Li, Z., Guo, H., Li, J., Ma, T., Zhou, S., Zhang, Z., et al. (2020). Sulforaphane Prevents Type 2 Diabetes-Induced Nephropathy via AMPK-Mediated Activation of Lipid Metabolic Pathways and Nrf2 Antioxidative Function. *Clin. Sci. (Lond)* 134, 2469–2487. doi:10.1042/CS20191088

Liao, H. H., Zhang, N., Meng, Y. Y., Feng, H., Yang, J. J., Li, W. J., et al. (2019). Myricetin Alleviates Pathological Cardiac Hypertrophy via TRAF6/TAK1/MAPK and Nrf2 Signaling Pathway. *Oxid Med. Cel Longev* 2019, 6304058. doi:10.1155/2019/6304058

Luo, W., Dai, Y., Chen, Z., Yue, X., Andrade-Powell, K. C., and Chang, J. (2020). Spatial and Temporal Tracking of Cardiac Exosomes in Mouse Using a Nano-Luciferase-CD63 Fusion Protein. *Commun. Biol.* 3, 114. doi:10.1038/s42003-020-0830-7

Ma, Z. G., Dai, J., Zhang, W. B., Yuan, Y., Liao, H. H., Zhang, N., et al. (2016). Protection against Cardiac Hypertrophy by Geniposide Involves the GLP-1 Receptor/AMPKα Signalling Pathway. *Br. J. Pharmacol.* 173, 1502–1516. doi:10.1111/bph.13449

Ma, Z. G., Yuan, Y. P., Zhang, X., Xu, S. C., Kong, C. Y., Song, P., et al. (2019). C1q-tumour Necrosis Factor-Related Protein-3 Exacerbates Cardiac Hypertrophy in Mice. *Cardiovasc. Res.* 115, 1067–1077. doi:10.1093/cvr/cvy279

Matzinger, M., Fischhuber, K., Pölöske, D., Mechtler, K., and Heiss, E. H. (2020). AMPK Leads to Phosphorylation of the Transcription Factor Nrf2, Tuning Transactivation of Selected Target Genes. *Redox Biol.* 29, 101393. doi:10.1016/j.redox.2019.101393

Murphy, S. P., Ibrahim, N. E., and Januzzi, J. L., Jr. (2020). Heart Failure with Reduced Ejection Fraction: A Review. *JAMA* 324, 488–504. doi:10.1001/jama.2020.10262

Packer, M. (2020). Autophagy-dependent and -independent Modulation of Oxidative and Organellar Stress in the Diabetic Heart by Glucose-Lowering Drugs. *Cardiovasc. Diabetol.* 19, 62. doi:10.1186/s12933-020-01041-4

Park, H. W., Park, H., Ro, S. H., Jang, I., Semple, I. A., Kim, D. N., et al. (2014). Hepatoprotective Role of Sestrin2 against Chronic ER Stress. *Nat. Commun.* 5, 4233. doi:10.1038/ncomms5233

Parmigiani, A., Nourbakhsh, A., Ding, B., Wang, W., Kim, Y. C., Akopiants, K., et al. (2014). Sestrins Inhibit mTORC1 Kinase Activation through the GATOR Complex. *Cell Rep* 9, 1281–1291. doi:10.1016/j.celrep.2014.10.019

Pasha, M., Eid, A. H., Eid, A. A., Gorin, Y., and Munusamy, S. (2017). Sestrin2 as a Novel Biomarker and Therapeutic Target for Various Diseases. *Oxid. Med. Cel Longev.* 2017, 3296294. doi:10.1155/2017/3296294

Qi, D., and Young, L. H. (2015). AMPK: Energy Sensor and Survival Mechanism in the Ischemic Heart. *Trends Endocrinol. Metab.* 26, 422–429. doi:10.1016/j.tem.2015.05.010

Quan, N., Li, X., Zhang, J., Han, Y., Sun, W., Ren, D., et al. (2020). Substrate Metabolism Regulated by Sestrin2-mTORC1 Alleviates Pressure Overload-Induced Cardiac Hypertrophy in Aged Heart. *Redox Biol.* 36, 101637. doi:10.1016/j.redox.2020.101637

Sciarretta, S., Forte, M., Frati, G., and Sadoshima, J. (2018). New Insights into the Role of mTOR Signaling in the Cardiovascular System. *Circ. Res.* 122, 489–505. doi:10.1161/CIRCRESAHA.117.311147

Shaw, R. J. (2009). LKB1 and AMP-Activated Protein Kinase Control of mTOR Signalling and Growth. *Acta Physiol. (Oxf)* 196, 65–80. doi:10.1111/j.1748-1716.2009.01972.x

Sun, W., Wang, Y., Zheng, Y., and Quan, N. (2020). The Emerging Role of Sestrin2 in Cell Metabolism, and Cardiovascular and Age-Related Diseases. *Aging Dis.* 11, 154–163. doi:10.14336/AD.2019.0320

Wu, Q. Q., Xiao, Y., Liu, C., Duan, M., Cai, Z., Xie, S., et al. (2019). The Protective Effect of High Mobility Group Protein HMGA2 in Pressure Overload-Induced Cardiac Remodeling. *J. Mol. Cel Cardiol* 128, 160–178. doi:10.1016/j.yjmcc.2019.01.027

Yang, Y., Cuevas, S., Yang, S., Villar, V. A., Escano, C., Asico, L., et al. (2014). Sestrin2 Decreases Renal Oxidative Stress, Lowers Blood Pressure, and Mediates Dopamine D2 Receptor-Induced Inhibition of Reactive Oxygen Species Production. *Hypertension* 64, 825–832. doi:10.1161/HYPERTENSIONAHA.114.03840

Yildiz, M., Oktay, A. A., Stewart, M. H., Milani, R. V., Ventura, H. O., and Lavie, C. J. (2020). Left Ventricular Hypertrophy and Hypertension. *Prog. Cardiovasc. Dis.* 63, 10–21. doi:10.1016/j.pcad.2019.11.009

Zaha, V. G., and Young, L. H. (2012). AMP-activated Protein Kinase Regulation and Biological Actions in the Heart. *Circ. Res.* 111, 800–814. doi:10.1161/CIRCRESAHA.111.255505

Zhang, P., Hu, X., Xu, X., Fassett, J., Zhu, G., Viollet, B., et al. (2008). AMP Activated Protein Kinase-Alpha2 Deficiency Exacerbates

Pressure-Overload-Induced Left Ventricular Hypertrophy and Dysfunction in Mice. *Hypertension* 52, 918–924. doi:10.1161/HYPERTENSIONAHA.108.114702

Zhang, N., Feng, H., Liao, H. H., Chen, S., Yang, Z., Deng, W., et al. (2018a). Myricetin Attenuated LPS Induced Cardiac Injury *In Vivo* and *In Vitro*. *Phytother Res.* 32, 459–470. doi:10.1002/ptr.5989

Zhang, N., Wei, W. Y., Liao, H. H., Yang, Z., Hu, C., Wang, S. S., et al. (2018b). AdipoRon, an Adiponectin Receptor Agonist, Attenuates Cardiac Remodeling Induced by Pressure Overload. *J. Mol. Med. (Berl)* 96, 1345–1357. doi:10.1007/s00109-018-1696-8

Zhang, X., Hu, C., Kong, C. Y., Song, P., Wu, H. M., Xu, S. C., et al. (2020). FNDC5 Alleviates Oxidative Stress and Cardiomyocyte Apoptosis in Doxorubicin-Induced Cardiotoxicity via Activating AKT. *Cell Death Differ* 27, 540–555. doi:10.1038/s41418-019-0372-z

Zuurbier, C. J., Bertrand, L., Beauloye, C. R., Andreadou, I., Ruiz-Meana, M., Jespersen, N. R., et al. (2020). Cardiac Metabolism as a Driver and Therapeutic Target of Myocardial Infarction. *J. Cel Mol Med* 24, 5937–5954. doi:10.1111/jcmm.15180

Conflict of Interest: The authors declare that the research was conducted in the absence of any commercial or financial relationships that could be construed as a potential conflict of interest.

frontiers in Pharmacology

ORIGINAL RESEARCH
published: 26 November 2021
doi: 10.3389/fphar.2021.771940

Enhancing Fatty Acids Oxidation *via* L-Carnitine Attenuates Obesity-Related Atrial Fibrillation and Structural Remodeling by Activating AMPK Signaling and Alleviating Cardiac Lipotoxicity

Yudi Zhang[1†], Yuping Fu[1†], Tiannan Jiang[2†], Binghua Liu[3], Hongke Sun[1], Ying Zhang[1], Boyuan Fan[1], Xiaoli Li[1], Xinghua Qin[3] and Qiangsun Zheng[1]**

[1]The Second Affiliate Hospital of Xi'an Jiaotong University, Xi'an, China, [2]Department of Cardiology, Beijing Anzhen Hospital, Capital Medical University, Beijing, China, [3]School of Life Sciences, Northwestern Polytechnical University, Xi'an, China

Atrial fibrillation (AF) is the most common sustained cardiac arrhythmia in clinical setting. Its pathogenesis was associated with metabolic disorder, especially defective fatty acids oxidation (FAO). However, whether promoting FAO could prevent AF occurrence and development remains elusive. In this study, we established a mouse model of obesity-related AF through high-fat diet (HFD) feeding, and used L-carnitine (LCA, 150 mg/kg·BW/d), an endogenous cofactor of carnitine palmitoyl-transferase-1B (CPT1B; the rate-limiting enzyme of FAO) to investigate whether FAO promotion can attenuate the AF susceptibility in obesity. All mice underwent electrophysiological assessment for atrial vulnerability, and echocardiography, histology and molecular evaluation for AF substrates and underlying mechanisms, which were further validated by pharmacological experiments *in vitro*. HFD-induced obese mice increased AF vulnerability and exhibited apparent atrial structural remodeling, including left atrial dilation, cardiomyocyte hypertrophy, connexin-43 remodeling and fibrosis. Pathologically, HFD apparently leads to defective cardiac FAO and subsequent lipotoxicity, thereby evoking a set of pathological reactions including oxidative stress, DNA damage, inflammation, and insulin resistance. Enhancing FAO *via* LCA attenuated lipotoxicity and lipotoxicity-induced pathological changes in the atria of obese mice, resulting in restored structural remodeling and ameliorated AF susceptibility. Mechanistically, LCA activated AMPK/PGC1α signaling both *in vivo* and *in vitro*, and pharmacological inhibition of AMPK *via* Compound C attenuated LCA-induced cardio-protection in palmitate-treated primary atrial cardiomyocytes. Taken together, our results demonstrated that FAO promotion *via* LCA attenuated obesity-mediated AF and structural remodeling by activating AMPK signaling and alleviating atrial lipotoxicity. Thus, enhancing FAO may be a potential therapeutic target for AF.

Abbreviations: AF, atrial fibrillation; AMPK, AMP-activated protein kinase; CPT1B, carnitine palmitoyltransferase-1B; CC, compound C; FAO, fatty acids oxidation; FAs, fatty acids; HFD, high-fat diet; LCA, L-carnitine; NRF2, nuclear factor erythroid 2-related factor2; PGC1α, peroxisome proliferator-activated receptor γ coactivator1α; STD, standard diet.

OPEN ACCESS

Edited by:
Jérôme Roncalli,
Centre Hospitalier Universitaire de Toulouse, France

Reviewed by:
Andrea Elia,
Temple University, United States
Yin Cai,
Hong Kong Polytechnic University, Hong Kong SAR, China

***Correspondence:**
Xinghua Qin
xinghuaqin@nwpu.edu.cn
Qiangsun Zheng
zhengqiangsun@126.com

†These authors have contributed equally to this work and share first authorship

Specialty section:
This article was submitted to Cardiovascular and Smooth Muscle Pharmacology, a section of the journal Frontiers in Pharmacology

Received: 07 September 2021
Accepted: 12 November 2021
Published: 26 November 2021

Citation:
Zhang Y, Fu Y, Jiang T, Liu B, Sun H, Zhang Y, Fan B, Li X, Qin X and Zheng Q (2021) Enhancing Fatty Acids Oxidation via L-Carnitine Attenuates Obesity-Related Atrial Fibrillation and Structural Remodeling by Activating AMPK Signaling and Alleviating Cardiac Lipotoxicity. Front. Pharmacol. 12:771940. doi: 10.3389/fphar.2021.771940

Keywords: atrial fibrillation, obesity, fatty acids oxidation, lipotoxicity, l-carnitine, AMPK (5′-AMP activated kinase)

INTRODUCTION

Atrial fibrillation (AF), the most common sustained cardiac arrhythmia in clinical practice affecting nearly 2% of general population, is associated with substantial complications and financial burden (Lippi et al., 2021). Metabolic disturbances have shown strong relationship with AF by ample clinical evidence, and have been represented as driving forces for adverse atrial remodelling mechanically (Mourtzinis et al., 2018). In addition, regarding cardiac high energy demand, disordered atrial metabolism is supposed to take a leading role in AF pathogenesis. However, far less is known about the impacts of atrial metabolism in AF.

Metabolic homeostasis and abnormalities have spurred major interest in the field of AF at present, with a focus on lipids, the predominant energy substrates (~70%) of heart. Under physiological conditions, absorbed cardiac FAs is delivered into mitochondria *via* the gateway enzyme carnitine palmitoyltransferase-1B (CPT1B), and fueled by mitochondrial FAs oxidation (FAO) and the TCA cycle. In context of AF, the metabolic disturbance of FAs was observed and proved to contribute to the predisposition and perpetuation of AF (Mourtzinis et al., 2018). Briefly, during AF, irregular high-frequency excitation and contraction of cardiomyocytes shift the metabolic balance from FAO to carbohydrate utilization, a more oxygen-saving way (Heijman and Dobrev, 2015). Supportively, AF patients and animals show the coordinated transcriptional down-regulation of FAO-related enzymes (especially AMP-activated protein kinase (AMPK), peroxisome proliferator-activated receptor γ coactivator1α (PGC1α), and CPT1B) and concomitant up-regulation of glycolysis-related enzymes in atria (Barth et al., 2005; Tu et al., 2014; Mourtzinis et al., 2018; Jie et al., 2019). Supportively, redressing lipid metabolism through factors, such as AMPK, PPARα/PGC1α, Hif1-α, VLCAD, and PLIN2, has been proved effective to prevent AF, exemplifying metabolic modulation as a potential therapeutic strategy for AF (Harada et al., 2017). Of note, pharmacological interventions targeting FAO regulators, AMPK and PGC1α (Yu et al., 2011; Liu et al., 2016; Bai et al., 2019; Deshmukh et al., 2021; Ostropolets et al., 2021), have been proved to reduce AF susceptibility, yet it is still unclear whether enhancing FAO alleviates AF.

AF risk escalates in parallel with increased BMI, thus obesity, a public health issue as well as the most common metabolic disorder in human, is regarded as the second biggest attributable risk factor for AF (Wong et al., 2015). Various pathological conditions including metabolic imbalance of glucose or lipid and metabolic stress has been observed in obesity (Vyas and Lambiase, 2019). Notably, diet-induced obesity increases the influx of FAs and downregulates the key enzymes involved in FAs expenditure (Haffar et al., 2015; Heier and Haemmerle, 2016; Garcia and Shaw, 2017). Particularly, in long-term obese individuals, CPT1B is decreased in expression and blunted in response to lipid (Maples et al., 2015), while L-carnitine (LCA), the obligatory cofactor of CPT1B (Söder et al., 2019), is decreased in serum and insufficient to cope with FAs overload (Pooyandjoo et al., 2016). Together, obesity and AF share the same pathogenesis, defective FAO, which might count for the increased AF susceptibility, especially in which are provoked by obesity. Therefore, FAO promotion maybe the first-line option to combat AF, especially obesity-related AF. In pathological context, ectopic lipid accumulation and consequently lipotoxicity occurred when FAO was defective in cardiomyocyte, serving as a mechanistic link between AF/obesity and metabolic disorder (Haffar et al., 2015; Ozcan et al., 2015; Opacic et al., 2016; Harada et al., 2017). Specifically, cardiac lipotoxicity could provoke oxidative stress, DNA damage, inflammation, and insulin intolerance, contributing morphological changes and cellular dysfunction of atria (Karam et al., 2017; Sletten et al., 2018), including cardiac hypertrophy, fibrosis, gap junction remodeling, and myocardial injury (Shenasa et al., 2015; Fukui et al., 2017; Meng et al., 2017; Sato et al., 2019), thus, providing substrates for AF.

Therefore, we adopted LCA (150 mg/kg·BW/d) to facilitate FAO, and further examined the AF vulnerability and atrial remodeling *in vivo* (a mice model of high-fat diet (HFD)-induced obesity-mediated AF) and *in vitro* (a primary atrial cardiomyocyte cell model of palmitate (PA)-mimicked lipid overloading), aiming to determine whether enhancing FAO can alter the process that underlie AF in obesity and explore possible mechanisms. Our results determined that defective cardiac FAO takes a leading role in obesity-related AF, and proved that FAO promotion *via* LCA exerts an anti-AF effect through activating AMPK signals and reducing atrial lipotoxicity in obese mice. Notably, this article firstly demonstrates the beneficial effects of enhanced FAO in the reversal of obesity-related AF, thus shedding light onto a feasible AF treatment.

METHODS AND MATERIALS

Animal and Treatment

Male C57BL/6J mice (aged 4–6 weeks) were purchased from Xi'an Jiaotong University (Xi'an, China) and bred under standard laboratory conditions. After 1 week of acclimatization, a total of forty mice were randomly divided into 4 groups (n = 10 per group): 1) Standard diet group (STD; 20% fat, 56% carbohydrate, 24% protein; Research Diets Inc., New Brunswick, NJ); 2) STD + LCA group; 3) HFD group (HFD; 60% fat, 20% carbohydrate, 20% protein; Research Diets Inc.); 4) HFD + LCA group. After feeding HFD for 8 weeks, the mice became obese and showed greater propensity for AF. Subsequently, FAO activator, LCA (150 mg/kg·BW/d; TargetMol, Boston, United States) (Bakermans et al., 2013), was administrated *via* drinking water for another 4 weeks. Based on our preliminary experiment, the experimental dose of LCA was set to be 150 mg/kg·BW/d, which had no significant impact on mice body weight (BW) but suppressed obesity-induced AF susceptibility. At the end of the experiment, AF induction, echocardiography, intraperitoneal glucose tolerance test (IPGTT) and insulin tolerance test (ITT) were performed in

each group before tissue sampling. After overnight fasting, atrial tissues and blood samples were collected from euthanized mice for further analysis. All the procedures of this study were approved by the Institutional Animal Care and Use Committee of Xi'an Jiaotong University.

Cell Culture and Treatment

Primary atrial cardiomyocytes were isolated from the atria of neonatal Sprague–Dawley rat (1~3-day-old; Xi'an Jiaotong University, Xi'an, China). Briefly, atria tissue were surgically removed, trypsinized (0.08% trypsin; Solarbio, Beijing, China), digested with 0.1% collagenase II (Solarbio), and the primary atrial cardiomyocytes were isolated by differential detachment and verified under the microscope. Isolated cells were cultured in 6-well plates at 37°C in 5% CO_2, with DMEM supplemented with 10% FBS and 1% penicillin/streptomycin solution. Final solutions of 200 μM PA (dissolved in 20% BSA; Sigma-Aldrich, St. Louis, United States) was added to replicate the effects of lipid overloading, while LCA (5 mM; TargetMol) was added to enhance FAO, and Compound C (CC, 0.5 μM; Sigma-Aldrich) was added to inhibit AMPK activation. After being treated for 24 h, cells were collected, washed and lysed for the following evaluations.

AF Induction and Electrophysiological Examination

Programmed *trans*-esophageal stimulation was performed to assess AF inducibility as described previously (Fu et al., 2021). Briefly, mice were anesthetized with pentobarbital intraperitoneally (50 mg/kg·BW) and then electrical stimulated by an external simulator (SCOPE, Kaifeng, China), and surface electrocardiogram (ECG) was recorded by a physiologic signal-acquisition system (RM6240; Chengdu instrument factory, Chengdu, China). At first, baseline ECG was analyzed by 10 consecutive beats recorded in the initial stabilization period with heart rates between 300 and 500 bpm at first. Later, AF was induced with burst pacing (pulse width 1 ms; 1.5× capture threshold; 30, 35, and 40 Hz), and was considered sustained as persisted rapid irregular f-waves with irregular R-R intervals lasting for more than 1 s. In addition, atrial effective refractory period (ERP) was assessed by continuous stimulation applied with decreasing R-R intervals from 140 to 40 ms at 1 ms decrements. Sinoatrial node recovery time ($SNRT_{max}$) was measured as the longest duration between the last stimulus and the first sinus P-wave, and corrected by the R-R interval ($_cSNRT_{max}$).

Echocardiography

2D echocardiography was employed to discern cardiac structural and functional differences among groups. Echocardiography (Vevo 2,100; VisualSonics Inc., Toronto, Ontario, Canada) was performed by an animal cardiologist blind to the experimental design in mice anaesthetized with inhalational isoflurane. Dimension of superoinferior (SI), anteroposterior (AP) and mediolateral (ML) were obtained in a long-axis view and a short-axis view, respectively. LA filling volume was calculated using the formula: LA Volume = $(4\pi\times SI\times AP\times ML)/(3\times 2\times 2\times 2)$ (Ujino et al., 2006). Cardiac function was calculated according to standard formulae, and the results were averaged of three cardiac cycles.

IPGTT and ITT

Glucose and insulin homeostasis were evaluated *in vivo* by IPGTT and ITT. For the IPGTT, D-glucose was injected intraperitoneally (2 g/kg·BW) into over-night fasted mice, and, subsequently, blood was taken from the tail vein at 5, 15, 30, 60, 90 and 120 min after glucose loading and blood glucose levels were measured by the Accu-Chek glucometer (Roche Diagnostics, Indianapolis, United States). Similarly, for the ITT, mice were fasted for 2 h before insulin administration intraperitoneally (1 U/kg·BW; Wanbang Biopharma, Xuzhou, China), following the glucose determination at 0, 15, 30, 45 and 60 min. Glucose tolerance and insulin sensitivity were calculated as the area under the curve (AUC) by GraphPad Prism 8.0 (GraphPad Software, San Diego, America).

Analysis of Histological Staining and Fluorescence

After being isolated from heart tissue, atrial appendages were fixed with 4% paraformaldehyde overnight, embedded in paraffin, and cut into 5 μm slides longitudinally. Paraffin-embedded specimens were finally stained with hematoxylin-eosin (H&E), Wheat Germ Agglutinin (WGA), Masson, Periodic acid-Schiffs (PAS), selected antibodies (connexin-43; 1:200; Invitrogen, California, United States, NRF2; 1:500; Proteintech, Chicago, United States, and 8-Hydroxy-2′-deoxyguanosine (8-OH-dG), 1: 100; JalCA, Shizuoka, Japan), and TUNEL (*in situ* cell death detection kit, TMR red; Roche Diagnostics). Respectively, frozen sections (10 μm thickness) of atria samples were prepared and stained with oil red O, MitoSOX and dihydroethidium (DHE). Slides were visualized and photographed by an optical microscope (Nikon, Melville, NY, United States) at a magnification of 100× for histology, or by a confocal microscope (Leica, Bensheim, Germany) at a magnification of 20× for immunofluorescence. Images were further analyzed by ImageJ software (version 1.46r; National Institutes of Health, Bethesda, United States). Data were expressed as the percentage of the positive-stained region to the total area of cardiomyocyte area, and averaged from six random fields in each slide.

Detection of Markers in Serum and Tissue

Biomarkers were assayed using commercially available kits in accordance with manufacturer's guidelines, including fasted non-esterified FAs (NEFA) (Solarbio), lactate dehydrogenase (LDH) (Nanjing Jiancheng Bioengineering Institute, Nanjing, China), creatine kinase-MB (CK-MB) (Nanjing Jiancheng Bioengineering Institute), malondialdehyde (MDA) (Beyotime Institute of Biotechnology, Shanghai, China) and superoxide dismutase (SOD) (Beyotime Institute of Biotechnology).

Assay of FAO *in vitro*

Cellular FAO was measured with a FAO Assay Kit (ab222944; Abcam, Cambridge, United States) according to the manufacturer's instruction. Fluorescence was detected using FLUOstar Omega

(BMG LABTECH, Aylesbury, United Kingdom) and the results were normalized by protein concentration in each well through a micro-bicinchoninic acid (BCA; Pierce Chemical Company, Rockford, United States) kit.

Western Blot

Protein levels were measured by WB with β-actin as the loading control. Protein was extracted from atria samples or cells and quantitated by a BCA assay. Equal amount (10–30 μg) of protein was loaded and separated by SDS-PAGE using 10 or 12% acrylamide gradients, and later transferred to nitrocellulose membranes. The membranes were blocked with 5% skim milk and incubated with antibodies against total-AMPK (1:1,000; Cell Signaling Technology/CST, Massachusetts, United States), CD36 (1:1,000; Abcam), collagen Ⅰ (1:1,000; Abcam), collagen Ⅲ (1:1,000; Abcam), connexin-43 (1:200; Invitrogen), CPT1B (1:1,000; Proteintech), GLUT4 (1:500; Proteintech), NFκB (1:1,000; Proteintech), NRF2 (1:1,000; Proteintech), phoso-AMPK (Thr172; 1:1,000; CST), phoso-Akt (Ser473; 1:1,000; CST), phoso-NFκB (1:1,000; CST), PGC1α (1:1,000; Proteintech), SOD2 (1:1,000; Proteintech), TGF-β (1:1,000; Abcam), α-SMA (1:1,000; CST), β-actin (1:5,000; Proteintech). Protein levels were quantified as the intensity of bands using ImageJ software (NIH systems) and standardized to β-actin. Abbreviations are fully illustrated in corresponding figure legends.

RNA Extraction and Real-Time Reverse Transcription Polymerase Chain Reaction

RT-qPCR was carried out to quantify gene expressions among the groups. Briefly, RNA from atria tissues was extracted using TRIzol reagent (Accurate Biology, Changsha, China). Then, the high-sensitivity RT-qPCR reaction was measured using the SYBR green chimeric fluorescence method (Accurate Biology) and detected by CFX96™ Real-Time PCR System (Bio-Rad, Hercules, CA, United States). Results were quantified using the $2^{-\triangle\triangle Ct}$ comparative method and normalized by β-actin. The primer sequences and full names of genes are listed in **Supplementary Table S1**.

Statistical Analysis

All data of animal and cell studies were analyzed by SPSS 23.0 (IBM SPSS software, New York, United States), visualized by GraphPad Prism 8.0 (GraphPad Software), and shown as mean ± SEM. Replicates are indicated in figure legends and table legends. Data normality was evaluated by Kolmogorov-Smirnov test, and comparisons between groups were performed with One-way ANOVA (in mice experiments) or Two-way ANOVA (in cell experiments) with Bonferroni *post-hoc* test. For all tests, $p < 0.05$ was considered significant.

RESULTS

LCA Supplementation Attenuates Obesity-Induced AF Susceptibility

In this study, we established a mouse model of obesity-related AF through 13-week HFD feeding, and LCA was administrated *via* drinking water (150 mg/kg·BW/d) during the last 4-week period to investigate whether enhancing FAO could attenuate obesity-mediated AF. The schematic of the experimental design is shown in **Figure 1A**, and basal characteristics of mice in each group are summarized in **Table 1**.

As expected, at the end of the experiment, HFD mice gained 20% more BW than STD mice (**Supplementary Figure S1A**), together with increased heart weight (HW) and serum NEFA (**Supplementary Figures S1B–D**). Obesity-mediated AF was successfully established, as supported by increased AF frequency and prolonged duration in HFD mice (**Figures 1B–D**). LCA decreased the ratio of HW/NAL (nasal-anal length) in HFD mice, yet no significant change of BW gain was observed with or without LCA supplementation (**Supplementary Figures S1A–C**). In addition, LCA suppressed HFD-induced elevation of serum NEFA (**Supplementary Figure S1D**). Of note, LCA supplementation alleviated pacing-induced AF susceptibility in the obese mice. Surface ECG (Lead II) at baseline showed that LCA supplementation significantly decreased P-wave duration (P_{max}) and P-wave area (P_{area}), two of the independent predictors for AF, in obese mice (**Figures 1E–G**). In addition, electrophysiological abnormalities, including prolonged $SNRT_{max}$ and shortened ERP, were regarded to increase the AF propensity. Supportively, LCA supplementation shortened $SNRT_{max}$ and extended ERP in obese mice (**Figures 1H–L**).

LCA Supplementation Constrains Obesity-Induced Atrial Structural Remodeling

Atrial structural remodeling, including atrial dilatation, cellular hypertrophy, gap junction disturbance, and interstitial fibrosis, offers substrates for AF. Thus, we later assessed atrial structural alterations among the groups.

Obese mice displayed excessive left atrial enlargement, as shown by marked increase of left atrium (LA) diameter and LA filling volume (**Figures 2A–C**). In atrial cardiomyocytes, obesity developed substantial cellular hypertrophy and disarray in the atria, as evidenced by H&E staining, WGA staining and β-MHC transcription (**Figures 2D–G**). Moreover, the main gap junction protein, connexin-43, was apparently upregulated in expression and heterogeneous distributed in the atrial cardiomyocyte of obese mice (**Figures 2H–J**). In addition, intra-myocardial fibrosis, a hallmark of AF, was observed to increase in the atria of obese mice, as evidenced by aggravated collagen deposition, upregulated pro-fibrosis signaling (TGF-β, α-SMA, Smad3, collagen Ⅰ, and collagen Ⅲ), and downregulated transcription of anti-fibrotic Smad7 (**Figures 2K–O**).

Coincided with reduced AF inducibility, LCA supplementation showed significant capacity to shrink LA, attenuate cellular hypertrophy, gap junction disturbance, and fibrosis while challenged by a long-term HFD (**Figure 2**), indicating FAO promotion *via* LCA supplementation constrained the AF substrates in obese mice.

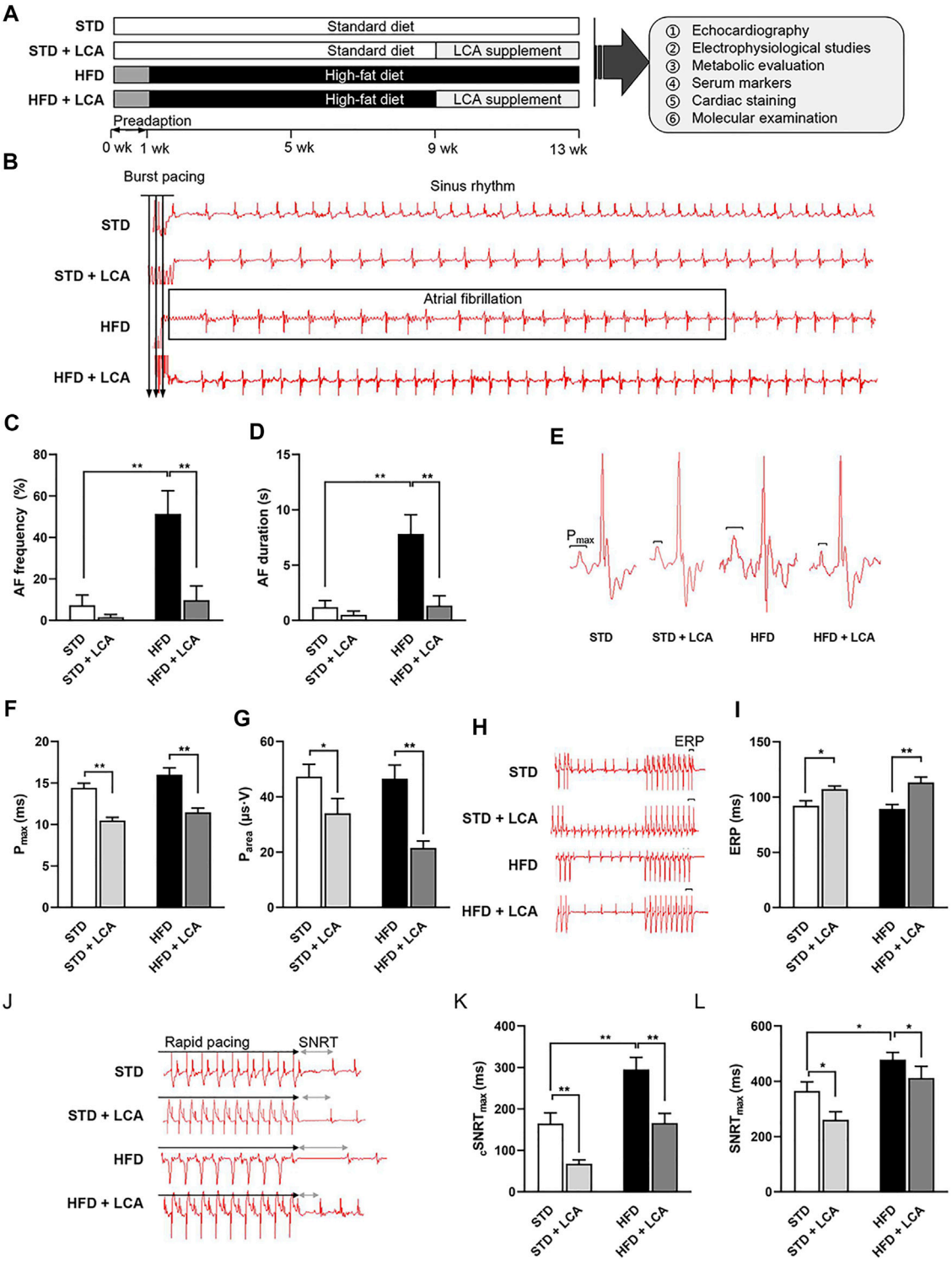

FIGURE 1 | LCA inhibits obesity–induced AF. **(A)** Experimental protocols of this study. **(B)** Representative AF induction by *trans*-esophageal burst pacing. **(C,D)** Analysis of AF frequency and duration. **(E)** Three-limb-lead electrocardiogram at baseline. **(F,G)** Analysis of P-wave. **(H–L)** Analysis of $SNRT_{max}$, $_{c}SNRT_{max}$ and ERP detected by programmed cardiac stimulation. n = 10 per group. One-way ANOVA with Bonferroni *post-hoc test* was used to compare data among groups. Data are expressed as mean ± SEM. $^{*}p < 0.05$, $^{**}p < 0.01$. STD, standard diet; HFD, high-fat diet; LCA, L-carnitine; FAO, fatty acids oxidation; P_{area}, P-wave area; P_{max}, P-wave duration; AF, atrial fibrillation; ERP, effective refractory period; SNRT, sinus node recovery time; $_{c}$SNRT, corrected sinus node recovery time.

TABLE 1 | Physical characteristics, echocardiographic, surface ECG and electrophysiological parameters, and serum marker levels of STD, STD + LCA, HFD and HFD + LCA mice.

Parameter	STD	STD + LCA	HFD	HFD + LCA
	(*n* = 10)	(*n* = 10)	(*n* = 10)	(*n* = 10)
Physical characteristics				
Food intake (g/d)	3.39 ± 0.18	3.36 ± 0.13	2.48 ± 0.06*	2.53 ± 0.18*
Energy intake (kcal/gm/d)	13.02	12.90	12.97	13.27
Water intake (ml/d)	5.12 ± 0.09	5.14 ± 0.13	4.82 ± 0.05*	4.83 ± 0.16
Body weight (g)	26.21 ± 0.69	27.17 ± 0.96	33.41 ± 0.55*	35.91 ± 1.24
Heart weight (mg)	132.10 ± 10.59	129.33 ± 3.83	155.70 ± 7.83*	143.50 ± 3.37†
NAL (cm)	10.04 ± 0.09	10.00 ± 0.04	10.17 ± 0.08	10.09 ± 0.11
HW/NAL (mg/cm)	13.16 ± 0.53	12.18 ± 0.53	15.32 ± 0.46*	14.01 ± 0.09†
Heart rate (bpm)	378.80 ± 20.64	364.70 ± 15.43	414.70 ± 22.12	386.1 ± 34.78
Echocardiography				
LA diameter (mm)	1.86 ± 0.07	1.61 ± 0.07	2.39 ± 0.09*	1.97 ± 0.12†
LA filling volume (ml)	23.26 ± 4.40	18.38 ± 3.26	58.68 ± 15.50*	21.26 ± 5.71†
Surface ECG				
P_{max} (ms)	14.43 ± 0.56	10.47 ± 0.39*	16.00 ± 0.83	11.45 ± 0.53†
P_{area} (μs·V)	47.32 ± 4.49	36.23 ± 2.74*	46.57 ± 4.95	21.52 ± 2.50†
Electrophysiology				
AF duration (s)	1.08 ± 7.00	0.50 ± 0.34	154.77 ± 49.33*	18.69 ± 14.63†
AF frequency (%)	9.70 ± 6.95	1.60 ± 1.30	51.40 ± 11.10*	7.30 ± 4.96†
AF incidence (%)	30	20	90.00*	30.00†
$SNRT_{max}$ (ms)	364.90 ± 33.07	261.10 ± 28.51*	478.40 ± 26.47*	412.20 ± 41.51†
$_cSNRT_{max}$ (ms)	164.80 ± 25.75	67.90 ± 90.4*	295.60 ± 29.08*	166.00 ± 23.24†
ERP (ms)	92.20 ± 4.57	107.20 ± 2.88*	89.40 ± 4.07	113.20 ± 4.97*†
Serum markers				
NEFA (mmol/L)	0.88 ± 0.18	0.76 ± 0.10	1.39 ± 0.16*	0.65 ± 0.11†
LDH (U/L)	57.85 ± 7.97	60.19 ± 8.26	90.38 ± 7.95*	75.97 ± 6.79
CK-MB (U/L)	126.00 ± 7.77	134.69 ± 15.33	137.69 ± 2.41	81.31 ± 26.68†
MDA (μmol/L)	0.78 ± 0.13	0.79 ± 0.37	1.67 ± 0.22*	0.53 ± 0.07†
SOD (U/ml)	34.55 ± 3.53	39.19 ± 2.03	32.18 ± 2.38	41.16 ± 6.37*†
Heart markers				
MDA (μmol/mg prot)	0.53 ± 0.03	0.43 ± 0.11	1.26 ± 0.02*	0.38 ± 0.09†
SOD (U/mg prot)	602.25 ± 42.36	677.25 ± 57.79*	417.19 ± 45.15*	838.61 ± 111.19†

n = *10 per group. One-way ANOVA, with Bonferroni* post-hoc *test was used to compare data among groups. The data were expressed as mean ± SEM.* *p < *0.05 vs STD,* †p < *0.05 vs HFD. AF, atrial fibrillation;* $_cSNRT$*, corrected sinus node recovery time; ECG, electrocardiogram; ERP, effective refractory period; HFD, high-fat diet; HW, heart weight; LA, left atrium; LCA,* $_L$*-carnitine; LDH, lactate dehydrogenase; CK-MB, creatine kinase-MB; MDA, molondialdehyde; NAL, naso-anal length; NEFA, non-esterified fatty acids;* P_{area}*, P-wave area;* P_{max}*, P-wave duration; SNRT, sinus node recovery time; SOD, superoxide dismutase; STD, standard diet.*

Enhanced FAO *via* LCA Supplementation Redresses Lipid Metabolism Imbalance, Thereby Decreasing Obesity-Induced Lipid Deposition in Atria

Epigenetic studies demonstrated that AF is highly associated with lipid metabolic abnormalities. In line with this, apparent lipid deposition was observed in obese mice. What's more, in accordance with reduced AF susceptibility and atrial remodeling, promoting FAO with LCA decreased the atrial lipid deposition effectively in obese mice (**Figures 3A,B**).

Promoted FAs influx and defective FAO can predispose to lipid deposition (**Figure 3C**). Thus, firstly, we assessed factors involved in lipid uptake and transportation. CD36, the main *trans*-membrane translocase of FAs, was decreased in gene level in obesity, and increased after LCA treatment (**Figure 3D**). However, CD36 was unchanged in total protein level among the groups (**Figure 3E**), but elevated in atrial membrane translocation in obese mice, and slightly reduced after LCA supplementation (**Figures 3F,G**). Besides, the transcription of other transportation-related genes, FABP3 and FABP-pm, was decreased in the atria of obesity and restored after LCA supplementation (**Figure 3D**).

Next, we evaluated the expression of the key enzymes of FAO, including CPT1B, AMPK and PGC1α, by RT-qPCR and Western blot. In contrast to increased FAs uptake, mitochondrial FAO was downregulated in obesity, as evidenced by the remarkable decrease of AMPK phosphorylation, and PGC1α expression in the atria of HFD mice compared to STD mice (**Figures 3H–L**). Notably, LCA supplementation upregulated the phosphorylation of AMPK as well as the expression of PGC1α and CPT1B in HFD mice (**Figures 3D–L**).

LCA Supplementation Restrains Cardiac Oxidative Stress and DNA Damage in the Atria of Obese Mice

Lipid over-deposition undermines the structure of cardiomyocytes, namely, cardiac lipotoxicity (Sletten et al., 2018), thereby provoking a set of pathological processes, including oxidative inflammation, DNA damage and insulin resistance, which have been implicated as possible mechanisms

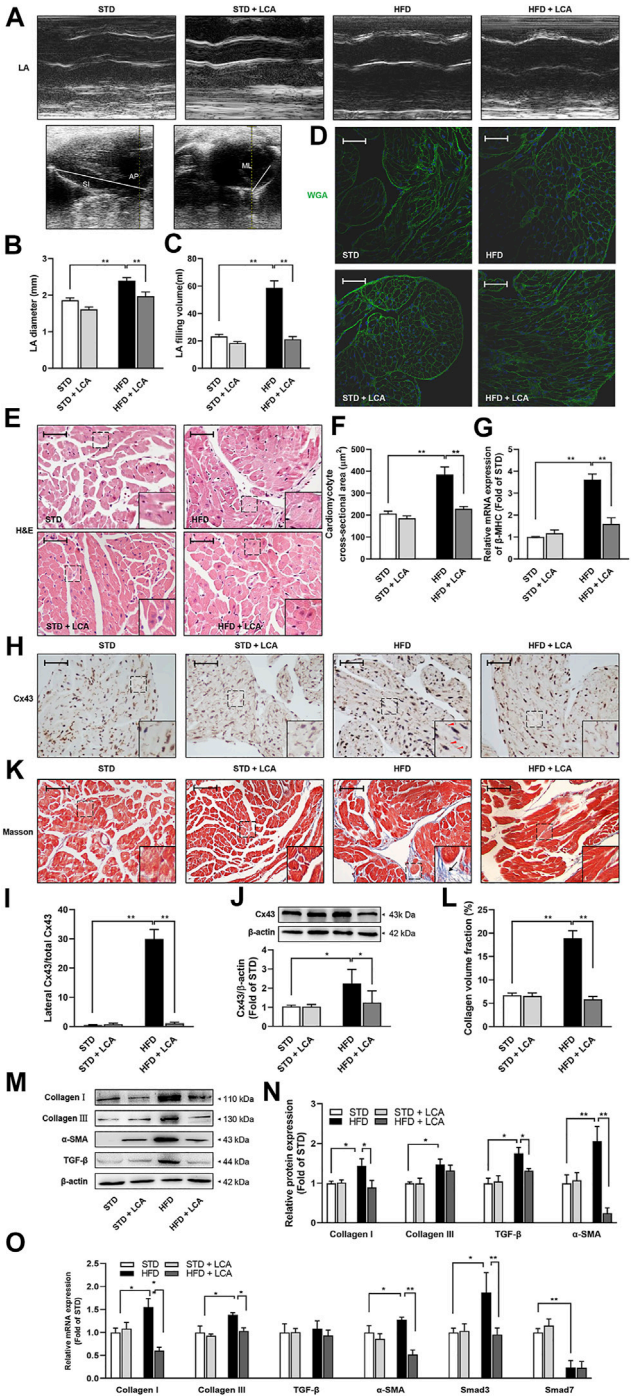

FIGURE 2 | LCA suppresses atrial remodeling in obese mice. **(A)** Representative echocardiographic images of LA among the groups. **(B)** Measurements of LA diameter and **(C)** LA filling volume detected by 2D-guided M-mode imaging. The SI and AP were obtained in a long-axis view, and ML was assessed in parasternal short-axis view. LA filling volume was calculated using the formula: LA filling volume = (4π×SI×AP×ML)/(3 × 2× 2 × 2). **(D)** Representative sections of WGA staining. **(E)** Representative sections of H&E staining. **(F)** Quantitative analysis of cellular morphology by ImageJ. **(G)** Relative mRNA levels of β-MHC using RT-qPCR. **(H,I)** Subcellular localization of Cx43 and immunohistochemistry. Triangles indicate

(*Continued*)

FIGURE 2 | lateralized Cx43. **(J)** Protein expression of Cx43 using Western blot. **(K,L)** Interstitial fibrosis (Arrow) using Masson's trichrome staining. **(M,N)** Representative images and analysis of TGF-β signaling-associated proteins (TGF-β, α-SMA, collagen I and collagen III) using Western blot. **(O)** Relative mRNA expression levels of the fibrosis-related genes (TGF-β, α-SMA, Smad3, Smad7, collagen I and collagen III) using RT-qPCR. Scale bar: 50 μm n = 10 **(A–C)** or 4 **(D–O)** per group. One-way ANOVA with Bonferroni *post-hoc* test was used to compare data among groups. Data are expressed as mean ± SEM. $^{*}p < 0.05$, $^{**}p < 0.01$. STD, standard diet; HFD, high-fat diet; LCA, L-carnitine; FAO, fatty acids oxidation; LA, left atrium; SI, superoinferior dimension; AP, anteroposterior dimension; MI, mediolateral dimension; WGA, wheat Germ Agglutinin; H&E, hematoxylin-eosin; β-MHC, β–cardiac myosin heavy chain; Cx43, connexin-43; TGF-β, transform growth factor-β; α-SMA, α-smooth muscle actin; Smad, *drosophila* mothers against decapentaplegic protein.

for AF. Thus, firstly, we evaluated oxidative stress. Obesity increased mitochondrial superoxide production (measured by MitoSOX staining) and increased cellular oxidative stress (measured by DHE staining) in the atria (**Figures 4A–D**). Besides, obesity increased MDA contents in the serum and atria, and decreased atrial SOD, but unaffected serum SOD level. LCA supplementation thwarted oxidative damages provoked by HFD, as supported by the decreased MitoSOX Red and DHE fluorescence signal, the reduced MDA levels and the rise of SOD levels in the serum and atria of obese mice (**Figures 4A–H**).

Nuclear factor erythroid 2-related factor (NRF2) is an accepted master regulator participating in the cellular adaptive response to redox or energy stress, which accumulates in nuclear to induce a battery of defensive genes encoding detoxifying enzymes and antioxidant proteins (such as SOD2 and NFκB) (**Figure 4E**) (Tonelli et al., 2018). Next, we evaluated the NRF2-mediated cardio-protective pathways. Nuclear levels of NRF2 were comparably decreased in the atria of obese mice, and increased after LCA supplementation (**Figures 4J,K**). In addition, total protein level of NRF2 was elevated after LCA supplementation. In parallel with the distinct NRF2 activation, SOD2, one of the downstream of NRF2 for antioxidant defense, was noticeably increased in the atria of obese mice after LCA treatment (**Figures 4L,M**).

Consistent with obesity-induced oxidative stress, oxidative DNA damage (as shown by 8-OH-dG staining) and DNA segment (as shown by TUNEL staining) in the atira was aggravated after HFD, and were alleviated by LCA (**Figures 4N–Q**). Moreover, we evaluated myocardial cellular damage by measuring serum LDH and CK-MB levels. Obesity increased LDH levels apparently, yet LCA treatment unaffected its levels in obese mice. CK-MB is a more specific marker of myocardial cellular damage, and results showed that obesity unaffected serum CK-MB levels, yet LCA treatment reduced its levels (**Figures 4R,S**) in obese mice.

LCA Supplementation Mitigates Obesity-Related Atrial Inflammatory Response

Next, we determined the transcription of pro-inflammation cytokines in the atria, including IL-1β, IL-6, IL-18, TNF-α,

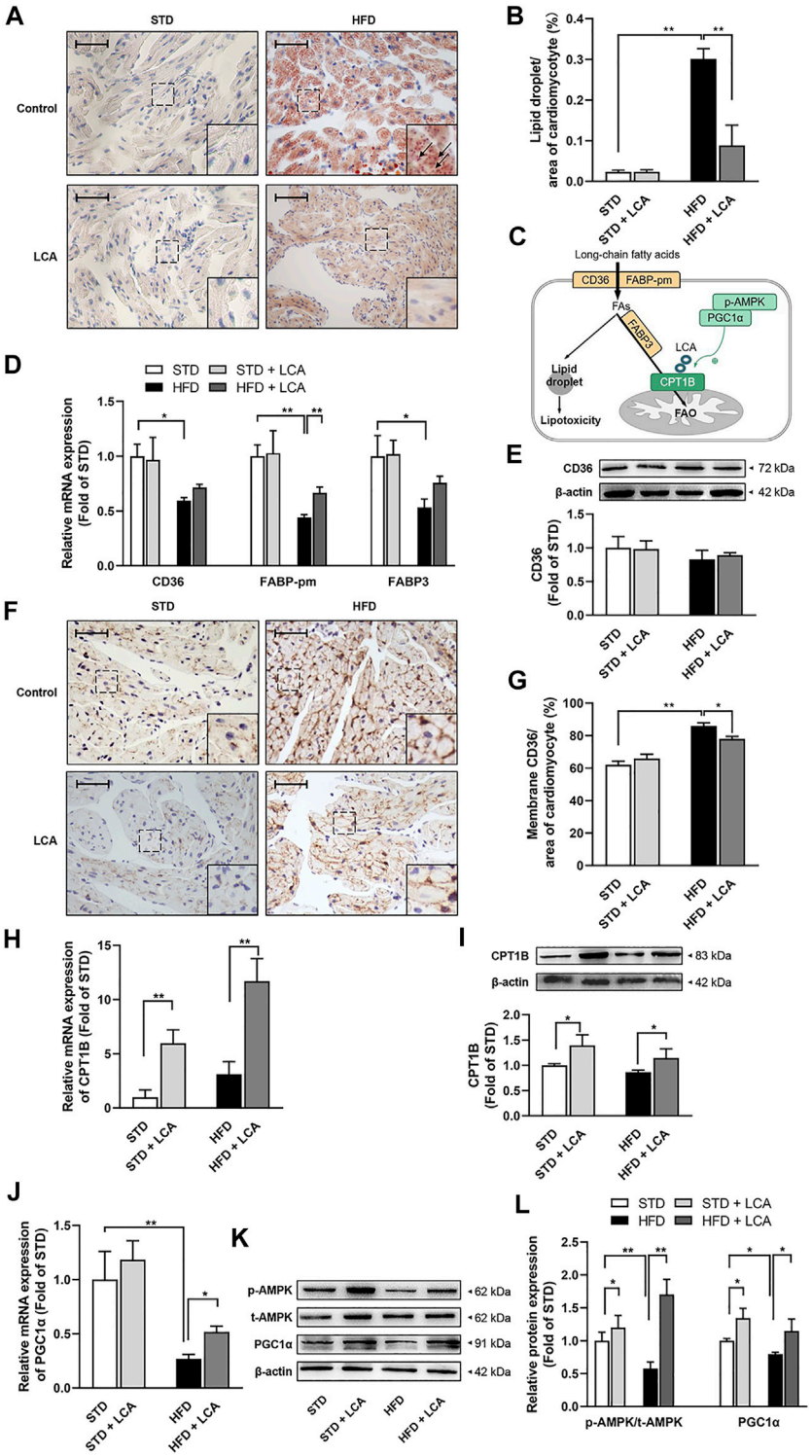

FIGURE 3 | LCA enhances FAO, thereby inhibits cardiac lipotoxicity by alleviating atrial steatosis in obese mice. **(A)** Representative sections of lipid accumulation (Arrow) using oil red O staining. **(B)** Quantitative analysis of lipid accumulation by ImageJ. **(C)** Schematic diagram illustrating cardiac lipid metabolism. **(D)** Quantitative analysis of the transcription of lipid uptake and transportation-related genes (CD36, FABP-pm, FABP3) by RT-PCR. **(E)** Representative image and quantitative analysis of CD36 by Western blot. **(F)** Representative images of membrane translocation of CD36 using immunohistochemistry. **(G)** Quantitative analysis of sarcolemma CD36 contents by ImageJ. **(H)** Quantitative analysis of the transcription of CPT1B using RT-qPCR. **(I)** Representative Image and quantitative analysis of CPT1B by Western blot. **(J)** Quantitative analysis of the transcription of PGC1α using RT-qPCR. **(K,L)** Representative images and quantitative analysis of FAO-related regulators (AMPK and

(*Continued*)

FIGURE 3 | PGC1α) by Western blot. Scale bar: 50 μm $n = 4$ per group. One-way ANOVA with Bonferroni *post-hoc* test was used to compare data among groups. Data are expressed as mean ± SEM. *$p < 0.05$, **$p < 0.01$. STD, standard diet; HFD, high-fat diet; LCA, L-carnitine; FAs, fatty acids; FAO, fatty acids oxidation; AMPK, AMP-activated protein kinase; CD36, FAT; CPT1B, carnitine palmitoyltransferase-1B; PGC1α, peroxisome proliferator-activated receptor γ coactivator1α; FABP-pm, plasma membrane fatty acid-binding protein; FABP3, fatty acid binding protein 3; p-, phoso-.

and MCP-1. Results demonstrated that HFD increased the transcription of IL-6 compared to STD, while LCA suppressed the transcription of most pro-inflammation cytokines, except for MCP-1, in both STD and HFD mice (**Figure 4T**). In addition, NFκB, a well-known downstream factor of NRF2, is a central activator of the immune response. Our results demonstrated that NFκB was activated in the atria of HFD mice, and was inhibited after LCA supplementation (**Figure 4U**), which is in line with our results showing LCA increased the expression and activation of NRF2 (**Figures 4I–M**).

LCA Supplementation Improves Insulin Sensitivity in Obese Mice

Disordered glucose metabolism and insulin resistance are also novel risk factors for AF and usually occur in obesity (Nakamura and Sadoshima, 2020). Therefore, apart from FAs metabolism, the impacts of LCA on glycometabolism, including insulin signaling and insulin resistance, glucose and insulin tolerance, are also investigated in this study.

Both IPGTT (**Figures 5A–C**) and ITT (**Figures 5D–F**) confirmed glucose metabolic imbalance in obesity, including increased fasting blood glucose (FBG), impaired glucose tolerance, and decreased insulin sensitivity. Intriguingly, LCA had no effect on glucose tolerance and FBG, yet increased insulin tolerance in obese mice, indicating improved insulin sensitivity in peripheral tissues. Mechanistic investigation using WB analysis showed that LCA restored the serine/threonine protein kinase PKB (Akt) phosphorylation in the atria of obese mice (**Figure 5G**). Moreover, although LCA treatment had no effect on GLUT4 expression, its activation, as reflected by its translocation to the intracellular membrane, was promoted in obese mice (**Figures 5H–J**). Next, we assessed the transcription of glucose metabolism-related genes, including GLUT1, GLUT4, HK2, PFKM, PKM2, and PDK4. Most of these genes, except for PFKM, were inhibited in the atria of obese mice. LCA supplementation increased the transcription of GLUT4, PKM2, and PDK4, whereas decreased PFKM transcription in obese mice (**Figure 5K**). In addition, PAS staining showed aggravated glycogen accumulation in the atria of obese mice. LCA further increased glycogen accumulation in atrial cardiomyocytes (**Figures 5L,M**), probably due to the fact that LCA upregulated glucose uptake more than glycolysis (**Figure 5N**).

Inhibition of AMPK Constrains the Cardio-Protective Effects of LCA Supplementation *in vitro*

To investigate whether AMPK is crucial in LCA-conferred cardio-protection, we used PA, a saturated fatty acid, to mimic obesity *in vitro, and* CC, a pharmacological inhibitor of AMPK, to block AMPK signaling in primary atrial cardiomyocytes (**Figure 6A**). LCA enhanced FAO significantly in PA-treated cells, which might be ascribe to the activation AMPK and upregulation of PGC1α and CPT1B; however, inhibition of AMPK by CC reversed these effects (**Figures 6C,D**).

MDA examination was performed to assess the levels of oxidative stress. In line with the animal studies, LCA supplementation induced a decrement of PA-induced oxidative stress (Decreased cellular MDA) and enhanced corresponding anti-oxidative system (Restored NRF2/SOD2 signaling) in primary atrial cardiomyocytes; however, pretreatment with CC abolished LCA-conferred antioxidant effects. Similarly, pretreatment with CC also attenuated LCA-conferred anti-inflammation effects, as judged by NFκB activation (**Figures 6E–G**).

Altogether, these results supported that activation of AMPK signaling pathway may be the relevant molecular basis of LCA-mediated cardio-protection.

DISCUSSION

Although defective FAO has long been pronounced in AF, its implication in AF is under-investigated. In this study, we established an obesity (induced by HFD)-related AF mice model, which showed increased AF vulnerability and exhibited apparent atrial structural remodeling (**Figures 1**, **2**). Pathologically, obesity caused defective cardiac FAO and induced cardiac lipotoxicity (**Figure 3**) (Haffar et al., 2015), thereby evoking a set of pathological reactions, including oxidative stress, DNA damage, inflammation and insulin resistance (**Figures 4**, **5**), which contributing to AF. Enhancing FAO *via* LCA supplementation (the cofactor of CPT1B), attenuated cardiac steatosis and lipotoxicity-induced pathological changes in the atria of obese mice, resulting in restored AF substrates and ameliorated AF susceptibility (**Figure 7**). Mechanistically, AMPK/PGC1α signaling was implicated in LCA-conferred beneficial effects against obesity-mediated AF (**Figure 6**).

The derangement of the energy substrate metabolism in the pathogenesis of AF has garnered extensive interest in the field of AF. Ample of proteomics and metabolomics studies have proved the considerable lipid metabolism remodeling in the myocardium of AF patients (Huang et al., 2011; Tu et al., 2014). Dyslipidemia is independently associated with AF incidence (Guan et al., 2020), and lipid metabolism related proteins serve as a potential AF biomarker (such as LDL, VLDL, HDL, and FABP3) (Golaszewska et al., 2019). Enzymes involved in FAO (such as CD36, CPT1B and VLCAD), as well as their regulators (such as PPAR-α and PGC1α), are demonstrated to inhibited in chronic AF (Liu et al., 2016). These evidence supported the impaired FAs uptake and

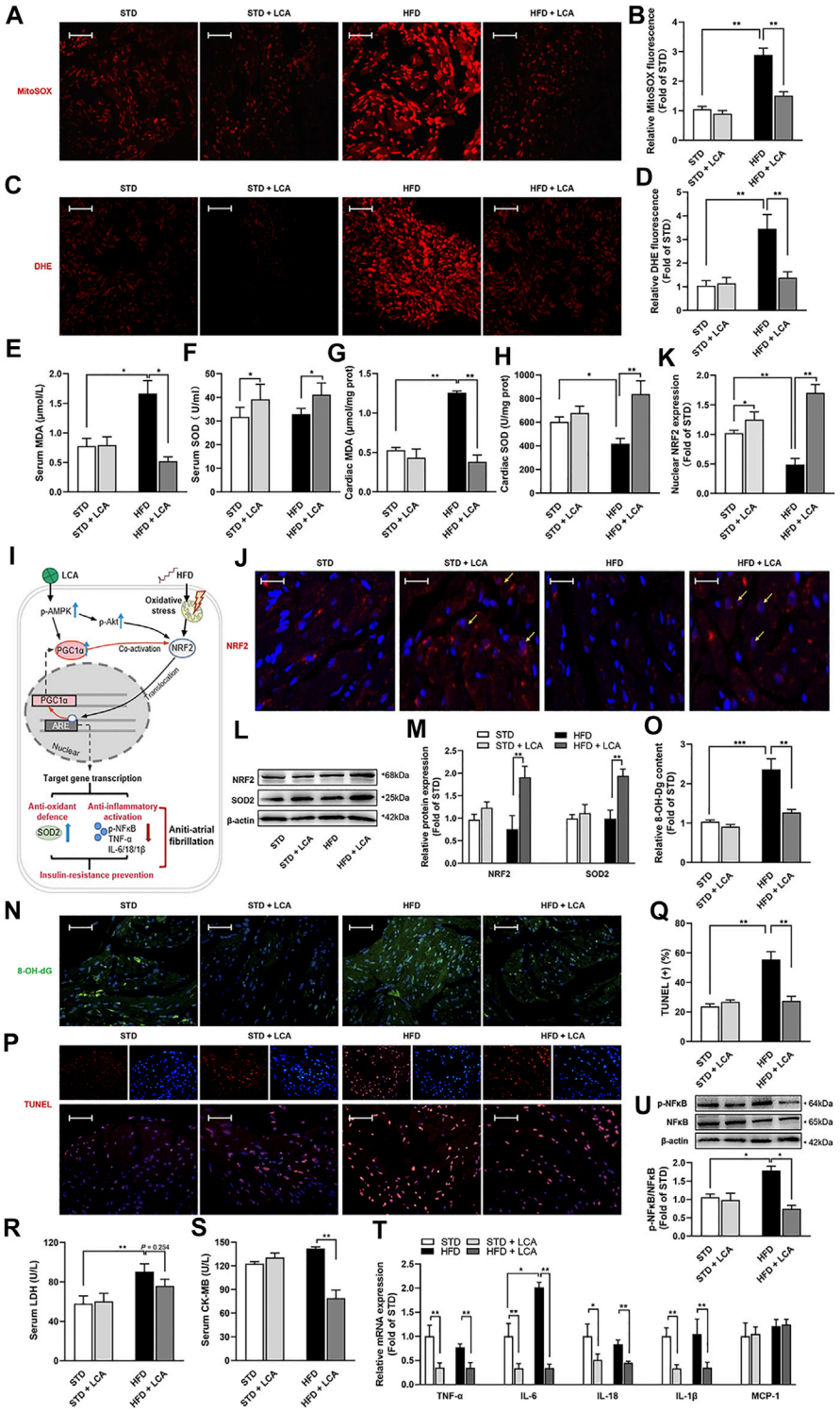

FIGURE 4 | LCA inhibits cardiac oxidative stress and mitigates inflammation. Representative images and analysis of the subcellular localization of the oxidation products of **(A,B)** MitoSOX and **(C,D)** DHE. Red: oxidation products-staining. Scar: 10 μm $n = 4$. **(E,F)** Comparisons of serum MDA and SOD using commercially available kits among the groups. **(G,H)** Levels of atrial MDA and SOD normalized to tissue protein concentration. **(I)** Schematic diagram illustrating NRF2-related signals. **(J,K)** Localization of NRF2 in atria by confocal immune-cyto-chemical analysis: Blue: nucleus (DAPI); Red: NRF2-staining; Pink: merge of blue and red indicated nuclear localization of NRF2 (Arrow). Scar: 30 μm $n = 4$. **(L,M)** Representative images and quantitative analysis of anti-oxidative system involved protein expressions (NRF2 and SOD2) using Western blot. **(N,O)** Representative images and analysis of oxidative DNA damage by 8-OH-dG staining. Green: 8-OH-dG -staining; Blue: DAPI.

(*Continued*)

FIGURE 4 | Scar: 50 μm $n = 4$. **(P,Q)** Representative images and analysis of DNA damage by TUNEL staining. Red: TUNEL-staining; Blue: DAPI; Pink: merge. Scar: 50 μm $n = 4$. Comparisons of **(R)** serum LDH and serum **(S)** CK-MB using commercially available kits. $n = 8$. **(T)** Quantitative analysis of the expression of inflammation-related genes in the atria using RT-qPCR. **(U)** Representative images and quantitative analysis of expression and phosphorylation of NFκB using Western blot. One-way ANOVA with Bonferroni *post-hoc* test was used to compare data among groups. Data are expressed as mean ± SEM. $^{*}p < 0.05$, $^{**}p < 0.01$. STD, standard diet; HFD, high-fat diet; LCA, L-carnitine; DHE, dihydroethidium; MDA, molondialdehyde; SOD, superoxide dismutase; NRF2, nuclear erythroid 2 p45-related factor 2; p-, phoso-; SOD2, manganese superoxide dismutase, superoxide dismutase 2; 8-OH-Dg, 8-hydroxydeoxyguanosine; IL, interleukin; TNF-α, tumor necrosis factor-α; MCP-1, monocyte chemoattractant protein-1; NFκB, the nuclear factor kappa B; LDH, lactate dehydrogenase; CK-MB, creatine kinase-MB.

defective FAO, along with increased atrial lipid deposition of AF (Lenski et al., 2015), suggesting disordered lipid metabolism is closely related to the occurrence and development of AF (Opacic et al., 2016). Consequently, from a broader metabolic perspective, redressing the disbalance of lipid metabolism should be considered as a novel a candidate strategy for AF. Supportively, AMPK, an effective lipid metabolism accelerator, and its downstream effectors, PPAR-α/PGC-1α signals, both have been proposed as alternative metabolic modulations to combat AF (Harada et al., 2015; Bai et al., 2019; Ostropolets et al., 2021). Genetic deletion of liver kinase B1, an activator of AMPK, can develop spontaneous AF in mice (Ozcan et al., 2015). Besides, in agreement with inactivated AMPK signaling in atria in long-standing AF (Harada et al., 2015), restoring FAO targeting AMPK, PPAR-α or PGC1α (Metformin, AICAR, Fenofibrate and β_3AR) (Yu et al., 2011; Liu et al., 2016; Bai et al., 2019; Deshmukh et al., 2021; Ostropolets et al., 2021) have been confirmed to suppress AF inducibility. However, AMPK, a key regulator of multi-pathways and multi-targets, also gets involved in inflammation mitigation, Ca^{2+}-handling and cell contraction, mitochondrial biogenesis, cell growth and proliferation, and so on, thus exerting cardiovascular protection with a combination of multiple mechanisms (Garcia and Shaw, 2017). Therefore, the cardio-protective effect of AMPK-mediated pathways cannot be differentiated from FAO promotion. It is worthy to evaluated the direct effects of accelerated FAO on AF, especially in circumstances of obesity, in which cardiac FAO is defective considerably compared to other well-known 'culprits' of the AF. As expected, we proved that boosting FAO *via* LCA, a natural and biologically active micronutrient enhancing physiological FAO through CPT1B (Marcovina et al., 2013) and activation of AMPK signaling pathway (**Figures 3**, **6**), can significantly reduce obesity-mediated AF propensity and the corresponding atrial remodeling (**Figures 1**, **2**), thus better supports the efficiency of FAO promotion in the AF therapeutic approach.

Whereas, in opposite to our theory, FAO suppression *via* Ranolazine has been demonstrated to attenuate AF occurrence in 1-week ACh-$CaCl_2$-exposed rats (Zou et al., 2016), probably by supporting the transient supply/demand mismatch during the stabilization of AF (Heijman and Dobrev, 2015). This controversial result can be further explained by the nonspecific confounding influence of Ranolazine, since it directly blocks the late sodium channel to terminate arrhythmia, and attenuates adverse myocardial alterations including hypertrophy and fibrosis (De Angelis et al., 2016). More notably, prolonged inhibition of FAO would presumably increase cardiac preference for carbohydrate sources, which represents a driving force for atrial electrical remodeling as well as followed irreversible structural remodeling after a long period (Kolwicz and Tian, 2011); and in addition induces atrial lipid accumulation, which promotes lipotoxicity-provoked AF (Young et al., 2002; Lundsgaard et al., 2020).

Over-accumulation of lipid in cardiomyocyte cytosol occurs when FAs supply fails to match the needs created by FAs expenditure, thus is commonly observed in obesity (Haffar et al., 2015) as well as AF (Lenski et al., 2015). Notably, cardiac steatosis in atria exerts detrimental impacts on heart (termed "lipotoxicity"), thus taking a leading role in AF, especially in obesity-related AF (Haffar et al., 2015; Opacic et al., 2016). For instance, excess myocardial FAs can convert into potentially "lipotoxic" metabolites, such as diacylglycerol and ceramides (Serra et al., 2013), which directly affect excitation-contraction coupling and ion channel/pump integrity, and later contribute to irreversible structure alterations (Harada et al., 2017). Besides, lipid-derived excessive oxidants generation and impaired antioxidant capacity (inactivated NRF2-cascade) lead to redox imbalance and trigger inflammatory response (Li et al., 2019), which are in line with progressively deterioration of myocardial structure and function (Goldberg et al., 2012), including LA enlargement, and myocardial hypertrophy, connexin-43 remodeling, interstitial fibrosis in the atria (Harada et al., 2017). What's more, cardiac lipotoxicity causes insulin dysregulation and glycometabolism impairment (Nakamura and Sadoshima, 2020), which are speculated to provide a metabolic arrhythmogenic substrate for AF (Maria et al., 2018). Cardiac lipotoxicity induced by HFD was further delineated in this study, and ameliorated after FAO promotion which redressed the disbalance of lipid metabolism and normalized the cardiac lipid content, thus explained the correlation between defective FAO and AF/obesity (**Figures 3**–**5**).

Disordered glucose metabolism and insulin homeostasis are also active metabolic subjects in the study of AF. Prior researchers have established strong correlation between inadequate glycemic control and AF episodes (Dublin et al., 2010). Within cardiomyocytes, suppressed atrial glucose oxidation and increased glycogen synthesis occur in AF and promote marked glycogen accumulation (Heijman and Dobrev, 2015). Besides, insulin resistance is considered as a novel independent risk factor for AF, which engenders both atrial structural remodeling and abnormal intracellular calcium homeostasis (Chan et al., 2019; Wu et al., 2014). What's more, insulin signaling loss, noted as impaired glucose transport (alterations in the expression and trafficking of GLUT4), has been proposed to be an early pathogenic factor of AF pathogenesis (Maria et al., 2018). Intra-myocardial toxic metabolites of FAs metabolism and

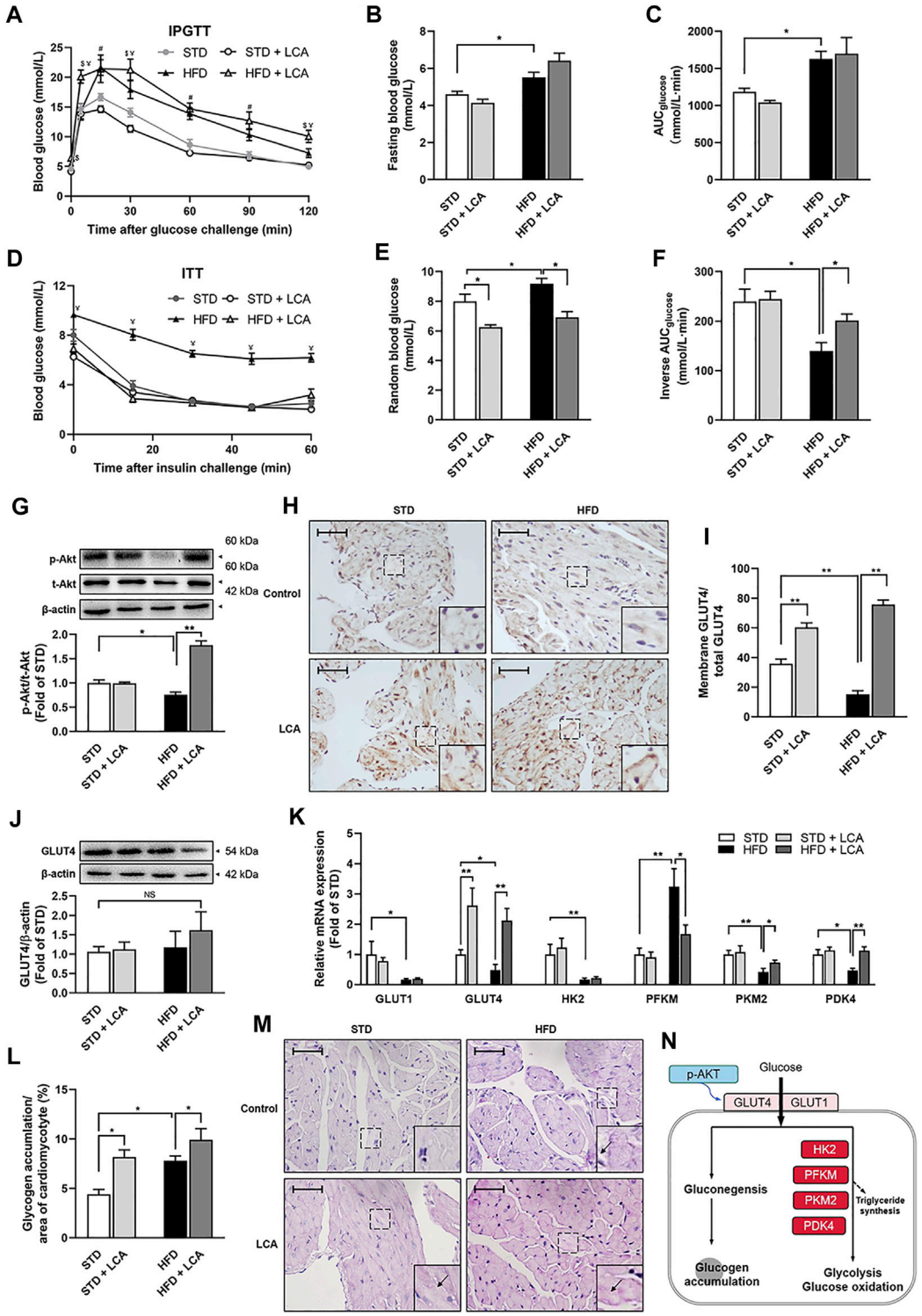

FIGURE 5 | LCA restores glucose and insulin homeostasis. **(A)** Plasma glucose levels in the IPGTT. **(B)** Fast blood glucose levels among groups. **(C)** Analysis of $AUC_{glucose}$ during IPGTT. **(D)** Plasma glucose levels in the ITT. **(E)** Random blood glucose levels among groups. **(F)** Analysis of inverse $AUC_{glucose}$ during ITT. **(G)** Representative images and quantitative analysis of expression and phosphorylation of Akt by Western blot. **(H,I)** Representative images of membrane translocation of GLUT4 using immunohistochemistry and quantitative analyzed by ImageJ. **(J)** Representative images and quantitative analysis of the expression of GLUT4 by Western blot. **(K)** Quantitative analysis of the expression of glucose metabolism-related genes (GLUT1, GLUT4, HK2, PFKM, PKM2, and PDK4) using RT-qPCR. **(L,M)** Glycogen accumulation (Arrow) demonstrated by Periodic acid-Schiff staining. **(N)** Schematic diagram illustrating glucose metabolism. Scale bar: 50 μm $n = 4$ for *in vivo* experiments and 10 for *in vitro* experiments in each group. One-way ANOVA with Bonferroni *post-hoc* test was used to compare data among groups. Data are

(*Continued*)

FIGURE 5 | expressed as mean ± SEM. *$p < 0.05$, **$p < 0.01$, $^{¥}p < 0.05$ HFD vs others, $^{\$}p < 0.05$ HFD + LCA vs others, $^{\#}p < 0.05$ STD/STD + LCA vs HFD/HFD + LCA. STD, standard diet; HFD, high-fat diet; LCA, L-carnitine; IPGTT, intraperitoneal glucose tolerance test; ITT, insulin tolerance test; AUC, area under the curve; Akt, protein kinase B; p-, phoso-; GLUT, glucose transporter; HK2, hexokinase2; PFKM, phosphofructokinase; PKM2, pyruvate kinase isozyme type M2; PDK4, pyruvate dehydrogenase kinase 4; p-, phoso-.

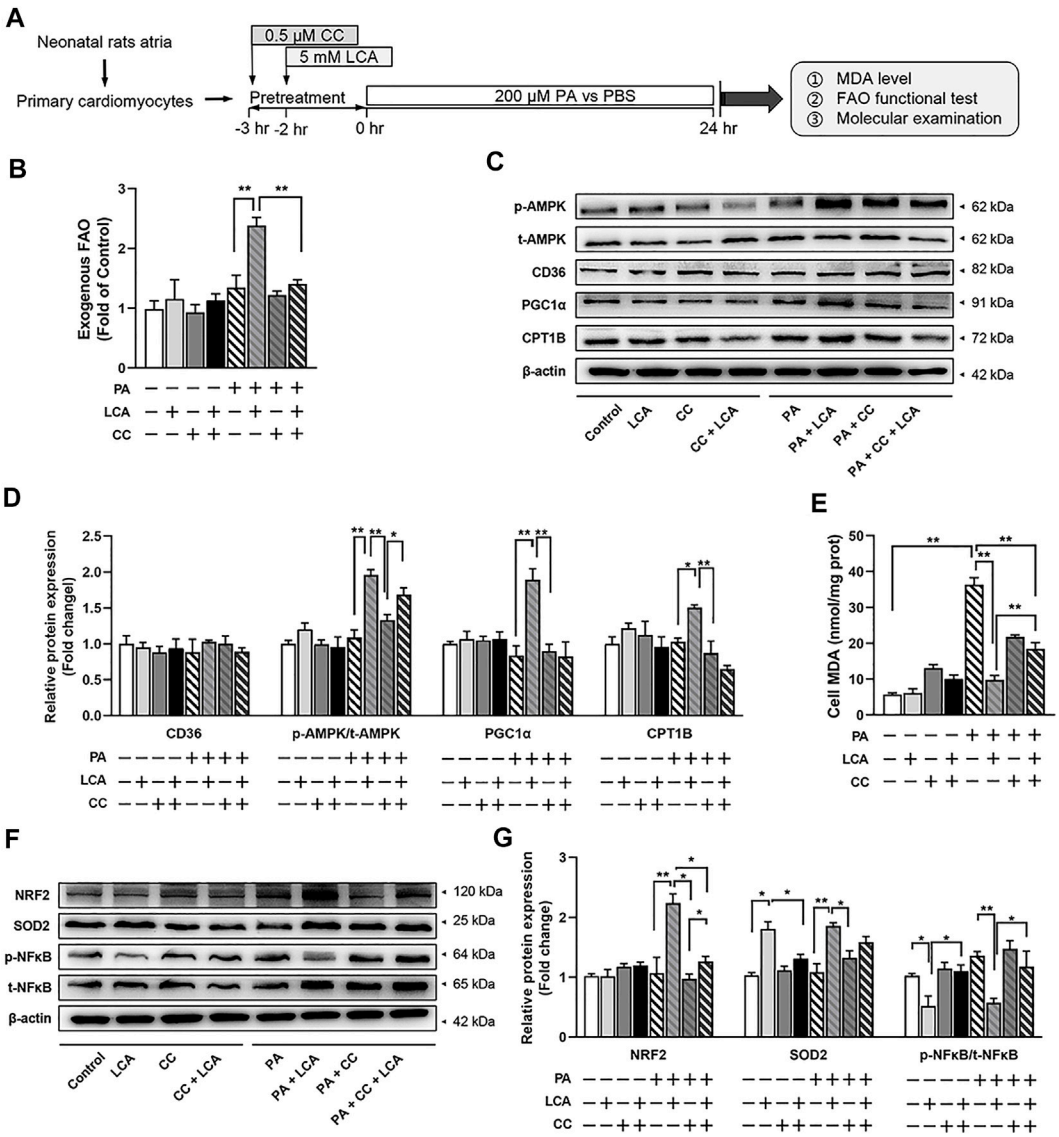

FIGURE 6 | Pharmacological inhibition of AMPK via CC attenuated LCA-conferred beneficial effects in palmitate-treated primary atrial cardiomyocytes. **(A)** Schematic diagram illustrating the cell isolation, culture and treatment. **(B)** FAO rate in different treatment groups. The measure of substrate utilization after 18°C unsaturated fatty acid (Oleate, 100 μM) addition was normalized with maximal O_2 consumption in Control cells. **(C)** Representative images and **(D)** quantitative analysis of the expression of FAO-related proteins using Western blot. **(E)** Cellular MDA concentrations among the groups. **(F)** Representative images and **(G)** quantitative analysis of the expression of oxidative stress-related proteins (NRFS and SOD2) and inflammation-related protein (NFκB) using Western blot. $n = 3$ or 4 each group. Two-way ANOVA with Bonferroni *post-hoc* test was used to compare data among groups. Data are expressed as mean ± SEM. *$p < 0.05$, **$p < 0.01$. CC, Compound C; LCA, L-carnitine; PA, palmitate; FAO, fatty acids oxidation; MDA, molondialdehyde; NRF2, nuclear erythroid 2 p45-related factor 2; AMPK, AMP-activated protein kinase; CD36, FAT; CPT1B, carnitine palmitoyltransferase-1B; p-, phoso-; PGC1α, peroxisome proliferator-activated receptor γ coactivator1α; NRF2, Nuclear factor erythroid 2-related factor 2; NFκB, the nuclear factor kappa B; SOD2, manganese superoxide dismutase, superoxide dismutase 2.

triacylglycerol, such as diacylglycerol, ceramides and acylcarnitines, are responsible for severe insulin resistance by interrupting insulin signal cascade at different levels and multiple steps of glucose metabolism (Belfort et al., 2005; Yazici and Sezer, 2017). In consistent to ameliorated lipid accumulation and lipotoxicity, enhanced FAO *via* LCA promoted insulin-

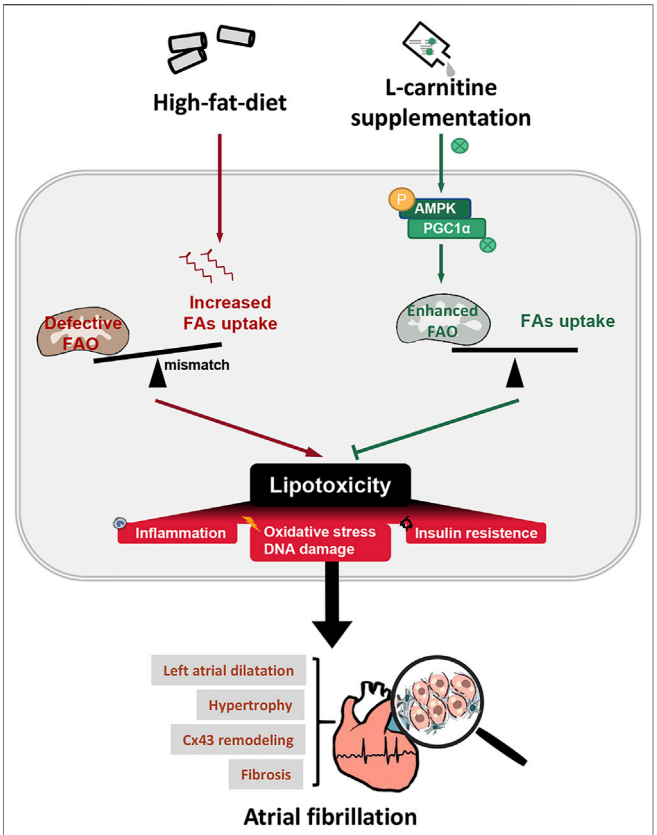

FIGURE 7 | Hypothetical mechanisms of LCA-conferred cardio-protection against obesity-related AF. Possible mechanism proposed in this study: HFD-induced imbalance between FAs uptake and expenditure causes lipid accumulation and lipotoxicity, which triggers a set of chain reactions, including oxidative stress, DNA damage, inflammation and insulin resistance, and finally contributing to atrial remodeling and greater propensity for AF. Promotion of FAO via LCA combats obesity-induced AF by reducing myocardial lipotoxicity, alleviating atrial remodeling, including left atrial dilatation, cardiac hypertrophy, gap junction remodeling and interstitial fibrosis. Mechanistically, LCA supplement amended lipid metabolism through AMPK-dependent pathway. STD, standard diet; HFD, high-fat diet; LCA, L-carnitine; FAO, fatty acids oxidation; AF, atrial fibrillation; AMPK, AMP-activated protein kinase; CD36, FAT; CPT1B, carnitine palmitoyltransferase-1B; p-, phoso-; PGC1α, peroxisome proliferator-activated receptor γ coactivator1α.

stimulated glucose uptake, thus restored random blood glucose in obesity (**Figure 5**). Some other experimental studies have given another explanation for the improved carbohydrate metabolism, that LCA supplementation can reduce the ratio of acetyl-CoA to free CoA in the mitochondria, thereby stimulating the activity of pyruvate dehydrogenase (PDH) (Calvani et al., 2000). However, our results implied the activated Akt and upregulated subsequent glucose utilization in the atria may be the reason why LCA supplementation can recover the glucose metabolism and insulin homeostasis, and thus expanding the potential role of FAO promotion *via* LCA in AF suppression.

Although present observations have unveiled the practical meaning of promoted FAO *via* LCA in obesity-dependent AF, and indicating the leading role of FAO in AF pathogenesis, this study failed to directly assess the efficiency of FAs uptake or FAO *in vivo*, and whether the LCA-conferred anti-AF effects is mediated by AMPK also needs confirmation *in vivo*. Further investigative work is warranted to address the limitation.

CONCLUSION

In conclusion, we present for the first time that FAO promotion *via* LCA could redress lipid metabolism imbalance and reduce cardiac lipotoxicity through AMPK activation, thereby ameliorating obesity-mediated AF and atrial structural remodeling. Enhancing FAO may optimize the therapeutic strategy for AF, especially in obesity.

DATA AVAILABILITY STATEMENT

The original contributions presented in the study are included in the article/**Supplementary Material**, further inquiries can be directed to the corresponding authors.

ETHICS STATEMENT

The animal study was reviewed and approved by the Institutional Animal Care and Use Committee of Xi'an Jiaotong University.

AUTHOR CONTRIBUTIONS

YuZ and XQ designed the study. YuZ, YF and BL performed the experiments. YuZ, BF and XL analyzed the data and prepared the figures. YuZ, YF, TJ, YiZ and HS analyzed and interpreted the data. YuZ wrote the main manuscript. YF, TJ, XQ and QZ revised the manuscript and supervised the project. All authors approved the final version of this manuscript.

FUNDING

This work was supported by the National Natural Science Foundation of China (Grant Number 81870257 and 31871172) and Key Research and Development Program of Shaanxi (Grant Number 2021SF-132).

ACKNOWLEDGMENTS

We appreciate the technical support of HY Yang (Air Force Medical University, Xi'an, China) and CY Li (Xijing Hospital, Xi'an, China) in this project.

SUPPLEMENTARY MATERIAL

The Supplementary Material for this article can be found online at: https://www.frontiersin.org/articles/10.3389/fphar.2021.771940/full#supplementary-material

REFERENCES

Bai, F., Liu, Y., Tu, T., Li, B., Xiao, Y., Ma, Y., et al. (2019). Metformin Regulates Lipid Metabolism in a Canine Model of Atrial Fibrillation through AMPK/PPAR-α/VLCAD Pathway. *Lipids Health Dis.* 18 (1), 109. doi:10.1186/s12944-019-1059-7

Bakermans, A. J., van Weeghel, M., Denis, S., Nicolay, K., Prompers, J. J., and Houten, S. M. (2013). Carnitine Supplementation Attenuates Myocardial Lipid Accumulation in Long-Chain Acyl-CoA Dehydrogenase Knockout Mice. *J. Inherit. Metab. Dis.* 36 (6), 973–981. doi:10.1007/s10545-013-9604-4

Barth, A. S., Merk, S., Arnoldi, E., Zwermann, L., Kloos, P., Gebauer, M., et al. (2005). Reprogramming of the Human Atrial Transcriptome in Permanent Atrial Fibrillation: Expression of a Ventricular-like Genomic Signature. *Circ. Res.* 96 (9), 1022–1029. doi:10.1161/01.RES.0000165480.82737.33

Belfort, R., Mandarino, L., Kashyap, S., Wirfel, K., Pratipanawatr, T., Berria, R., et al. (2005). Dose-response Effect of Elevated Plasma Free Fatty Acid on Insulin Signaling. *Diabetes* 54 (6), 1640–1648. doi:10.2337/diabetes.54.6.1640

Calvani, M., Reda, E., and Arrigoni-Martelli, E. (2000). Regulation by Carnitine of Myocardial Fatty Acid and Carbohydrate Metabolism under normal and Pathological Conditions. *Basic Res. Cardiol.* 95 (2), 75–83. doi:10.1007/s003950050167

Chan, Y. H., Chang, G. J., Lai, Y. J., Chen, W. J., Chang, S. H., Hung, L. M., et al. (2019). Atrial Fibrillation and its Arrhythmogenesis Associated with Insulin Resistance. *Cardiovasc. Diabetol.* 18 (1), 125. doi:10.1186/s12933-019-0928-8

De Angelis, A., Cappetta, D., Piegari, E., Rinaldi, B., Ciuffreda, L. P., Esposito, G., et al. (2016). Long-term Administration of Ranolazine Attenuates Diastolic Dysfunction and Adverse Myocardial Remodeling in a Model of Heart Failure with Preserved Ejection Fraction. *Int. J. Cardiol.* 217, 69–79. doi:10.1016/j.ijcard.2016.04.168

Deshmukh, A., Ghannam, M., Liang, J., Saeed, M., Cunnane, R., Ghanbari, H., et al. (2021). Effect of Metformin on Outcomes of Catheter Ablation for Atrial Fibrillation. *J. Cardiovasc. Electrophysiol.* 32 (5), 1232–1239. doi:10.1111/jce.14954

Dublin, S., Glazer, N. L., Smith, N. L., Psaty, B. M., Lumley, T., Wiggins, K. L., et al. (2010). Diabetes Mellitus, Glycemic Control, and Risk of Atrial Fibrillation. *J. Gen. Intern. Med.* 25 (8), 853–858. doi:10.1007/s11606-010-1340-y

Fu, Y., Jiang, T., Sun, H., Li, T., Gao, F., Fan, B., et al. (2021). Necroptosis Is Required for Atrial Fibrillation and Involved in Aerobic Exercise-conferred Cardioprotection. *J. Cel. Mol. Med.* 25, 8363–8375. doi:10.1111/jcmm.16796

Fukui, A., Ikebe-Ebata, Y., Kondo, H., Saito, S., Aoki, K., Fukunaga, N., et al. (2017). Hyperleptinemia Exacerbates High-Fat Diet-Mediated Atrial Fibrosis and Fibrillation. *J. Cardiovasc. Electrophysiol.* 28 (6), 702–710. doi:10.1111/jce.13200

Garcia, D., and Shaw, R. J. (2017). AMPK: Mechanisms of Cellular Energy Sensing and Restoration of Metabolic Balance. *Mol. Cel.* 66 (6), 789–800. doi:10.1016/j.molcel.2017.05.032

Golaszewska, K., Harasim-Symbor, E., Polak-Iwaniuk, A., and Chabowski, A. (2019). Serum Fatty Acid Binding Proteins as a Potential Biomarker in Atrial Fibrillation. *J. Physiol. Pharmacol.* 70 (1). doi:10.26402/jpp.2019.1.11

Goldberg, I. J., Trent, C. M., and Schulze, P. C. (2012). Lipid Metabolism and Toxicity in the Heart. *Cell Metab* 15 (6), 805–812. doi:10.1016/j.cmet.2012.04.006

Guan, B., Li, X., Xue, W., Tse, G., Waleed, K. B., Liu, Y., et al. (2020). Blood Lipid Profiles and Risk of Atrial Fibrillation: A Systematic Review and Meta-Analysis of Cohort Studies. *J. Clin. Lipidol.* 14 (1), 133–142.e3. doi:10.1016/j.jacl.2019.12.002

Haffar, T., Bérubé-Simard, F., and Bousette, N. (2015). Impaired Fatty Acid Oxidation as a Cause for Lipotoxicity in Cardiomyocytes. *Biochem. Biophys. Res. Commun.* 468 (1-2), 73–78. doi:10.1016/j.bbrc.2015.10.162

Harada, M., Melka, J., Sobue, Y., and Nattel, S. (2017). Metabolic Considerations in Atrial Fibrillation - Mechanistic Insights and Therapeutic Opportunities. *Circ. J.* 81 (12), 1749–1757. doi:10.1253/circj.CJ-17-1058

Harada, M., Tadevosyan, A., Qi, X., Xiao, J., Liu, T., Voigt, N., et al. (2015). Atrial Fibrillation Activates AMP-dependent Protein Kinase and its Regulation of Cellular Calcium Handling: Potential Role in Metabolic Adaptation and Prevention of Progression. *J. Am. Coll. Cardiol.* 66 (1), 47–58. doi:10.1016/j.jacc.2015.04.056

Heier, C., and Haemmerle, G. (2016). Fat in the Heart: The Enzymatic Machinery Regulating Cardiac Triacylglycerol Metabolism. *Biochim. Biophys. Acta* 1861 (10), 1500–1512. doi:10.1016/j.bbalip.2016.02.014

Heijman, J., and Dobrev, D. (2015). Irregular Rhythm and Atrial Metabolism Are Key for the Evolution of Proarrhythmic Atrial Remodeling in Atrial Fibrillation. *Basic Res. Cardiol.* 110 (4), 41. doi:10.1007/s00395-015-0498-1

Huang, W. J., Zhou, R., Zeng, X. R., Tan, X. Q., Cheng, Z. H., Tang, M. H., et al. (2011). Comparative Proteomic Analysis of Atrial Appendages from Rheumatic Heart Disease Patients with Sinus Rhythm and Atrial Fibrillation. *Mol. Med. Rep.* 4 (4), 655–661. doi:10.3892/mmr.2011.468

Jie, Q. Q., Li, G., Duan, J. B., Li, X. B., Yang, W., Chu, Y. P., et al. (2019). Remodeling of Myocardial Energy and Metabolic Homeostasis in a Sheep Model of Persistent Atrial Fibrillation. *Biochem. Biophys. Res. Commun.* 517 (1), 8–14. doi:10.1016/j.bbrc.2019.05.112

Karam, B. S., Chavez-Moreno, A., Koh, W., Akar, J. G., and Akar, F. G. (2017). Oxidative Stress and Inflammation as central Mediators of Atrial Fibrillation in Obesity and Diabetes. *Cardiovasc. Diabetol.* 16 (1), 120. doi:10.1186/s12933-017-0604-9

Kolwicz, S. C., and Tian, R. (2011). Glucose Metabolism and Cardiac Hypertrophy. *Cardiovasc. Res.* 90 (2), 194–201. doi:10.1093/cvr/cvr071

Lenski, M., Schleider, G., Kohlhaas, M., Adrian, L., Adam, O., Tian, Q., et al. (2015). Arrhythmia Causes Lipid Accumulation and Reduced Glucose Uptake. *Basic Res. Cardiol.* 110 (4), 40. doi:10.1007/s00395-015-0497-2

Li, R., Liu, Y., Shan, Y. G., Gao, L., Wang, F., and Qiu, C. G. (2019). Bailcalin Protects against Diabetic Cardiomyopathy through Keap1/Nrf2/AMPK-Mediated Antioxidative and Lipid-Lowering Effects. *Oxid. Med. Cel. Longev.* 2019, 3206542. doi:10.1155/2019/3206542

Lippi, G., Sanchis-Gomar, F., and Cervellin, G. (2021). Global Epidemiology of Atrial Fibrillation: An Increasing Epidemic and Public Health challenge. *Int. J. Stroke.* 16 (2), 217–221. doi:10.1177/1747493019897870

Liu, G. Z., Hou, T. T., Yuan, Y., Hang, P. Z., Zhao, J. J., Sun, L., et al. (2016). Fenofibrate Inhibits Atrial Metabolic Remodelling in Atrial Fibrillation through PPAR-A/sirtuin 1/PGC-1α Pathway. *Br. J. Pharmacol.* 173 (6), 1095–1109. doi:10.1111/bph.13438

Lundsgaard, A. M., Fritzen, A. M., Nicolaisen, T. S., Carl, C. S., Sjøberg, K. A., Raun, S. H., et al. (2020). Glucometabolic Consequences of Acute and Prolonged Inhibition of Fatty Acid Oxidation. *J. Lipid Res.* 61 (1), 10–19. doi:10.1194/jlr.RA119000177

Maples, J. M., Brault, J. J., Witczak, C. A., Park, S., Hubal, M. J., Weber, T. M., et al. (2015). Differential Epigenetic and Transcriptional Response of the Skeletal Muscle Carnitine Palmitoyltransferase 1B (CPT1B) Gene to Lipid Exposure with Obesity. *Am. J. Physiol. Endocrinol. Metab.* 309 (4), E345–E356. doi:10.1152/ajpendo.00505.2014

Marcovina, S. M., Sirtori, C., Peracino, A., Gheorghiade, M., Borum, P., Remuzzi, G., et al. (2013). Translating the Basic Knowledge of Mitochondrial Functions to Metabolic Therapy: Role of L-Carnitine. *Transl. Res.* 161 (2), 73–84. doi:10.1016/j.trsl.2012.10.006

Maria, Z., Campolo, A. R., Scherlag, B. J., Ritchey, J. W., and Lacombe, V. A. (2018). Dysregulation of Insulin-Sensitive Glucose Transporters during Insulin Resistance-Induced Atrial Fibrillation. *Biochim. Biophys. Acta Mol. Basis Dis.* 1864 (4 Pt A), 987–996. doi:10.1016/j.bbadis.2017.12.038

Mayama, T., Matsumura, K., Lin, H., Ogawa, K., and Imanaga, I. (2007). Remodelling of Cardiac gap junction Connexin 43 and Arrhythmogenesis. *Exp. Clin. Cardiol.* 12 (2), 67–76.

Meng, T., Cheng, G., Wei, Y., Ma, S., Jiang, Y., Wu, J., et al. (2017). Exposure to a Chronic High-Fat Diet Promotes Atrial Structure and gap junction Remodeling in Rats. *Int. J. Mol. Med.* 40 (1), 217–225. doi:10.3892/ijmm.2017.2982

Mourtzinis, G., Kahan, T., Bengtsson Boström, K., Schiöler, L., Cedstrand Wallin, L., Hjerpe, P., et al. (2018). Relation between Lipid Profile and New-Onset Atrial Fibrillation in Patients with Systemic Hypertension (From the Swedish Primary Care Cardiovascular Database [SPCCD]). *Am. J. Cardiol.* 122 (1), 102–107. doi:10.1016/j.amjcard.2018.03.024

Nakamura, M., and Sadoshima, J. (2020). Cardiomyopathy in Obesity, Insulin Resistance and Diabetes. *J. Physiol.* 598 (14), 2977–2993. doi:10.1113/JP276747

Opacic, D., van Bragt, K. A., Nasrallah, H. M., Schotten, U., and Verheule, S. (2016). Atrial Metabolism and Tissue Perfusion as Determinants of Electrical and Structural Remodelling in Atrial Fibrillation. *Cardiovasc. Res.* 109 (4), 527–541. doi:10.1093/cvr/cvw007

Ostropolets, A., Elias, P. A., Reyes, M. V., Wan, E. Y., Pajvani, U. B., Hripcsak, G., et al. (2021). Metformin Is Associated with a Lower Risk of Atrial Fibrillation and Ventricular Arrhythmias Compared with Sulfonylureas: An Observational Study. *Circ. Arrhythm Electrophysiol.* 14 (3), e009115. doi:10.1161/CIRCEP.120.009115

Ozcan, C., Battaglia, E., Young, R., and Suzuki, G. (2015). LKB1 Knockout Mouse Develops Spontaneous Atrial Fibrillation and Provides Mechanistic Insights into Human Disease Process. *J. Am. Heart Assoc.* 4 (3), e001733. doi:10.1161/JAHA.114.001733

Pooyandjoo, M., Nouhi, M., Shab-Bidar, S., Djafarian, K., and Olyaeemanesh, A. (2016). The Effect of (L-)carnitine on Weight Loss in Adults: a Systematic Review and Meta-Analysis of Randomized Controlled Trials. *Obes. Rev.* 17 (10), 970–976. doi:10.1111/obr.12436

Sato, S., Suzuki, J., Hirose, M., Yamada, M., Zenimaru, Y., Nakaya, T., et al. (2019). Cardiac Overexpression of Perilipin 2 Induces Atrial Steatosis, Connexin 43 Remodeling, and Atrial Fibrillation in Aged Mice. *Am. J. Physiol. Endocrinol. Metab.* 317 (6), E1193–E1204. doi:10.1152/ajpendo.00227.2019

Serra, D., Mera, P., Malandrino, M. I., Mir, J. F., and Herrero, L. (2013). Mitochondrial Fatty Acid Oxidation in Obesity. *Antioxid. Redox Signal.* 19 (3), 269–284. doi:10.1089/ars.2012.4875

Shenasa, M., Shenasa, H., and El-Sherif, N. (2015). Left Ventricular Hypertrophy and Arrhythmogenesis. *Card. Electrophysiol. Clin.* 7 (2), 207–220. doi:10.1016/j.ccep.2015.03.017

Sletten, A. C., Peterson, L. R., and Schaffer, J. E. (2018). Manifestations and Mechanisms of Myocardial Lipotoxicity in Obesity. *J. Intern. Med.* 284 (5), 478–491. doi:10.1111/joim.12728

Söder, J., Höglund, K., Dicksved, J., Hagman, R., Eriksson Röhnisch, H., Moazzami, A. A., et al. (2019). Plasma Metabolomics Reveals Lower Carnitine Concentrations in Overweight Labrador Retriever Dogs. *Acta Vet. Scand.* 61 (1), 10. doi:10.1186/s13028-019-0446-4

Tonelli, C., Chio, I. I. C., and Tuveson, D. A. (2018). Transcriptional Regulation by Nrf2. *Antioxid. Redox Signal.* 29 (17), 1727–1745. doi:10.1089/ars.2017.7342

Tu, T., Zhou, S., Liu, Z., Li, X., and Liu, Q. (2014). Quantitative Proteomics of Changes in Energy Metabolism-Related Proteins in Atrial Tissue from Valvular Disease Patients with Permanent Atrial Fibrillation. *Circ. J.* 78 (4), 993–1001. doi:10.1253/circj.cj-13-1365

Ujino, K., Barnes, M. E., Cha, S. S., Langins, A. P., Bailey, K. R., Seward, J. B., et al. (2006). Two-dimensional Echocardiographic Methods for Assessment of Left Atrial Volume. *Am. J. Cardiol.* 98 (9), 1185–1188. doi:10.1016/j.amjcard.2006.05.040

Vyas, V., and Lambiase, P. (2019). Obesity and Atrial Fibrillation: Epidemiology, Pathophysiology and Novel Therapeutic Opportunities. *Arrhythm Electrophysiol. Rev.* 8 (1), 28–36. doi:10.15420/aer.2018.76.2

Wang, Z. Y., Liu, Y. Y., Liu, G. H., Lu, H. B., and Mao, C. Y. (2018). l-Carnitine and Heart Disease. *Life Sci.* 194, 88–97. doi:10.1016/j.lfs.2017.12.015

Wong, C. X., Sullivan, T., Sun, M. T., Mahajan, R., Pathak, R. K., Middeldorp, M., et al. (2015). Obesity and the Risk of Incident, Post-Operative, and Post-Ablation Atrial Fibrillation: A Meta-Analysis of 626,603 Individuals in 51 Studies. *JACC Clin. Electrophysiol.* 1 (3), 139–152. doi:10.1016/j.jacep.2015.04.004

Wu, S. B., Wu, Y. T., Wu, T. P., and Wei, Y. H. (2014). Role of AMPK-Mediated Adaptive Responses in Human Cells with Mitochondrial Dysfunction to Oxidative Stress. *Biochim. Biophys. Acta* 1840 (4), 1331–1344. doi:10.1016/j.bbagen.2013.10.034

Yazıcı, D., and Sezer, H. (2017). Insulin Resistance, Obesity and Lipotoxicity. *Adv. Exp. Med. Biol.* 960, 277–304. doi:10.1007/978-3-319-48382-5_12

Young, M. E., Guthrie, P. H., Razeghi, P., Leighton, B., Abbasi, S., Patil, S., et al. (2002). Impaired Long-Chain Fatty Acid Oxidation and Contractile Dysfunction in the Obese Zucker Rat Heart. *Diabetes* 51 (8), 2587–2595. doi:10.2337/diabetes.51.8.2587

Yu, J., Li, W., Li, Y., Zhao, J., Wang, L., Dong, D., et al. (2011). Activation of β(3)-adrenoceptor Promotes Rapid Pacing-Induced Atrial Electrical Remodeling in Rabbits. *Cell. Physiol. Biochem.* 28 (1), 87–96. doi:10.1159/000331717

Zhang, L., Huang, B., Scherlag, B. J., Ritchey, J. W., Embi, A. A., Hu, J., et al. (2015). Structural Changes in the Progression of Atrial Fibrillation: Potential Role of Glycogen and Fibrosis as Perpetuating Factors. *Int. J. Clin. Exp. Pathol.* 8 (2), 1712–1718.

Zou, D., Geng, N., Chen, Y., Ren, L., Liu, X., Wan, J., et al. (2016). Ranolazine Improves Oxidative Stress and Mitochondrial Function in the Atrium of Acetylcholine-CaCl2 Induced Atrial Fibrillation Rats. *Life Sci.* 156, 7–14. doi:10.1016/j.lfs.2016.05.026

Conflict of Interest: The authors declare that the research was conducted in the absence of any commercial or financial relationships that could be construed as a potential conflict of interest.

Publisher's Note: All claims expressed in this article are solely those of the authors and do not necessarily represent those of their affiliated organizations, or those of the publisher, the editors and the reviewers. Any product that may be evaluated in this article, or claim that may be made by its manufacturer, is not guaranteed or endorsed by the publisher.

frontiers in Pharmacology

ORIGINAL RESEARCH
published: 07 December 2021
doi: 10.3389/fphar.2021.690371

Hydrogen Sulfide Ameliorates Angiotensin II-Induced Atrial Fibrosis Progression to Atrial Fibrillation Through Inhibition of the Warburg Effect and Endoplasmic Reticulum Stress

*Heng-Jing Hu[1,2], Xiu-Heng Wang[3], Yao Liu[1], Tian-Qing Zhang[1], Zheng-Rong Chen[1], Chi Zhang[4], Zhi-Han Tang[4], Shun-Lin Qu[4], Hui-Fang Tang[1] and Zhi-Sheng Jiang[1,2,4]**

[1]Department of Cardiology Laboratory, First Affiliated Hospital of University of South China, Hengyang, China, [2]Postdoctoral Research Station of Basic Medicine, University of South China, Hengyang, China, [3]Department of Nuclear Medicine Lab, First Affiliated Hospital of University of South China, Hengyang, China, [4]Institute of Cardiovascular Disease and Key Lab for Arteriosclerology of Hunan Province, University of South China, Hengyang, China

OPEN ACCESS

Edited by:
Jérôme Roncalli,
Centre Hospitalier Universitaire de Toulouse, France

Reviewed by:
Mariarosaria Bucci,
University of Naples Federico II, Italy
Claudio de Lucia,
Istituti Clinici Scientifici Maugeri (ICS Maugeri), Italy
Helen E. Collins,
University of Louisville, United States

***Correspondence:**
Zhi-Sheng Jiang
zsjiang2005@163.com

Specialty section:
This article was submitted to Cardiovascular and Smooth Muscle Pharmacology, a section of the journal Frontiers in Pharmacology

Received: 02 April 2021
Accepted: 24 November 2021
Published: 07 December 2021

Citation:
Hu H-J, Wang X-H, Liu Y, Zhang T-Q, Chen Z-R, Zhang C, Tang Z-H, Qu S-L, Tang H-F and Jiang Z-S (2021) Hydrogen Sulfide Ameliorates Angiotensin II-Induced Atrial Fibrosis Progression to Atrial Fibrillation Through Inhibition of the Warburg Effect and Endoplasmic Reticulum Stress. Front. Pharmacol. 12:690371. doi: 10.3389/fphar.2021.690371

Atrial fibrosis is the basis for the occurrence and development of atrial fibrillation (AF) and is closely related to the Warburg effect, endoplasmic reticulum stress (ERS) and mitochondrion dysfunctions-induced cardiomyocyte apoptosis. Hydrogen sulfide (H_2S) is a gaseous signalling molecule with cardioprotective, anti-myocardial fibrosis and improved energy metabolism effects. Nevertheless, the specific mechanism by which H_2S improves the progression of atrial fibrosis to AF remains unclear. A case-control study of patients with and without AF was designed to assess changes in H_2S, the Warburg effect, and ERS in AF. The results showed that AF can significantly reduce cystathionine-γ-lyase (CSE) and 3-mercaptopyruvate thiotransferase (3-MST) expression and the H_2S level, induce cystathionine-β-synthase (CBS) expression; increase the Warburg effect, ERS and atrial fibrosis; and promote left atrial dysfunction. In addition, AngII-treated SD rats had an increased Warburg effect and ERS levels and enhanced atrial fibrosis progression to AF compared to wild-type SD rats, and these conditions were reversed by sodium hydrosulfide (NaHS), dichloroacetic acid (DCA) or 4-phenylbutyric acid (4-PBA) supplementation. Finally, low CSE levels in AngII-induced HL-1 cells were concentration- and time-dependent and associated with mitochondrial dysfunction, apoptosis, the Warburg effect and ERS, and these effects were reversed by NaHS, DCA or 4-PBA supplementation. Our research indicates that H_2S can regulate the AngII-induced Warburg effect and ERS and might be a potential therapeutic drug to inhibit atrial fibrosis progression to AF.

Keywords: atrial fibrosis, atrial fibrillation, angiotensin II, endoplasmic reticulum stress, hydrogen sulfide, warburg effect

INTRODUCTION

Atrial fibrillation (AF) is the most common malignant cardiac arrhythmia, affecting 2% of the general population worldwide (Xiong et al., 2019), especially those over 70 years old (Piatek et al., 2016). It is expected that more than 20 million people worldwide will be affected by AF by 2050 (Christophersen et al., 2017). AF is a major risk factor for cardiovascular events, stroke and sudden death, imposing heavy financial and health care burdens on both individuals and society. Atrial fibrosis is a hallmark feature of AF, promotes atrial structural remodelling, such as induced left atrial dysfunction (LADS), and atrial electrophysiological remodelling, such as increased susceptibility to AF. The AF caused by renin-angiotensin-aldosterone system (RAAS) is closely related to the progression of atrial fibrosis. RAAS inhibitors can inhibited the occurrence and development of AF induced by atrial fibrosis and realized significant benefits for the long-term survival of AF patients (Han et al., 2013; Turin et al., 2018). However, these conventional drugs cannot completely cure atrial fibrosis (McMurray et al., 2012). Therefore, we are currently working on studying the mechanisms and interventions of atrial fibrosis to reduce the atrial structural remodelling and electrical remodelling caused by atrial fibrosis and reduce the occurrence and development of AF.

The endoplasmic reticulum (ER) is a multifunctional signalling organelle with complex stress signalling pathways and regulates the transport and apoptosis of cell membrane proteins, thereby achieving the correct folding of proteins (Welchen and Gonzalez, 2016). Induced dysfunction of the ER under glucose deficiency, hypoxia, inflammation and oxidative stress, which interfere with protein folding, posttranslational modification and secretion, is called ER stress (ERS). PKR-like ER kinase (PERK/eIF2AK3), inositol-requiring enzyme 1 (IRE1) and activating transcription factor 6 (ATF6) are three transmembrane ER signalling proteins mediated by ERS and the unfolded protein response (UPR). When ERS occurs, increase PERK, IRE1 and ATF6 protein expression and activity (Xin et al., 2011; Yan et al., 2019). Subsequently, phosphorylated PERK (p-PERK) can cause eukaryotic initiation factor 2α (eIF2α) phosphorylation (p-eIF2α) and increase activating transcription factor 4 (ATF4) expression, thereby inhibiting mRNA translation and global protein synthesis and promoting apoptosis (Wen et al., 2017). In experimental models and patients with AF, protein production and breakdown of dysfunctional proteins is disrupted, which contributes to myocardial remodelling and AF susceptibility (Deshmukh et al., 2015; Wiersma et al., 2017; Yuan et al., 2020). Furthermore, recent studies have demonstrated that local uncommon energy metabolism, such as insulin resistance and impaired glucose transport and uptake, leads to the accumulation of unfolded proteins in the lumen of the ER, which can lead to ERS (Luoma, 2013; Sun et al., 2019). The Warburg effect refers to a state in which tissues produce energy through glycolysis despite the presence of normal aerobic conditions, and increased local lactate accumulation is characteristic of the Warburg effect. An acidic environment can be induced in cardiovascular diseases (CHDs) and myocardial fibrosis and is closely related to ERS (Cottrill and Chan, 2013; Imle et al., 2019).

Current research has defined hydrogen sulfide (H_2S), a toxic gas with the smell of rotten eggs, as the third gas signalling molecule after nitric oxide (NO) and carbon monoxide (CO). Cystathionine-γ-lyase (CSE), cystathionine-β-synthase (CBS) and 3-mercaptopyruvate thiotransferase (3-MST) are the three most common ways to synthesize hydrogen sulfide. CBS is a key enzyme for H_2S production in the cardiovascular system (Leffler et al., 2006), and the CSE/H_2S pathway plays an important role in regulating CHD (Pan et al., 2012). In addition, 3-MST is a key enzyme for H_2S production in mitochondria (Beltowski, 2015). As a gaseous signalling molecule, H_2S participates in maintenance of the physiology of the cardiovascular system through its anti-oxidant, anti-inflammatory, neuromodulatory, energy metabolism regulation (Liang et al., 2015), and cardioprotective. Therefore, it can improve atrial remodelling and AF (Xue et al., 2020) and myocardial ischaemia-reperfusion injury (Snijder et al., 2013) and has been shown to promote myocardial repair and long-term cardiac function recovery after infarction in CSE-KO mice (Ellmers et al., 2020). In addition, attenuation of pathological fibrosis by modulating signals involved in cardiac fibrosis is an area of great interest due to its obvious therapeutic implications for the treatment of AF (Su et al., 2021). It is well established that reduced H_2S levels are associated with cardiomyocyte apoptosis, myocardial fibrosis, and ERS induced by ischaemia-reperfusion injury (Snijder et al., 2013; George et al., 2017; Ren et al., 2019). Nevertheless, to the best of our knowledge, it is not clear whether H_2S can attenuate AngII-induced Warburg effect and ERS, thereby ameliorating atrial fibrosis progression to AF.

In this study, we hypothesized that H_2S exerts cardioprotective against AngII-induced Warburg effect and ERS and further affects atrial fibrosis progression to AF. The mechanism was investigated using patient tissue specimens, rat models of AF, and HL-1 cell models of AF, with the aim of providing new molecular targets for prevention and treatment of AF.

MATERIALS AND METHODS

Human Left Atrial Appendage

Human research was approved by the ethics committee of the First Affiliated Hospital of University of South China and was performed in compliance with the Declaration of Helsinki. Left atrial appendage (LAA) tissue specimens were collected from rheumatic heart disease (RHD) patients undergoing mitral regurgitation surgery in the First Affiliated Hospital of University of South China. Informed consent for clinical observation experiments was signed by the patient or a family member before surgery. Patients with benign/malignant tumours, acute/chronic heart failure, hypertension, chronic obstructive pulmonary disease, pulmonary heart disease, CHD, cardiomyopathy, hyperthyroidism and obesity as well as overweight patients and patients with diabetes mellitus (including type 1 and type 2 diabetes mellitus and impaired

TABLE 1 | Main characteristics of 12 patients with rheumatic heart disease with mitral valve replacement combined with AF or SR.

Parameter	AF patients	SR patients	P
Number of patients	6	6	
Sex (male/female)			
male	3	3	
female	3	3	
Age, y	58.1 ± 12.9	57.9 ± 13.2	0.62
Systolic blood pressure, mm Hg	121 ± 14	122 ± 13	0.91
Diastolic blood pressure, mm Hg	76 ± 12	75 ± 10	0.96
Body mass index, kg/m2	24.5 ± 3.4	24.3 ± 3.0	0.58

glucose tolerance) were excluded before enrolment. According to the presence or absence of AF, the enrolled patients were divided into a permanent AF group ($n = 6$) and a sinus rhythm (SR) group ($n = 6$). General patient information is shown in **Table 1**.

Animal Models

In female animals, the incidence of supraventricular tachycardia is closely related to menstrual cycle, more common in luteal phase, and negatively related to estrogen level (Gowd and Thompson, 2012). Therefore, in order to exclude the effect of estrogen, combined with relevant AF research reports (Chan et al., 2019; Ge et al., 2020), we select male Sprague–Dawley (SD) rats, weighing 200–250 g, purchased from the Animal Department of University of South China, as research target. The animal studies were approved by the Ethics Committee of the First Affiliated Hospital of University of South China. Ang-II (200 ng/kg/min) was subcutaneously infused into the rats using a mini-pump (Model 2004; Alzet) for 4 weeks to induce atrial fibrosis (Ge et al., 2020). AF was induced by transesophageal stimulation. The inducibility of AF was clarified by atrial rapid programmed stimulation (ARPS) via oesophageal electrodes after 4 weeks of continuous Ang-II administration with a subcutaneous mini-pump as previously described (Song et al., 2019). AF vulnerability was assessed by stimulation for 5 s per cycle starting at 50 ms of the RR interval and ending at 2 ms decrements until termination at 10 ms decrements and resting for 5 s if no AF occurred. If AF occurred, the time from the end of stimulation to the first sinus P recovery, which was defined as AF duration, was recorded. To recover the sinus P wave, another stimulation of the next perimeter was performed until stimulation ended at 10 ms. AF was defined as a rapid and irregular atrial rhythm with irregular RR intervals lasting at least 1 s on ECG. AF was considered inducible if one or more bursts in the series caused an AF event. The number of AF episodes and AF duration were recorded and analysed. Minipump implantation and ARPS stimulation with oesophageal pacing were performed under 2% v/v isoflurane/oxygen inhalation anaesthesia. When ARPS stimulation was finished and the heart rate returned to the SR P wave, the SD rats were euthanized using potassium chloride (10% concentration, 75–150 mg/kg KCl administered via rapid intravenous injection) until cardiac function stopped. The left atrial tissue was stored in liquid nitrogen.

Animal Experimental Design

SD rats were randomly divided into eight groups with six rats in each group. SD rats in each group received the following treatments (see **Supplementary Figure S1**).

Sham group: SD rats were infusion of 0.9% saline (200 ng/kg per minute) using continuous subcutaneous mini-pump for 4 weeks, and then ARPS stimulation was given through the oesophagus.

Ang-II group: SD rats were infusion of Ang-II (200 ng/kg per minute) using continuous subcutaneous mini-pump for 4 weeks, and then ARPS stimulation was given through the oesophagus (Ge et al., 2020).

Ang-II + NaHS group: SD rats were infusion of Ang-II (200 ng/kg per minute) using continuous subcutaneous mini-pump combined with intraperitoneal injection of NaHS (56 μM/kg qd) for 4 weeks, and then ARPS stimulation was given through the oesophagus (Pan et al., 2014).

Ang-II + 4-PBA group: SD rats were infusion of Ang-II (200 ng/kg per minute) using continuous subcutaneous mini-pump combined with intraperitoneal injection of 4-PBA (20 mg/kg qd) for 4 weeks, and then ARPS stimulation was given through the oesophagus (Luo et al., 2015).

Ang-II + DCA group: SD rats were infusion of Ang-II (200 ng/kg per minute) using continuous subcutaneous mini-pump combined with intraperitoneal injection of dichloroacetic acid (DCA, 50 mg/kg qd) for 4 weeks, and then ARPS stimulation was given through the oesophagus (Sun et al., 2016).

NaHS group: SD rats were infusion of NaHS (56 μM/kg qd) using continuous intraperitoneal injections for 4 weeks, and then ARPS stimulation was given through the oesophagus.

4-PBA group: SD rats were infusion of 4-PBA (20 mg/kg qd) using continuous intraperitoneal injections for 4 weeks, and then ARPS stimulation was given through the oesophagus.

DCA group: SD rats were infusion of DCA (50 mg/kg qd) using continuous intraperitoneal injections for 4 weeks, and then ARPS stimulation was given through the oesophagus.

HL-1 Experimental Design

The HL-1 cell line was purchased from Shanghai (TongPai, China), used for *in vitro* research and cultivated in DMEM containing 10% foetal bovine serum (Gibco, MA, United States), 0.1 mM norepinephrine and 2 mM L-glutamine in a 37°C cell incubator with 5% CO_2. Before each experiment, HL-1 cells were plated in six-well plates and treated as described below when the cells reached 70–80% confluence. (see **Supplementary Figure S2**):

Control group: HL-1 cells were cultured in DMEM for 24 h.

Ang II group: HL-1 cells were treated with Ang II (200 nM) for 24 h (Lee et al., 2020).

Ang II + NaHS group: HL-1 cells were pre-incubated with NaHS (100 μM) for 24 h, and then treated with Ang-II for another 24 h (Lee et al., 2019).

Ang II + 4-PBA group: HL-1 cells were pre-incubated with 4-PBA (500 μM) for 24 h, and then treated with Ang-II for another 24 h (Yuan et al., 2020).

Ang II + DCA group: HL-1 cells were pre-incubated with DCA (1.5 mM) for 24 h, and then treated with Ang-II for another 24 h (Li et al., 2019a).

NaHS group: HL-1 cells were pre-incubated with NaHS (100 μM) for 24 h, and then incubated with DMEM for another 24 h.

4-PBA group: HL-1 cells were pre-incubated with 4-PBA (500 μM) for 24 h, and then incubated with DMEM for another 24 h.

DCA group: HL-1 cells were pre-incubated with DCA (1.5 mM) for 24 h, and then incubated with DMEM for another 24 h.

Cell Viability Assay

CCK-8 assays were used to investigate the viability of HL-1 cells cultured in 96-well plates. Our experimental methods were performed as described in a previous report by Li et al. (2020).

Detection of Intracellular ROS

Intracellular ROS levels were determined by the oxidative conversion of cell-permeable DCFH-DA to fluorescent dichlorofluorescein (DCF). Our experimental methods were performed as previously reported by Thakur et al. (2015).

Detection of Left Atrial Function

The patients and rats were placed on a test bench on the left side and connected with a synchronous 12-lead ECG. The left atrial diameter (LAD), left atrial diameter (LASED) and left ventricular ejection fraction (LVEF) were measured by the M-mode echocardiography. End systolic left atrial volume (LAESV) and end diastolic left atrial volume (LAEDV) were measured by the biplane Simpson's method at apical four chamber and apical two chamber views. The left ventricular outflow tract velocity time integral (LVOT-VTI) was measured by the left ventricular outflow tract blood flow spectrum. The mitral annular motion spectrum (Ea, Aa) were measured by the tissue Doppler, and calculated the Ea/Aa ratio.

The body surface area (BSA) of patient's was calculated according to the Stevenson's formula (Si et al., 2018).

BSA = 0.0061 * height (CM) + 0.0128 * weight (kg) - 0.1529.

The body surface area of the rats was calculated using the Meeh-Rubner formula (Spiers and Candas, 1984).

BSA = K * weight 7) 2/3÷10,000, and K value in rats = 9.1.

The left atrial end-systolic volume index (LAESVI) was calculated as LAESVI = LAESV/BSA.

The left atrial ejection fraction (LAEF) was calculated as LAEF = (LAESV-LAEDV)/LAESV.

The left atrial function index (LAFI) was finally obtained as LAFI = (LAEF*LVOT-VTI)/LAESVI.

Western Blotting

Collected the total protein of left atrium tissue and HL-1 cells in lysis buffer (Beyotime P0013F). Protein concentration was determined using a BCA protein assay kit (Beyotime P0012S). Equal amounts (70 μg) of protein were separated in a 12% sodium dodecyl sulfate (SDS)-polyacrylamide gel. Proteins were transferred to polyvinylidene difluoride (PVDF) membranes (Beyotime FFP33), blocked in Tris-buffered saline (TBS) with 5% milk/0.1% Tween 20 and incubated overnight at 4°C with anti-pyruvate dehydrogenase kinase 4 (PDK-4) (1:500, Abcam ab89295), anti-PDH (1:5,000, Abcam ab172617), anti-lactate dehydrogenase (LDHA) (1:1,500, Abcam ab222910), anti-matrix metallopeptidase 9 (MMP-9) (1:500, Abcam ab58803), anti-p-PERK (1:2000, Affinity DF7576), anti-PERK (1:1,000, Affinity AF5304), anti-p-eIF2α (1:1,000, Cell Signaling, #9721), anti-eIF2α (1:1,000, Cell Signaling, #9722), anti-Caspase-12 (1:1,000, Abcam ab8117), anti-ATF 4 (1:1,000, Abcam ab23760), anti-C/EBP homologous protein (CHOP, 1:200, Abcam ab11419), anti-CBS (1:800, Abnova H00000875-M01), anti-CSE (1:800, BIOSS bs-9515R), anti-3-MST (1:500, Abcam ab224043) or anti-glyceraldehyde 3-phosphate dehydrogenase (GAPDH, 1:5,000, Abcam ab 9,484) antibody in blocking buffer. The membranes were washed in 0.1% Tween/TBS and incubated with HRP-labelled goat anti-rabbit IgG (H + L) (Beyotime A0208) or HRP-labelled goat anti-mouse IgG (H + L) (Beyotime A0216) secondary antibody for 2 h at room temperature, followed by detection of chemiluminescence. Gel Imaging system (Bio-Rad Laboratories, Inc.) and Quantity One software (version 4.6.6; Bio-Rad Laboratories, Inc.) were used to image and analyse the western blot bands. Band intensities were detected with Super Signal West Pico Chemiluminescent Substrate (Thermo, United States).

Myocardial Masson Staining

Fresh tissue was fixed in 4% paraformaldehyde for more than 24 h. The tissue was taken out of the fixative solution and placed in a fume hood for trimming of the target site tissue with a scalpel, and the trimmed tissue and the corresponding label was placed in a dehydration box. The dehydration box was put into a hanging basket, and the trimmed tissue was treated with a sequential alcohol gradient for dehydration in a dehydrator. Wax-soaked tissue was then embedded in an embedding machine. First, the melted wax was placed into the embedding frame, and before the wax solidified, the tissue was removed from the dehydration box and put into the embedding frame according to the requirements of the embedding surface, and the corresponding label was attached. The samples were cooled in a refrigerator at −20°. After the wax solidified, the wax block was removed from the embedding frame and trimmed. The trimmed wax block was sliced on a paraffin microtome to a thickness of 4 μm. The slices were floated on a spreader in warm water at 40°C to flatten the tissue, and the tissue was picked up with a glass slide and placed in a 60°C oven to bake for subsequent histochemical staining. The steps for Masson staining were as follows. Samples were fixed with neutral formalin, sectioned, deparaffinized in absolute alcohol, stained with the iron hematoxylin A liquid and B liquid (according to 1:1) for 3 min, differentiation for a few seconds with 1% hydrochloric acid alcohol, 60% ammonia water return blue and washed with water, stained with Ponceau red dye for 7 min and washed with distilled water slightly, differentiation for 3 min in Phosphomolybdate acid, stained with Aniline blue liquid for 5 min and differentiation for 1 min in glacial acetic acid solution, dehydrated in absolute alcohol, putting in xylene for transparency, and mounted with

neutral gum. Collagen fibers were bluish in color and myocardial cell were orange. All sections with Masson staining were observed and the pictures were photograPEd by an Olympus microscope (IX-70 OLYMPUS, Japan) (Li et al., 2019b).

Assessing the Levels of Lactic Acid, Glucose Consumption and Cellular ATP

After various treatments, 10 μl of homogenate (1:10 dilution) was collected and analysed using a lactic acid kit (NanJing Jiancheng Corp, A019-2), a glucose consumption kit (Sigma MAK083) and an ATP assay kit (Cloud Clone Corp, CEA349Ge) according to the manufacturers' instructions (Xiao et al., 2017).

Programmable Electrical Stimulator Detection of AERP and AERPd

Electrophysiological investigation was performed as previously described (Hu et al., 2019).

Detection of HL-1 Cell Apoptosis *via* Flow Cytometry

The degree of apoptosis in HL-1 cells cultured in 6-well plates was detected by flow cytometry. Our experimental method was performed as previously reported by Gu et al. (Gu et al., 2018).

Detection of Oxidative Damage by Assessing 8-OHdG Content in HL-1 Cell Mitochondrial DNA

Mitochondrial DNA oxidative damage was evaluated by detecting the 8-hydroxy-2-deoxyguanosine (8-OHdG) content. Our experimental method was performed as previously reported by Ni et al. (2021).

Test of Carbonyl Protein Content in HL-1 Cells

After various treatments, HL-1 cells were collected and lysed, and the carbonyl protein content in HL-1 cells was measured as described by Ni et al. (2021).

Determination of Lipid Peroxidation Level in HL-1 Cells

After various treatments, HL-1 cells were collected and lysed, and the lipid peroxidation levels in HL-1 cells were determined as previously reported by Ni et al. (2021).

Determination of Mitochondrial Respiratory Function

The mitochondrial oxygen consumption in HL-1 cells was assayed based on the method described by Sun et al., 2018. Mitochondrial respiration buffer (125 mmol/L KCl, 5 mmol/L K2HPO4, 20 mmol/L MOPS, 2.5 mmol/L EGTA, 1 μmol/L Na4P2O7, and 0.1% bovine serum albumin, pH 7.4). Mitochondrial oxygen consumption was measured by Clark type oxygen electrode (Hansatech Instruments, Norfolk, United Kingdom) in mitochondrial respiration buffer at 30°C. Pyruvate (5 mmol/L) and malate (5 mmol/L) were used as substrates for complex I-containing mitochondria at a final concentration of 500 μg protein/ml. ADP-stimulated oxygen consumption (state three respiration) was measured in the presence of 200 μmol/L ADP, and ADP independent oxygen consumption (state four respiration) was also monitored. The respiratory control ratio (RCR, state three divided by state 4) reflects oxygen consumption by phosphorylation (coupling). The ADP/O ratio (number of ADP molecules added for each oxygen atom consumed) is an index of the efficiency of oxidative phosphorylation. State three shows the oxygen consumption of the ADP phosphorylation process during transformation to ATP. State four indicates ADP consumption after the base oxygen consumption and reflects invalid oxygen consumption.

Quantitative PCR

Total RNA was isolated from cultured cells using TRIzol® reagent (Tiangen Biotech Co., Ltd.). First-strand cDNA was synthesized from 4 mg total RNA using M-MLV reverse transcriptase (Promega Corporation) and oligo (dT). The cDNA for collagen I*α*, collagen III*α* and GAPDH was amplified using specific primers and conditions. The PCR products were subjected to electrophoresis in 1% agarose gels and visualized with ethylene bromide. Real-time quantitative PCR (qPCR) was performed with SYBRPremix Ex Taq (Perfect Real Time) (Takara, Japan). The relative mRNA levels were calculated by normalization to GAPDH, according to the 2-ΔΔCT method. The following specific primers were used: forward 5′-GTCGTATCC AGTGCGTGTC-3′ and reverse 5′-GTGGAGTCGGCAATT GCA-3′; collagen IIIα, forward 5′-CAATTCCTGGCGTTA CCTTG-3′ and reverse 5′-AGCCCTGTATTCCGTCTCCT-3'; GAPDH, forward 5′-GGC AAGGTCATCCCAGAG CT-3′ and reverse 5′-CGCCTGCTT CACCACCTTCT-3'.

Determination of the H_2S Level in Patient and Rat Plasma

The plasma of patients and rats in each group was collected, and detection was performed according to the Methylene blue method described by Geng Bin et al. (Zheng et al., 2012).

Measurement of CSE Activity

Prepare NaHS as standard curve: set the concentration gradient of NaHS standard to 1000, 800, 400, 200, 100, 50μM, and use deionized water instead of 0 μM. After configuration, add 500 μl each to the centrifuge tube, add 2.5 ml deionized water to each tube, then add 1% zinc acetate (400 μl), N,N-dimethyl-p-phenylenediamine sulfate (20 mM; 40 μl) in 7.2 mol/l HCl was added, which was immediately followed by the addition of FeCl3 (30 mM; 40 μl) in 1.2 mol/l HCl. Subsequently, the absorbance at 670 nm was measured using a microplate reader (Molecular Devices, LLC). The standard curve of NaHS is Y = 0.00038x + 0.09475, r2 = 0.99951. Following treatment, HL-1

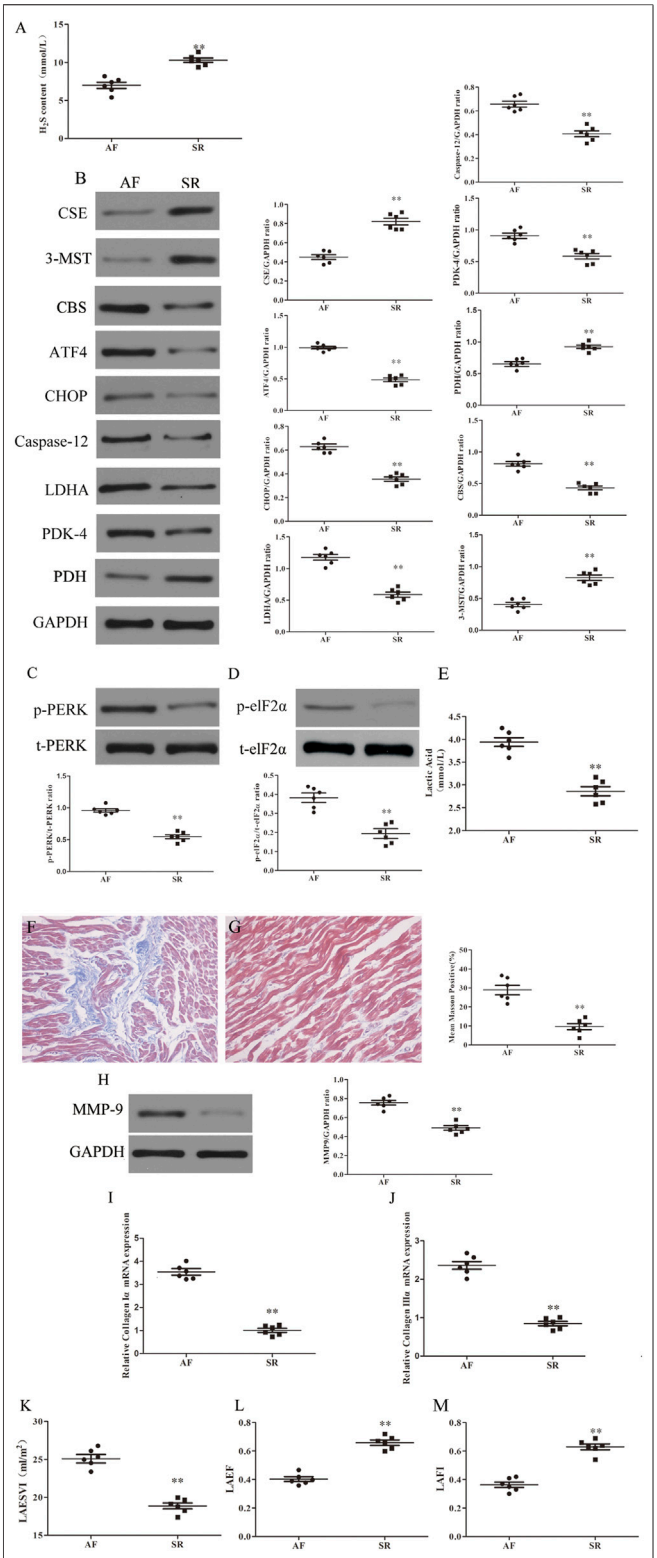

FIGURE 1 | Increased fibrosis, ERS and Warburg effect and decreased CSE expression and left atrial function were found in AF patients compared with SR patients. **(A)** H_2S content was determined by Methylene blue method in the LAA of patients with SR or AF (n = 6 in each group). **(B)**

(*Continued*)

FIGURE 1 | Representative Western blotting and relative densitometry analysis of CSE, CBS, 3-MST, PDK-4, LDHA, PDH, ATF-4, CHOP, caspase-12 and GAPDH in the LAA of patients with SR or AF (n = 6 in each group). **(C)** Western blotting was used to analyze the protein levels of p-PERK and t-PERK in the LAA of patients with SR or AF (n = 6 in each group). **(D)** Western blotting was used to analyze the protein levels of p-elf2α and t-elf2α in the LAA of patients with SR or AF (n = 6 in each group). **(E)** Lactate acid was determined by kit analysis in the LAA of patients with SR or AF (n = 6 in each group). Blue staining with representative Masson staining (scale bar = 50 μm) and quantification of atrial fibrosis (n = 6 in each group, with ≥40 fields in each group) were used in the **(F)** AF group and **(G)** SR group. **(H)** Western blotting was used to analyze the protein levels of MMP-9 and GAPDH in the LAA of patients with SR or AF (n = 6 in each group). Representative RT-PCR and relative densitometry analysis of **(I)** collagen Iα and **(J)** collagen IIIα in the LAA of patients with SR or AF (n = 6 in each group). Left atrial function was measured by color Doppler echocardiography **(K)** LAESVI, **(L)** LAEF and **(M)** LAFI (n = 6 in each group) in the patients with SR or AF during the echocardiographic studies. $^{**}p < 0.01$ *VS AF*. A Student's t-test was used for each of these comparisons between AF and SR groups.

cells were collected and homogenized in 50 mM ice-cold potassium phosphate buffer (pH, 6.8). Each 1 ml of the reaction mixture contained potassium phosphate buffer (100 mM; pH, 7.4), L-cysteine (10 mM), pyridoxal 5′-phosphate (2 mM) and cell lysis solution. In the central pool, 1% zinc acetate (400 μl) was added to trap the evolved H_2S. The reaction was performed in tightly stoppered cryovial test tubes in a shaking water bath at 37°C. After incubating for 120 min, the zinc acetate was collected, and N,N-dimethyl-p-phenylenediamine sulfate (20 mM; 40 μl) in 7.2 mol/l HCl was added, which was immediately followed by the addition of FeCl3 (30 mM; 40 μl) in 1.2 mol/l HCl. Subsequently, the absorbance at 670 nm was measured using a microplate reader (Molecular Devices, LLC). According to the standard curve, the protein concentrations of Control and each treatment group were calculated, and the release of endogenous H_2S was calculated. The amount of H_2S present was standardized according to the protein concentration in the Control and each treatment groups. The experiment was repeated ≥6 times (Hu et al., 2021).

Statistical Analyses

All the values are expressed as the mean ± standard error of the mean (SEM) or a percentage of at least three independent experiments. Statistical analysis was performed with unpaired Student's t-test for comparisons between two groups. One-way analysis of variance (ANOVA) (Tukey's) was used to evaluate AF duration, AERPd, AERP, ATP production, glucose consumption, lactate production, cell apoptosis, reactive oxygen species, carbonyl protein, 8-OHdG, respiratory control rate (RCR), ADP/O ratio, mitochondrial state3 oxygen consumption, mitochondrial state4 oxygen consumption and the expression of PDK-4, LDH, PDH p-PERK, ATF4, p-elf2α, CHOP, CSE caspase-12 and MMP-9. Fisher's exact test was used to evaluate AF inducibility. p values <0.05 were considered statistically significant. All statistical analyses were performed using GraphPad Prism six software (GraphPad Software Inc., La

Jolla, CA, version 6.42). The number of experiments per group is indicated in the figure legends.

RESULTS

AF and SR Patient Characteristics

Table 1 shows the clinical characteristics of six patients with SR and six patients with AF. LAA were obtained from the 12 patients through cardiothoracic mitral valve replacement surgery (male, 50%, female, 50%). There were no significant differences in baseline data between SR and AF patients (**Table 1**).

Specific Changes in LAA Tissue in Patients With AF

H_2S deficiency often leads to the occurrence of a variety of CHDs (Wang et al., 2009). To investigate the role of H_2S in the development of AF, first we examined the levels of H_2S in the plasma of RHD patients with AF or SR. We found that plasma levels of H_2S was significantly lower in patients with AF compared with SR patients (**Figure 1A**). Second, we detected the expression of H_2S synthase CSE, CBS and 3-MST in LAA obtained from RHD patients with AF or SR. We found that CSE and 3-MST expression were downregulated and CBS expression was upregulated in the LAA from AF patients compared with SR patients (**Figure 1B**). In addition, the expression levels of ERS axes, including caspase-12, CHOP, ATF4 (**Figure 1B**), p-elF2α and p-PERK (**Figures 1C,D**), and the Warburg effect markers, including LDHA, PDK-4 (**Figure 1B**) and lactic acid (**Figure 1E**), were increased in the LAA from AF patients compared with SR patients. Finally, we examined the extent of fibrosis in LAA from patients with AF or SR and we found masson positivity (**Figures 1F,G**) and the expression of MMP-9 (**Figure 1H**), collagen Iα and collagen IIIα (**Figures 1I**,**J**) were upregulated and cardiac colour Doppler ultrasound indicated that LAESVI was increased (**Figure 1J**) and LAEF and LAFI were decreased (**Figures 1K,L**) in AF patients compared with SR patients.

NaHS Inhibits the Ang II-Induced Atrial Warburg Effect in SD Rats

Continuous stimulation with Ang-II can lead to the formation of atrial fibrosis (Ge et al., 2020). As shown in **Figure 2**, the decreased expression of PDH (**Figure 2A**) and increased expression of LDHA and PDK-4 (**Figures 2B,C**), accompanied by enhanced local lactate acid accumulation (**Figure 2D**), decreased ATP production (**Figure 2E**) and promoted glycogen consumption (**Figure 2F**) in the left atrium of SD rats with Ang-II infusion, it suggests that the Warburg effect in the left atrium of SD rats is enhanced after Ang-II infusion. Additionally, NaHS supplementation dramatically enhanced PDH expression (**Figure 2A**) and inhibited the expression of PDK-4 and LDHA (**Figures 2B,C**), accompanied by decreased local lactate acid (**Figure 2D**), increased ATP production (**Figure 2E**) and reduced glycogen consumption (**Figure 2F**) in the left atrium of SD rats with Ang-II infusion, suggesting that exogenous supplementation with H_2S was able to prevent the Warburg effect in the left atrium of SD rats after Ang-II infusion. This effect of H_2S is consistent with the effect of exogenous supplementation with DCA, a specific inhibitor of the Warburg effect key enzyme PDK.

NaHS Inhibits Ang-II-Induced Atrial ERS in SD Rats

Apoptosis of cardiomyocytes results in myocardial fibrosis (Zhang et al., 2019). ERS is positively associated with myocardial apoptosis and contributes to the development of myocardial fibrosis, which leads to various CHDs. To determine whether H_2S prevents atrial fibrosis through inhibition of apoptosis caused by ERS, we treated SD rats upon Ang II infusion with NaHS. As shown in **Figure 3**, Ang-II induced ERS in the left atrium of SD rats, evidenced by increased expression of p-PERK (**Figure 3A**), p-elF2a (**Figure 3B**), ATF4 (**Figure 3C**), CHOP (**Figure 3D**) and caspase 12 (**Figure 3F**). Cotreatment with NaHS significantly inhibited the expression of p-PERK (**Figure 3A**), p-elF2a (**Figure 3B**), ATF4 (**Figure 3C**), CHOP (**Figure 3D**) and caspase12 (**Figure 3F**) in the left atrium of SD rats induced by Ang-II infusion, which was consistent with the effect of supplementation with 4-PBA, a specific inhibitor of ERS.

NaHS Inhibits Left Atrial Remodelling Induced by Ang-II in SD Rats and is Associated With Inhibition of the Warburg Effect and ERS

Left atrial remodelling induced by AF involves atrial structural and electrophysiological remodelling (Wang et al., 2019). Myocardial fibrosis causes structural remodelling that can lead to cardiac dysfunction, whereas atrial fibrosis leads to LADS. Lower plasma H_2S content is closely related to atrial fibrosis. First, we observed that Ang-II infusion significantly decreased CSE and 3-MST expression and increased CBS expression in the left atrium of SD rats (**Figure 4A**), and decreased H_2S content in the plasma of SD rats (**Figure 4B**). In addition, we observed that Ang-II infusion significantly increased atrial fibrosis in SD rats with positive Masson staining, increased MMP-9, collagen Iα and collagen III α expression (**Figures 4C–M**), and increased susceptibility to AF, including promoted the number of AF episodes and extended AF duration, shortened AERP and prolonged AERPd (**Figures 4N–R**), and cardiac color Doppler ultrasound confirmed left atrial dysfunction (LADS), including enlarged LAESVI and decreased LAEF and LAFI (**Figures 4S–U**) compared with saline injected SD rats. Finally, SD rats treated with NaHS, DCA or 4-PBA were protected against Ang II-induced atrial fibrosis, evidenced by negative Masson staining, decreased MMP-9, collagen Iα and collagen III *α* expression (**Figures 4C–M**), and decreased susceptibility to AF, including reduced number of AF episodes and shortened AF duration, prolonged AERP and shortened AERPd, (**Figures 4N–R**), and improved LADS, including narrowed LAESVI and increased LAEF and LAFI(**Figures 4S–U**) compared with Ang-II

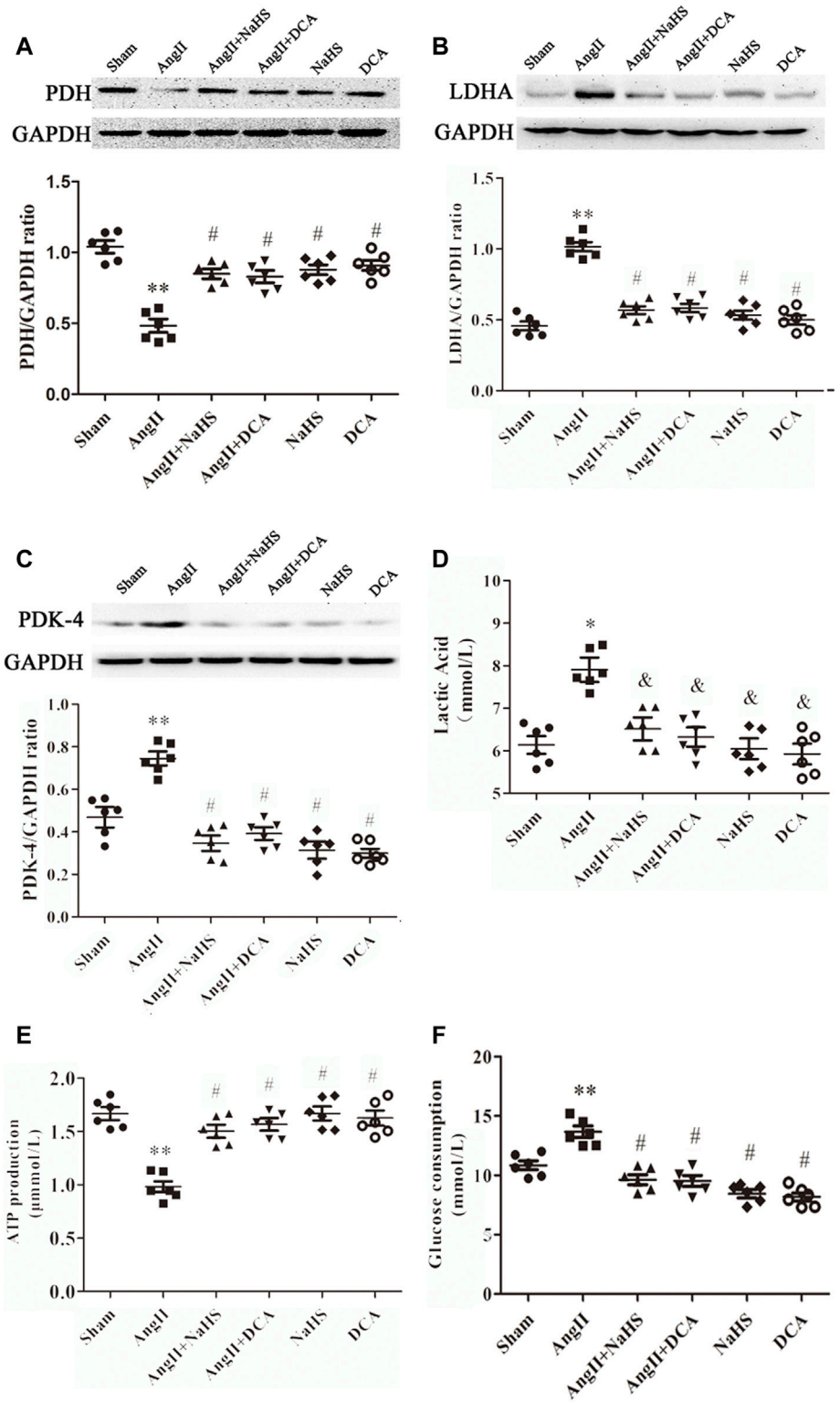

FIGURE 2 | NaHS attenuated the Warburg effect in the left atrium gained from rats under Ang-II treatment. Representative Western blotting and relative densitometry analysis of **(A)** PDH, **(B)** LDHA and **(C)** PDK-4 with GAPDH as a loading control in the rats left atrial tissue of the indicated groups. Lactate acid **(D)** and the production of ATP **(E)** and glucose consumption **(F)** were determined by kit analysis in the rats left atrial tissue of the indicated groups **(***n* = 6 in each group**)**. ***p < 0.01 VS Sham, *p < 0.05 VS Sham, #p < 0.01 VS Ang II, &p < 0.05 VS Ang II.* Groups were compared using one-way analysis of variance (ANOVA) (Tukey's) in **(A–F)**.

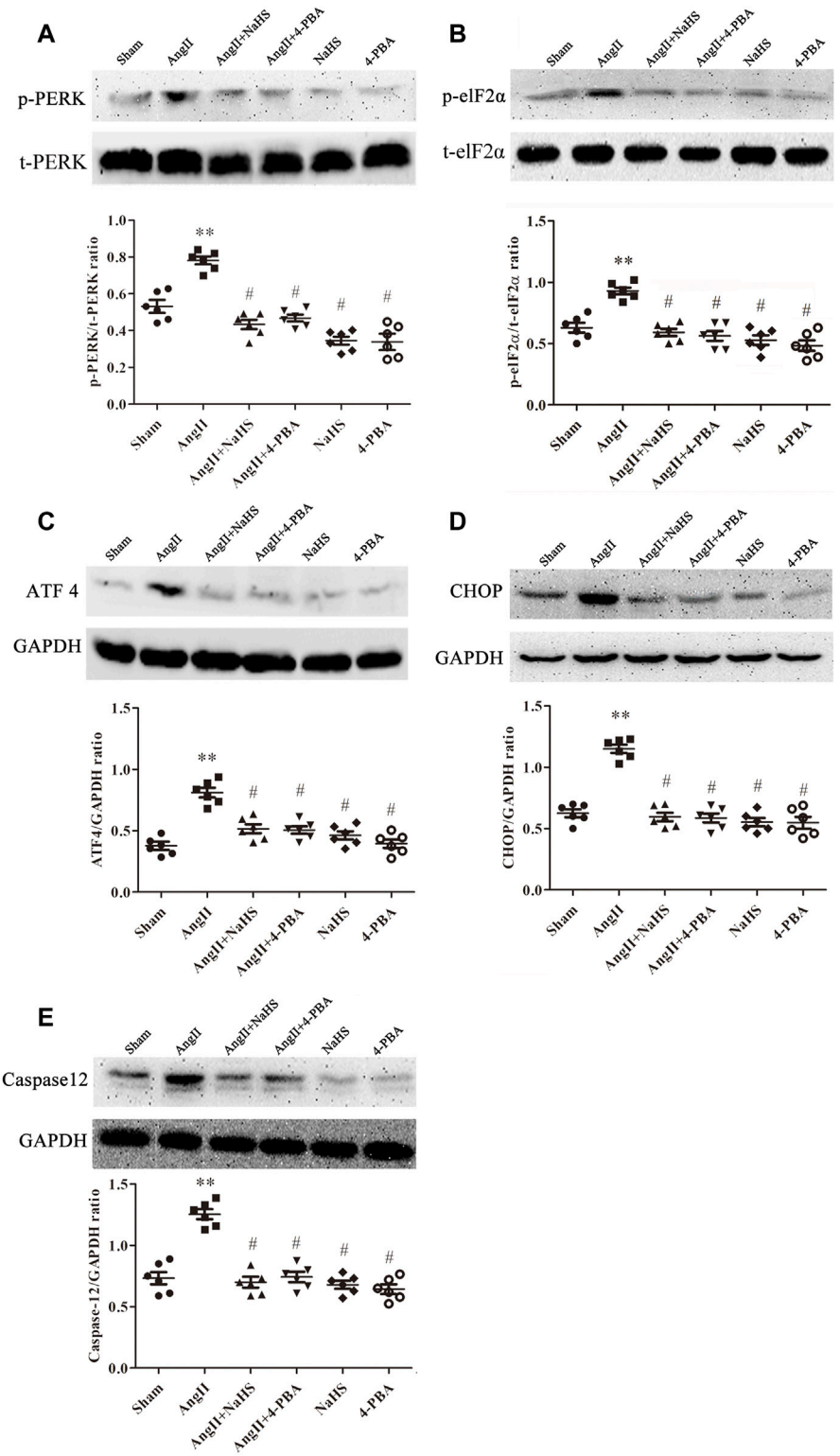

FIGURE 3 | NaHS attenuated the ERS in the left atrium gained from rats under Ang II treatment. Representative Western blotting and relative densitometry analysis of **(A)** p-PERK with t-PERK as the loading control, **(B)** p-eIF2α with t-eIF2α as the loading control and **(C)** ATF 4, **(D)** CHOP and **(E)** caspase12 with GAPDH as the loading control in the rats left atrial tissue of the indicated groups. (n = 6 in each group) ***p < 0.01 VS Sham, #p < 0.01 VS Ang II.* Groups were compared using one-way analysis of variance (ANOVA) (Tukey's) in **(A–E)**.

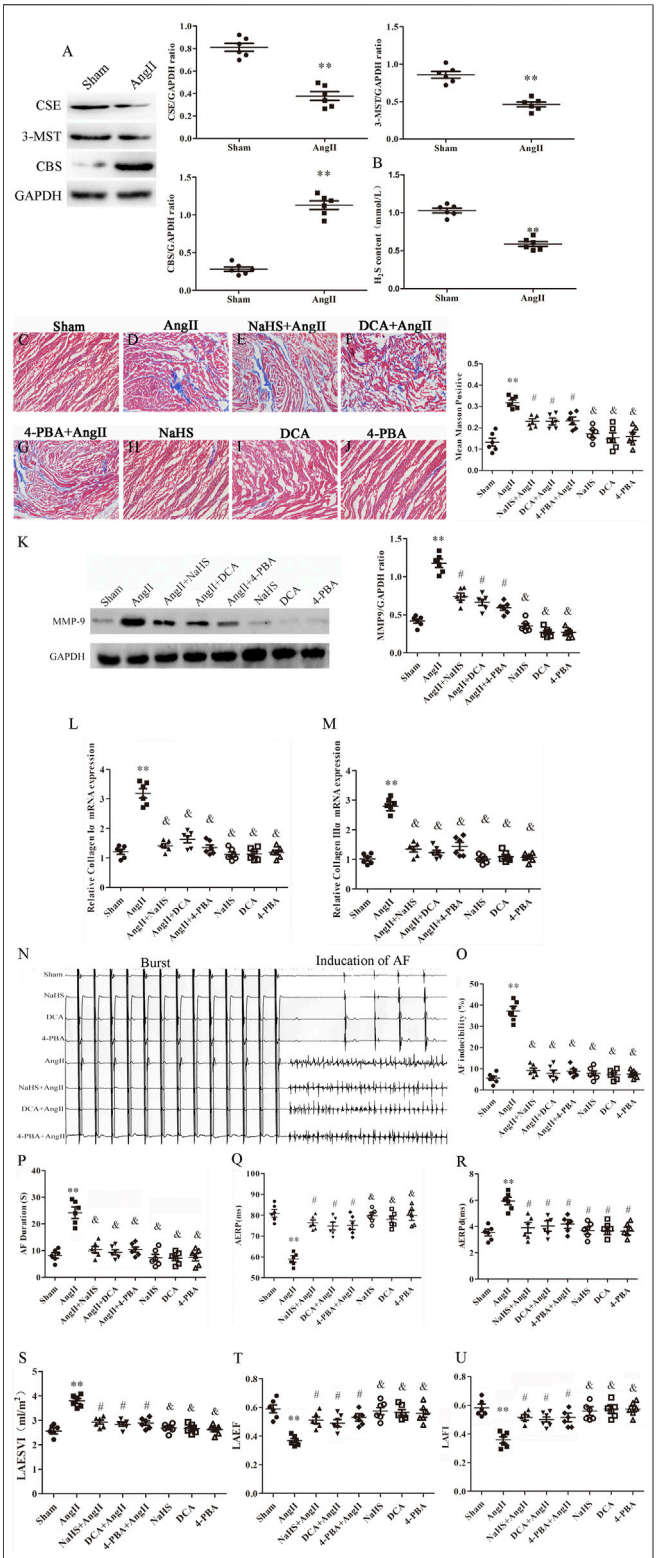

FIGURE 4 | NaHS inhibits left atrial remodeling induced by Ang II in SD rats and is associated with the inhibition of the Warburg effect and ERS. **(A)** Representative Western blotting and relative densitometry analysis of CSE, 3-MST and CBS with GAPDH as the loading control in the rats left atrial

(*Continued*)

FIGURE 4 | tissue of the indicated groups. (*n* = 6 in each group). **(B)** H_2S content was determined by Methylene blue method in the rats plasma of the indicated groups (*n* = 6 in each group). Blue staining with representative Masson staining (scale bar = 50 μm) and quantification of atrial fibrosis (*n* = 6 in each group, with ≥40 fields in each group) were used in the **(C)** Sham group, **(D)** Ang II group, **(E)** NaHS + Ang II group, **(F)** DCA + Ang II group, **(G)** 4-PBA + Ang II group, **(H)** NaHS group, **(I)** DCA group and **(J)** 4-PBA group. **(K)** Representative Western blotting and relative densitometry analysis of MMP-9 with GAPDH as the loading control in the rats left atrial tissue of the indicated groups (*n* = 6 in each group). Representative RT-PCR and relative densitometry analysis of **(L)** Collagen Iα and **(M)** Collagen IIIαin the rats left atrial tissue of the indicated groups (*n* = 6 in each group). **(N)** ARPS was performed via the esophagus, and AF episodes and duration were recorded in the rats indicated groups. Electrophysiological analysis of numbers of AF episodes **(O)** and durations of AF **(P)**, AERP **(Q)** and AERPd **(R)** in the rats indicated groups during the electrophysiological studies (*n* = 6 in each group). Left atrial function was measured by color Doppler echocardiography **(S)** LAESVI, **(T)** LAEF, and **(U)** LAFI in the rats indicated groups during the echocardiographic studies (*n* = 6 in each group). ***p < 0.01 VS Control, and p < 0.01 VS Ang II, #p < 0.05 VS Ang II.* Groups were compared using one-way analysis of variance (ANOVA) (Tukey's) in C to M and P to U, Fisher's exact test was used to compare groups in O, and Student's t-test was used to compare groups in **(A,B)**.

injected SD rats. However, treatment with DCA or NAHS or 4-PBA alone had no effect on the formation of atrial fibrosis, left atrial function and susceptibility to AF.

NaHS Inhibited HL-1 Apoptosis Induced by Ang II *via* Prevention of the Warburg Effect and ERS

To further determine the roles of H_2S, ERS and the Warburg effect in HL-1 cell apoptosis, we treated HL-1 cells with Ang-II in the presence or absence of NaHS, DCA or 4-PBA. We found that Ang-II significantly reduced the expression and activity of CSE in a concentration-dependent and time-dependent manner, and decreased cell viability in a time-dependent manner (**Figures 5A–C**). First, we investigated the expression of key enzymes involved in the Warburg effect and key enzymes involved in ERS, glucose consumption and ATP production, as shown in **Figure 5**. We found that Ang-II significantly increased the expression of LDH, PDK-4, p-PERK, ATF4, p-elF2α, CHOP and caspase-12 and the lactic acid content in HL-1 cells, and these changes were blocked by treatment with NaHS or DCA or 4-PBA (**Figures 5D–K**). Treatment with NaHS or DCA or 4-PBA alone did not affect the expression of LDH, PDK-4, p-PERK, ATF4, p-elF2α, CHOP and caspase-12 and the lactic acid content in HL-1 cells (**Figures 5D–K**). In addition, Ang-II significantly increased glucose consumption and decreased ATP production in HL-1 cells, and these effects were blocked by treatment with NaHS or DCA or 4-PBA (**Figures 5L,M**). Treatment of HL-1 cells with NaHS, DCA or 4-PBA alone did not affect glucose consumption or ATP production (**Figures 5L,M**). Second, using flow cytometry and CCK-8 to detect apoptosis, we further demonstrated that Ang-II significantly promoted HL-1 cell apoptosis and reduced the viability of HL-1 cells, whereas NaHS, DCA and 4-PBA significantly prevented HL-1 cell apoptosis induced by Ang II. Treatment with NaHS, DCA or

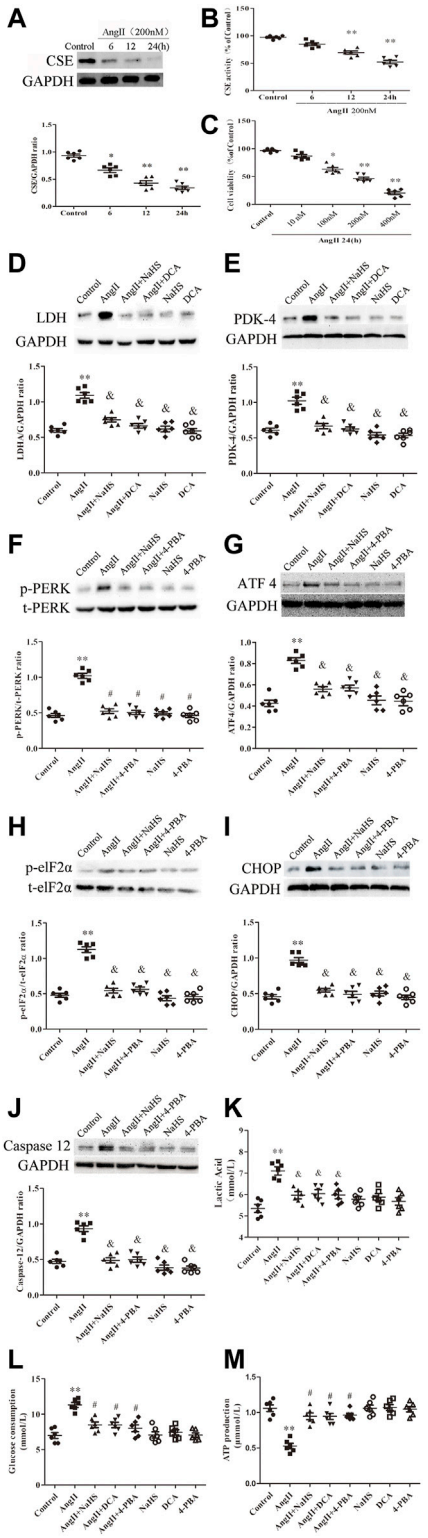

FIGURE 5 | NaHS attenuated the Warburg effect and ERS in HL-1 cells under Ang II treatment. Representative Western blotting and relative densitometry analysis of **(A)** CSE with GAPDH as a loading control induced by Ang-II concentration in the HL-1 cell of the indicated groups (n = 6 in (*Continued*)

FIGURE 5 | each group). **(B)** Detection of CSE activity by methylene blue assay in the HL-1 cell of the indicated groups (n = 6 in each group). CCK-8 was used to detect the changes in HL-1 cell viability induced by Ang II at different times **(C)** (n = 6 in each group). Representative Western blotting and relative densitometry analysis of **(F)** p-PERK with t-PERK as the loading control and **(H)** p-eIF2α with t-eIF2α as the loading control and **(D)** LDH, **(E)** PDK-4, **(G)** ATF 4, **(I)** CHOP and **(J)** caspase12 with GAPDH as the loading control in the HL-1 cell of the indicated groups (n = 6 in each group). Lactate acid **(K)** and glucose consumption **(L)** and the production of ATP **(M)** were determined by kit analysis in the HL-1 cell of the indicated groups (n = 6 in each group). $^{**}p < 0.01$ *VS Control, and* $p < 0.01$ *VS Ang II.* Groups were compared using one-way analysis of variance (ANOVA) (Tukey's) in **(A–J)**.

4-PBA alone did not affect HL-1 cell apoptosis (**Figures 6A–C**). Oxidative stress induced ERS in cardiomyocytes. In the present study, we demonstrated that Ang-II significantly increased ROS generation, carbonyl protein expression, 8-OHdG content and lipid peroxides in HL-1 cells, whereas NaHS, DCA and 4-PBA significantly blocked Ang-II-induced ROS production, carbonyl protein expression, 8-OHdG content and lipid peroxides in HL-1 cells. NaHS, DCA and 4-PBA alone did not affect ROS production, carbonyl protein expression, 8-OHdG content or lipid peroxides in HL-1 cells (**Figures 6D–N**). When mitochondria are damaged by oxidative stress, the production of ATP is reduced. To detect whether mitochondrial function was damaged, we tested mitochondrial respiratory function, including state three and four respiration, RCR and the ADP/O ratio. We observed that the state 3, RCR and ADP/O ratios in Ang II-treated HL-1 cells were significantly reduced compared with those in control HL-1 cells, and state four was significantly increased (**Figures 6O–R**). Compared with HL-1 cells in the Ang-II group, NaHS or DCA or 4-PBA treatment of HL-1 cells significantly increased RCR, ADP/O ratio and the state 3 (**Figure 6Q**) and significantly reduced the state 4 (**Figure 6R**). HL-1 cells treated with NaHS or DCA or 4-PBA alone showed no significant differences in state three or state four or RCR or the ADP/O ratio compared to control HL-1 cells (**Figures 6O–R**).

DISCUSSION

AF is a common cause of cardiovascular death and a major public health problem worldwide. Increasing research has demonstrated that atrial fibrosis is a key step leading to the development and progression of AF and is positively correlated with the Warburg effect and ERS activation (Wiersma et al., 2017; Hu et al., 2019). At the same time, the degree of atrial fibrosis is also positively correlated with atrial structural and electrophysiological remodelling. Although the mechanisms by which H_2S regulates the occurrence and development of AF have been documented, the effects of H_2S on atrial fibrosis progression to AF induced by the Warburg effect and ERS are still unknown. First, our study revealed that AF reduces serum H_2S content by inhibiting H_2S synthase and that AF can promote the Warburg effect and increase ERS in atrial tissue, with increased atrial fibrosis progression to AF. Second, compared with the sham group, the Warburg effect and ERS in the atrial tissue of AF rats

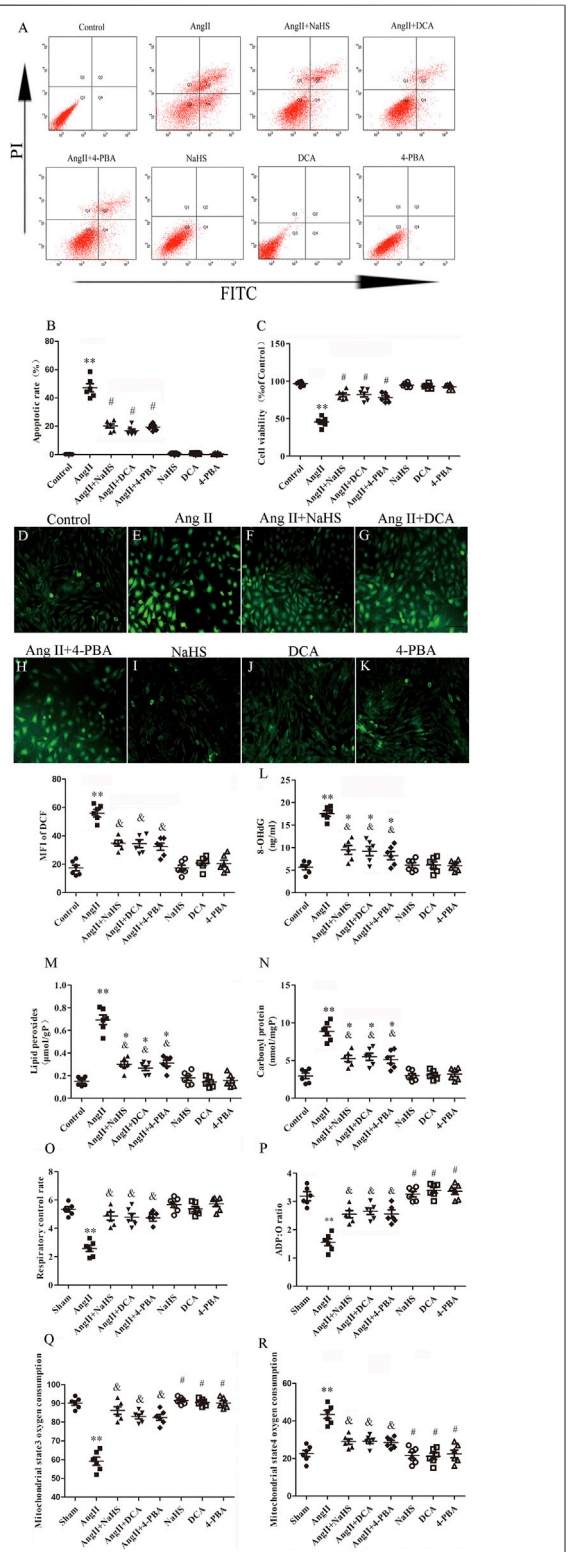

FIGURE 6 | NaHS inhibits HL-1 oxidative stress induced by Ang II and is associated with attenuation of the Warburg effect and ERS. **(A)** Red staining with representative flow cytometry and quantification of the HL-1 cell apoptotic rate **(B)** were used as indication treatments (n = 6 in each

(*Continued*)

FIGURE 6 | group). **(C)** CCK-8 was used to detect the changes in HL-1 cell viability induced by the indicated treatments (n = 6 in each group). After different treatments, ROS were measured using DCFH-DA staining followed by photofluorography (n = 6 in each group, scale bar = 50 μm) and quantitative analysis of the mean fluorescence intensity (MFI) in each group. **(D)** Control, **(E)** Ang II, **(F)** Ang II + NaHS, **(G)** Ang II + DCA, **(H)** Ang II + 4-PBA, **(I)** NaHS, **(J)** DCA and **(K)** 4-PBA. 8-OHdG **(L)**, lipid peroxides **(M)** and Carbonyl protein **(N)** were determined by kit analysis in the HL-1 cell of the indicated groups (n = 6 in each group). Mitochondrial oxygen consumption was measured using a Clark-type oxygen electrode to detect **(O)** The respiratory control rate (RCR), **(P)** The ADP/O ratio, **(Q)** The mitochondrial state3 oxygen consumption, **(R)** The mitochondrial state4 oxygen consumption in the HL-1 cell of the indicated groups (n = 6 in each group)**$p < 0.01$ VS Control, *$p < 0.05$ VS Control, and $p < 0.05$ VS Ang II, #$p < 0.01$ VS Ang II*. Groups were compared using one-way analysis of variance (ANOVA) (Tukey's) in **(D–R)**, Fisher's exact test was used to compare groups in **(B,C)**.

treated with NaHS were significantly reduced, and atrial fibrosis progression to AF was inhibited. Finally, through *in vitro* cytology experiments, we found that NaHS reduced HL-1 cell apoptosis by inhibiting the Warburg effect and ER stress occurrence in Ang-II treat HL-1 cell, manifested by improved mitochondrial function and energy metabolism impairment as well as reduced ROS generation. Collectively, these data suggest that H_2S plays a critical role in regulating atrial structural remodelling and electrical remodelling induced by the Warburg effect and ERS in AF. Our findings establish that H_2S can be used as a potential therapeutic strategy to prevent the development of AF induced by atrial fibrosis.

The heart is characterized by high energy consumption and oxygen supply and is intolerant of hypoxia. The myocardium requires a sufficient energy supply to maintain normal circulation. Mitochondrial dysfunction is one of the main features of AF. Our previous studies showed that AF leads to an increase in the atrial Warburg effect, which is closely related to atrial fibrosis and increased susceptibility to AF (Hu et al., 2019), and mitochondrial dysfunction is one of the main features of AF. Therefore, when AF occurs, the substrate of atrial energy metabolism is converted from fatty acids to glucose, and energy is provided through the Warburg effect, thereby promoting atrial fibrosis and atrial electrical remodelling and reducing the pumping function of the heart. Current research has verified that atrial fibrosis is the basis for structural remodelling and the persistence of AF. The occurrence and development of atrial fibrosis are inseparable from the excessive deposition of extracellular matrix proteins. Therefore, the balance between atrial fibrosis and anti-fibrosis is disrupted, which is reflected in high expression of collagen 1α, collagen 3α and MMP-9 in pathological results, and the response of the heart pumping function is an increase in LAESVIZ and decrease in LAEF and LAFI (Begg et al., 2017; Njoku et al., 2018). In addition, Ang II can induce left ventricular insufficiency caused by myocardial infarction or continuous progression of HF, as well as left atrial fibrosis progression to AF (Suo et al., 2019). In the current study, Western blot analysis showed that the expression of PDK-4, LDHA and MMP-9 was higher in AF patients than in SR patients. Masson staining showed that the degree of atrial fibrosis in AF patients was significantly higher

than that in SR patients. In addition, collagen 1α and collagen 3α expression and lactic acid content in the atrial tissue of AF patients were significantly higher than in SR patients, and the left atrial function indices LAESVI, LAEF and LAEI were significantly worse in AF patients than in SR patients. Combined with our previous research reports (Hu et al., 2019), the Warburg effect is related to atrial fibrosis progression to AF and can be used as a target for AF prevention and treatment.

The renin-angiotensin-aldosterone system induces the occurrence of atrial fibrosis by secreting endogenous Ang-II and is believed to play an important role in the occurrence and development of AF (Fan et al., 2015). In animal models, continuous subcutaneous stimulation with Ang II can induce atrial fibrosis in rats and promote the occurrence and development of AF (Ge et al., 2020). In addition, Ang-II induces atrial cell apoptosis, which is the basis of atrial fibrosis (Zhu et al., 2021). In addition to atrial myocytes, the heart also contains ventricular cardiomyocytes, fibroblasts, smooth muscle cells and endothelial cells. The functions of these cells are also regulated by Ang-II. For example, Ang-II has multiple effects on cardiomyocytes and cardiac fibroblasts and can cause cardiomyocyte hypertrophy, cardiac fibroblast proliferation and cardiac interstitial fibrosis. It is particularly noteworthy that interstitial fibrosis is associated with cardiac wall stiffness after myocardial infarction and HF and decreased electrical coupling of myocardial cells, thereby promoting the occurrence of AF (Zlochiver et al., 2008). In addition, endothelial cells are the most numerous cell type among cardiac mesenchymal cells and play an important role in heart remodelling. The phenotypic transition from endothelial cells to mesenchymal cells is called endothelial-to-mesenchymal transition (EndoMT), and endothelial cells mainly regulate myocardial fibrosis through EndoMT. Current studies have confirmed that Ang-II can induce excessive activation of EndoMT in endothelial cells and cause myocardial fibrosis and extracellular matrix protein accumulation (Piera-Velazquez et al., 2011; Zou et al., 2021). In our study, Masson staining showed that the atrial fibrosis in the rats in the Ang-II treatment group was significantly more serious than that in rats in the sham group, and the expression of PDK-4, LDHA, collagen Iα, collagen IIIα and MMP-9 was significantly increased, the susceptibility to AF was increased, and the left atrial function deteriorated. In the *in vitro* cell experiment, compared with the control group, the HL-1 cell activity in the Ang-II treatment group was significantly decreased, and the degree of apoptosis was significantly increased, accompanied by the expression of PDK-4 and LDHA. Whether *in vivo* or *in vitro*, the use of DCA, a specific inhibitor of the Warburg effect, significantly improved the pathophysiological changes caused by Ang-II treatment. Notably, Scientific studies have identified DCA not only reverses metabolic derangements but also effectively targets mitochondrial related pathways of apoptosis, and significantly improve cardiomyocyte apoptosis and myocardial fibrosis in rats with right ventricular cardiomyopathy (Sun et al., 2016). Our previous research results show that DCA alone will not increase atrial fibrosis in normal dogs (Hu et al., 2019). Then, we further explored the relationship between the Warburg effect and atrial fibrosis caused by atrial cell apoptosis.

Disruption of ER homeostasis triggers ERS, which can be restored by activating the UPR in the short term. Activation of CHOP by the upstream PERK-eIF2α-ATF4 axis plays an important role in ERS-related apoptosis in cardiomyocytes (Fels and Koumenis, 2006). CHOP activates a series of signal transduction pathways to upregulate the expression of caspase-3, ultimately leading to apoptosis (Feng et al., 2019). When the myocardium develops lesions, the oxidation of beta fatty acids is limited, and instead these fatty acids provide energy for glucose metabolism. In the myocardium of diabetic rats, disturbed glucose metabolism leads to downregulation of the expression of glycometabolic proteins, such as PPARα and PGC-1α, which in turn activate the expression of p-PERK, p-eIF2α, ATF6, CHOP and ATF4, suggesting that disturbed glucose metabolism is a key step in the activation of myocardial ERS (Lakshmanan et al., 2013). In the AF state, myocardial tissue obtains energy through the Warburg effect, leading to tissue microenvironment acidosis. On the one hand, acidosis can directly reduce the activity of myocardial ER and further aggravate the occurrence of ERS and cardiac fibrosis and remodelling (Glembotski et al., 2012; Yong et al., 2019); on the other hand, acidosis can induce ERS in many cell types; for example, acidosis can lead to ERS and induce cardiac fibrosis in patients with HF (Schaffer and Kim, 2018). It should be noted that ERS is involved in the occurrence of AF (Wiersma et al., 2017). In our study, Western blotting analysis revealed that the expression of the p-PERK-p-eIF2-α-ATF4-CHOP-Caspase 12 axis in the left atrial tissue of patients with atrial fibrillation was significantly increased compared with that in SR patients and that Ang-II treatment significantly increased the expression of the p-PERK-p-eIF2-α-ATF4-CHOP-Caspase 12 axis in rat left atrium tissue and HL-1 cells. The ERS-specific inhibitor 4-PBA inhibited the Ang-II-induced p-PERK-p-eIF2-α-ATF4-CHOP-Caspase 12-axis expression in HL-1 cells and rat left atrial tissue, improving atrial fibrosis, AF susceptibility and deterioration of left atrial function and reducing HL-1 cell apoptosis. 4-PBA has been approved by the U.S. Food and Drug Administration (FDA) as an ammonia scavenger for children with urea cycle disorders. It is a low molecular weight fatty acid and non-toxic pharmacological compound, and has been proved to promote myocardial repair and prevent myocardial fibrosis after MI (Luo et al., 2015). Therefore, the use of 4-PBA alone will not lead to myocardial fibrosis.

Alterations in mitochondrial energy metabolism contribute to the development of cardiac fibrosis-related diseases (Mihm et al., 2007). Glucose, the other major energy substrate of the heart, is oxidized via glycolysis and converted into energy in the mitochondria. Our previous study showed mitochondrial tricarboxylic acid cycle dysfunction in the development of AF, and such changes resulted in increased myocardial O2 consumption and reduced cardiac efficiency (Yamada et al., 2006). In addition, mitochondria are the main production site of ROS, and mitochondrial proteins, lipids, and mtDNA are considered the main targets of oxidative damage after excessive release of mitochondrial ROS. Moreover, when mitochondrial ROS are abundantly produced, they can induce a large release of

Ca^{2+} into the cytoplasm, causing the occurrence of ER stress and promoting mitochondrial membrane permeability transition pore opening, which allows cytoplasmic Ca^{2+} to enter the mitochondria and further accumulate, creating a vicious cycle (Harisseh et al., 2019). The current study revealed that Ang-II increased mitochondrial oxidative stress and mtDNA damage in cardiomyocytes and interstitial cells, leading to cardiac fibrogenesis, cardiac hypertrophy, and apoptosis (Meng et al., 2018). In this study, we also confirmed that Ang-II induced the expression of reactive oxygen species, carbonyl proteins, 8-OHdG, and lipid peroxides; promoted a significant increase in cardiomyocyte apoptosis; and impaired mitochondrial respiratory function and energy metabolism in HL-1 cells. This suggests that both the Warburg effect and ER stress ultimately occur in response to mitochondrial oxidative stress that causes cardiomyocyte injury and thus effectively protect cardiomyocytes from oxidative damage, which is the direction of our further in-depth research.

Endogenous H_2S is the final metabolite produced by H_2S synthase in the body to convert sulfur-containing amino acids. It exists in gaseous form and as dissolved NaHS. NaHS can be hydrolysed into Na^+ and HS^- in the body, the latter of which can produce H_2S. The current research on the role of H_2S in animal models uses the exogenous H_2S donor NaHS, which can be used to increase the level of H_2S in plasma and the content of H_2S in the myocardium. In recent years, it has been generally believed that H_2S exerts cardioprotective effects through antiapoptotic, anti-inflammatory and antifibrotic properties, especially in CHD, HF, AF and other diseases characterized by myocardial fibrosis. Our current research combined with our previous research reports (Hu et al., 2019) found that both Warburg effect and ERS can lead to atrial myocyte apoptosis, which is closely related to the inflammatory damage caused by oxidative stress. Therefore, this is one of the main ways to explore whether H_2S can improve the occurrence of AF. First, we compared the difference between H_2S synthase and H_2S content in patients with AF and SR. Studies have shown that when AF occurs, stable sulfides stored in the mitochondria are mobilized to generate free sulfides in the blood and used to counteract myocardial damage caused by oxidative stress (Watts et al., 2021). Therefore, the longer the AF occurs, the more the long-term stable sulfide storage reserve is exhausted, resulting in a decrease in the H_2S content in the plasma and an intensified oxidative stress response, thereby aggravating the occurrence of atrial fibrosis (Watts et al., 2021). Our study also confirmed lower CSE expression and significantly higher atrial fibrosis in AF atrial tissue than in SR atrial tissue. Interestingly, the CBS levels in AF patients were significantly higher than those in SR patients, which may be related to CSE and CBS feedback regulation (Nandi and Mishra, 2017). We often think that CBS is mainly expressed in the nervous system, but current studies have confirmed that this enzyme also exists in the cardiovascular system and exerts a cardiovascular protective effect (Bucci et al., 2014). When glucose metabolism is abnormal, CBS is upregulated in myocardial tissue and myocardial interstitial tissue. Unfortunately, this increase in CBS is not sufficient to cause an increase in overall H_2S production. In contrast, because the expression of CSE and 3-MST is reduced, the overall H_2S content is still low; thus, myocardial fibrosis is still developing at this time (Jin et al., 2015). In the SD rat model, we also further confirmed that SD rats treated with Ang-II can significantly reduce the expression of CSE and 3-MST, increase the expression of CBS, and increase the occurrence of atrial fibrosis. Regrettably, although the expression of CBS increased, the content of H_2S in the plasma of SD rats induced by Ang-II did not increase significantly, but decreased, which is consistent with the study of Watts (Watts et al., 2021). It is suggested that CSE is the main synthase of H_2S in the cardiovascular system, and the decrease of H_2S content induced by Ang-II is closely related to atrial fibrosis.

Previous studies have reported that db/db mice are susceptible to diabetic cardiomyopathy, which is related to the decrease of H_2S content in the circulation and glucose metabolism disorders (Sun et al., 2018). H_2S can improve mitochondrial function and glycolysis and promote aerobic oxidation of glucose in mitochondria to provide energy. It is worth noting that when mitochondrial dysfunction occurs, the tricarboxylic acid cycle is inhibited, thereby promoting the remodelling of myocardial fibrosis, which is manifested by upregulation of MMP-9 and collagen I expression (Liang et al., 2015). At this time, tricarboxylic acid cycle disorder can also activate autophagy-related proteins and ERS to promote myocardial fibrosis, and this pathophysiological effect of mitochondrial dysfunction can be reversed by NaHS (Kumar et al., 2019; Nie et al., 2021). Ang-II inhibits miR-133a and induces mitochondrial oxidative stress and mtDNA damage in cardiomyocytes, and these Ang-II-induced pathophysiological effects can also be reversed by NaHS (Ceylan-Isik et al., 2013; Su et al., 2021). Our previous research results show that the Warburg effect inhibits the key enzymes of TCA and causes the occurrence of AF (Hu et al., 2019). However, the significantly increases expression of PDK-4, a key Warburg effect enzyme, is the key to this change. PDK-4 has strong activity in glucose metabolism disorders, can activate AF and inhibit the expression of MMP genes, and promote the synthesis of extracellular matrix (Ding et al., 2017). Based on this finding, we found that exogenous H_2S supplementation can significantly reduce the expression of PDK-4 induced by Ang-II and improve the Warburg effect, which is manifested by reducing the expression of LDHA, reducing the content of lactic acid and abnormal glucose consumption, and increasing the production of ATP. PDK4 is not only a key enzyme of the Warburg effect, but also an important mitochondrial matrix enzyme in cell energy regulation, and is closely related to mitochondrial function. The high expression of PDK-4 leads to the increase of local tissue lactic acid content, which causes the expression of a variety of ERS genes, such as the expression of CHOP, ATF4 and p-eIF2α (Dong et al., 2017; Ma et al., 2020). Consistent with those study, our research shows that H_2S can improve the Warburg effect and mitochondrial function by inhibiting PDK-4 expression, reducing mitochondrial ROS and oxidative stress, and it's also by inhibiting p-PERK-p-eIF2-α-ATF4 -CHOP-Caspase12 axis to reduce the occurrence of ERS and atrial muscle cell apoptosis, thereby improving the progression of atrial fibrosis to AF.

Current research shows that ROS-induced oxidation of ryanodine receptors promotes SR calcium leakage and AF (Xie

et al., 2015). Impaired glucose metabolism also leads to mitochondrial oxidative stress, which causes increased MMP-9 expression to promote impaired left atrial function and cause AF (Liang et al., 2018; Gong et al., 2020). In the atria of CSE-KO mice, the level of superoxide was found to increase, which was negatively correlated with changes in H_2S content and positively correlated with atrial action potential and AF inducibility (Watts et al., 2021). In addition, ROS can cause atrial electrical remodelling by activating the ultrafast outward rectifying potassium current (Ikur), thereby causing AF (Christophersen et al., 2013). It is worth noting that even in myocardium with impaired glucose metabolism, oxidative stress and related structural remodelling are the basis of abnormal electrical activity. H_2S improves mitochondrial oxidative stress, respiratory dysfunction, and reduces apoptosis in HL-1 cells caused by glucose metabolism disorder, and in turn can improve atrial function in mice (Garcia et al., 2017; Lee et al., 2019). This has similar effects to reducing oxidative stress to inhibit HL-1 cell apoptosis and improve left atrial structural remodelling induced by AF in mice (Johnston et al., 1990). Moreover, studies have confirmed that H_2S can reduce the instantaneous outward potassium current, maintain the stability of cardiac electrical activity, and shorten the action potential of rat atrial myocytes caused by H_2S deficiency but does not affect normal atrial electrical activity, so as to improve the occurrence of atrial fibrillation. This phenomenon has also been proved in the mouse atrial fibrillation model (Sheng et al., 2013; Xue et al., 2020; Watts et al., 2021). In our study, the reduction in H_2S levels was related to the Warburg effect in the atrium and the activation of endoplasmic reticulum stress to induce oxidative stress and led to an increase in susceptibility to AF. Supplementation with H_2S can significantly reduce oxidative stress and improve susceptibility to AF.

In summary, H_2S has been shown to improve left atrial dysfunction and AF susceptibility by inhibiting AngII-induced Warburg effect and ERS-induced atrial fibrosis, thereby reducing the occurrence and development of AF. Our research also provides a new strategy involving the use of H_2S synthase as a key factor in the diagnosis and treatment of atrial fibrosis-related AF and as a new therapeutic target for these diseases. First, there may be other signalling pathways that regulate the Warburg effect and ERS-related atrial fibrosis, such as the MAPK pathway. Whether H_2S regulates the Warburg effect and endoplasmic reticulum stress through signalling pathways affecting atrial fibrosis should be determined in further studies. In addition, we did not conduct high and low expression studies on endogenous H_2S synthase. Therefore, to obtain more convincing results, a sufficient number of rats with conditional cardiac knockout and high expression should be created in subsequent studies.

DATA AVAILABILITY STATEMENT

The original contributions presented in the study are included in the article/supplementary material; further inquiries can be directed to the corresponding author.

ETHICS STATEMENT

The studies involving human participants were reviewed and approved by the ethics committee of the First Affiliated Hospital of University of South China. The patients/participants provided their written informed consent to participate in this study. The animal study was reviewed and approved by the ethics committee of the First Affiliated Hospital of University of South China. Written informed consent was obtained from the owners for the participation of their animals in this study. Written informed consent was obtained from the individual(s) for the publication of any potentially identifiable images or data included in this article.

AUTHOR CONTRIBUTIONS

H-JH and Z-SJ coordinated and led the experimental design and participated in the manuscript writing. H-JH, X-HW, YL, T-QZ, Z-RC, CZ, Z-HT, and S-LQ were tested. H-JH and H-FT conducted literature search, and completed the verification and revision of important knowledge content. H-JH and Z-SJ conducted the final verification and proofreading of the article, and were responsible for confirming the authenticity of the data in this section. All authors have read and approved the final manuscript.

FUNDING

The present work was supported by grants from the National Natural Science Foundation of China (Grant no. 81700306), the Natural Science Foundation of Hunan Province (Grant no. 2018JJ3469), the China Postdoctoral Science Foundation (Grant no. 2017M622588), the Key Project of Hunan provincial science and technology innovation (Grant no. 2020SK1013-2), and the Scientific Research Fund Project of Hunan Provincial Health Commission (Grant no. 20201920).

SUPPLEMENTARY MATERIAL

The Supplementary Material for this article can be found online at: https://www.frontiersin.org/articles/10.3389/fphar.2021.690371/full#supplementary-material

REFERENCES

Begg, G. A., Karim, R., Oesterlein, T., Graham, L. N., Hogarth, A. J., Page, S. P., et al. (2017). Intra-cardiac and Peripheral Levels of Biochemical Markers of Fibrosis in Patients Undergoing Catheter Ablation for Atrial Fibrillation. *Europace* 19 (12), 1944–1950. doi:10.1093/europace/euw315

Beltowski, J. (2015). Hydrogen Sulfide in Pharmacology and Medicine--An Update. *Pharmacol. Rep.* 67 (3), 647–658. doi:10.1016/j.pharep.2015.01.005

Bucci, M., Vellecco, V., Cantalupo, A., Brancaleone, V., Zhou, Z., Evangelista, S., et al. (2014). Hydrogen Sulfide Accounts for the Peripheral Vascular Effects of Zofenopril Independently of ACE Inhibition. *Cardiovasc. Res.* 102 (1), 138–147. doi:10.1093/cvr/cvu026

Ceylan-Isik, A. F., Kandadi, M. R., Xu, X., Hua, Y., Chicco, A. J., Ren, J., et al. (2013). Apelin Administration Ameliorates High Fat Diet-Induced Cardiac Hypertrophy and Contractile Dysfunction. *J. Mol. Cel Cardiol* 63, 4–13. doi:10.1016/j.yjmcc.2013.07.002

Chan, Y. H., Chang, G. J., Lai, Y. J., Chen, W. J., Chang, S. H., Hung, L. M., et al. (2019). Atrial Fibrillation and its Arrhythmogenesis Associated with Insulin Resistance. *Cardiovasc. Diabetol.* 18 (1), 125. doi:10.1186/s12933-019-0928-8

Christophersen, I. E., Olesen, M. S., Liang, B., Andersen, M. N., Larsen, A. P., Nielsen, J. B., et al. (2013). Genetic Variation in KCNA5: Impact on the Atrial-specific Potassium Current IKur in Patients with Lone Atrial Fibrillation. *Eur. Heart J.* 34 (20), 1517–1525. doi:10.1093/eurheartj/ehs442

Christophersen, I. E., Rienstra, M., Roselli, C., Yin, X., Geelhoed, B., Barnard, J., et al. (2017). Large-scale Analyses of Common and Rare Variants Identify 12 New Loci Associated with Atrial Fibrillation. *Nat. Genet.* 49 (6), 946–952. doi:10.1038/ng.3843

Cottrill, K. A., and Chan, S. Y. (2013). Metabolic Dysfunction in Pulmonary Hypertension: the Expanding Relevance of the Warburg Effect. *Eur. J. Clin. Invest.* 43 (8), 855–865. doi:10.1111/eci.12104

Deshmukh, A., Barnard, J., Sun, H., Newton, D., Castel, L., Pettersson, G., et al. (2015). Left Atrial Transcriptional Changes Associated with Atrial Fibrillation Susceptibility and Persistence. *Circ. Arrhythm Electrophysiol.* 8 (1), 32–41. doi:10.1161/CIRCEP.114.001632

Ding, H., Jiang, L., Xu, J., Bai, F., Zhou, Y., Yuan, Q., et al. (2017). Inhibiting Aerobic Glycolysis Suppresses Renal Interstitial Fibroblast Activation and Renal Fibrosis. *Am. J. Physiol. Ren. Physiol* 313 (3), F561–F575. doi:10.1152/ajprenal.00036.2017

Dong, L., Krewson, E. A., and Yang, L. V. (2017). Acidosis Activates Endoplasmic Reticulum Stress Pathways through GPR4 in Human Vascular Endothelial Cells. *Int. J. Mol. Sci.* 18 (2), 278. doi:10.3390/ijms18020278

Ellmers, L. J., Templeton, E. M., Pilbrow, A. P., Frampton, C., Ishii, I., Moore, P. K., et al. (2020). Hydrogen Sulfide Treatment Improves Post-Infarct Remodeling and Long-Term Cardiac Function in CSE Knockout and Wild-type Mice. *Int. J. Mol. Sci.* 21 (12), 4284. doi:10.3390/ijms21124284

Fan, J., Zou, L., Cui, K., Woo, K., Du, H., Chen, S., et al. (2015). Atrial Overexpression of Angiotensin-Converting Enzyme 2 Improves the Canine Rapid Atrial Pacing-Induced Structural and Electrical Remodeling. Fan, ACE2 Improves Atrial Substrate Remodeling. *Basic Res. Cardiol.* 110 (4), 45. doi:10.1007/s00395-015-0499-0

Fels, D. R., and Koumenis, C. (2006). The PERK/eIF2alpha/ATF4 Module of the UPR in Hypoxia Resistance and Tumor Growth. *Cancer Biol. Ther.* 5 (7), 723–728. doi:10.4161/cbt.5.7.2967

Feng, K., Ge, Y., Chen, Z., Li, X., Liu, Z., Li, X., et al. (2019). Curcumin Inhibits the PERK-eIF2α-CHOP Pathway through Promoting SIRT1 Expression in Oxidative Stress-Induced Rat Chondrocytes and Ameliorates Osteoarthritis Progression in a Rat Model. *Oxid Med. Cel Longev* 2019, 8574386. doi:10.1155/2019/8574386

Garcia, N. A., Moncayo-Arlandi, J., Vazquez, A., Genovés, P., Calvo, C. J., Millet, J., et al. (2017). Hydrogen Sulfide Improves Cardiomyocyte Function in a Cardiac Arrest Model. *Ann. Transpl.* 22, 285–295. doi:10.12659/aot.901410

Ge, Z., Chen, Y., Wang, B., Zhang, X., Yan, Y., Zhou, L., et al. (2020). MFGE8 Attenuates Ang-II-Induced Atrial Fibrosis and Vulnerability to Atrial Fibrillation through Inhibition of TGF-β1/Smad2/3 Pathway. *J. Mol. Cel Cardiol* 139, 164–175. doi:10.1016/j.yjmcc.2020.01.001

George, A. K., Behera, J., Kelly, K. E., Zhai, Y., and Tyagi, N. (2017). Hydrogen Sulfide, Endoplasmic Reticulum Stress and Alcohol Mediated Neurotoxicity. *Brain Res. Bull.* 130, 251–256. doi:10.1016/j.brainresbull.2017.02.002

Glembotski, C. C., Thuerauf, D. J., Huang, C., Vekich, J. A., Gottlieb, R. A., and Doroudgar, S. (2012). Mesencephalic Astrocyte-Derived Neurotrophic Factor Protects the Heart from Ischemic Damage and Is Selectively Secreted upon Sarco/endoplasmic Reticulum Calcium Depletion. *J. Biol. Chem.* 287 (31), 25893–25904. doi:10.1074/jbc.M112.356345

Gong, M., Yuan, M., Meng, L., Zhang, Z., Tse, G., Zhao, Y., et al. (2020). Wenxin Keli Regulates Mitochondrial Oxidative Stress and Homeostasis and Improves Atrial Remodeling in Diabetic Rats. *Oxid Med. Cel Longev* 2020, 2468031. doi:10.1155/2020/2468031

Gowd, B. M., and Thompson, P. D. (2012). Effect of Female Sex on Cardiac Arrhythmias. *Cardiol. Rev.* 20 (6), 297–303. doi:10.1097/CRD.0b013e318259294b

Gu, M., Wang, J., Wang, Y., Xu, Y., Zhang, Y., Wu, W., et al. (2018). MiR-147b Inhibits Cell Viability and Promotes Apoptosis of Rat H9c2 Cardiomyocytes via Down-Regulating KLF13 Expression. *Acta Biochim. Biophys. Sin (Shanghai)* 50 (3), 288–297. doi:10.1093/abbs/gmx144

Han, M., Zhang, Y., Sun, S., Wang, Z., Wang, J., Xie, X., et al. (2013). Renin-angiotensin System Inhibitors Prevent the Recurrence of Atrial Fibrillation: a Meta-Analysis of Randomized Controlled Trials. *J. Cardiovasc. Pharmacol.* 62 (4), 405–415. doi:10.1097/FJC.0b013e3182a094a1

Harisseh, R., Abrial, M., Chiari, P., Al-Mawla, R., Villedieu, C., Tessier, N., et al. (2019). A Modified Calcium Retention Capacity Assay Clarifies the Roles of Extra- and Intracellular Calcium Pools in Mitochondrial Permeability Transition Pore Opening. *J. Biol. Chem.* 294 (42), 15282–15292. doi:10.1074/jbc.RA119.009477

Hu, H. J., Zhang, C., Tang, Z. H., Qu, S. L., and Jiang, Z. S. (2019). Regulating the Warburg Effect on Metabolic Stress and Myocardial Fibrosis Remodeling and Atrial Intracardiac Waveform Activity Induced by Atrial Fibrillation. *Biochem. Biophys. Res. Commun.* 516 (3), 653–660. doi:10.1016/j.bbrc.2019.06.055

Hu, H. J., Qiu, J., Zhang, C., Tang, Z. H., Qu, S. L., and Jiang, Z. S. (2021). Hydrogen Sulfide Improves oxLDLinduced Expression Levels of LpPLA2 in THP1 Monocytes via the p38MAPK Pathway. *Mol. Med. Rep.* 23 (5), 358. doi:10.3892/mmr.2021.11997

Imle, R., Wang, B. T., Stützenberger, N., Birkenhagen, J., Tandon, A., Carl, M., et al. (2019). ADP-dependent Glucokinase Regulates Energy Metabolism via ER-Localized Glucose Sensing. *Sci. Rep.* 9 (1), 14248. doi:10.1038/s41598-019-50566-6

Jin, S., Pu, S. X., Hou, C. L., Ma, F. F., Li, N., Li, X. H., et al. (2015). Cardiac H2S Generation Is Reduced in Ageing Diabetic Mice. *Oxid Med. Cel Longev* 2015, 758358. doi:10.1155/2015/758358

Johnston, J. B., Israels, L. G., Goldenberg, G. J., Anhalt, C. D., Verburg, L., Mowat, M. R., et al. (1990). Glutathione S-Transferase Activity, Sulfhydryl Group and Glutathione Levels, and DNA Cross-Linking Activity with Chlorambucil in Chronic Lymphocytic Leukemia. *J. Natl. Cancer Inst.* 82 (9), 776–779. doi:10.1093/jnci/82.9.776

Kumar, A., Davuluri, G., Welch, N., Kim, A., Gangadhariah, M., Allawy, A., et al. (2019). Oxidative Stress Mediates Ethanol-Induced Skeletal Muscle Mitochondrial Dysfunction and Dysregulated Protein Synthesis and Autophagy. *Free Radic. Biol. Med.* 145, 284–299. doi:10.1016/j.freeradbiomed.2019.09.031

Lakshmanan, A. P., Harima, M., Suzuki, K., Soetikno, V., Nagata, M., Nakamura, T., et al. (2013). The Hyperglycemia Stimulated Myocardial Endoplasmic Reticulum (ER) Stress Contributes to Diabetic Cardiomyopathy in the Transgenic Non-obese Type 2 Diabetic Rats: a Differential Role of Unfolded Protein Response (UPR) Signaling Proteins. *Int. J. Biochem. Cel Biol* 45 (2), 438–447. doi:10.1016/j.biocel.2012.09.017

Lee, M. A., Raad, N., Song, M. H., Yoo, J., Lee, M., Jang, S. P., et al. (2020). The Matricellular Protein CCN5 Prevents Adverse Atrial Structural and Electrical Remodelling. *J. Cel Mol Med* 24 (20), 11768–11778. doi:10.1111/jcmm.15789

Lee, T. I., Kao, Y. H., Baigalmaa, L., Lee, T. W., Lu, Y. Y., Chen, Y. C., et al. (2019). Sodium Hydrosulphide Restores Tumour Necrosis Factor-α-Induced Mitochondrial Dysfunction and Metabolic Dysregulation in HL-1 Cells. *J. Cel Mol Med* 23 (11), 7641–7650. doi:10.1111/jcmm.14637

Leffler, C. W., Parfenova, H., Jaggar, J. H., and Wang, R. (2006). Carbon Monoxide and Hydrogen Sulfide: Gaseous Messengers in Cerebrovascular Circulation. *J. Appl. Physiol.* 100 (3), 1065–1076. doi:10.1152/japplphysiol.00793.2005

Li, C., Zhang, J., Xue, M., Li, X., Han, F., Liu, X., et al. (2019). SGLT2 Inhibition with Empagliflozin Attenuates Myocardial Oxidative Stress and Fibrosis in Diabetic Mice Heart. *Cardiovasc. Diabetol.* 18 (1), 15. doi:10.1186/s12933-019-0816-2

Li, X., Liu, J., Hu, H., Lu, S., Lu, Q., Quan, N., et al. (2019). Dichloroacetate Ameliorates Cardiac Dysfunction Caused by Ischemic Insults through AMPK Signal Pathway-Not Only Shifts Metabolism. *Toxicol. Sci.* 167 (2), 604–617. doi:10.1093/toxsci/kfy272

Li, Y., Ren, S., Xia, J., Wei, Y., and Xi, Y. (2020). EIF4A3-Induced Circ-BNIP3 Aggravated Hypoxia-Induced Injury of H9c2 Cells by Targeting miR-27a-3p/BNIP3. *Mol. Ther. Nucleic Acids* 19, 533–545. doi:10.1016/j.omtn.2019.11.017

Liang, M., Jin, S., Wu, D. D., Wang, M. J., and Zhu, Y. C. (2015). Hydrogen Sulfide Improves Glucose Metabolism and Prevents Hypertrophy in Cardiomyocytes. *Nitric Oxide* 46, 114–122. doi:10.1016/j.niox.2014.12.007

Liang, X., Zhang, Q., Wang, X., Yuan, M., Zhang, Y., Xu, Z., et al. (2018). Reactive Oxygen Species Mediated Oxidative Stress Links Diabetes and Atrial Fibrillation. *Mol. Med. Rep.* 17 (4), 4933–4940. doi:10.3892/mmr.2018.8472

Luo, T., Kim, J. K., Chen, B., Abdel-Latif, A., Kitakaze, M., and Yan, L. (2015). Attenuation of ER Stress Prevents post-infarction-induced Cardiac Rupture and Remodeling by Modulating Both Cardiac Apoptosis and Fibrosis. *Chem. Biol. Interact* 225, 90–98. doi:10.1016/j.cbi.2014.10.032

Luoma, P. V. (2013). Elimination of Endoplasmic Reticulum Stress and Cardiovascular, Type 2 Diabetic, and Other Metabolic Diseases. *Ann. Med.* 45 (2), 194–202. doi:10.3109/07853890.2012.700116

Ma, W. Q., Sun, X. J., Zhu, Y., and Liu, N. F. (2020). PDK4 Promotes Vascular Calcification by Interfering with Autophagic Activity and Metabolic Reprogramming. *Cell Death Dis* 11 (11), 991. doi:10.1038/s41419-020-03162-w

McMurray, J. J., Adamopoulos, S., Anker, S. D., Auricchio, A., Böhm, M., Dickstein, K., et al. (2012). ESC Guidelines for the Diagnosis and Treatment of Acute and Chronic Heart Failure 2012: The Task Force for the Diagnosis and Treatment of Acute and Chronic Heart Failure 2012 of the European Society of Cardiology. Developed in Collaboration with the Heart Failure Association (HFA) of the ESC. *Eur. J. Heart Fail.* 14 (14), 803–869. doi:10.1093/eurjhf/hfs105

Meng, G., Liu, J., Liu, S., Song, Q., Liu, L., Xie, L., et al. (2018). Hydrogen Sulfide Pretreatment Improves Mitochondrial Function in Myocardial Hypertrophy via a SIRT3-dependent Manner. *Br. J. Pharmacol.* 175 (8), 1126–1145. doi:10.1111/bph.13861

Mihm, M. J., Amann, D. M., Schanbacher, B. L., Altschuld, R. A., Bauer, J. A., and Hoyt, K. R. (2007). Cardiac Dysfunction in the R6/2 Mouse Model of Huntington's Disease. *Neurobiol. Dis.* 25 (2), 297–308. doi:10.1016/j.nbd.2006.09.016

Nandi, S. S., and Mishra, P. K. (2017). H2S and Homocysteine Control a Novel Feedback Regulation of Cystathionine Beta Synthase and Cystathionine Gamma Lyase in Cardiomyocytes. *Sci. Rep.* 7 (1), 3639. doi:10.1038/s41598-017-03776-9

Ni, Y., Deng, J., Liu, X., Li, Q., Zhang, J., Bai, H., et al. (2021). Echinacoside Reverses Myocardial Remodeling and Improves Heart Function via Regulating SIRT1/FOXO3a/MnSOD axis in HF Rats Induced by Isoproterenol. *J. Cel Mol Med* 25 (1), 203–216. doi:10.1111/jcmm.15904

Nie, L., Liu, M., Chen, J., Wu, Q., Li, Y., Yi, J., et al. (2021). Hydrogen Sulfide Ameliorates Doxorubicininduced Myocardial Fibrosis in Rats via the PI3K/AKT/mTOR Pathway. *Mol. Med. Rep.* 23 (4), 299. doi:10.3892/mmr.2021.11938

Njoku, A., Kannabhiran, M., Arora, R., Reddy, P., Gopinathannair, R., Lakkireddy, D., et al. (2018). Left Atrial Volume Predicts Atrial Fibrillation Recurrence after Radiofrequency Ablation: a Meta-Analysis. *Europace* 20 (1), 33–42. doi:10.1093/europace/eux013

Pan, L. L., Liu, X. H., Gong, Q. H., Yang, H. B., and Zhu, Y. Z. (2012). Role of Cystathionine γ-lyase/hydrogen Sulfide Pathway in Cardiovascular Disease: a Novel Therapeutic Strategy. *Antioxid. Redox Signal.* 17 (1), 106–118. doi:10.1089/ars.2011.4349

Pan, L. L., Wang, X. L., Wang, X. L., and Zhu, Y. Z. (2014). Sodium Hydrosulfide Prevents Myocardial Dysfunction through Modulation of Extracellular Matrix Accumulation and Vascular Density. *Int. J. Mol. Sci.* 15 (12), 23212–23226. doi:10.3390/ijms151223212

Piatek, J., Konstanty-Kalandyk, J., Kedziora, A., Hyochan Song, B., Wierzbicki, K., Darocha, T., et al. (2016). Total Arterial Myocardial Revascularization in Patients over 70 Years Old - a New Trend in Coronary Surgery in Elderly. *Przegl Lek* 73 (11), 813–815.

Piera-Velazquez, S., Li, Z., and Jimenez, S. A. (2011). Role of Endothelial-Mesenchymal Transition (EndoMT) in the Pathogenesis of Fibrotic Disorders. *Am. J. Pathol.* 179 (3), 1074–1080. doi:10.1016/j.ajpath.2011.06.001

Ren, L., Wang, Q., Chen, Y., Ma, Y., and Wang, D. (2019). Involvement of MicroRNA-133a in the Protective Effect of Hydrogen Sulfide against Ischemia/Reperfusion-Induced Endoplasmic Reticulum Stress and Cardiomyocyte Apoptosis. *Pharmacology* 103 (1-2), 1–9. doi:10.1159/000492969

Schaffer, S., and Kim, H. W. (2018). Effects and Mechanisms of Taurine as a Therapeutic Agent. *Biomol. Ther. (Seoul)* 26 (3), 225–241. doi:10.4062/biomolther.2017.251

Sheng, J., Shim, W., Wei, H., Lim, S. Y., Liew, R., Lim, T. S., et al. (2013). Hydrogen Sulphide Suppresses Human Atrial Fibroblast Proliferation and Transformation to Myofibroblasts. *J. Cel Mol Med* 17 (10), 1345–1354. doi:10.1111/jcmm.12114

Si, H., Lei, Z., Han, C., Wu, Z., and Li, S. (2018). Evaluation of Body Surface Area Formulae for Scaling GFR of Adult Renal Patients: More Between-Subject Variability Explained by the DuBois & DuBois Formula. *Q. J. Nucl. Med. Mol. Imaging* 62 (2), 185–189. doi:10.23736/S1824-4785.16.02714-X

Snijder, P. M., de Boer, R. A., Bos, E. M., van den Born, J. C., Ruifrok, W. P., Vreeswijk-Baudoin, I., et al. (2013). Gaseous Hydrogen Sulfide Protects against Myocardial Ischemia-Reperfusion Injury in Mice Partially Independent from Hypometabolism. *PLoS One* 8 (5), e63291. doi:10.1371/journal.pone.0063291

Song, S., Zhang, R., Mo, B., Chen, L., Liu, L., Yu, Y., et al. (2019). EZH2 as a Novel Therapeutic Target for Atrial Fibrosis and Atrial Fibrillation. *J. Mol. Cel Cardiol* 135, 119–133. doi:10.1016/j.yjmcc.2019.08.003

Spiers, D. E., and Candas, V. (1984). Relationship of Skin Surface Area to Body Mass in the Immature Rat: a Reexamination. *J. Appl. Physiol. Respir. Environ. Exerc. Physiol.* 56 (1), 240–243. doi:10.1152/jappl.1984.56.1.240

Su, H., Su, H., Liu, C. H., Hu, H. J., Zhao, J. B., Zou, T., et al. (2021). H2S Inhibits Atrial Fibrillation-Induced Atrial Fibrosis through miR-133a/CTGF axis. *Cytokine* 146, 155557. doi:10.1016/j.cyto.2021.155557

Sun, M., Zhao, W., Li, S., Li, C., Feng, Y., and Geng, D. (2019). Gastric Sleeve Surgery Alleviates Obesity-Associated Insulin Resistance and Suppresses Endoplasmic Reticulum Stress in Adipose Tissue of Db/db Mice. *Obes. Surg.* 29 (10), 3220–3227. doi:10.1007/s11695-019-03966-6

Sun, X. Q., Zhang, R., Zhang, H. D., Yuan, P., Wang, X. J., Zhao, Q. H., et al. (2016). Reversal of Right Ventricular Remodeling by Dichloroacetate Is Related to Inhibition of Mitochondria-dependent Apoptosis. *Hypertens. Res.* 39 (5), 302–311. doi:10.1038/hr.2015.153

Sun, Y., Tian, Z., Liu, N., Zhang, L., Gao, Z., Sun, X., et al. (2018). Exogenous H2S Switches Cardiac Energy Substrate Metabolism by Regulating SIRT3 Expression in Db/db Mice. *J. Mol. Med. (Berl)* 96 (3-4), 281–299. doi:10.1007/s00109-017-1616-3

Suo, Y., Yuan, M., Li, H., Zhang, Y., Li, Y., Fu, H., et al. (2019). Sacubitril/Valsartan Improves Left Atrial and Left Atrial Appendage Function in Patients with Atrial Fibrillation and in Pressure Overload-Induced Mice. *Front. Pharmacol.* 10, 1285. doi:10.3389/fphar.2019.01285

Thakur, A., Alam, M. J., Ajayakumar, M. R., Ghaskadbi, S., Sharma, M., and Goswami, S. K. (2015). Norepinephrine-induced Apoptotic and Hypertrophic Responses in H9c2 Cardiac Myoblasts Are Characterized by Different Repertoire of Reactive Oxygen Species Generation. *Redox Biol.* 5, 243–252. doi:10.1016/j.redox.2015.05.005

Turin, A., Bax, J. J., Doukas, D., Joyce, C., Lopez, J. J., Mathew, V., et al. (2018). Interactions Among Vitamin D, Atrial Fibrillation, and the Renin-Angiotensin-Aldosterone System. *Am. J. Cardiol.* 122 (5), 780–784. doi:10.1016/j.amjcard.2018.05.013

Wang, A., Green, J. B., Halperin, J. L., and Piccini, J. P., Sr. (2019). Atrial Fibrillation and Diabetes Mellitus: JACC Review Topic of the Week. *J. Am. Coll. Cardiol.* 74 (8), 1107–1115. doi:10.1016/j.jacc.2019.07.020

Wang, X. B., Jin, H. F., and Du, J. B. (2009). Role of Gas Signaling Molecule Hydrogen Sulfide in Cardiovascular Diseases. *Zhongguo Dang Dai Er Ke Za Zhi* 11 (9), 790–793.

Watts, M., Kolluru, G. K., Dherange, P., Pardue, S., Si, M., Shen, X., et al. (2021). Decreased Bioavailability of Hydrogen Sulfide Links Vascular Endothelium and Atrial Remodeling in Atrial Fibrillation. *Redox Biol.* 38, 101817. doi:10.1016/j.redox.2020.101817

Welchen, E., and Gonzalez, D. H. (2016). Cytochrome C, a Hub Linking Energy, Redox, Stress and Signaling Pathways in Mitochondria and Other Cell Compartments. *Physiol. Plant* 157 (3), 310–321. doi:10.1111/ppl.12449

Wen, L., Xiao, B., Shi, Y., and Han, F. (2017). PERK Signalling Pathway Mediates Single Prolonged Stress-Induced Dysfunction of Medial Prefrontal Cortex Neurons. *Apoptosis* 22 (6), 753–768. doi:10.1007/s10495-017-1371-5

Wiersma, M., Meijering, R. A. M., Qi, X. Y., Zhang, D., Liu, T., Hoogstra-Berends, F., et al. (2017). Endoplasmic Reticulum Stress Is Associated with Autophagy

and Cardiomyocyte Remodeling in Experimental and Human Atrial Fibrillation. *J. Am. Heart Assoc.* 6 (10), e006458. doi:10.1161/JAHA.117.006458

Xiao, Y., Peng, H., Hong, C., Chen, Z., Deng, X., Wang, A., et al. (2017). PDGF Promotes the Warburg Effect in Pulmonary Arterial Smooth Muscle Cells via Activation of the PI3K/AKT/mTOR/HIF-1α Signaling Pathway. *Cell Physiol Biochem* 42 (4), 1603–1613. doi:10.1159/000479401

Xie, W., Santulli, G., Reiken, S. R., Yuan, Q., Osborne, B. W., Chen, B. X., et al. (2015). Mitochondrial Oxidative Stress Promotes Atrial Fibrillation. *Sci. Rep.* 5, 11427. doi:10.1038/srep11427

Xin, W., Li, X., Lu, X., Niu, K., and Cai, J. (2011). Involvement of Endoplasmic Reticulum Stress-Associated Apoptosis in a Heart Failure Model Induced by Chronic Myocardial Ischemia. *Int. J. Mol. Med.* 27 (4), 503–509. doi:10.3892/ijmm.2011.612

Xiong, H., Yang, Q., Zhang, X., Wang, P., Chen, F., Liu, Y., et al. (2019). Significant Association of Rare Variant p.Gly8Ser in Cardiac Sodium Channel β4-subunit SCN4B with Atrial Fibrillation. *Ann. Hum. Genet.* 83 (4), 239–248. doi:10.1111/ahg.12305

Xue, X., Ling, X., Xi, W., Wang, P., Sun, J., Yang, Q., et al. (2020). Exogenous Hydrogen Sulfide Reduces Atrial Remodeling and Atrial Fibrillation Induced by Diabetes Mellitus via Activation of the PI3K/Akt/eNOS Pathway. *Mol. Med. Rep.* 22 (3), 1759–1766. doi:10.3892/mmr.2020.11291

Yamada, H., Popović, Z. B., Martin, D. O., Civello, K. C., and Wallick, D. W. (2006). The Effects of Altering Time Delays of Coupled Pacing during Acute Atrial Fibrillation. *Heart Rhythm* 3 (6), 722–727. doi:10.1016/j.hrthm.2006.02.007

Yan, B., Liu, S., Li, X., Zhong, Y., Tong, F., and Yang, S. (2019). Preconditioning with Endoplasmic Reticulum Stress Alleviated Heart Ischemia/reperfusion Injury via Modulating IRE1/ATF6/RACK1/PERK and PGC-1α in Diabetes Mellitus. *Biomed. Pharmacother.* 118, 109407. doi:10.1016/j.biopha.2019.109407

Yong, J., Bischof, H., Burgstaller, S., Siirin, M., Murphy, A., Malli, R., et al. (2019). Mitochondria Supply ATP to the ER through a Mechanism Antagonized by Cytosolic Ca2. *Elife* 8, e49682. doi:10.7554/eLife.49682

Yuan, M., Gong, M., Zhang, Z., Meng, L., Tse, G., Zhao, Y., et al. (2020). Hyperglycemia Induces Endoplasmic Reticulum Stress in Atrial Cardiomyocytes, and Mitofusin-2 Downregulation Prevents Mitochondrial Dysfunction and Subsequent Cell Death. *Oxid Med. Cel Longev* 2020, 6569728. doi:10.1155/2020/6569728

Zhang, X., Dong, S., Jia, Q., Zhang, A., Li, Y., Zhu, Y., et al. (2019). The microRNA in Ventricular Remodeling: the miR-30 Family. *Biosci. Rep.* 39 (8), BSR20190788. doi:10.1042/BSR20190788

Zheng, Y., Liao, F., Du, J. B., Tang, C. S., Xu, G. H., and Geng, B. (2012). Modified Methylene Blue Method for Measurement of Hydrogen Sulfide Level in Plasma. *Sheng Li Xue Bao* 64 (6), 681–686.

Zhu, X., Zhang, X., Cong, X., Zhu, L., and Ning, Z. (2021). ANGPTL4 Attenuates Ang II-Induced Atrial Fibrillation and Fibrosis in Mice via PPAR Pathway. *Cardiol. Res. Pract.* 2021, 9935310. doi:10.1155/2021/9935310

Zlochiver, S., Muñoz, V., Vikstrom, K. L., Taffet, S. M., Berenfeld, O., and Jalife, J. (2008). Electrotonic Myofibroblast-To-Myocyte Coupling Increases Propensity to Reentrant Arrhythmias in Two-Dimensional Cardiac Monolayers. *Biophys. J.* 95 (9), 4469–4480. doi:10.1529/biophysj.108.136473

Zou, X., Song, X. M., and Wang, J. (2021). Biological Features of Cardiac Endothelial Cells and Their Role and Mechanism on Regulating Heart Failure. *Zhonghua Xin Xue Guan Bing Za Zhi* 49 (4), 318–323. doi:10.3760/cma.j.cn112148-20200521-00418

Conflict of Interest: The authors declare that the research was conducted in the absence of any commercial or financial relationships that could be construed as a potential conflict of interest.

Publisher's Note: All claims expressed in this article are solely those of the authors and do not necessarily represent those of their affiliated organizations, or those of the publisher, the editors and the reviewers. Any product that may be evaluated in this article, or claim that may be made by its manufacturer, is not guaranteed or endorsed by the publisher.

frontiers | Frontiers in Pharmacology

REVIEW
published: 11 April 2022
doi: 10.3389/fphar.2022.792798

Cyclic GMP and PKG Signaling in Heart Failure

Genri Numata[1,2] *and Eiki Takimoto*[1,3]*

[1]Department of Cardiovascular Medicine, The University of Tokyo Hospital, Tokyo, Japan, [2]Department of Advanced Translational Research and Medicine in Management of Pulmonary Hypertension, The University of Tokyo Hospital, Tokyo, Japan, [3]Division of Cardiology, Department of Medicine, The Johns Hopkins Medical Institutions, Baltimore, MD, United States

Cyclic guanosine monophosphate (cGMP), produced by guanylate cyclase (GC), activates protein kinase G (PKG) and regulates cardiac remodeling. cGMP/PKG signal is activated by two intrinsic pathways: nitric oxide (NO)-soluble GC and natriuretic peptide (NP)-particulate GC (pGC) pathways. Activation of these pathways has emerged as a potent therapeutic strategy to treat patients with heart failure, given cGMP-PKG signaling is impaired in heart failure with reduced ejection fraction (HFrEF) and preserved ejection fraction (HFpEF). Large scale clinical trials in patients with HFrEF have shown positive results with agents that activate cGMP-PKG pathways. In patients with HFpEF, however, benefits were observed only in a subgroup of patients. Further investigation for cGMP-PKG pathway is needed to develop better targeting strategies for HFpEF. This review outlines cGMP-PKG pathway and its modulation in heart failure.

Keywords: NO, SGC, NPR, PGC, cGMP, PKG

OPEN ACCESS

Edited by:
Antonio Lax,
University of Murcia, Spain

Reviewed by:
Kristen Bubb,
Monash University, Australia
Robert Lukowski,
University of Tübingen, Germany

***Correspondence:**
Eiki Takimoto
eikitakimoto@gmail.com

Specialty section:
This article was submitted to Cardiovascular and Smooth Muscle Pharmacology, a section of the journal Frontiers in Pharmacology

Received: *11 October 2021*
Accepted: *09 February 2022*
Published: *11 April 2022*

Citation:
Numata G and Takimoto E (2022) Cyclic GMP and PKG Signaling in Heart Failure. Front. Pharmacol. 13:792798. doi: 10.3389/fphar.2022.792798

INTRODUCTION

Heart failure is a major health problem, and its prevalence is increasing worldwide. The traditional guideline directed therapies target the renin-angiotensin-aldosterone system and the sympathetic nervous system, but recently, cyclic guanosine 3′,5′-monophosphate (cGMP) and its downstream protein kinase G (PKG) signaling has attracted attention as a novel therapeutic target (Tsai and Kass, 2009). cGMP-PKG pathway regulates diverse cellular mechanisms to maintain cellular homeostasis and is activated by two different pathways. One is natriuretic peptide (NP)-NP receptor (NPR)-particulate guanylate cyclase (pGC) pathway, and the other is NO-soluble GC (sGC) pathway. cGMP-PKG pathway has been suggested to be blunted or dysregulated in patients with HFrEF or HFpEF (Paulus et al., 2013; Redfield et al., 2013). Increased plasma levels of inflammatory cytokines including TNF-α and IL-6 in HF are related to endothelial dysfunction with low NO-sGC-cGMP signaling in the heart and vasculature (Torre-Amione et al., 1996; Lommi et al., 1997), where its degradation by cGMP-PDEs might be enhanced. In HFpEF patients, myocardial homogenates from biopsy samples revealed low PKG activity and cGMP concentration compared with HFrEF and aortic stenosis patients (Van Heerebeek et al., 2012). Thus, the therapeutic strategy to recover blunted cGMP/PKG signaling in heart failure is very reasonable. Sacubitril/valsartan is the first agent in this class that has been approved for use in heart failure. It consists of the neprilysin (NEP) inhibitor and the angiotensin receptor blocker, and is described as an angiotensin receptor-neprilysin inhibitor (ARNi). NEP hydrolyzes several peptide hormones including NPs (ANP, BNP, CNP), adrenomedullin, glucagon, enkephalins, substance P, neurotensin, oxytocin, and bradykinin. Thus, its inhibition enhances NPs-pGC-cGMP. ARNi improved clinical outcomes in patients with HFrEF (McMurray et al., 2014; Velazquez et al., 2018) and also exhibited favorable outcomes in a particular sub-group (female) in HFpEF (Solomon et al., 2019; Pieske et al.,

2021). Vericiguat, an sCG stimulator that enhances (NO)-sGC-cGMP pathway independently of NO, was approved for the treatment of heart failure. Vericugat is effective in patients with HFrEF (Armstrong et al., 2020a), but it failed to reveal clinical improvement in HFpEF (Armstrong et al., 2020b; Udelson et al., 2020) (**Table 1**). The clinical importance of cGMP-PKG pathway is clear; however, a better understanding of underlying mechanisms is necessary for the optimal therapeutic strategy with enhancement of cGMP-PKG signaling pathway. This review focuses on the regulatory mechanisms of cGMP-PKG pathway in heart failure.

Phosphodiesterase and cGMP/PKG Signaling

Phosphodiesterase (PDE) has 11 superfamilies and more than 100 isoform variants that hydrolyze cAMP or cGMP to their inactive respective 5′-monophosphate form. Seven PDEs (PDE1, 2, 3, 4, 5, 8, and 9) are currently known to be expressed in myocardium. PDE1, 2, and 3 hydrolyze both cAMP and cGMP, while PDE5 and 9 are selective for cGMP and PDE4 and 8 are selective for cAMP (Kim and Kass, 2017). PDEs are differentially localized within the cells, contributing to the compartmentalized regulation of cGMP and cAMP signaling in both space and time.

Inhibition of PDE1, a dual substrate esterase, demonstrates acute inotropic and lusitropic effects largely via cAMP pathway (Hashimoto et al., 2018), demonstrated in large animal models. PDE1A, one the three isoforms of PDE1, modulates pathological hypertrophy via cGMP-PKG in rodent and cell models, while PDE1C, coupled with adenosine A2A receptor and TRPC3, hydrolyzes cAMP and regulates apoptosis in cardiac myocytes (Miller et al., 2009; Zhang et al., 2018).

PDE2 is also a dual substrate esterase and involved in the regulation of cardiac hypertrophy via cGMP. PDE2 specifically plays an important role in the crosstalk between cGMP and cAMP pathways because its activity is stimulated by cGMP (Baliga et al., 2018). PDE2 has three splice variants (PDE2A1, 2A2, 2A3), which are differently localized: PDE2A1 in cytoplasm, PDE2A2 in mitochondrial matrix, and PDE2A3 at membrane (mostly PDE2A3) (Geoffroy et al., 1999; Lugnier et al., 1999; Mongillo et al., 2006; Weber et al., 2017). In the heart, in particular, PDE2A might be localized in both cytosolic and particulate fractions of cardiac ventricle, though it differs from species to species (Le Trong et al., 1990; Bode et al., 1991; Muller et al., 1992; Sugioka et al., 1994; Geoffroy et al., 1999; Mongillo et al., 2006). In humans, PDE2A3 is expressed in cardiomyocytes and vascular endothelial cells (Sadhu et al., 1999). Under the normal conditions, PDE2 is less abundant in cardiomyocytes than in fibroblasts and endothelial cells (Stephenson et al., 2009; Vettel et al., 2014), but under the pathological conditions, PDE2 expressions and cAMP-hydrolyzing activity significantly increase (Levy, 2013; Mehel et al., 2013). (Chen et al., 2016). Cardiac PDE2A expressions increase in rat cardiac hypertrophy and also in human ischemic or non-ischemic heart failure (Mehel et al., 2013). PDE2 can hydrolyze cGMP produced by either pGC (Stangherlin et al., 2011) and sGC (Mongillo et al., 2006) with the allosteric hydrolyzing ability activated by cGMP, but this might depend on the stress conditions and cGMP concentrations (Terasaki and Appleman, 1975; Prigent et al., 1988; Mery et al., 1993; Dittrich et al., 2001; Herring et al., 2001; Weber et al., 2017). PDE2A overexpression blunts norepinephrine-induced cellular hypertrophy with marked decrease in cAMP levels (Mehel et al., 2013). On the other hand, PDE2A inhibition suppresses cardiac hypertrophy induced by norepinephrine in rats (Zoccarato et al., 2015). These apparently opposite results might be attributable to the cAMP and cGMP regulation levels which might depend on the contexts. In the computer modeling, Zhao et al. reported that PDE2A hydrolyzed increasing amount of cAMP with increasing levels of β adrenergic stimulation, and hydrolyzed increasing amounts of cGMP with decreasing levels of NO stimulation (Zhao et al., 2016).

We elaborate on cGMP-specific PDEs (PDE5 and PDE9) in the next section, reviewing their effects on cardiac remodeling. PDE5 hydrolyzes cGMP derived from NO-sGC pathway and PDE9 degrades cGMP from NP-pGC pathway, modulating various signaling related to cardiac remodeling (**Figure 1**).

NO-sGC Pathway (PDE5)

Nitric oxide (NO) stimulates sGC to produce cGMP, which is hydrolyzed specifically by PDE5. PDE5A is localized at Z-disks in cardiac myocytes under physiological conditions but it is diffusely distributed under diseased conditions (Takimoto et al., 2005; Zhang et al., 2008). The expression of PDE5A is up-regulated in failing hearts (Shan et al., 2012), though it is very low under physiological conditions. In experimental animal models, PDE5 inhibition (PDE5i) provides cardiac protection against pressure-overload, ischemia-reperfusion injury, and doxorubicin-toxicity (Takimoto et al., 2005; Burley et al., 2007; Kukreja et al., 2012; Jin et al., 2013), with multiple myocardial signaling pathways altered (Takimoto, 2012). A regulator of G-protein signaling (RGS), 2/4 is phospho-activated to inhibit Gq-signaling (Takimoto et al., 2009) and transient receptor potential canonical Ca^{2+} channel-type6 (TRPC6) coupled with calcinurin (Cn) signaling (Koitabashi et al., 2010; Seo et al., 2014) is deactivated by PDE5i-PKG-phosphorylation. Mechanisms related to proteostasis are also regulated. PDE5i-activated PKG enhances proteasome function, blocking the accumulation of misfolded proteins via posttranslational modifications of proteasome subunits (Ranek et al., 2013). PDE5i also phosphorylates tuberin (TSC2), an intrinsic regulator of the mechanistic target of rapamycin complex-1 (mTORC1), and enhances autophagy. In a model of ischemia re-perfusion injury, PDE5i-cGMP-PKG exerts cardio-protective effects against necrosis and apoptosis through modulating mitochondrial functions (RAMZI et al., 2002; Salloum et al., 2008; Li et al., 2016; Patel et al., 2019) Additionally, PDE5i alone or in combination with natriuretic peptide, phosphorylates sarcomeric proteins including titin (Bishu et al., 2011a), troponin-I (Layland et al., 2005; Wijnker et al., 2014), and cardiac myosin-binding protein C (Thoonen et al., 2015), which improves systolic and diastolic function. Some may still have debate on PDE5A or PKG effects on cardiomyocyte. Straubinger et al. reported that sildenafil failed to limit the progressive cardiomyocyte growth, fibrosis, or cardiac dysfunctions in the cardiomyocyte-specific overexpression of the

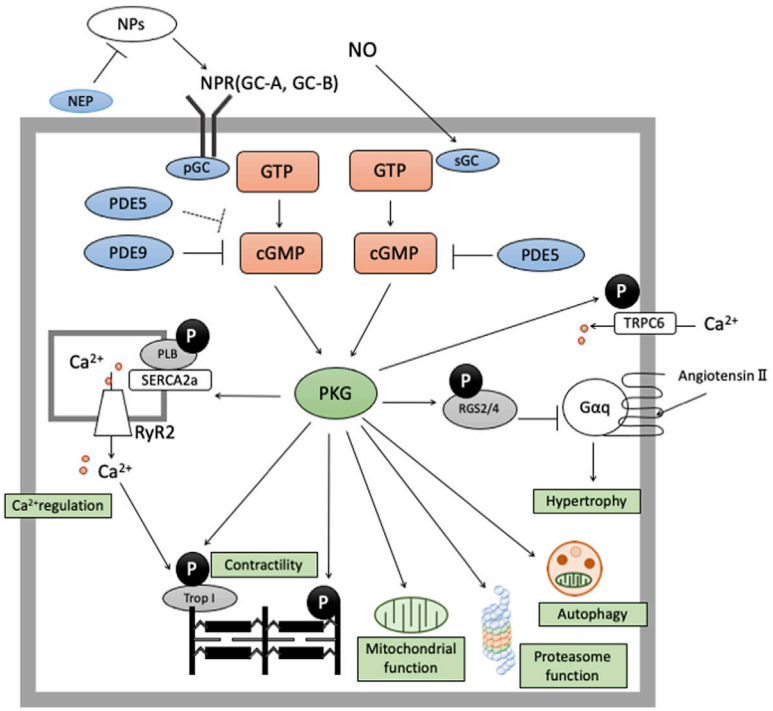

FIGURE 1 | cGMP/PKG signaling in cardiomyocyte cGMP-PKG signaling is enhanced by two pathways. The former is NO-sGC-cGMP pathway and the latter is NP-NPR-pGC pathway. cGMP derived from NO-sGC pathway takes hydrolyzation by PDE5, and cGMP from NP-pGC pathway by PDE9 and PDE5 (especially in stressed conditions). cGMP/PKG signaling exerts protective effects in cardiomyocyte by phosphorylate various proteins like RGS2/4, Troponin I, TSC2, cMyBP-C, or Titin.

AT1 receptor mice (Straubinger et al., 2015). Lukowski et al. showed that the deletion of cardiomyocyte-specific PKG had no effect on cardiac hypertrophy caused by pressure overload and isoproterenol administration (Lukowski et al., 2010). Patrucco et al. reported that the lack of PKG in cardiomyocyte, endothelial cells, or cardiac fibroblast did not augment hypertrophic response and sildenafil had modest effects on angiotensin II-induced cardiac hypertrophy (Patrucco et al., 2014). On the other hand, however, cardiomyocyte-specific overexpression of PDE5A recovered impaired cardiac functions from pressure overload (Zhang et al., 2010) and myocardial infarction (Pokreisz et al., 2009). Frantz and Kuhn et al. generated animals with cardiomyocyte-restricted deletion of PKG, and demonstrated the animals developed severe hypertrophy by chronic angiotensin II infusion or pressure overload (Frantz et al., 2013). Recently, we have consistently reported that sildenafil exhibited protective effects against cardiac hypertrophy via proliferator activated receptor γ co-activator-1α-PKG cascade (Zhu et al., 2021). Together it would be reasonable to conclude that cGMP-PKG signaling in cardiomyocyte would be important in cardiac hypertrophy and remodeling. With regard to the cardiac-specific role and regulation of PDE5, a tissue-specific conditional deletion model would be awaited.

sGC stimulators and sGC activators are direct modulators of sGC, increasing the production of cGMP: the former stimulates NO-sensitive (unoxidized) sGC and the latter can activate NO-insensitive (oxidized) sGC. sGC stimulators have shown cardiac benefits in an HFpEF model (Wilck et al., 2018) as well as in an HFrEF model. Double-transgenic rats (dTGR) harboring the renin and angiotensinogen genes exhibit an HFpEF phenotype of diastolic dysfunction, preserved EF, systemic hypertension, cardiac hypertrophy, fibrosis, inflammation, and endothelial dysfunction, and dies between 7 and 8 weeks from severe heart failure (Damage et al., 1999; Mervaala et al., 2001; Wellner et al., 2005; Fischer et al., 2008; Finckenberg et al., 2012; Haase et al., 2014). Treatment with an sGC stimulator improved cardiac function, cardiac fibrosis, and inflammation, with minimal effects on cardiac hypertrophy (Wilck et al., 2018). sGC activators have also shown cardio-protective effects in another HFpEF model (Dahl salt-sensitive model: DSS) (Kolijn et al., 2020), where an sGC activator (cinaciguat) phosphorylates titin and improves passive stiffness. In human cardiomyocytes from HFpEF patients, cinaciguat phosphorylates titin and improves passive tension, associated with a reduction in proinflammatory cytokines and oxidative stress markers (Kolijn et al., 2020). sGC-bound cofactor heme (Fe2+) is oxidized to Fe^{3+} under oxidative conditions, leading to the inactive Apo form that no longer is responsive to NO. sGC stimulators stimulate only Fe^{2+}-sGC, while sGC activators act on oxidated sGC(Fe^{3+}-sGC or Apo-sGC) (Krishnan et al., 2018) to produce cGMP. In oxidated conditions such as HFpEF, sGC activator might have an advantage.

Although preclinical studies have revealed cardio-protective and anti-remodeling effects from NO-sGC-cGMP activation in either type of heart failure (HFrEF or HFpEF), clinical studies

TABLE 1 | Clinical trials associated with sGC inhibitors and neprilysin inhibitors.

Study	Drugs	meanEF (%)	Number	Female (%)	NPs (pg/ml)	Outcomes	Notes
McMurray et al. (2014), PARADIGM-HF	Sacubitril-Valsartan (LCZ696)	29.6	4187	21.0	BNP 255 NT-proBNP 1631	A composite of death from CVD or hospitalization 21.8% vs 26.5% HR 0.80, 95% CI 0.73 to 0.87, $p < 0.001$	
	enalapril	29.4	4212	22.6	BNP 251 NT-proBNP 1594		
Velazquez et. al. (2019) PIONEER-HF	Sacubitril-Valsartan	24	440	25.7	NT-proBNP 4821	The time-averaged reduction in the NT-proBNP at weeks 4 and 8 to the baseline -46.7% vs -25.3%(ratio of change 0.76, 95% CI 0.69 to 0.85)	
	enalapril	25	441	30.2	4710		
Solomon et al. (2019) PARAGON-HF	Sacbitril-Vaslsartan	57.6	2419	51.6	NT-proBNP 904	Cardiovascular death 8.5% vs 8.9% HR 0.95, 95% CI 0.79 to 1.16	A composite outcome of hospitalization and cardiovascular death in female RR 0.73 95% CI 0.59 to 0.90
	Valsartan	57.5	2403	51.8	915	Total Hospitalization 690 vs 797 HR 0.85, 95% CI 0.72 to 1.0	
Pieske et al. (2021) PARALLAX	acbitril-Vaslsartan	56.7	1286	50.2	NT-proBNP 786	The reduction in NTproBNP at week 12 The adjusted geometric mean ratio 0.84 (95% CI, 0.80- 0.88; $p < 0.001$)	No significant between-group difference in the Kansas City Cardiomyopathy Questionnaire clinical summary score 12.3 vs 11.8 (mean difference, 0.52; 95% CI, −0.93 to 1.97) No improvement in NYHA class 23.6% vs 24.0% of patients (adjusted odds ratio, 0.98; 95% CI, 0.81 to 1.18)
	Individualized comparator	56.2	1286	51.2	760	6-minute walk difference at week 24. No significant between-group from baseline 9.7 m vs 12.2 m (adjusted mean difference, −2.5 m; 95% CI, −8.5 to 3.5; $p = 0.42$)	6-minute walking distance improved among women but decreased among men 6.59 vs −12.07 ($p = 0.0024$) Individualized comparator: enalapril at a target dose of 10, valsartan at a target dose of 160 mg, or placebo (no RAS inhibitor).
Armstrong et al. (2020a) VICTORIA	Vericiguat	29.3	2526	24.0	NT-proBNP 2803	The composite of death from any cause or hospitalization for heart failure 37.9% vs 40.9% HR 0.90, (95% CI 0.83 to 0.98, $p = 0.02$)	
	Placebo	27.9	2524	23.9	2821		
Udelson et al. (2020) CAPACITY HFpEF	Praliciguat	61.9	91	38.5	NT-proBNP 260	Changes in peak VO_2 −0.26 vs −0.04 mL/kg/min 1286 (95% CI, −0.83 to 0.31 and −0.49 to 0.56)	
	Placebo	59.8	90	44.4	228.5		
Armstrong et al. (2020b) VITALITY-HFpEF	Vericiguat 15 mg	56.8	264	53.0	NT-proBNP 1364.5	The mean changes in the KCCQ PLS 5.5 points in the 15-mg/d vericiguat group 6.5 points in the 10-mg/d vericiguat group 6.9 points in the placebo group	The overall mortality rate was 4.1% (n = 32) 10 (3.8%) in the 15-mg vericiguat group 15 (5.7%) in the 10 mg vericiguat group 7 (2.7%) in the placebo group 8 cardiovascular deaths (3.0%) in the 15-mg vericiguat group
	Vericiguat 10mg	55.8	263	47.1	1339.1	differences between either vericiguat dosage and placebo were not statistically significant	12 (4.6%) in the 10-mg vericiguat group
	Placebo	56.3	262	46.2	1644.2		4 (1.5%) in the placebo group

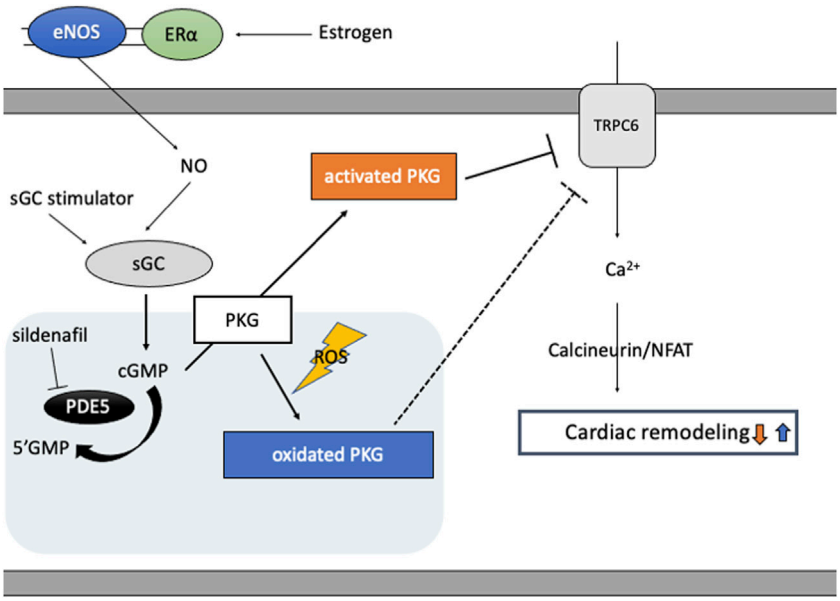

FIGURE 2 | cGMP/PKG signaling and PKG oxidation. Estrogen plays a pivotal role in cGMP-PKG signaling coupled with eNOS via estrogen receptor (ERα)-mediated non-nuclear signaling. In diseased conditions like heart failure, eNOS activity is impaired and PKG undertakes oxidation and localizes in cytosol, inhibiting protective effects of PKG signaling independent of cGMP and enhancing cardiac remodeling via target proteins like TRPC6. PDE5 inhibitor, sildenafil, reveals protective effects only under the condition of sufficient oxidated PKG1α, while sGC stimulator improves cardiac remodeling independent of PKG redox status.

have yielded mixed results. Two meta-analyses of controlled clinical trials (928 patients in 14 studies (De Vecchis et al., 2017), 555 patients in 13 studies (De Vecchis et al., 2018)) demonstrate that PDE5 inhibitors improve clinical outcomes, exercise capacity, and pulmonary hemodynamics in patients with HFrEF, but not HFpEF. The negative results in HFpEF might be partially attributable to the female-specific response of PDE5i depending on estrogen levels, given the prevalence of HFpEF in older women: nearly half of the patients were older women (average age 67) in the negative RELAX trial. Epidemiological studies have demonstrated that women are likely to develop HFpEF. In clinical trials of HFpEF women account for around 50–60% of the trial cohorts (Forman and Gaziano, 2009; Savill, 2014), whereas they account for 20–25% of those of HFrEF (Pablo, 2017; Zannad et al., 2018; Pieske et al., 2019). In a recent multicenter, observational study, female sex was reported to be independently associated with the presence of diastolic dysfunction and worse clinical outcomes (Sotomi et al., 2021). Sex-hormone estrogen plays a pivotal role in cGMP-PKG signal coupled with NO via estrogen receptor (ERα)-mediated non-nuclear signaling, also known as rapid signaling or membrane-initiated steroid signaling (Adlanmerini et al., 2014; Arnal et al., 2017). In a female mouse model of heart failure, PDE5i fails to provide heart-protective effects in the absence of estrogen. We previously demonstrated that sildenafil treatment failed to exert anti-remodeling effects in female pathological hypertrophy heart in from Gαq-overexpressing or pressure-overloaded mice after ovary removal; on the contrary, estrogen replacement recovered the protective effects of sildenafil (Sasaki et al., 2014). Rüdebusch et al. (2020) also demonstrated that sGC stimulation has protective effects associated with improved gene expressions in mice heart failure model induced by pressure overload (Rüdebusch et al., 2020) and interestingly we have recently reported that this sGC protective effects are independent of estrogen status in rodent pressure-overload model (Nobuaki et al., 2020).

Despite promising preclinical results, however, a clinical study testing vericiguat in patients with HFpEF turned out negative (Vitality HFpEF). Although the reason for the negative results remains an open question, the redox status related to HFpEF might be speculated to be involved. NO–sGC–cGMP signaling can be compromised either by reducing the bioavailability of NO or by altering the redox state of sGC itself (Costell et al., 2012). Several groups reported that redox conditions altered cysteine residues (Cys) on sGC, affecting its catalytic or regulatory functions (Craven and DeRubertis, 1978a; Craven and DeRubertis, 1978b; Braughler, 1983). The redox status also alters the heme conditions within sGC. Heme iron in the reduced status (Fe^{2+}) is necessary for NO binding, and sGC stimulator can stimulate only the reduced form of sGC, while the sGC activator can activate both reduced sGC and oxidized sGC (containing Fe^{3+}) (Evgenov et al., 2006). In rat external iliac arteries without endothelium, peroxynitrite was reported to alter the redox state of sGC. Under the exposure of peroxynitrite, vascular relaxation induced by an sGC stimulator was impaired, whereas that by an sGC activator was enhanced. Additionally, this response correlated well with tissue levels of cGMP (Tawa et al., 2014). In Sprague Dawley rats fed with high salt/fat diet, an sGC activator, but not an

sGC stimulator, attenuated the development of cardiac hypertrophy in a blood pressure-independent manner (Evgenov et al., 2006). Although there are no data about sGC redox status in patients with heart failure, inflammation and oxidative stress conditions in HFpEF might critically affect the efficacy of cGMP-modifying drugs (Tawa et al., 2014).

Thus, an sGC activator might serve as a potential novel treatment of HFpEF. So far, cinaciguat, an sGC activator, has been tested only in acute heart failure, with increased hypotensive events but no clear benefits, and sGC activators have not yet been explored in patients with chronic heart failure.

NP-pGC Pathway (PDE9 and PDE5)

Natriuretic peptides stimulate transmembrane receptor guanylate cyclase to produce cGMP. Atrial and B-type natriuretic peptides (ANP, BNP) bind to receptor particulate guanylyl cyclase A (pGC-A or NPRA), while C-type natriuretic peptide (CNP) binds to particulate guanylyl cyclase B (pGC-B or NPRB). pGC-A is localized at T-tubules and pGC-B is distributed throughout the sarcolemma. This spatial difference renders compartmentalized ANP/NPRA/cGMP signaling vs. CNP/NPRB/cGMP: the former have little impact on contractility and the latter have positive-lusitropic effects (Kuhn, 2016; Subramanian et al., 2018; Michel et al., 2020). cGMP from NP-pGC axis is degraded by PDE9 (Volpe et al., 2016; Goetze et al., 2020), which is expressed prominently in the brain and less in the heart (GraceKim et al., 2017). Similar to PDE5, myocardial PDE9 expression is low under physiological conditions but is upregulated under disease conditions such as HFpEF and aortic stenosis (Lee et al., 2015). PDE9 inhibition, either with a pharmacological or a genetic approach, suppressed cardiac hypertrophy in rodent pressure-overload (PO) model (Lee et al., 2015; Kokkonen-Simon et al., 2018; Richards et al., 2021). Importantly, both PDE5i and PDE9i similarly improve diastolic distensibility and ameliorate cardiac remodeling, associated with better profiles of hypertrophic/fibrosis-related gene expression (Lee et al., 2015), (Bishu et al., 2011a); however, comprehensive analyses of RNA-sequence data of myocardium reveals significant differences between PDE5i and PDE9i (Kokkonen-Simon et al., 2018), particularly in miRNA profiles related to hypertrophy and fibrosis: marked down-regulation of pro-hypertrophic and pro-fibrotic miRs by PDE5i vs. virtually no effect by PDE9i.

As previously described, ARNI exhibited favorable outcome in female patients with HFpEF (Solomon et al., 2019; Pieske et al., 2021). There has been no explanation provided for this observation of female-only benefit. We would speculate that this might be possibly related to difference of plasma NPs levels. Female patients with HFpEF are reported to exhibit lower plasma NPs levels as follows. ARNI might compensate lower levels of NPs in female patients with HFpEF. In HFpEF patients, plasma BNP levels are reported to be lower than in HFrEF (Harada et al., 2017); interestingly, women with HFpEF had lower BNP levels than men [43.9 vs. 76.1 pmol/L, p = 0.0193 (Tasevska-Dinevska et al., 2011), 104 vs 133, $p < 0.001$ (Savarese and D'Amario, 2018)] while in HFrEF the levels of NPs were inconsistent. One group reported that the plasma levels of ANP and BNP were similar in both genders (ANP: 114.9 vs. 141.2 pg/ml, $p = 0.2606$, BNP: 252.0 vs. 381.9 pg/ml, $p = 0.1577$). Another group reported that the plasma levels of NT-proBNP were higher in female HFrEF (8481 vs. 7543 pg/ml, $p < 0.001$) (Kim et al., 2017) and there is another group reporting that plasma NT-proBNP levels were similar in both genders (2532 vs. 2677 pg/ml, $p = 0.978$) (Sobhani et al., 2018). Another possible reason why ARNI is effective in female HFpEF might be related to CNP regulation. CNP exerts biological effects by binding to two types of natriuretic receptors; cGMP-coupled NPR-B and NPR-C (Chauhan et al., 2003; Villar et al., 2007). Endothelial deletion of CNP or global deletion of NPR-C revealed hypertensive phenotype only in female mice (Moyes et al., 2014), while the absence of eNOS and COX-1 in endothelial cells had no effect on mean blood pressure in female mice, but resulted in significantly high blood pressure in male animals (Scotland et al., 2005).

These suggest the pivotal contribution of CNP to female blood pressure maintenance. It is thus tempting to speculate that cardiac protection from ARNI therapy might depend more on the regulation of CNP in females than in males, although the contribution of cGMP might be unclear.

Although PDE5 hydrolyzes cGMP coupled with NO under normal conditions. PDE5 could become interactive with NPs-derived cGMP under stressed conditions (Zhang et al., 2012). Cardiomyocyte PDE5 is normally localized at Z-bands of sarcomeres, but becomes diffusely localized when exposed to pathological stress such as TAC or NOS inhibition (Nagayama et al., 2008; Zhang et al., 2012). In a dog hypertension model produced by bilateral renal wrapping, sildenafil treatment with concomitant BNP administration enhances plasma cGMP concentration, and recovers left ventricular diastolic capacitance in association with titin phosphorylation compared with sildenafil treatment alone (Bishu et al., 2011b). The beneficial synergistic effects of the combined PDE5 and NPs were also reported in pulmonary hypertension (PH). In a mouse model of hypoxia-induced PH, global deletion of NPRA blunts the beneficial effects of sildenafil on right ventricular systolic pressure (Zhao et al., 2003). Also, in hypoxia-induced PH rats, ANP and sildenafil show synergistic effects on decreasing right ventricular systolic pressure and on increasing plasma cGMP levels (Preston et al., 2004). Furthermore, a recent clinical trial of pulmonary arterial hypertension also demonstrated that the combined inhibition of neprilysin and PDE5 increase both plasma NP and cGMP levels and decreased pulmonary vascular resistance without affecting systemic blood pressure (Hobbs et al., 2019), which makes contrast to the concomitant use of PDE5 inhibitor (sildenafil) with sGC stimulator (riociguat) having been reported to be associated with hypotension but without beneficial effects on hemodynamics or exercise capacity (Galiè et al., 2015). The combination of pGC-related pathway and PDE5 might be a potential therapeutic option also in heart failure.

PKG Oxidation in Failing Heart

cGMP activated PKG targets various molecules to regulate cellular function in cardiomyocytes (Takimoto, 2012),

including RGS2/4, TRPC6, proteasome systems, mitochondria, and sarcomere components. Two PKG genes, *prkg1* and *prkg2,* encode PKG1 and PKG2, respectively, and PKG1 is the primary isotype in cardiomyocyte. PKG1 is activated classically by cGMP, but also by oxidation (**Figure 2**): When oxidized, a cysteine residue C43(C42 in mice) forms a disulfide bond to form a homodimer of PKG1 (Burgoyne et al., 2007). Oxidized PKG1 is increased in failing hearts, though it accounts for only a small portion of PKG1 in normal hearts (Paulus et al., 2013; Nakamura et al., 2015; Prysyazhna et al., 2016). Oxidative PKG1 resides only at cytosol but not at the plasma membrane, while unoxidized PKG1 resides in both (Nakamura et al., 2015). Therefore, oxidized PKGI is no longer able to exert beneficial effects by the mechanisms mediated by membrane-localized PKGI, including inhibition of TRPC6-Cn-NFAT hypertrophy signaling and TSC2-mTORC1 metabolic/autophagy signaling (Oeing et al., 2020). Interestingly, PKG1 oxidation is required for the anti-remodeling effects from PDE5i as cytosol-localized PDE5 needs cGMP-activation via its GAF domain, while sGC stimulation exerts anti-remodeling effects independent of redox status of PKG1 (Nakamura et al., 2018). PDE5 inhibitor could be effective only under the sufficient myocardial stress to oxidate PKG1α, whereas an sGC stimulator provides benefits independent of redox conditions.

CONCLUSION

cGMP/PKG signaling can be augmented by stimulation of either NO-sGC pathway or NP-pGC pathway. Although activation of either provides anti-remodeling benefits, they do not necessarily share the same molecular mechanisms in common. Furthermore, benefits might be also affected by the PKG redox status. Although ample preclinical evidence shows the benefits of cGMP/PKG augmentation in HFrEF or HFpEF models, clinical studies thus far provide consistent efficacy of cGMP/PKG augmentation in patients with HFrEF and limited efficacy in patients with HFpEF. Further studies would be helpful to better understand the pathophysiology of HFpEF and the development of novel treatments.

AUTHOR CONTRIBUTIONS

All authors listed have made a substantial, direct, and intellectual contribution to the work and approved it for publication.

FUNDING

This work was supported by the research grants from Fukuda Foundation for Medical Technology and JSPS KAKENHI (Grant-in-Aid for Scientific Research #21K08047).

REFERENCES

Adlanmerini, M., Solinhac, R., Abot, A., Fabre, A., Raymond-Letron, I., Guihot, A.-L., et al. (2014). Mutation of the Palmitoylation Site of Estrogen Receptor α *In Vivo* Reveals Tissue-specific Roles for Membrane versus Nuclear Actions. *Proc. Natl. Acad. Sci.* 111, E283 LP–E290. doi:10.1073/pnas.1322057111

Armstrong, P. W., Lam, C. S. P., Anstrom, K. J., Ezekowitz, J., Hernandez, A. F., O'Connor, C. M., et al. (2020). Effect of Vericiguat vs Placebo on Quality of Life in Patients with Heart Failure and Preserved Ejection Fraction: The VITALITY-HFpEF Randomized Clinical Trial. *JAMA - J. Am. Med. Assoc.* 324, 1512–1521. doi:10.1001/jama.2020.15922

Armstrong, P. W., Pieske, B., Anstrom, K. J., Ezekowitz, J., Hernandez, A. F., Butler, J., et al. (2020). Vericiguat in Patients with Heart Failure and Reduced Ejection Fraction. *N. Engl. J. Med.* 382, 1883–1893. doi:10.1056/NEJMoa1915928

Arnal, J.-F., Lenfant, F., Metivier, R., Flouriot, G., Henrion, D., Adlanmerini, M., et al. (2017). Membrane and Nuclear Estrogen Receptor Alpha Actions: From Tissue Specificity to Medical Implications. *Physiol. Rev.* 97, 1045–1087. doi:10.1152/physrev.00024.2016

Baliga, R. S., Preedy, M. E. J., Dukinfield, M. S., Chu, S. M., Aubdool, A. A., Bubb, K. J., et al. (2018). Phosphodiesterase 2 Inhibition Preferentially Promotes NO/guanylyl cyclase/cGMP Signaling to Reverse the Development of Heart Failure. *Proc. Natl. Acad. Sci. U. S. A.* 115, E7428–E7437. doi:10.1073/pnas.1800996115

Bishu, K., Hamdani, N., Mohammed, S. F., Kruger, M., Ohtani, T., Ogut, O., et al. (2011). Sildenafil and B-type Natriuretic Peptide Acutely Phosphorylate Titin and Improve Diastolic Distensibility *In Vivo*. *Circulation* 124, 2882–2891. doi:10.1161/CIRCULATIONAHA.111.048520

Bishu, K., Hamdani, N., Mohammed, S. F., Kruger, M., Ohtani, T., Ogut, O., et al. (2011). Sildenafil and B-type Natriuretic Peptide Acutely Phosphorylate Titin and Improve Diastolic Distensibility *In Vivo*. *Circulation* 124, 2882–2891. doi:10.1161/CIRCULATIONAHA.111.048520

Bode, D. C., Kanter, J. R., and Brunton, L. L. (1991). Cellular Distribution of Phosphodiesterase Isoforms in Rat Cardiac Tissue. *Circ. Res.* 68, 1070–1079. doi:10.1161/01.res.68.4.1070

Braughler, J. M. (1983). Soluble Guanylate Cyclase Activation by Nitric Oxide and its Reversal. Involvement of Sulfhydryl Group Oxidation and Reduction. *Biochem. Pharmacol.* 32, 811–818. doi:10.1016/0006-2952(83)90581-6

Burgoyne, J. R., Madhani, M., Cuello, F., Charles, R. L., Brennan, J. P., Schröder, E., et al. (2007). Cysteine Redox Sensor in PKGIa Enables Oxidant-Induced Activation. *Science* 317, 13931397. doi:10.1126/science.1144318

Burley, D. S., Ferdinandy, P., and Baxter, G. F. (2007). Cyclic GMP and Protein Kinase-G in Myocardial Ischaemia-Reperfusion: Opportunities and Obstacles for Survival Signaling. *Br. J. Pharmacol.* 152, 855–869. doi:10.1038/sj.bjp.0707409

Chauhan, S. D., Nilsson, H., Ahluwalia, A., and Hobbs, A. J. (2003). Release of C-type Natriuretic Peptide Accounts for the Biological Activity of Endothelium-Derived Hyperpolarizing Factor. *Proc. Natl. Acad. Sci. U. S. A.* 100, 1426–1431. doi:10.1073/pnas.0336365100

Chen, W., Spitzl, A., Mathes, D., Nikolaev, V. O., Werner, F., Weirather, J., et al. (2016). Endothelial Actions of ANP Enhance Myocardial Inflammatory Infiltration in the Early Phase after Acute Infarction. *Circ. Res.* 119, 237–248. doi:10.1161/CIRCRESAHA.115.307196

Costell, M. H., Ancellin, N., Bernard, R. E., Zhao, S. F., Upson, J. J., Morgan, L. A., et al. (2012). Comparison of Soluble Guanylate Cyclase Stimulators and Activators in Models of Cardiovascular Disease Associated with Oxidative Stress. *Front. Pharmacol.* 3 (JUL), 1–14. doi:10.3389/fphar.2012.00128

Craven, P. A., and DeRubertis, F. R. (1978). Effects of Thiol Inhibitors on Hepatic Guanylate Cyclase Activity Evidence for the Involvement of Vicinal Dithiols in the Expression of Basal and Agonist-Stimulated Activity. *BBA - Enzymol.* 524, 231–244. doi:10.1016/0005-2744(78)90121-3

Craven, P. A., and DeRubertis, F. R. (1978). Restoration of the Responsiveness of Purified Guanylate Cyclase to Nitrosoguanidine, Nitric Oxide, and Related Activators by Heme and Hemeproteins. Evidence for Involvement of the Paramagnetic nitrosyl.Heme Complex in Enzyme Activation. *J. Biol. Chem.* 253, 8433–8443. doi:10.1016/s0021-9258(17)34310-7

Damage, H. E., Luft, F. C., Mervaala, E., Mu, D. N., Gross, V., Schmidt, F., et al. (1999). Influence of Exercise Training on Neurogenic Control of Blood Pressure

in Spontaneously Hypertensive Rats. *State-of-the-Art Lecture* 34, 212–218. doi:10.1161/01.HYP.34.4.720

De Vecchis, R., Cesaro, A., and Ariano, C. (2018). Differential Effects of the Phosphodiesterase Inhibition in Chronic Heart Failure Depending on the Echocardiographic Phenotype (HFREF or HFpEF): a Meta-Analysis. *Minerva Cardioangiol* 66, 659–670. doi:10.23736/S0026-4725.17.04382-1

De Vecchis, R., Cesaro, A., Ariano, C., Giasi, A., and Cioppa, C. (2017). Phosphodiesterase-5 Inhibitors Improve Clinical Outcomes, Exercise Capacity and Pulmonary Hemodynamics in Patients with Heart Failure with Reduced Left Ventricular Ejection Fraction: A Meta-Analysis. *J. Clin. Med. Res.* 9, 488–498. doi:10.14740/jocmr3008w

Dittrich, M., Jurevicius, J., Georget, M., Rochais, F., Fleischmann, B. K., Hescheler, J., et al. (2001). Local Response of L-type Ca2+ Current to Nitric Oxide in Frog Ventricular Myocytes. *J. Physiol.* 534, 109–121. doi:10.1111/j.1469-7793.2001.00109.x

Evgenov, O. V., Pacher, P., Schmidt, P. M., Haskó, G., Schmidt, H. H. H. W., and Stasch, J. P. (2006). NO-independent Stimulators and Activators of Soluble Guanylate Cyclase: Discovery and Therapeutic Potential. *Nat. Rev. Drug Discov.* 5, 755–768. doi:10.1038/nrd2038

Finckenberg, P., Eriksson, O., Baumann, M., Merasto, S., Lalowski, M. M., Levijoki, J., et al. (2012). Caloric Restriction Ameliorates Angiotensin II-Induced Mitochondrial Remodeling and Cardiac Hypertrophy. *Hypertension* 59, 76–84. doi:10.1161/HYPERTENSIONAHA.111.179457

Fischer, R., Dechend, R., Qadri, F., Markovic, M., Feldt, S., Herse, F., et al. (2008). Dietary N-3 Polyunsaturated Fatty Acids and Direct Renin Inhibition Improve Electrical Remodeling in a Model of High Human Renin Hypertension. *Hypertension* 51, 540–546. doi:10.1161/HYPERTENSIONAHA.107.103143

Forman, D., and Gaziano, J. M. (2009). Irbesartan in Patients with Heart Failure and Preserved Ejection Fraction. *Curr. Cardiovasc. Risk Rep.* 3, 311–312. doi:10.1007/s12170-009-0056-1

Frantz, S., Klaiber, M., Baba, H. A., Oberwinkler, H., Völker, K., Gaßner, B., et al. (2013). Stress-dependent Dilated Cardiomyopathy in Mice with Cardiomyocyte- Restricted Inactivation of Cyclic GMP-dependent Protein Kinase I. *Eur. Heart J.* 34, 1233–1244. doi:10.1093/eurheartj/ehr445

Galiè, N., Müller, K., Scalise, A. V., and Grünig, E. (2015). PATENT PLUS: A Blinded, Randomised and Extension Study of Riociguat Plus Sildenafil in Pulmonary Arterial Hypertension. *Eur. Respir. J.* 45, 1314–1322. doi:10.1183/09031936.00105914

Geoffroy, V., Fouque, F., Nivet, V., Clot, J. P., Lugnier, C., Desbuquois, B., et al. (1999). Activation of a cGMP-Stimulated cAMP Phosphodiesterase by Protein Kinase C in a Liver Golgi-Endosomal Fraction. *Eur. J. Biochem.* 259, 892–900. doi:10.1046/j.1432-1327.1999.00123.x

Goetze, J. P., Bruneau, B. G., Ramos, H. R., Ogawa, T., de Bold, M. K., and de Bold, A. J. (2020). Cardiac Natriuretic Peptides. *Nat. Rev. Cardiol.* 17, 698–717. doi:10.1038/s41569-020-0381-0

GraceKim, E., PhDaDavid, A., and Kass, M. (2017). Cardiac Phosphodiesterases and Their Modulation for Treating Heart Disease Grace. *Handb. Exp. Pharmacol.* 243, 249–269. doi:10.1007/164_2016_82

Haase, N., Rugor, J., Przybyl, L., Qadri, F., Müller, D. N., and Dechend, R. (2014). Relaxin Does Not Improve Angiotensin II-Induced Target-Organ Damage. *PLoS One* 9, 1–7. doi:10.1371/journal.pone.0093743

Harada, E., Mizuno, Y., Kugimiya, F., Shono, M., Maeda, H., Yano, N., et al. (2017). B-type Natriuretic Peptide in Heart Failure with Preserved Ejection Fraction: Relevance to Age-Related Left Ventricular Modeling in Japanese. *Circ. J.* 81, 1006–1013. doi:10.1253/circj.CJ-16-1282

Hashimoto, T., Kim, G. E., Tunin, R. S., Adesiyun, T., Hsu, S., Nakagawa, R., et al. (2018). Acute Enhancement of Cardiac Function by Phosphodiesterase Type 1 Inhibition Translational Study in the Dog and Rabbit. *Circulation* 138, 1974–1987. doi:10.1161/CIRCULATIONAHA.117.030490

Herring, N., Rigg, L., Terrar, D. A., and Paterson, D. J. (2001). NO-cGMP Pathway Increases the Hyperpolarisation-Activated Current, if, and Heart Rate during Adrenergic Stimulation. *Cardiovasc. Res.* 52, 446–453. doi:10.1016/s0008-6363(01)00425-4

Hobbs, A. J., Moyes, A. J., Baliga, R. S., Ghedia, D., Ochiel, R., Sylvestre, Y., et al. (2019). Neprilysin Inhibition for Pulmonary Arterial Hypertension: a Randomized, Double-Blind, Placebo-Controlled, Proof-Of-Concept Trial. *Br. J. Pharmacol.* 176, 1251–1267. doi:10.1111/bph.14621

Jin, Z., Zhang, J., Zhi, H., Hong, B., Zhang, S., Guo, H., et al. (2013). The Beneficial Effects of Tadalafil on Left Ventricular Dysfunction in Doxorubicin-Induced Cardiomyopathy. *J. Cardiol.* 62, 110–116. doi:10.1016/j.jjcc.2013.03.018

Kim, G. E., and Kass, D. A. (2017). Cardiac Phosphodiesterases and Their Modulation for Treating Heart Disease. *Handb. Exp. Pharmacol.* 243, 249–269. doi:10.1007/164_2016_82

Kim, H. L., Kim, M. A., Choi, D. J., Han, S., Jeon, E. S., Cho, M. C., et al. (2017). Gender Difference in the Prognostic Value of N-Terminal Pro-B Type Natriuretic Peptide in Patients with Heart Failure — a Report from the Korean Heart Failure Registry (KorHF). *Circ. J.* 81, 1329–1336. doi:10.1253/circj.CJ-16-1345

Koitabashi, N., Aiba, T., Hesketh, G. G., Rowell, J., Zhang, M., Takimoto, E., et al. (2010). Cyclic GMP/PKG-dependent Inhibition of TRPC6 Channel Activity and Expression Negatively Regulates Cardiomyocyte NFAT Activation: Novel Mechanism of Cardiac Stress Modulation by PDE5 Inhibition. *J. Mol. Cell. Cardiol.* 48, 713–724. doi:10.1016/j.yjmcc.2009.11.015

Kokkonen-Simon, K. M., Saberi, A., Nakamura, T., Ranek, M. J., Zhu, G., Bedja, D., et al. (2018). Marked Disparity of microRNA Modulation by cGMP-Selective PDE5 versus PDE9 Inhibitors in Heart Disease. *JCI Insight* 3, e121739. doi:10.1172/jci.insight.121739

Kolijn, D., Kovács, Á., Herwig, M., Lódi, M., Sieme, M., Alhaj, A., et al. (2020). Enhanced Cardiomyocyte Function in Hypertensive Rats with Diastolic Dysfunction and Human Heart Failure Patients after Acute Treatment with Soluble Guanylyl Cyclase (sGC) Activator. *Front. Physiol.* 11, 1–21. doi:10.3389/fphys.2020.00345

Krishnan, S. M., Kraehling, J. R., Eitner, F., Bénardeau, A., and Sandner, P. (2018). The Impact of the Nitric Oxide (No)/soluble Guanylyl Cyclase (sGC) Signaling cascade on Kidney Health and Disease: A Preclinical Perspective. *Int. J. Mol. Sci.* 19. doi:10.3390/ijms19061712

Kuhn, M. (2016). Molecular Physiology of Membrane Guanylyl Cyclase Receptors. *Physiol. Rev.* 96, 751–804. doi:10.1152/physrev.00022.2015

Kukreja, R. C., Salloum, F. N., and Das, A. (2012). Cyclic Guanosine Monophosphate Signaling and Phosphodiesterase-5 Inhibitors in Cardioprotection. *J. Am. Coll. Cardiol.* 59, 1921–1927. doi:10.1016/j.jacc.2011.09.086

Layland, J., Solaro, R. J., and Shah, A. M. (2005). Regulation of Cardiac Contractile Function by Troponin I Phosphorylation. *Cardiovasc. Res.* 66, 12–21. doi:10.1016/j.cardiores.2004.12.022

Le Trong, H., Walsh, K. A., Charbonneau, H., Beier, N., Sonnenburg, W. K., Stroop, S. D., et al. (1990). Amino Acid Sequence of the Cyclic GMP Stimulated Cyclic Nucleotide Phosphodiesterase from Bovine Heart. *Biochemistry* 29, 10280–10288. doi:10.1021/bi00496a018

Lee, D. I., Zhu, G., Sasaki, T., Cho, G.-S., Hamdani, N., Holewinski, R., et al. (2015). Phosphodiesterase 9A Controls Nitric-oxide-independent cGMP and Hypertrophic Heart Disease. *Nature* 519, 472–476. doi:10.1038/nature14332

Levy, F. O. (2013). Cardiac PDEs and Crosstalk between cAMP and cGMP Signalling Pathways in the Regulation of Contractility. *Naunyn. Schmiedebergs. Arch. Pharmacol.* 386, 665–670. doi:10.1007/s00210-013-0874-z

Li, N., Yuan, Y., Li, S., Zeng, C., Yu, W., Shen, M., et al. (2016). Pde5 Inhibitors Protect against post-infarction Heart Failure. *Front. Biosci. - Landmark* 21, 1194–1210. doi:10.2741/4450

Lommi, J., Pulkki, K., Koskinen, P., Naveri, H., Leinonen, H., Harkonen, M., et al. (1997). Haemodynamic, Neuroendocrine and Metabolic Correlates of Circulating Cytokine Concentrations in Congestive Heart Failure. *Eur. Heart J.* 18, 1620–1625. doi:10.1093/oxfordjournals.eurheartj.a015142

Lugnier, C., Keravis, T., Le Bec, A., Pauvert, O., Proteau, S., and Rousseau, E. (1999). Characterization of Cyclic Nucleotide Phosphodiesterase Isoforms Associated to Isolated Cardiac Nuclei. *Biochim. Biophys. Acta - Gen. Subj.* 1472, 431–446. doi:10.1016/s0304-4165(99)00145-2

Lukowski, R., Rybalkin, S. D., Loga, F., Leiss, V., Beavo, J. A., and Hofmann, F. (2010). Cardiac Hypertrophy Is Not Amplified by Deletion of cGMP-dependent Protein Kinase I in Cardiomyocytes. *Proc. Natl. Acad. Sci. U. S. A.* 107, 5646–5651. doi:10.1073/pnas.1001360107

McMurray, J. J. V., Packer, M., Desai, A. S., Gong, J., Lefkowitz, M. P., Rizkala, A. R., et al. (2014). Angiotensin–Neprilysin Inhibition versus Enalapril in Heart Failure. *N. Engl. J. Med.* 371, 993–1004. doi:10.1056/NEJMoa1409077

Mehel, H., Emons, J., Vettel, C., Wittköpper, K., Seppelt, D., Dewenter, M., et al. (2013). Phosphodiesterase-2 Is Up-Regulated in Human Failing Hearts and Blunts β-adrenergic Responses in Cardiomyocytes. *J. Am. Coll. Cardiol.* 62, 1596–1606. doi:10.1016/j.jacc.2013.05.057

Mervaala, E. M. A., Cheng, Z. J., Tikkanen, I., Lapatto, R., Nurminen, K., Vapaatalo, H., et al. (2001). Endothelial Dysfunction and Xanthine Oxidoreductase Activity in Rats with Human Renin and Angiotensinogen Genes. *Hypertension* 37, 414–418. doi:10.1161/01.hyp.37.2.414

Mery, P., Pavoines, C., Belhassen, L., and Peckers, F. (1993). Nitric Oxide Regulates Cardiac Ca2+ Current. *J. Biol. Chem.* 268, 26286–26295. doi:10.1016/s0021-9258(19)74313-0

Michel, K., Herwig, M., Werner, F., Spes, K. Š., Abeßer, M., Schuh, K., et al. (2020). C-type Natriuretic Peptide Moderates Titin-Based Cardiomyocyte Stiffness. *JCI Insight* 5. doi:10.1172/jci.insight.139910

Miller, C. L., Oikawa, M., Cai, Y., Wojtovich, A. P., Nagel, D. J., Xu, X., et al. (2009). Role of Ca2+/calmodulin-Stimulated Cyclic Nucleotide Phosphodiesterase 1 in Mediating Cardiomyocyte Hypertrophy. *Circ. Res.* 105, 956–964. doi:10.1161/CIRCRESAHA.109.198515

Mongillo, M., Tocchetti, C. G., Terrin, A., Lissandron, V., Cheung, Y. F., Dostmann, W. R., et al. (2006). Compartmentalized Phosphodiesterase-2 Activity Blunts β-adrenergic Cardiac Inotropy via an NO/cGMP-dependent Pathway. *Circ. Res.* 98, 226–234. doi:10.1161/01.RES.0000200178.34179.93

Moyes, A. J., Khambata, R. S., Villar, I., Bubb, K. J., Baliga, R. S., Lumsden, N. G., et al. (2014). Endothelial C-type Natriuretic Peptide Maintains Vascular Homeostasis. *J. Clin. Invest.* 124, 4039–4051. doi:10.1172/JCI74281

Muller, B., Stoclet, J. C., and Lugnier, C. (1992). Cytosolic and Membrane-Bound Cyclic Nucleotide Phosphodiesterases from guinea Pig Cardiac Ventricles. *Eur. J. Pharmacol. Mol. Pharmacol.* 225, 263–272. doi:10.1016/0922-4106(92)90028-t

Nagayama, T., Zhang, M., Hsu, S., Takimoto, E., and Kass, D. A. (2008). Sustained Soluble Guanylate Cyclase Stimulation Offsets Nitric-Oxide Synthase Inhibition to Restore Acute Cardiac Modulation by Sildenafil. *J. Pharmacol. Exp. Ther.* 326, 380–387. doi:10.1124/jpet.108.137422

Nakamura, T., Ranek, M. J., Lee, D. I., Hahn, V. S., Kim, C., Eaton, P., et al. (2015). Prevention of PKG1α Oxidation Augments Cardioprotection in the Stressed Heart. *J. Clin. Invest.* 125, 2468–2472. doi:10.1172/JCI80275

Nakamura, T., Zhu, G., Ranek, M. J., Kokkonen-Simon, K., Zhang, M., Kim, G. E., et al. (2018). Prevention of PKG-1α Oxidation Suppresses Antihypertrophic/Antifibrotic Effects from PDE5 Inhibition but Not sGC Stimulation. *Circ. Hear. Fail.* 11, e004740. doi:10.1161/CIRCHEARTFAILURE.117.004740

Nobuaki, F., Eiki, T., Kazutaka, U., Pangyen, L., Miyu, T., Yu, O., et al. (2020). Estrogen Receptor-α Non-nuclear Signaling Confers Cardioprotection and Is Essential to cGMP-PDE5 Inhibition Efficacy. *JACC Basic Transl. Sci.* 5, 282–295.

Oeing, C. U., Nakamura, T., Pan, S., Mishra, S., Dunkerly-Eyring, B. L., Kokkonen-Simon, K. M., et al. (2020). PKG1a Cysteine-42 Redox State Controls mTORC1 Activation in Pathological Cardiac Hypertrophy. *Circ. Res.* 127, 522–533. doi:10.1161/CIRCRESAHA.119.315714

Pablo, A. (2017). Olavegogeascoechea. De la evidencia a la práctica en la insuficiencia cardíaca. *Rev. Argentina Med.* 5, 132–133.

Patel, C. H., Nakamura, T., Zhu, G., Bedja, D., Sasaki, M., Holewinski, R. J., et al. (2019). PKG1-modified TSC2 Regulates mTORC1 Activity to Counter Adverse Cardiac Stress. *Nature* 566, 264–269.

Patrucco, E., Domes, K., Sbroggió, M., Blaich, A., Schlossmann, J., Desch, M., et al. (2014). Roles of cGMP-dependent Protein Kinase I (cGKI) and PDE5 in the Regulation of Ang II-Induced Cardiac Hypertrophy and Fibrosis. *Proc. Natl. Acad. Sci. U. S. A.* 111, 12925–12929. doi:10.1073/pnas.1414364111

Paulus, W. J., Tschöpe, C., and D, P. H. (2013). A Novel Paradigm for Heart Failure with Preserved Ejection Fraction: Comorbidities Drive Myocardial Dysfunction and Remodeling through Coronary Microvascular Endothelial Inflammation. *J. Am. Coll. Cardiol.* 62, 263–271. doi:10.1016/j.jacc.2013.02.092

Pieske, B., Patel, M. J., Westerhout, C. M., Anstrom, K. J., Butler, J., Ezekowitz, J., et al. (2019). Baseline Features of the VICTORIA (Vericiguat Global Study in Subjects with Heart Failure with Reduced Ejection Fraction) Trial. *Eur. J. Heart Fail.* 21, 1596–1604. doi:10.1002/ejhf.1664

Pieske, B., Wachter, R., Shah, S. J., Baldridge, A., Szeczoedy, P., Ibram, G., et al. (2021). Effect of Sacubitril/Valsartan vs Standard Medical Therapies on Plasma NT-proBNP Concentration and Submaximal Exercise Capacity in Patients with Heart Failure and Preserved Ejection Fraction: The PARALLAX Randomized Clinical Trial. *JAMA - J. Am. Med. Assoc.* 326, 1919–1929.

Pokreisz, P., Vandenwijngaert, S., Bito, V., Van Bergh, A. Den., Lenaerts, I., Busch, C., et al. (2009). Ventricular Phosphodiesterase-5 Expression Is Increased in Patients with Advanced Heart Failure and Contributes to Adverse Ventricular Remodeling after Myocardial Infarction in Mice. *Circulation* 119, 408–416. doi:10.1161/CIRCULATIONAHA.108.822072

Preston, I. R., Hill, N. S., Gambardella, L. S., Warburton, R. R., and Klinger, J. R. (2004). Synergistic Effects of ANP and Sildenafil on cGMP Levels and Amelioration of Acute Hypoxic Pulmonary Hypertension. *Exp. Biol. Med.* 229, 920–925. doi:10.1177/153537020422900908

Prigent, A. F., Fougier, S., Nemoz, G., Anker, G., Pacheco, H., Lugnier, C., et al. (1988). Comparison of Cyclic Nucleotide Phosphodiesterase Isoforms from Rat Heart and Bovine Aorta. Separation and Inhibition by Selective Reference Phosphodiesterase Inhibitors. *Biochem. Pharmacol.* 37, 3671–3681. doi:10.1016/0006-2952(88)90400-5

Prysyazhna, O., Burgoyne, J. R., Scotcher, J., Grover, S., Kass, D., and Eaton, P. (2016). Phosphodiesterase 5 Inhibition Limits Doxorubicin-Induced Heart Failure by Attenuating Protein Kinase G Iα Oxidation. *J. Biol. Chem.* 291, 17427–17436. doi:10.1074/jbc.M116.724070

Ramzi, O., Salloum, F., Hawkins, J., and Kukreja, R. C. (2002). Sildenafil (Viagra) Induces Powerful Cardioprotective Effect via Opening of Mitochondrial KATP Channels in Rabbits. *Am. J. Physiol. Hear. Circ. Physiol.* 283, H1263–H1269. doi:10.1152/ajpheart.00324.2002

Ranek, M. J., Terpstra, E. J. M., Li, J., Kass, D. A., and Wang, X. (2013). Protein Kinase G Positively Regulates Proteasome-Mediated Degradation of Misfolded Proteins. *Circulation* 128, 365–376. doi:10.1161/CIRCULATIONAHA.113.001971

Redfield, M. M., Chen, H. H., Borlaug, B. A., Semigran, M. J., Lee, K. L., Lewis, G., et al. (2013). Effect of Phosphodiesterase-5 Inhibition on Exercise Capacity and Clinical Status in Heart Failure with Preserved Ejection Fraction: A Randomized Clinical Trial. *JAMA - J. Am. Med. Assoc.* 309, 1268–1277. doi:10.1001/jama.2013.2024

Richards, D. A., Aronovitz, M. J., Liu, P., Martin, G. L., Tam, K., Pande, S., et al. (2021). CRD-733, a Novel PDE9 (Phosphodiesterase 9) Inhibitor, Reverses Pressure Overload-Induced Heart Failure. *Circ. Hear. Fail.* 14, e007300. doi:10.1161/circheartfailure.120.007300

Rüdebusch, J., Benkner, A., Nath, N., Fleuch, L., Kaderali, L., Grube, K., et al. (2020). Stimulation of Soluble Guanylyl Cyclase (sGC) by Riociguat Attenuates Heart Failure and Pathological Cardiac Remodelling. *Br. J. Pharmacol.* 1, 13. doi:10.1111/bph.15333

Sadhu, K., Hensley, K., Florio, V. A., and Wolda, S. L. (1999). Differential Expression of the Cyclic GMP-Stimulated Phosphodiesterase PDE2A in Human Venous and Capillary Endothelial Cells. *J. Histochem. Cytochem.* 47, 895–905. doi:10.1177/002215549904700707

Salloum, F. N., Abbate, A., Das, A., Houser, J. E., Mudrick, C. A., Qureshi, I. Z., et al. (2008). Sildenafil (Viagra) Attenuates Ischemic Cardiomyopathy and Improves Left Ventricular Function in Mice. *Am. J. Physiol. - Hear. Circ. Physiol.* 294, 1398–1406. doi:10.1152/ajpheart.91438.2007

Sasaki, H., Nagayama, T., Blanton, R. M., Seo, K., Zhang, M., Zhu, G., et al. (2014). PDE5 Inhibitor Efficacy Is Estrogen Dependent in Female Heart Disease. *J. Clin. Invest.* 124, 2464–2471. doi:10.1172/JCI70731

Savarese, G., and D'Amario, D. (2018). Sex Differences in Heart Failure. *Adv. Exp. Med. Biol.* 1065, 529–544. doi:10.1007/978-3-319-77932-4_32

Savill, P. (2014). Spironolactone in Heart Failure with Preserved Ejection Fraction. *Practitioner* 258, 10.

Scotland, R. S., Madhani, M., Chauhan, S., Moncada, S., Andresen, J., Nilsson, H., et al. (2005). Investigation of Vascular Responses in Endothelial Nitric Oxide Synthase/cyclooxygenase-1 Double-Knockout Mice: Key Role for Endothelium-Derived Hyperpolarizing Factor in the Regulation of Blood Pressure *In Vivo*. *Circulation* 111, 796–803. doi:10.1161/01.CIR.0000155238.70797.4E

Seo, K., Rainer, P. P., Lee, D. I., Hao, S., Bedja, D., Birnbaumer, L., et al. (2014). Hyperactive Adverse Mechanical Stress Responses in Dystrophic Heart Are Coupled to Transient Receptor Potential Canonical 6 and Blocked by Cgmp-Protein Kinase G Modulation. *Circ. Res.* 114, 823–832. doi:10.1161/CIRCRESAHA.114.302614

Shan, X., Quaile, M. P., Monk, J. K., French, B., Cappola, T. P., and Margulies, K. B. (2012). Differential Expression of Pde5 in Failing and Nonfailing Human Myocardium. *Circ. Hear. Fail.* 5, 79–86. doi:10.1161/CIRCHEARTFAILURE.111.961706

Sobhani, K., Nieves Castro, D. K., Fu, Q., Gottlieb, R. A., Van Eyk, J. E., and Noel Bairey Merz, C. (2018). Sex Differences in Ischemic Heart Disease and Heart Failure Biomarkers. *Biol. Sex. Differ.* 9, 1–13. doi:10.1186/s13293-018-0201-y

Solomon, S. D., McMurray, J. J. V., Anand, I. S., Ge, J., Lam, C. S. P., Maggioni, A. P., et al. (2019). Angiotensin–Neprilysin Inhibition in Heart Failure with Preserved Ejection Fraction. *N. Engl. J. Med.* 381, 1609–1620. doi:10.1056/NEJMoa1908655

Sotomi, Y., Hikoso, S., Nakatani, D., Mizuno, H., Okada, K., Dohi, T., et al. (2021). Sex Differences in Heart Failure with Preserved Ejection Fraction. *J. Am. Heart Assoc.* 10, 1–20. doi:10.1161/jaha.120.018574

Stangherlin, A., Gesellchen, F., Zoccarato, A., Terrin, A., Fields, L. A., Berrera, M., et al. (2011). CGMP Signals Modulate Camp Levels in a Compartment-specific Manner to Regulate Catecholamine-dependent Signaling in Cardiac Myocytes. *Circ. Res.* 108, 929–939. doi:10.1161/CIRCRESAHA.110.230698

Stephenson, D. T., Coskran, T. M., Wilhelms, M. B., Adamowicz, W. O., O'Donnell, M. M., Muravnick, K. B., et al. (2009). Immunohistochemical Localization of Phosphodiesterase 2A in Multiple Mammalian Species. *J. Histochem. Cytochem.* 57, 933–949. doi:10.1369/jhc.2009.953471

Straubinger, J., Schöttle, V., Bork, N., Subramanian, H., Dünnes, S., Russwurm, M., et al. (2015). Sildenafil Does Not Prevent Heart Hypertrophy and Fibrosis Induced by Cardiomyocyte Angiotensin II Type 1 Receptor Signalings. *J. Pharmacol. Exp. Ther.* 354, 406–416. doi:10.1124/jpet.115.226092

Subramanian, H., Froese, A., Jönsson, P., Schmidt, H., Gorelik, J., and Nikolaev, V. O. (2018). Distinct Submembrane Localisation Compartmentalises Cardiac NPR1 and NPR2 Signalling to cGMP. *Nat. Commun.* 9, 1–9. doi:10.1038/s41467-018-04891-5

Sugioka, M., Ito, M., Masuoka, H., Ichikawa, K., Konishi, T., Tanaka, T., et al. (1994). Identification and Characterization of Isoenzymes of Cyclic Nucleotide Phosphodiesterase in Human Kidney and Heart, and the Effects of New Cardiotonic Agents on These Isoenzymes. *Naunyn. Schmiedebergs. Arch. Pharmacol.* 350, 284–293. doi:10.1007/BF00175034

Takimoto, E. (2012). Cyclic GMP-dependent Signaling in Cardiac Myocytes. *Circ. J.* 76, 1819–1825. doi:10.1253/circj.cj-12-0664

Takimoto, E., Koitabashi, N., Hsu, S., Ketner, E. A., Zhang, M., Nagayama, T., et al. (2009). The. Regulator of G Protein Signaling 2 Mediates Cardiac Compensation to Pressure Overload and Antihypertrophic Effects of PDE5 Inhibition in Mice. *J. Clin. Invest.* 119, 408–420. doi:10.1172/JCI35620

Takimoto, E., Champion, H. C., Li, M., Belardi, D., Ren, S., Rodriguez, E. R., et al. (2005). Chronic Inhibition of Cyclic GMP Phosphodiesterase 5A Prevents and Reverses Cardiac Hypertrophy. *Nat. Med.* 11, 214–222. doi:10.1038/nm1175

Tasevska-Dinevska, G., Kennedy, L. M., Cline-Iwarson, A., Cline, C., Erhardt, L., and Willenheimer, R. (2011). Gender Differences in Variables Related to B-Natriuretic Peptide, Left Ventricular Ejection Fraction and Mass, and Peak Oxygen Consumption, in Patients with Heart Failure. *Int. J. Cardiol.* 149, 364–371. doi:10.1016/j.ijcard.2010.02.018

Tawa, M., Shimosato, T., Iwasaki, H., Imamura, T., and Okamura, T. (2014). Effects of Peroxynitrite on Relaxation through the NO/sGC/cGMP Pathway in Isolated Rat Iliac Arteries. *J. Vasc. Res.* 51, 439–446. doi:10.1159/000371491

Terasaki, W. L., and Appleman, M. M. (1975). The Role of Cyclic GMP in the Regulation of Cyclic AMP Hydrolysis. *Metabolism* 24, 311–319. doi:10.1016/0026-0495(75)90112-2

Thoonen, R., Giovanni, S., Govindan, S., Lee, D. I., Wang, G.-R., Calamaras, T. D., et al. (2015). Molecular Screen Identifies Cardiac Myosin-Binding Protein-C as a Protein Kinase G-Iα Substrate. *Circ. Heart Fail.* 8, 1115–1122. doi:10.1161/CIRCHEARTFAILURE.115.002308

Torre-Amione, G., Kapadia, S., Benedict, C., Oral, H., Young, J. B., and Mann, D. L. (1996). Proinflammatory Cytokine Levels in Patients with Depressed Left Ventricular Ejection Fraction: A Report from the Studies of Left Ventricular Dysfunction (SOLVD). *J. Am. Coll. Cardiol.* 27, 1201–1206. doi:10.1016/0735-1097(95)00589-7

Tsai, E. J., and Kass, D. A. (2009). Cyclic GMP Signaling in Cardiovascular Pathophysiology and Therapeutics. *Pharmacol. Ther.* 122, 216–238. doi:10.1016/j.pharmthera.2009.02.009

Udelson, J. E., Lewis, G. D., Shah, S. J., Zile, M. R., Redfield, M. M., Burnett, J., et al. (2020). Effect of Praliciguat on Peak Rate of Oxygen Consumption in Patients with Heart Failure with Preserved Ejection Fraction: The CAPACITY HFpEF Randomized Clinical Trial. *JAMA - J. Am. Med. Assoc.* 324, 1522–1531. doi:10.1001/jama.2020.16641

Van Heerebeek, L., Hamdani, N., Falcão-Pires, I., Leite-Moreira, A. F., Begieneman, M. P. V., Bronzwaer, J. G. F., et al. (2012). Low Myocardial Protein Kinase G Activity in Heart Failure with Preserved Ejection Fraction. *Circulation* 126, 830–839. doi:10.1161/CIRCULATIONAHA.111.076075

Velazquez, E. J., Morrow, D. A., DeVore, A. D., Duffy, C. I., Ambrosy, A. P., McCague, K., et al. (2018). Angiotensin–Neprilysin Inhibition in Acute Decompensated Heart Failure. *N. Engl. J. Med.* 380, 539–548. doi:10.1056/NEJMoa1812851

Vettel, C., Lämmle, S., Ewens, S., Cervirgen, C., Emons, J., Ongherth, A., et al. (2014). PDE2-mediated cAMP Hydrolysis Accelerates Cardiac Fibroblast to Myofibroblast Conversion and Is Antagonized by Exogenous Activation of cGMP Signaling Pathways. *Am. J. Physiol. - Hear. Circ. Physiol.* 306, 1246–1252. doi:10.1152/ajpheart.00852.2013

Villar, I. C., Panayiotou, C. M., Sheraz, A., Madhani, M., Scotland, R. S., Nobles, M., et al. (2007). Definitive Role for Natriuretic Peptide Receptor-C in Mediating the Vasorelaxant Activity of C-type Natriuretic Peptide and Endothelium-Derived Hyperpolarising Factor. *Cardiovasc. Res.* 74, 515–525. doi:10.1016/j.cardiores.2007.02.032

Volpe, M., Carnovali, M., and Mastromarino, V. (2016). The Natriuretic Peptides System in the Pathophysiology of Heart Failure: From Molecular Basis to Treatment. *Clin. Sci.* 130, 57–77. doi:10.1042/CS20150469

Weber, S., Zeller, M., Guan, K., Wunder, F., Wagner, M., and El-Armouche, A. (2017). PDE2 at the Crossway between cAMP and cGMP Signalling in the Heart. *Cell. Signal.* 38, 76–84. doi:10.1016/j.cellsig.2017.06.020

Wellner, M., Dechend, R., Park, J. K., Shagdarsuren, E., Al-Saadi, N., Kirsch, T., et al. (2005). Cardiac Gene Expression Profile in Rats with Terminal Heart Failure and Cachexia. *Physiol. Genomics* 20, 256–267. doi:10.1152/physiolgenomics.00165.2004

Wijnker, P. J. M., Murphy, A. M., Stienen, G. J. M., and van der Velden (2014). J. Troponin I Phosphorylation in Human Myocardium in Health and Disease. *Neth. Heart J.* 22, 463–469. doi:10.1007/s12471-014-0590-4

Wilck, N., Markó, L., Balogh, A., Kräker, K., Herse, F., Bartolomaeus, H., et al. (2018). Nitric Oxide-Sensitive Guanylyl Cyclase Stimulation Improves Experimental Heart Failure with Preserved Ejection Fraction. *JCI insight* 3. doi:10.1172/jci.insight.96006

Zannad, F., Anker, S. D., Byra, W. M., Cleland, J. G. F., Fu, M., Gheorghiade, M., et al. (2018). Rivaroxaban in Patients with Heart Failure, Sinus Rhythm, and Coronary Disease. *N. Engl. J. Med.* 379, 1332–1342. doi:10.1056/NEJMoa1808848

Zhang, M., Koitabashi, N., Nagayama, T., Rambaran, R., Feng, N., Takimoto, E., et al. (2008). Expression, Activity, and Pro-hypertrophic Effects of PDE5A in Cardiac Myocytes. *Cell. Signal.* 20, 2231–2236. doi:10.1016/j.cellsig.2008.08.012

Zhang, M., Takimoto, E., Hsu, S., Lee, D. I., Nagayama, T., Danner, T., et al. (2010). Myocardial Remodeling Is Controlled by Myocyte-Targeted Gene Regulation of Phosphodiesterase Type 5. *J. Am. Coll. Cardiol.* 56, 2021–2030. doi:10.1016/j.jacc.2010.08.612

Zhang, M., Takimoto, E., Lee, D. I., Santos, C. X. C., Nakamura, T., Hsu, S., et al. (2012). Pathological Cardiac Hypertrophy Alters Intracellular Targeting of Phosphodiesterase Type 5 from Nitric Oxide Synthase-3 to Natriuretic Peptide Signaling. *Circulation* 126, 942–951. doi:10.1161/CIRCULATIONAHA.112.090977

Zhang, Y., Knight, W., Chen, S., Mohan, A., and Yan, C. (2018). Multiprotein Complex with TRPC (Transient Receptor Potential-Canonical) Channel, PDE1c (Phosphodiesterase 1C), and A2R (Adenosine A2 Receptor) Plays a Critical Role in Regulating Cardiomyocyte cAMP and Survival. *Circulation* 138, 1988–2002. doi:10.1161/CIRCULATIONAHA.118.034189

Zhao, C. Y., Greenstein, J. L., and Winslow, R. L. (2016). Roles of Phosphodiesterases in the Regulation of the Cardiac Cyclic Nucleotide Cross-Talk Signaling Network. *J. Mol. Cell. Cardiol.* 91, 215–227. doi:10.1016/j.yjmcc.2016.01.004

Zhao, L., Mason, N. A., Strange, J. W., Walker, H., and Wilkins, M. R. (2003). Beneficial Effects of Phosphodiesterase 5 Inhibition in Pulmonary Hypertension Are Influenced by Natriuretic Peptide Activity. *Circulation* 107, 234–237. doi:10.1161/01.cir.0000050653.10758.6b

Zhu, G., Ueda, K., Hashimoto, M., Zhang, M., Sasaki, M., Kariya, T., et al. (2021). The Mitochondrial Regulator PGC1α Is Induced by cGMP–PKG Signaling and Mediates the Protective Effects of Phosphodiesterase 5 Inhibition in Heart Failure. *FEBS Lett.* 596, 17–28. doi:10.1002/1873-3468.14228

Zoccarato, A., Surdo, N. C., Aronsen, J. M., Fields, L. A., Mancuso, L., Dodoni, G., et al. (2015). Cardiac Hypertrophy Is Inhibited by a Local Pool of cAMP Regulated by Phosphodiesterase 2. *Circ. Res.* 117, 707–719. doi:10.1161/CIRCRESAHA.114.305892

Conflict of Interest: The authors declare that the research was conducted in the absence of any commercial or financial relationships that could be construed as a potential conflict of interest.

Publisher's Note: All claims expressed in this article are solely those of the authors and do not necessarily represent those of their affiliated organizations, or those of the publisher, the editors, and the reviewers. Any product that may be evaluated in this article, or claim that may be made by its manufacturer, is not guaranteed or endorsed by the publisher.

Advantages of publishing in Frontiers

OPEN ACCESS
Articles are free to read for greatest visibility and readership

FAST PUBLICATION
Around 90 days from submission to decision

HIGH QUALITY PEER-REVIEW
Rigorous, collaborative, and constructive peer-review

TRANSPARENT PEER-REVIEW
Editors and reviewers acknowledged by name on published articles

Frontiers
Avenue du Tribunal-Fédéral 34
1005 Lausanne | Switzerland

Visit us: www.frontiersin.org
Contact us: frontiersin.org/about/contact

REPRODUCIBILITY OF RESEARCH
Support open data and methods to enhance research reproducibility

DIGITAL PUBLISHING
Articles designed for optimal readership across devices

FOLLOW US
@frontiersin

IMPACT METRICS
Advanced article metrics track visibility across digital media

EXTENSIVE PROMOTION
Marketing and promotion of impactful research

LOOP RESEARCH NETWORK
Our network increases your article's readership